# The interacting boson approximation

R. F. Casten

*Brookhaven National Laboratory, Upton, New York 11973*
*and Institut für Kernphysik der Universität zu Köln, 5000 Köln 41, West Germany*

D. D. Warner

*Science and Engineering Research Council Daresbury Laboratory, Warrington WA4 4AD, England*
*and Brookhaven National Laboratory, Upton, New York 11973*

The IBA-1 is reviewed with particular emphasis on the symmetry structure that arises naturally from its inherently algebraic approach. The formulation of the model, in both its algebraic and its numerical aspects, is presented and the basic character of its predictions is discussed and compared with nuclear data. The limitations of the model, and efforts to ameliorate these by appropriate extensions, are also reviewed in some detail. An effort is made to provide a simple, transparent understanding of the basic physics by clarifying the relation of the mathematical structure to underlying physical ideas, and to provide guidance in understanding and carrying out practical calculations.

## CONTENTS



## I. INTRODUCTION

In 1974, a new nuclear model was proposed, by Arima and Iachello, called the interacting boson approximation model or IBA (Arima and Iachello, 1975, 1976; see also Iachello and Arima, 1974). At the time of its proposal, models for medium- and heavy-mass nuclei generally centered on one of two types of approach, either a large-basis, shell-model diagonalization, along with related approximations, such as the random-phase approximation (RPA), to deal with nuclei that are not near closed shells or major subshells, or geometrical models in which a nuclear shape and excitations of that shape are envisioned. The IBA invoked instead an algebraic and group-

theoretical approach that recalls a methodology employed successfully for light nuclei in the late 1950s and early 1960s by Elliott (1958a, 1958b) and others. Over the last decade the IBA has generated considerable interest, as well as its fair share of controversy, and has prompted a large number of new studies in nuclear structure and spectroscopy. It is the purpose of this review to discuss the model and its predictions, its successes and limitations, and some extensions of it that have appeared in recent years.

The basic idea of the IBA (Arima and Iachello, 1975, 1976; Iachello, 1979; Scholten, 1980; Lipas, 1984) is to assume that low-lying collective states in even-even nuclei can be described by a system of interacting $s$ and $d$ bosons carrying angular momentums 0 and 2, respectively. This assumption is not an *ad hoc* one, but rather is based on the well-known features of generalized seniority (Talmi, 1983) calculations in the shell-model scheme and of the empirical structure of near-closed-shell nuclei, in which $0^+$ and $2^+$ states lie considerably lower in energy than those of higher angular momentum. More specifically, this is a characteristic feature of shell-model calculations of levels resulting from a short-range residual interaction in a two-particle configuration of identical nucleons in the same orbit (deShalit and Feshbach, 1974). Hence it is reasonable to view the boson states as being constructed from the valence space only and to identify the bosons as correlated pairs of like nucleons. As such, their number $N=n_s+n_d$ is finite and conserved in a given nucleus and is simply given by half the total number of valence nucleons. In the original version of the model, the IBA-1, with which this review deals, no distinction is made between protons and neutrons. Moreover, the valence number counting is always done relative to the nearest closed shells. For example, the nucleus $^{146}_{56}Ba_{90}$ has six valence protons (relative to $Z=50$) and eight neutrons (relative to $N=82$), and so the boson number is $N=3+4=7$. Similarly, both $^{196}_{78}Pt_{118}$ and $^{128}_{54}Xe_{74}$ have $N=N_\pi+N_\nu=2+4=6$ bosons and are taken to have the same basis states in the model, even though in one case both protons and neutrons are holes, while in the other the protons are particles and the neutrons holes. Nevertheless, despite this simplification, the key ingredient remains, namely, the explicit incorporation in the formalism of the finite number of valence nucleons available. This feature leads to many of the characteristic differences between the predictions of the IBA and earlier phenomenological models of collective nuclear structure, and also lends the former a microscopic aspect, in that a substantial part of the predicted structural changes across a major shell arise automatically from the changes in boson number.

Together, the $s(l=0)$ and $d(l=2)$ bosons of the IBA-1 have six components (substates) and therefore define a six-dimensional space. As will be discussed in detail later, this leads to a description in terms of the unitary group in six dimensions, U(6). As a consequence, many of the characteristic properties of the IBA can be derived by group-theoretical methods and expressed analytically. When we consider the different reductions of U(6), three dynamical symmetries emerge (Arima and Iachello, 1976, 1978a, 1978b, 1979), known as U(5), SU(3), and O(6), which are related to the geometrical idea of the spherical vibrator (Scharff-Goldhaber and Weneser, 1955), deformed rotor (Bohr and Mottelson, 1953), and asymmetric ($\gamma$-soft) deformed rotor (Wilets and Jean, 1956), respectively.

The existence and role of symmetries in the IBA framework represents its most unique and characteristic feature. Their description is simple and analytic, they have clear geometrical relationships and physical interpretations, and—a highly important practical point—their predictions depend on an absolute minimum of parameters. Indeed, many, such as $E2$ branching ratios, are parameter free. Moreover, even though most nuclei of course do not exhibit one or another of the IBA symmetries and hence require a numerical diagonalization of the IBA Hamiltonian for their description, an understanding of the symmetry properties of the IBA greatly simplifies that numerical treatment as well as the interpretation of the resulting wave functions, energy levels, and transition rates.

In addition, because of its symmetry structure, the IBA is a particularly apt vehicle for treating transitional regions, since such calculations can often be carried out in terms of a single free parameter that specifies the relative structural evolution along the transition path between pairs of symmetries. In this sense, the model provides an alternative to the situation that existed previously, in which a number of geometrical models, each applicable to a different structure, would be applied according to the empirically observed characteristics. It is worth emphasizing at this point, incidentally, that many references throughout the text to "geometric" models generally refer to the simplest "harmonic" versions originally introduced and most easily employed. It is not the place here to discuss the extensive subsequent evolution of these models, but the interested reader will find some apt comments in Lipas (1986b).

In these introductory comments, it should be noted that a model proposed by Janssen, Jolos, and Donau (1974), although starting from a quasiparticle framework with no fixed boson number, produces results equivalent to the IBA-1. In practice, the specific formalism of the IBA, with $s$ and $d$ bosons, generally renders it more easily usable. Although this review will therefore concentrate on the structure, properties, and tests of the IBA model and its offshoots, its equivalence to the quadrupole phonon approach of Janssen, Jolos, and Donau (1974), which has been emphasized by Paar (1979), should not be forgotten.

Although the IBA is primarily a model for low-lying collective excitations, recent extensions of the model have begun to extend these boundaries considerably. Perhaps the most natural of these extensions of the IBA-1 is the model known as the IBA-2 (Arima *et al.*, 1977;

Otsuka *et al.*, 1978), in which the proton and neutron degrees of freedom are specified separately and the Hamiltonian includes proton-boson–neutron-boson interactions. This development is a major one, not only because of the possibility of improved calculations, but also because it reveals still further systematics and new collective excitation modes and, most importantly, because it allows the link to the underlying shell model to be pursued. The IBA was originally formulated for even-even nuclei. Its extensions to odd-even nuclei (Iachello and Scholten, 1979) and recently to odd-odd spectra as well (Van Isacker *et al.*, 1985) are also major extensions of the original model.

It is important at the outset to emphasize clearly the purpose and nature of this review. The aim is to address the structure and physical content of the model, its simplicity and geometrical understanding, and to offer practical guidance in its use. A special effort will be made to remove some of the mystery from the model, especially in its reliance on abstract group theory. While the detailed use of group-theoretical techniques requires a specialized expertise, an understanding of the basic concepts and of the way they work can be rather simply conveyed.

This review will be limited to the IBA-1. Unfortunately, this forces us to ignore many exciting developments in the IBA-2 in recent years. The IBA-2 was for a long time viewed mostly as a much more complicated, but sometimes necessary, approach to detailed calculations necessitated by the obvious empirical dependence of certain properties (e.g., quadrupole moments, $M1$ transitions) on proton-neutron degrees of freedom. It was also essential in relating the IBA to its microscopic foundations. However, in recent years the discovery of symmetries in the IBA-2, of collective $M1$ modes, of the central importance of $F$ spin, and of the use of the IBA-2 to extract information analytically on effective charges and on effective substructure in the valence space have fostered an emerging appreciation of its independent importance. For the most part, these developments will be bypassed in the present article. The reader is referred to reviews by Barrett (1984), Dieperink (1984), Dieperink and Wenes (1985), and Lipas (1986a). The application of the IBA to odd-mass nuclei, in which an odd nucleon is coupled to an IBA-1 description of the even-even core in the so-called interacting boson-fermion approximation (IBFA), will also not be covered. This is a burgeoning field that can support a dedicated review.

As far as the experimental situation is concerned, only illustrative examples will be used to highlight specific ideas. This review is therefore in *no* sense intended to be an exhaustive and complete survey of the IBA literature. Partly because the IBA has now become a standard model for comparison with experimental data, that literature is already far too extensive to even attempt such a task. Moreover, there already exist many reviews that cover at least part of the overall territory. The interested reader is referred, for example, to Iachello (1979, 1981a, 1983b), Scholten (1979b), Arima and Iachello (1981), Casten and Warner (1983), Lipas (1984), Elliott (1985), Feng (1986), and Iachello and Arima (1987).

The emphasis here will be on the nuclear structure content of the model and on what the model has in turn disclosed as to the empirical structure of medium and heavy nuclei. Of course, the shortcomings of the model will be highlighted as appropriate, as well as extensions of the model designed to overcome these. The review will be divided into five sections. After this Introduction, Sec. II will give an outline of the model and its symmetry structure and characteristic predictions, along with a discussion of, and practical guidance in, its use for the vast majority of nuclei that are not close to one of the limiting symmetries. It will include discussions of the geometrical relationships of the model and of the intrinsic state for the IBA. Section III will discuss the applications of the model to empirical data. Section IV will discuss a number of important extensions of the IBA-1, and Sec. V will contain some brief concluding remarks. There will be only passing comments on the relationship of the IBA to its microscopic foundations in the shell model, since this is the subject of a recent review by Iachello and Talmi (1987).

## II. STRUCTURE OF THE MODEL

### A. Hamiltonian

The interacting boson model in its simplest form, as originally proposed (Arima and Iachello, 1975, 1976), describes a system of $s(l=0)$ and $d(l=2)$ bosons which may interact with one another via one- or two-body interactions. The neglect of higher-order terms does not represent any fundamental constraint, and indeed has been relaxed in some later applications of the model (see Sec. IV), but rather stems from the desire to keep the complexity of the overall Hamiltonian at a manageable level. The additional, and perhaps unique, constraint applied in this model is to conserve the total number of bosons in the system at a value given by one-half the number of valence nucleons. This restriction originates from the assumption that the $s$- and $d$-boson degrees of freedom can be related directly to $L=0$ and 2 excitations of pairs of fermions in a spherical shell-model basis. The counting of bosons must then be done with respect to the nearest closed shell in the neutron (or proton) space, so that the bosons are counted as particles if the neutron (or proton) number is before midshell, and as holes otherwise.

A first impression might be that, given the well-known particle-hole symmetry of most shell-model problems, it should be possible to count a particular type of boson from either shell and obtain identical results. However, the underlying reason for counting always to the nearest closed shell can be easily understood by the following simple example. Consider a shell that consists only of a $j=\frac{7}{2}$ orbit. The maximum number of particles in the

shell is eight, and midshell corresponds to four valence particles or two bosons. Assume now that there are six nucleons in the shell. If this system is treated as three particle bosons instead of one hole boson, then there will be basis states consisting of three $d$ bosons which, in the fermionic space, would correspond to states with seniority 6. The Pauli principle, however, mandates that the maximum seniority in a $j=\frac{7}{2}$ shell be 4. The rule of counting from the nearest closed shell therefore stems directly from the Pauli principle and hence from the assumed fermionic origins of the boson degrees of freedom.

Given the above simple definitions of the number and type of bosons and of the limits on the complexity of the possible interactions between them, it is a relatively straightforward matter to construct the basis, Hamiltonian, and operators that appear in the IBA-1 description. Any complete basis may be used, and, indeed, in occasional applications, basis states constructed in terms of the SU(3) or O(6) symmetry wave functions are useful. However, for most applications, and for the greatest ease in understanding the structure of the model and gaining insight into its predictions, it is most convenient to utilize the U(5) basis. Here the basis states can be simply specified by the number of $s$ and $d$ bosons and two additional quantum numbers which describe the manner in which the $d$ bosons couple to give the final total angular momentum. They can therefore be written as

$$|Nn_d v n_\Delta L\rangle \text{ or sometimes as } |Nn_d n_\beta n_\Delta L\rangle , \qquad (2.1)$$

where $N$ is the total number of bosons, $n_d$ is the number of $d$ bosons, $v$ is the $d$-boson seniority and hence the number of $d$ bosons *not* paired to angular momentum zero, and $n_\Delta$ represents the number of $d$-boson triplets coupled to zero angular momentum. Rigorously, $v$ and $n_\Delta$ cannot be simultaneous eigenvalues, but this is a technical point of small practical importance which we ignore here. In the second form $n_\beta$ is the number of $d$-boson zero-coupled pairs and hence is identical to $\frac{1}{2}(N-v)$. $L$ is the total angular momentum quantum number. The possible values of these quantum numbers are easily deduced. First of all, $N$ must equal $n_d+n_s$, so that $n_d$ can take values ranging from 0 to $N$ with $n_s=N-n_d$ in each case. Clearly, depending on the number of $d$ bosons paired to zero angular momentum, $v$ will take the values $n_d, n_d-2, \ldots, 1$, or 0 (equivalently, $n_\beta=0, 1, \ldots$), while $n_\Delta$ can take values 0, 1, ..., $[n_d/3]$ where the brackets indicate the largest integer $\leq n_d/3$. The first few basis states available for $n_d$ values from 0 to 3 are illustrated in Fig. 1, where it is immediately obvious that they correspond to the states of the simple harmonic oscillator. However, a fundamental difference from this geometric analog, where the phonons are generally understood as quasiparticle excitations, is the IBA-1 constraint on the total number of bosons, which results in a limitation on the total number of basis states available and, of course, on the maximum angular momentum that can be constructed ($L_{\max}=2N$). This distinction results

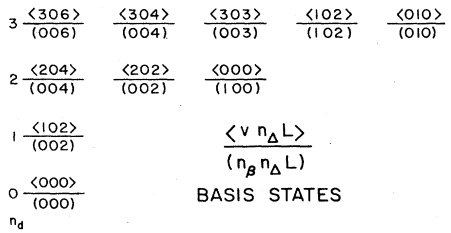


FIG. 1. Quantum numbers for the basis states of the IBA. The numbers above and below the lines give two alternate but equivalent sets of labels.

in many significant differences between the IBA and geometrical models, as will be discussed below.

The Hamiltonian, which connects the basis states, is written in the language of second quantization and, as such, can only involve combinations of the operators $s, s^\dagger, d, d^\dagger$. The specific combinations that appear are defined by the restriction limiting the complexity to a maximum of two-body interactions and by the need to conserve the total number of bosons. The former constraint implies that terms containing, for example, $d^\dagger d^\dagger$ or $s^\dagger s^\dagger$ are allowed, while combinations such as $d^\dagger d^\dagger d^\dagger$ are not. The latter demands that every creation operator be accompanied by an annihilation operator and vice versa. These rules result in the following form for the most general IBA-1 Hamiltonian (Arima and Iachello, 1976):

$$H=\varepsilon_s s^\dagger s+\varepsilon_d d^\dagger\cdot\tilde{d}+\tfrac{1}{2}\sum_{L=0,2,4} C_L(d^\dagger d^\dagger)^{(L)}\cdot(\tilde{d}\tilde{d})^{(L)}$$
$$+\frac{v_2}{\sqrt{10}}[(d^\dagger d^\dagger)^{(2)}\cdot\tilde{d}s+\text{H.c.}]+\frac{v_0}{2\sqrt{5}}(d^{\dagger 2}s^2+\text{H.c.})$$
$$+\frac{u_2}{\sqrt{5}}d^\dagger s^\dagger\cdot\tilde{d}s+\frac{u_0}{2}s^{\dagger 2}s^2 , \qquad (2.2)$$

where the coefficient in front of each term has been chosen according to the definitions of Arima and Iachello (1978a). The operator $\tilde{d}$ is defined by $\tilde{d}_m=(-1)^m d_{-m}$, so that it maintains the character of a spherical tensor operator of rank two. It is apparent that the full Hamiltonian of Eq. (2.2) involves two single-boson energies and seven boson-boson interaction strengths. The notation used follows that of Lipas (1984), in which tensor products, which involve angular momentum coupling, are denoted in the form $(d^\dagger d^\dagger)^{(L)}$ and scalar products as $d^\dagger\cdot d^\dagger$ with the further abbreviation that $d^\dagger\cdot d^\dagger\equiv d^{\dagger 2}$. Terms that contribute only to the binding energy in Eq. (2.2) can be removed when considering the excitation energy spectrum of a given nucleus by making use of the constraint on the total boson number, i.e.,

$$N=n_s+n_d , \quad n_s=s^\dagger s , \quad n_d=d^\dagger\cdot\tilde{d} , \qquad (2.3)$$

so that the Hamiltonian is reduced to its most useful six-parameter form,

$$H=\varepsilon'\hat{n}_d+\tfrac{1}{2}\sum_L C'_L(d^\dagger d^\dagger)^{(L)}\cdot(\tilde{d}\tilde{d})^{(L)}$$
$$+\frac{v_2}{\sqrt{10}}[(d^\dagger d^\dagger)^{(2)}\cdot ds+\text{H.c.}]$$
$$+\frac{v_0}{2\sqrt{5}}(d^{\dagger 2}s^2+\text{H.c.})\ . \qquad (2.4)$$

The primed parameters appearing in Eq. (2.4) are linear combinations of those in Eq. (2.2), and the detailed relationship between the two sets is given by Lipas (1984). For symbols such as $n_d$, which can denote either operators or their eigenvalues, the operator form is distinguished by a circumflex (e.g., $\hat{n}_d$).

Clearly it is possible to combine the terms in Eq. (2.4) in different ways and, in particular, to produce operators in the Hamiltonian that have a more intuitive interpretation. In particular, a multipole form for the Hamiltonian has been very commonly used, since it better displays the symmetry structure of the IBA-1. However, even when using that form, it often aids a physical understanding of the operation of the different terms to cast them in the direct second-quantized form of Eq. (2.4). Moreover, Eq. (2.4) is important because it is used in the computer program PHINT (Scholten, 1979a) to construct the final matrix for diagonalization.

As just alluded to, however, the most commonly used form of the IBA Hamiltonian, and the one in which it is easiest to understand the role of each term in determining the final structure of the nucleus under consideration, is the so-called multipole expansion. In this parametrization the various boson-boson interactions are grouped so that the Hamiltonian takes the form (Scholten, Iachello, and Arima, 1978)

$$H=\varepsilon''\hat{n}_d+a_0P^\dagger P+a_1\hat{L}^2+a_2Q^2+a_3T_3^2+a_4T_4^2\ , \qquad (2.5)$$

where

$$P=\tfrac{1}{2}(\tilde{d}^{\,2}-s^2)\ ,$$
$$T_l=(d^\dagger\tilde{d})^{(l)}\ ,\quad l=0,1,2,3,4\ ,$$
$$Q=(d^\dagger s+s^\dagger\tilde{d})-\frac{\sqrt{7}}{2}(d^\dagger\tilde{d})^{(2)}$$
$$=(d^\dagger s+s^\dagger\tilde{d})-\frac{\sqrt{7}}{2}T_2\ ,$$
$$\hat{n}_d=\sqrt{5}T_0\ ,\quad \hat{L}=\sqrt{10}T_1\ .$$

In this form there appear terms that have, at least superficially, a more physical connotation, specifically an angular momentum operator, a quadrupole operator, octupole and hexadecapole terms, as well as the so-called pairing operator $P$. Note, however, that these are operators acting on boson states, not in the fermion space. It is in this form, therefore, that we shall usually consider the application of the IBA-1 Hamiltonian to the set of basis states described earlier. We note that the definition of $Q$ above uses a specific [SU(3)] choice of numerical coefficients. A more general form will be given below.

At this point it is unfortunately necessary to digress for a moment on the issue of notation. There have been innumerable notations and definitions of the parameters used in the IBA Hamiltonian, even if one considers only the multipole form. For example, $\varepsilon''$, $a_0$, and $a_1$ are often denoted $\varepsilon$, $\kappa''$, and $-\kappa'$, while $a_2$ is most commonly replaced by $-\kappa$ but also by $-2\kappa$ and $QQ$. Indeed, in this work, $\varepsilon''$ will be written as $\varepsilon$ for simplicity. Since our primary motive is to convey a sense of the *physics* of the model we have, albeit reluctantly, occasionally glossed over this issue. In many cases, we have converted published parameter values or scales on figures to the consistent conventions adopted here. However, in a few applications discussed, the parameters involved will be defined only to within a multiplicative factor. It should be clear from the context and notation when this occurs. The reader who needs detailed information in these specific cases should consult the original literature. Where the parameter values make a difference of *physical* importance to the argument, however, they will be specified. For convenient reference, we list, in Table I, other notations frequently found for the parameters of Eq. (2.5).

In order to understand the role played by each of the operators in Eq. (2.5) in determining the structure of the final wave functions in a given problem, it is worthwhile to consider first the application of each term separately to the U(5) basis states of Fig. 1. The term in $\varepsilon''$ simply generates a diagonal contribution for each basis state proportional to the number of $d$ bosons contained within it; hence it is equivalent to assigning an energy to the $d$ boson and contributes a total energy to $H$ given by $\varepsilon''$ times the expectation value of the number of $d$ bosons, $\langle n_d\rangle$. The resultant energy spectrum is thus that of a quadrupole harmonic oscillator with phonon energy $\varepsilon''$ in which all the levels in a particular phonon multiplet are degenerate. This degeneracy can be lifted, without mix-

TABLE I. Relations between some IBA parameters.

| Parameters of Eq. (2.5) | PHINT[a] parameters | Equivalent parameters sometimes used in the literature[b] |
|---|---|---|
| $\varepsilon''$ | EPS | $\varepsilon$ |
| $a_0$ | 2 PAIR | $2\kappa''$ |
| $a_1$ | $\frac{1}{2}$ ELL | $-\kappa'$ |
| $a_2$ | $\frac{1}{2}$ QQ | $-2\kappa$ |
| $a_3$ | 5 OCT | |
| $a_4$ | 5 HEX | |

[a]Here PHINT refers to the program as written by O. Scholten and described in Scholten (1979a).

[b]For this column, the equivalences apply only to the PHINT parameters. In the past, in some cases, different forms of the operators were implicit in the Hamiltonians quoted. For example, the term in the Hamiltonian $-2\kappa Q^2$ has sometimes been written as $-\kappa Q^2$. In general, differences of a factor of 2 or in sign also appear in the literature.

ing the basis states of the model, by introducing any of the $\hat{L}^2$, $T_3^2$, or $T_4^2$ terms in the Hamiltonian, since inspection of Eq. (2.5) indicates that these terms cannot change the total $d$-boson number. Each simply provides a specific diagonal contribution. For example, the $\hat{L}^2$ term is proportional to the square of the total angular momentum of the system and hence yields a contribution proportional to $L(L+1)$.

The only terms that change the number of $d$ bosons, and therefore mix the basis states, are the pairing and quadrupole operators of Eq. (2.5). Therefore one or both of these must be used in order to induce a change in structure, for example, a transition from a spherical vibrational structure towards some type of deformed character, be it O(6), SU(3), or an intermediate case. It is therefore important to examine the specific role of these two terms in more detail. The pairing term, when expanded, clearly gives rise to contributions of the forms

$$d^{\dagger 2}s^2$$

and

$$d^{\dagger 2}\tilde{d}^2, \quad \Delta n_d = 0 ,$$

$$s^{\dagger 2}\tilde{d}^2, \quad \Delta n_d = \pm 2 ,$$

$$s^{\dagger 2}s^2, \quad \Delta n_d = 0 ,$$

where the effect of each term on the $d$-boson number $n_d$ is explicitly indicated. Thus $P^\dagger P$ either is diagonal or changes $n_d$ by 2 units. Moreover, given the appearance of only scalar products in $P$ and $P^\dagger$, the $\Delta n_d = \pm 2$ part is equivalent to changing the number of $d$-boson pairs coupled to angular momentum zero $n_\beta$ by $\pm 1$. The quadrupole operator, on the other hand, contains tensor products and pieces which change $n_d$ by one and by zero, so that $Q^2$ has elements with

$$d^{\dagger 2}s^2 \text{ and } s^{\dagger 2}\tilde{d}^2 , \quad \Delta n_d = \pm 2 ,$$

$$(d^\dagger \tilde{d})^{(2)} \cdot d^\dagger s \text{ and } (d^\dagger \tilde{d})^{(2)} \cdot s^\dagger \tilde{d} , \quad \Delta n_d = \pm 1 ,$$

$$d^\dagger s \cdot s^\dagger \tilde{d} \text{ and } (d^\dagger \tilde{d})^{(2)} \cdot (d^\dagger \tilde{d})^{(2)} , \quad \Delta n_d = 0 ,$$

and will therefore mix all basis states. Thus a Hamiltonian with $P^\dagger P$ and no $Q^2$ terms produces wave functions containing specific mixtures of those basis states differing only by $\Delta(n_d, n_\beta) = (2,1)$ or $(-2,-1)$, whereas one with a $Q^2$ term yields much more complex states containing amplitudes for all basis states. As will be seen, however, though each of these operators acting alone leads to complex mixtures of U(5) basis states, each also produces wave functions with definite, and simple, symmetry properties. That simplicity is, in effect, only apparent upon transformation to a different intrinsic system (different basis set), although its effects appear clearly in predictions of energy levels, transition rates, and so on.

This type of simple understanding of the characteristics of each of the operators in the general IBA-1 Hamiltonian, in terms of the way in which they connect the basis states of the model, provides an immediate insight into the structure induced by any combination of them in a particular calculation and into the structure of the different symmetry limits that emerge from a group-theoretical treatment of the Hamiltonian. Since these limiting symmetries provide benchmarks in defining the different structures obtainable within the general framework of the IBA, further discussion of the role of the various terms in the Hamiltonian will be left to a later section, after the algebraic method has been introduced. Prior to that, however, it is useful to consider the form of the operators that enter into the IBA-1 formalism in the description of various other observables.

### B. Transition operators

The construction of operators for the various nuclear structure observables of interest is again straightforward, given the fact that they must be built from the basis elements $s$, $s^\dagger$, $\tilde{d}$, or $d^\dagger$. In the vast majority of applications to date, only the lowest-order contributions to these operators have been included. Thus the electromagnetic transition operators can be written down by inspection as

$$T(E0) = \alpha \hat{n}_s + \frac{\beta'}{\sqrt{5}} \hat{n}_d , \tag{2.6}$$

$$T(M1) = g_B \hat{L} , \tag{2.7}$$

$$T(E2) = e_B[(s^\dagger \tilde{d} + d^\dagger s) + \chi (d^\dagger \tilde{d})^{(2)}] = e_B Q . \tag{2.8}$$

The $E0$ operator can be rewritten as

$$T(E0) = \alpha(\hat{N} - \hat{n}_d) + \frac{\beta'}{\sqrt{5}} \hat{n}_d = \alpha \hat{N} + \frac{\beta}{\sqrt{5}} \hat{n}_d . \tag{2.9}$$

The first term in $T(E0)$ vanishes, since $N$ is conserved and therefore cannot induce transitions between the orthogonal basis states. Hence $E0$ transitions are simply proportional to the matrix elements of the $d$-boson number operator and thus rather directly sample the wave-function structure. In contrast, the $M1$ operator is proportional to the total angular momentum and therefore gives rise to no transitions. To investigate $M1$ transitions in the IBA-1 framework, it has therefore been necessary to introduce second-order terms (Arima and Iachello, 1978a; Warner, 1981; Wood and Morrison, 1985). In this case, one has

$$T(M1) = (g_B + A\hat{N})\hat{L} + B\hat{n}_d \hat{L} + C(Q\hat{L})^{(1)} , \tag{2.10}$$

where $Q$ now has the more general form of Eq. (2.8).

Finally, the $E2$ operator, which is identical in form to the $Q$ operator in the Hamiltonian, consists of one piece that changes $n_d$ by unity and another that leaves $n_d$ unchanged, the ratio of the two terms being given by the parameter $\chi$.

Turning now to other properties, the operator for the mean-square radius is, of course, closely related to that for the $E0$ transitions and is given by

$$r^2 = \langle r^2 \rangle_c + a\hat{n}_d + b\hat{N} , \tag{2.11}$$

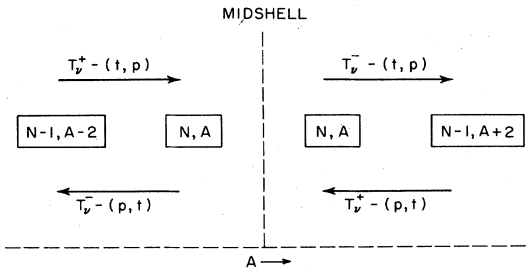


FIG. 2. Schematic representation of the role of the two-particle transfer operators above and below midshell.

where the first term represents the mean-square radius of the closed-shell core.

It is also possible in principle to treat two-nucleon transfer amplitudes within the framework of the IBA-1 model. For $L=0$ transfer, the operator is obviously either $s$ or $s^\dagger$, i.e.,

$$T^+=\alpha_+ s^\dagger , \quad T^-=\alpha_- s . \tag{2.12}$$

Thus the transfer of two identical nucleons in a relative angular momentum zero state is regarded as the creation or destruction of an $s$ boson. Of course, since such reactions change specifically the proton or neutron boson number, they cannot be explicitly realized within the IBA-1 formalism. A consideration of the problem within the framework of the neutron-proton version of the IBA, however, leads (Arima and Iachello, 1977) to the following forms for the two expressions:

$$T_\rho^+=\alpha_+ s^\dagger \left[\Omega_\rho-\hat{N}_\rho-\frac{\hat{N}_\rho}{\hat{N}}\hat{n}_d\right]^{1/2}\left[\frac{\hat{N}_\rho+1}{\hat{N}+1}\right]^{1/2} , \tag{2.13}$$

$$T_\rho^-=\alpha_- \left[\Omega_\rho-\hat{N}_\rho-\frac{\hat{N}_\rho}{\hat{N}}\hat{n}_d\right]^{1/2}\left[\frac{\hat{N}_\rho+1}{\hat{N}+1}\right]^{1/2} s , \tag{2.14}$$

where $\rho=\pi$ or $\nu$. Here $\Omega_\rho$ is the pair degeneracy in the appropriate major shell (e.g., for neutrons in the $N=82-126$ shell, $\Omega=22$). It is important to note that the role of the two-particle transfer operator changes at midshell when the bosons change from particles to holes. This situation is illustrated schematically in Fig. 2. Thus below midshell $T^+$ increases $A$ by 2 units and describes, for example, a $(t,p)$ reaction, whereas above midshell $T^+$, by increasing $n_s$ and therefore $N$ by 2 units, decreases $A$ by 2 units and describes a $(p,t)$ reaction.

### C. Algebraic treatment of the IBA-1 Hamiltonian

The previous sections showed how the IBA approach can be viewed as the application of a rather simple Hamiltonian, constructed by the application of a few, well-defined rules, to a set of basis states that correspond closely to those of a quadrupole harmonic oscillator. However, the unique characteristics of the IBA, and its historical motivation, are founded in the principles of group theory. A full treatise on the relevant algebraic techniques is beyond both the scope of the present article and the competence of its authors. Nevertheless, a certain familiarity with the basic principles, terminology, and methods of group theory applied in the IBA formalism is necessary to understand its origins and philosophy, as well as to simplify the use of the general Hamiltonian. Unfortunately for many nonspecialists, this is a topic that abounds in specialized terminology and obscure lemmas and theorems, without recourse to which many results are difficult to obtain and more so to visualize. As will become evident, the approach offered below has been liberally purloined from the excellent review article by Lipas (1984) on the IBA-1 formalism, but is aimed at an even more elementary level. It attempts to make clear the basic concepts and terminology by working out, step by step, examples of some of the key ideas. We hope that those not very familiar with group theory may benefit from the approach in this section.

The five magnetic substates of the $d$ boson and the single $s$ state can be regarded as forming a six-dimensional vector space. Then, just as in the analogous case of angular momentum, where the components $J_x,J_y,J_z$ generate rotations or transformations of the angular momentum vector and form the group O(3), bilinear combinations of the operators $s,s^\dagger,d_\mu,d_\mu^\dagger$ define basic "rotations" of the corresponding six-dimensional state vectors in the $s$-$d$ space and form the group U(6).

The essential group-theoretical apparatus is founded on the properties of commutation of various pairs of operators. The first step in working out a group structure is to look for combinations of the basic operators that close on commutation, that is, for which the commutator of any pair is equal to a linear combination of the members of the set (including the trivial result $[A,B]=0$). Complete sets of these operator combinations are called the *generators* of the group.

For O(3) the generators are $J_x$, $J_y$, and $J_z$ or, alternatively, the more convenient set $J_\pm,J_z$ where $J_\pm\equiv J_x\pm iJ_y$. The commutation relations for these latter are well known and are given by

$$[J_+,J_-]=2J_z \quad \text{and} \quad [J_z,J_\pm]=\pm J_\pm \quad (\hbar=1) ,$$

showing that, indeed, they close on commutation.

For the case of the U(6) group, there are 36 possible bilinear operator combinations that satisfy the requirement of boson number conservation,

$$\begin{aligned} &s^\dagger s, s^\dagger \tilde{d}_\mu, d_\mu^\dagger s, (d^\dagger \tilde{d})_\mu^{(l)} , \\ &l=0,1,2,3,4 , \\ &\mu=+4,+3,\ldots -3,-4, \quad |\mu|\le l . \end{aligned} \tag{2.15}$$

This set closes on commutation and thus comprises the generators. This can be made plausible by calculating, as an example, the commutator $[d^\dagger s,s^\dagger s]$. In order to do

this, we must state the basic rules for the eigenvalues of operators in the second-quantization formalism. In terms of a general creation (destruction) operator $b^\dagger(b)$ operating on a state with $n_b$ bosons, we have

$$b \mid n_b \rangle = \sqrt{n_b} \mid n_b - 1 \rangle \tag{2.16}$$

and

$$b^\dagger \mid n_b \rangle = \sqrt{n_b + 1} \mid n_b + 1 \rangle \ , \tag{2.17}$$

from which it follows also that $b^\dagger b \mid n_b \rangle \equiv \hat{n}_b \mid n_b \rangle = n_b \mid n_b \rangle$.

Thus, for the example of the operators of Eq. (2.15) just cited, we have

$$\begin{aligned}[d^\dagger s, s^\dagger s] \mid n_d n_s \rangle &= (d^\dagger s s^\dagger s - s^\dagger s d^\dagger s) \mid n_d n_s \rangle \\ &= d^\dagger s n_s \mid n_d n_s \rangle - \hat{n}_s d^\dagger s \mid n_d n_s \rangle\end{aligned}$$

or, since the eigenvalues of $\hat{n}_s$, namely $n_s$, are factorable,

$$\begin{aligned}&= (n_s - \hat{n}_s) d^\dagger s \mid n_d n_s \rangle \\ &= (n_s - \hat{n}_s) \sqrt{n_d + 1} \sqrt{n_s} \mid n_d + 1, n_s - 1 \rangle \\ &= [n_s - (n_s - 1)] \sqrt{n_d + 1} \sqrt{n_s} \mid n_d + 1, n_s - 1 \rangle \\ &= \sqrt{n_d + 1} \sqrt{n_s} \mid n_d + 1, n_s - 1 \rangle \equiv d^\dagger s \mid n_d, n_s \rangle\end{aligned}$$

or

$$[d^\dagger s, s^\dagger s] = d^\dagger s \ . \tag{2.18}$$

The other commutators can be similarly evaluated and indeed close on commutation. This set of 36 generators of the group of transformations of U(6) is said to form the Lie algebra U(6).

As will become evident, an important concept is that of a *Casimir* operator of a group. This is an operator that commutes with *all* of the generators of the group. Such operators can be composed of linear or higher-order combinations of the generators and are appropriately called linear, quadratic , . . . , Casimir operators.

For example, in the case of O(3), the operator $J^2 = J_x^2 + J_y^2 + J_z^2 = J_+ J_- + J_z^2$ commutes with $J_z$, $J_+$, and $J_-$ and is therefore the (quadratic) Casimir operator of O(3).

The linear Casimir operator of U(6), which commutes with all 36 generators, is the total boson number operator $C_{1U6} = \hat{N} \equiv d^\dagger \cdot \tilde{d} + s^\dagger s$. This result stems trivially from the fact that all bilinear combinations of the $s$ and $d$ operators must conserve the total boson number. Hence, for an arbitrary bilinear combination of the generators of U(6), $x^\dagger y$,

$$\begin{aligned}[\hat{N}, x^\dagger y]\Psi &= \hat{N}(x^\dagger y)\Psi - (x^\dagger y \hat{N})\Psi \\ &= \hat{N}(x^\dagger y)\Psi - N(x^\dagger y)\Psi = 0 \ .\end{aligned} \tag{2.19}$$

The quadratic Casimir operator of U(6) is $C_{2U6} = \hat{N}(\hat{N} + 5)$.

It is now possible to search for *smaller* sets of generators, contained within the original 36, which themselves close on commutation. These define *subalgebras* or subgroups of U(6). Each will have linear and/or quadratic Casimir operators associated with it which commute with all the generators of the subgroup [and hence also with the Casimirs of U(6)]. In the analogous O(3) case, the only subalgebra is generated by $J_z$: the associated group is O(2), and $J_z$ is also the Casimir operator of O(2). For U(6), there are several subgroups, so the reduction process continues until the subgroup O(3) is reached. This latter requirement is a physical one, since the nuclear wave functions must be rotationally invariant. One example (of many) of a subgroup of U(6) is U(5). It has the 25 generators

$$(d^\dagger \tilde{d})^{(l)}_\mu \ ,$$

which form a subset of the 36 given in Eq. (2.15) and which also close on commutation, as can be shown by direct calculation in the same manner as illustrated in Eq. (2.18). The linear Casimir operator of U(5) is $\hat{n}_d$. This can be seen trivially, since the generators of U(5) conserve the number of $d$ bosons and therefore must commute with $\hat{n}_d$. Note, however, that $\hat{n}_d$ *cannot* be a Casimir of the larger group U(6) because it does not commute, for example, with $s^\dagger \tilde{d}$, which does not conserve $n_d$. The quadratic Casimir of U(5) is $C_{2U5} = \hat{n}_d(\hat{n}_d + 4)$.

It is now necessary to find the quantum numbers that label the basis states. In general, as seen in the examples above, the generators of a group may change some quantum numbers (e.g., $n_d$), but there will be one (or more) that are *not* changed by *any* of the generators. For the angular momentum case, for example, the generators $J_z, J_\pm$ always conserve the total $J$. For the U(6) group, the 36 generators always conserve $N$. The set of basis states that transform into each other under the action of any of the generators and that therefore have a particular fixed value of an unchanged quantum number (or numbers) is called an *irreducible representation* of the group. For O(3) the set of states

$$\mid j, m = j \rangle, \mid j, m = j - 1 \rangle, \ldots, \mid jm = -j \rangle$$

forms an irreducible representation or basis of O(3). This irreducible representation is notationally labeled by $j$, which is then a characteristic quantum number for the representation. The basis states are distinguished by $m$, which itself labels the irreducible representations of the *subgroup* O(2). For U(6), the representation label is specified by $N$ (or commonly, for reasons relating to the proton-neutron symmetry of the wave functions, by the notation $[N]$).

Since the generators of a given group do not connect different irreducible representations, the Casimir operator(s) of a group, which, by definition, commute with all the generators, must be diagonal and therefore must conserve all quantum numbers, including those of the subgroups (such as $m$ in the angular momentum

case). Then it follows that a Hamiltonian consisting only of Casimir operators of a chain of a group and subgroups cannot mix different representations of any of the groups involved, and its eigenvalues are just linear combinations of those of its component Casimir operators. Moreover, at any stage in a group chain decomposition, all states with the same representation labels are degenerate. In addition, a transition operator consisting of generators of a given group or subgroup cannot connect states in different representations of that group. This trivially leads to many essential selection rules.

As is evident from the above discussion, for any group chain reduction, the basis states for which the Hamiltonian is diagonal will be defined by the representation labels of the various groups and subgroups appearing in the group chain reduction.

As an example of these concepts, the angular momentum problem can be summarized as follows:

$$\begin{array}{llll} \text{groups:} & O(3) & \supset & O(2), \\ \text{generators:} & J_{\pm}, J_z & & J_z, \\ \text{Casimirs:} & J^2 & & J_z, \\ \text{labels:} & j & & m, \end{array} \tag{2.20}$$

where the representation labels define the basis $|jm\rangle$. A Hamiltonian for the system can be written as a sum of the Casimir operators involved,

$$H = aJ^2 + bJ_z \ , \tag{2.21}$$

and the corresponding eigenvalue expression is, of course,

$$E = aj(j+1) + bm \ . \tag{2.22}$$

If one considers only the group O(3), i.e., $b=0$, then all the states of a representation of O(3) specified by $j$ are degenerate. The degeneracy is broken by going to the subgroup, in which case the energies depend on the value of $m$.

A central task in developing any group chain or group reduction scheme is thus to identify the quantum numbers that label the irreducible representations of each subgroup, and this is the basic procedure followed in the algebraic treatment of the IBA. Group chains are constructed starting from U(6), where all the states are degenerate for a given value of $N$, and ending with O(3). A Hamiltonian for any such chain is written as a sum over the Casimir operators of the subgroups of the specific chain, and therefore will be diagonal in a basis defined by the corresponding representation labels. Each step in the chain reduction thus introduces one or more free parameters (coefficients of terms in $H$) into the eigenvalue expression and requires one or more quantum numbers to distinguish the representations of the particular subgroup; it also breaks a previous degeneracy. Thus the solution of the eigenvalue problem for such a chain reduces to that of the (known) eigenvalues of each of the Casimir operators.

The structure defined by such a Hamiltonian is referred to as a *dynamical symmetry*. One of the elegant aspects of these symmetries is that, although they may correspond to a complex physical situation and, in terms of Eq. (2.5), to a complex Hamiltonian, the excitation energy spectrum can be immediately written down and each state can be labeled by appropriate quantum numbers. As noted, since transition operators can also often be written in terms of the group generators, transition selection rules also appear naturally, and the rates for allowed transitions can be written analytically. Moreover, many ratios of transition rates depend only on general characteristics of the symmetry (group chain) and are parameter free. [This is not surprising: the Alaga rules (Alaga *et al.*, 1955) for $E2$ branching ratios in deformed nuclei are a familiar geometrical analog.]

Returning now to the basic problem in the IBA-1, there are three, and only three, group chains of U(6) that end in O(3). They can be written

$$\begin{aligned} &\text{(I)} \quad U(6) \supset U(5) \supset O(5) \supset O(3) \ , \\ &\text{(II)} \quad U(6) \supset SU(3) \supset O(3) \ , \\ &\text{(III)} \quad U(6) \supset O(6) \supset O(5) \supset O(3) \ . \end{aligned} \tag{2.23}$$

Having summarized the basic group-theory approach and illustrated it with the angular momentum case, we should find the procedure here (if not the details of how they are carried out) clear. In the following we shall simply cite the principal results.

The linear and quadratic Casimir operators of U(6) and its various subgroups can be written in terms of the operators of Eq. (2.5) as

$$\begin{aligned} &C_{1U6} = \hat{N} \ , \quad C_{2U6} = \hat{N}(\hat{N}+5) \ , \\ &C_{1U5} = \hat{n}_d \ , \quad C_{2U5} = \hat{n}_d(\hat{n}_d+4) \ , \\ &C_{2SU3} = \tfrac{4}{3}Q^2 + \tfrac{1}{2}\hat{L}^2 \ , \\ &C_{2O6} = 2\hat{N}(\hat{N}+4) - 8P^{\dagger}P \ , \\ &C_{2O5} = \tfrac{2}{5}\hat{L}^2 + 4T_3^2 \ , \quad C_{2O3} = 2\hat{L}^2 \ . \end{aligned} \tag{2.24}$$

It should be commented that since these Casimir operators are defined by a set of vanishing commutators, any multiplicative form is also a generator. The definitions above are conventional and convenient ones. It now remains to identify the representation labels for each chain, and hence the quantum numbers of the basis states, as well as the physical structure for each limiting symmetry. In doing so, we shall from time to time make correspondences with various geometrical models.

### 1. Chain I: The U(5) limit

The representation labels for the U(5) limit (Arima and Iachello, 1976) have already been introduced in the previous section, in terms of the basis states used in the treatment of the general IBA-1 Hamiltonian. The correspon-

dence with the group decomposition of Eq. (2.23) is as follows:

$$\begin{array}{ccccc} U(6) & \supset & U(5) & \supset & O(5) \supset O(3) \\ [N] & & n_d & & v \quad n_\Delta L \end{array} . \tag{2.25}$$

As can be seen, an additional quantum number $n_\Delta$ has been introduced to describe the reduction from O(5) to O(3). This requirement indicates that within the basis states $|Nn_d v\rangle$ which describe the representations of O(5) there can be more than one state with a particular value of $L$.

As pointed out above, this chain was chosen to describe the basis of the general IBA-1 treatment, and the meanings and possible values of the quantum numbers have already been described. The Hamiltonian for chain I can be written down by inspection of Eqs. (2.24) and (2.25):

$$H_I = \alpha C_{1U5} + \beta C_{2U5} + \gamma C_{2O5} + \delta C_{2O3} . \tag{2.26}$$

Its eigenvalues are

$$E = \alpha n_d + \beta n_d(n_d+4) + 2\gamma v(v+3) + 2\delta L(L+1) , \tag{2.27}$$

where each term in Eq. (2.27) is the eigenvalue of the corresponding Casimir operator of Eq. (2.26). In terms of the operators of the multipole expansion, the Hamiltonian $H_I$ reduces to

$$H_I = \varepsilon \hat{n}_d + a_1 \hat{L}^2 + a_3 T_3^2 + a_4 T_4^2 . \tag{2.28}$$

The relationship between the different coefficients of Eqs. (2.26) and (2.28) is obtained by comparison of Eqs. (2.5) and (2.24) and is discussed in Lipas (1984).

A typical example of the energy spectrum in the harmonic U(5) limit where $H_I = \varepsilon \hat{n}_d$ is shown in Fig. 3 and corresponds, except for high-spin cutoffs, to that of a harmonic vibrator in a geometrical framework. The characteristic features of the corresponding wave functions can be deduced from the terms appearing in $H_I$, all of which are diagonal with respect to the $n_d$ quantum

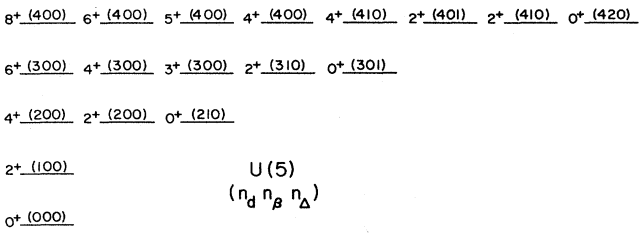


FIG. 3. Low-lying levels of the U(5) symmetry of the IBA in the harmonic limit.

number; thus, in U(5), there are no terms that mix states of different $d$-boson numbers. Examples of the wave functions are included in Table II, which gives the wave functions for the lowest $0^+$ states in all three dynamical symmetries. The selection rules for the various electromagnetic and transfer operators are then easily deduced.

It is interesting to note the rich flexibility in the level-energy spectrum provided by the eigenvalues expression (2.27). The U(5) limit is in fact a very general anharmonic vibrator, and levels with different $L$ but the same $n_d$ need not be degenerate. It is informative to pursue a little further the relationship between U(5) and the geometric anharmonic vibrator. Both spectra, of course, display multiplets of levels (with degeneracies broken by anharmonic effects) which have successively higher $n_d$ values or phonon quantum numbers. [Frequently below, for convenience, we shall use the phonon terminology in reference to the U(5) multiplets because of the similarity to the geometrical picture, just as in discussing SU(3) we shall call certain excitations $\beta$ and $\gamma$ vibrations.] The close relation to a vibrational picture is also clear in the nuclear potential corresponding to U(5), which is spherically symmetric with a minimum at deformation $\beta=0$ (see Sec. II.E). (Note, incidentally, a point that will be important later, that such a potential also has no structure in the $\gamma$ degree of freedom: it is completely $\gamma$ soft.)

TABLE II. Wave functions expressed in the U(5) basis for the first three $0^+$ states in each limit of the IBA.

| | | Basis states $(n_d n_\beta n_\Delta)$ | | | | | | |
|---|---|---|---|---|---|---|---|---|
| State[a] | Limit | (000) | (210) | (301) | (420) | (511) | (602) | (630) |
| $0_1^+$ | U(5) | 1 | 0 | 0 | 0 | 0 | 0 | 0 |
| | 0(6) | −0.43 | −0.75 | 0 | −0.491 | 0 | 0 | −0.095 |
| | SU(3) | 0.134 | 0.463 | −0.404 | 0.606 | −0.422 | −0.078 | 0.233 |
| $0_2^+$ | U(5) | 0 | 1 | 0 | 0 | 0 | 0 | 0 |
| | 0(6) | 0.685 | 0.079 | 0 | −0.673 | 0 | 0 | −0.269 |
| | SU(3) | 0.385 | 0.600 | −0.204 | −0.175 | 0.456 | 0.146 | −0.437 |
| $0_3^+$ | U(5) | 0 | 0 | 1 | 0 | 0 | 0 | 0 |
| | 0(6) | 0 | 0 | −0.866 | 0 | −0.463 | 0 | 0 |
| | SU(3) | −0.524 | −0.181 | −0.554 | 0.030 | −0.114 | −0.068 | −0.606 |

[a]The states are ordered for pedagogical clarity and not necessarily in the order of increasing energy. Indeed, the $\tau=3$ $0^+$ state in O(6) (here labeled $0_3^+$) is usually the $0_2^+$ state.

The similarity of the U(5) limit and the geometrical anharmonic vibrator runs deeper than this, however. Brink, de Toledo Piza, and Kerman (1965) have discussed a vibrator model with cubic and quartic anharmonicities in lowest-order perturbation theory. Since their Hamiltonian has several free parameters that affect the predicted degeneracy splitting, they adopted the approach of expressing the splittings of the three-phonon quintuplet in terms of those of the two-phonon triplet. Their results are given in Table III, in terms of $\varepsilon_0$, $\varepsilon_2$, and $\varepsilon_4$, which are the deviations of the two-phonon energies from $2E_{2_1^+}$. As pointed out by Arima and Iachello (1976) and shown more explicitly in a recent analysis of the U(5) symmetry (Aprahamian *et al.*, 1987), the energy levels of U(5) have exactly the same interrelationships as those given in Table III for the geometric anharmonic vibrator model. In both, there is an inherent connection between the energy splittings in different multiplets. It is interesting that some of the results in Table III can be trivially derived. For example, the three-phonon $0^+$ state can be constructed only by coupling the one-phonon $2^+$ state ($d$ boson) to the two-phonon $2^+$ state. The three indistinguishable phonons thus coupled have three pairwise anharmonic interactions, each of which is identical to that in the two-phonon $2^+$ state. Hence the anharmonicity is $3\varepsilon_2$. Similarly, the $6^+$ state is composed of a one-phonon $2^+$ state coupled to the two-phonon $4^+$ level. Again, there are three pairwise interactions identical to that occurring in the $4^+$ state, and the anharmonicity is $3\varepsilon_4$. The other results can be easily derived using the coefficients of fractional parentage tabulated by Bohr and Mottelson (1975).

### a. E0 transitions

As noted earlier, since the $E0$ operator is proportional to $\hat{n}_d$, $\langle i \mid T(E0) \mid j \rangle \propto n_{d_j} \langle i \mid j \rangle = 0$ if $i \neq j$, and there can be no $E0$ transitions in the U(5) limit.

TABLE III. Energies of the three-phonon quintuplet in terms of the two-phonon anharmonicities (Brink, de Toledo Piza, and Kerman, 1965).

| $N_{\text{ph}}$ | $L$ | Energy[a] (relative units) |
|---|---|---|
| 0 | 0 | 0 |
| 1 | 2 | 1 |
| 2 | 0 | $2+\varepsilon_0$ |
| 2 | 2 | $2+\varepsilon_2$ |
| 2 | 4 | $2+\varepsilon_4$ |
| 3 | 0 | $3+3\varepsilon_2$ |
| 3 | 2 | $3+7/5\varepsilon_0+4/7\varepsilon_2+36/35\varepsilon_4$ |
| 3 | 3 | $3+15/7\varepsilon_2+6/7\varepsilon_4$ |
| 3 | 4 | $3+11/7\varepsilon_2+10/7\varepsilon_4$ |
| 3 | 6 | $3+3\varepsilon_4$ |

[a] $\varepsilon_0$, $\varepsilon_2$, and $\varepsilon_4$ are defined as the deviations of the $0^+$, $2^+$, and $4^+$ level energies of the two-phonon triplet from $2E_{2_1^+}$.

### b. E2 transitions

The $E2$ operator of Eq. (2.8) has a term that changes $n_d$ by $\pm 1$ and a term with $\Delta n_d = 0$. If the operator is chosen to be a generator of the U(5) symmetry, then only the latter term would be used. However, the predicted $E2$ matrix elements would then be 0 between states differing by 1 or more $d$ bosons, while they would yield nonzero diagonal contributions (quadrupole moments). This situation is essentially the inverse of that expected and observed for vibrational nuclei, and hence it has been customary to use the first term of the $E2$ operator in the U(5) limit, which produces results very similar to those of the geometric vibrational picture.

For example, one obtains the general result

$$\sum_{L'} B(E2{:}L, n_d+1 \rightarrow L', n_d) = e_B^2 (n_d+1)(N-n_d) , \quad (2.29)$$

where $e_B$ is a boson effective charge. The sum on the left side of Eq. (2.29) accounts for the distribution of strength from a given initial state if the angular momentum selection rules allow decay to more than one level of the next lower multiplet. This sum contains more than one term only for decay of $n_d \geq 3$ states.

The expression analogous to Eq. (2.29) in the phonon model is proportional to $(n_{\text{ph}}+1)$. The factor $(N-n_d)$ in the IBA case arises from the finite boson number, and its origin can easily be seen. For example, if we denote the first few U(5) states only by $\mid n_d, n_s \rangle$ and use Eqs. (2.16) and (2.17), we have for the matrix element $\langle n_d, n_s \mid s^\dagger d \mid n_d+1, n_s-1 \rangle$:

$$\langle n_d, n_s \mid s^\dagger d \mid n_d+1, n_s-1 \rangle = \sqrt{(n_d+1)}\sqrt{n_s} \langle n_d, n_s \mid n_d, n_s \rangle \quad (2.30)$$

$$= \sqrt{n_d+1}\sqrt{N-n_d} . \quad (2.31)$$

Note that these results are intimately linked to the inclusion of finite $N$ in the IBA. In terms of quadrupole excitations only (i.e., $d$ bosons or quadrupole phonons), the U(5) limit and the geometrical vibrator are identical. The $2_1^+$ level has one such excitation, the levels of the $0^+, 2^+, 4^+$ triplet have two, and so on. The difference is that, in such excitations in the IBA, the restriction to a finite fixed $N$ imposes an additional constraint, which gives rise to the second factor on the right in Eqs. (2.29) and (2.31).

Equation (2.29) gives, for the transitions between the lowest levels,

$$B(E2{:}2_1^+ \rightarrow 0_1^+) = e_B^2 N \quad (2.32)$$

and

$$B(E2{:}2_2^+ \rightarrow 2_1^+) = 2e_B^2 (N-1) . \quad (2.33)$$

The ratio of these two gives the useful result that

$$R=\left[\frac{B(E2:2_2^+\rightarrow 2_1^+)}{B(E2:2_1^+\rightarrow 0_1^+)}\right]_{U(5)}$$
$$=\frac{N-1}{N}\left[\frac{B(E2:2_2^+\rightarrow 2_1^+)}{B(E2:2_1^+\rightarrow 0_1^+)}\right]_{ph}. \quad (2.34)$$

Since U(5) is usually relevant only near closed shells, where $N$ is rather small, differences from the geometric model can thus be significant. For example, for $N=5$, Eq. (2.34) gives $R=1.6$, compared to 2.0 for the geometric picture. Finally, note that when the initial state [with $N=n_d+1$ $d$ bosons; see Eq. (2.29)] is the fully aligned $I=2N$ excitation, the factor $(N-n_d)$ has reduced to unity. This is an example of the well-known cutoff effects in $B(E2)$ values involving high-spin states that are another characteristic distinction of the IBA from the geometric models.

As a final comment, it should be reemphasized that the choice of $E2$ operator used here, $T(E2)=\alpha(s^\dagger\tilde{d}+d^\dagger s)$, is not mandated by, nor is it in the spirit of, the U(5) symmetry itself. Under such circumstances [which are unique to U(5)], it would appear most reasonable in practical calculations to treat $B(E2)$ transitions in this limit with the full operator, the ratio $\chi$ of the two terms being a free parameter.

### c. Two-nucleon transfer

The ground states in U(5) consist solely of $n_s=N$ $s$ bosons. Thus the operator $s$ or $s^\dagger$ can connect the ground states of adjacent even-even U(5) nuclei with $N$ and $N-1$ or $N+1$, respectively, but cannot reach any excited $0^+$ states, since they all have $n_d>0$. The transfer strength between ground states is given by Eq. (2.13) as

$$S_g(N_\rho\rightarrow N_\rho+1)=\alpha_\rho^2(N_\rho+1)(\Omega_\rho-N_\rho)\,,\quad \rho=\pi,\nu\,. \quad (2.35)$$

## 2. Chain II: The SU(3) limit

The representation labels of the chain II (Arima and Iachello, 1978a) decomposition are

$$\begin{array}{ccccc} U(6) & \supset & SU(3) & \supset & O(3)\,. \\ [N] & & (\lambda,\mu) & K' & L \end{array} \quad (2.36)$$

The Hamiltonian is just a linear combination of the Casimir operators of SU(3) and O(3) and can be written

$$H_{II}=a_1\hat{L}^2+a_2Q^2\,. \quad (2.37)$$

Comparison with Eq. (2.24) shows that this form is equivalent to

$$H_{II}=\tfrac{3}{4}a_2C_{2SU3}+\left[\frac{a_1}{2}-\frac{3}{16}a_2\right]C_{2O3}\,.$$

The eigenvalue of the SU(3) Casimir operator as defined in Eq. (2.24) is given by

$$E_{C_{2SU3}}(\lambda,\mu)=\tfrac{2}{3}(\lambda^2+\mu^2+\lambda\mu+3\lambda+3\mu)\,, \quad (2.38)$$

and thus the resulting eigenvalue expression is

$$E=\frac{a_2}{2}(\lambda^2+\mu^2+\lambda\mu+3\lambda+3\mu)+(a_1-3a_2/8)L(L+1)\,. \quad (2.39)$$

Note that $Q$ in Eq. (2.37) takes the specific form of Eq. (2.5).

The step SU(3)⊃O(3) in Eq. (2.36) requires an extra quantum number and some explanation. Traditionally, this label is chosen to be $K'$ corresponding to the Vergados basis (Vergados, 1968). It is important to note that $K'$ is not exactly identical to the familiar projection quantum number $K$ of Elliott (1958a, 1958b; Elliott and Harvey, 1963). More specifically, the basis states of the Vergados basis of Eq. (2.36), here labeled by $K'$, are, in general, linear combinations of more than one Elliott (geometric) $K$ value, although for most $N$ and $L$ values the amplitudes with $K_{\text{Elliott}}\neq K_{\text{Vergados}}$ are very small (Casten and Warner, 1983). Nevertheless, effects of their presence show up in some characteristic predictions and are evident empirically as well (see below). Unless the distinction is important, however, we shall henceforth generally use the symbol $K$ for the SU(3) representation label.

A full discussion of the group-theoretical details of this symmetry, and of the ranges that the various quantum numbers can take, is best found in the more expert articles on the subject by Elliott (1958a, 1958b) and Vergados (1968) and, in the IBA context, by Arima and Iachello (1978a) and Lipas (1984). Here, it will be sufficient to outline a few of the rules for determining the labels and content of the lower SU(3) representations.

The quantum numbers $(\lambda,\mu)$ are best described and derived using the method of Young tableaux, which is illustrated in Fig. 4. The boson system is represented by a total of $2N$ boxes, arranged among three rows, and the SU(3) quantum numbers $\lambda$ and $\mu$ describe that arrangement in the manner shown in the figure. Physically, the rows can be thought of as representing the $z$, $x$, and $y$ directions for the oscillator quanta available to the system, so that $\lambda$ is equivalent to $n_z-n_x$, and $\mu$ to $n_x-n_y$. The ground-state representation of a (prolate) nucleus is then denoted by a single row of $2N$ boxes (all quanta in the $z$ direction) and hence has $(\lambda,\mu)=(2N,0)$. Since boson degrees of freedom are being considered, the next representation is formed by moving two boxes into the second row, giving $(\lambda',\mu')=(2N-4,2)$. The next two boxes can be placed in either the second or the third row, yielding $(2N-8,4)$ and $(2N-6,0)$, respectively, and so on. The $K$ values within each representation are given by

$$K=\min\{\lambda',\mu'\},\min\{\lambda',\mu'\}-2,\ldots,0\,, \quad (2.40)$$

which, for the lowest-lying representations (and large $N$), yields

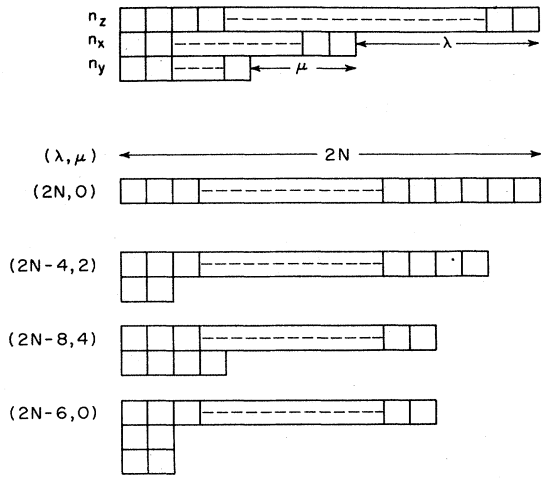


FIG. 4. Examples of the determination of the $(\lambda,\mu)$ values of the lowest SU(3) representations using the method of Young tableaux.

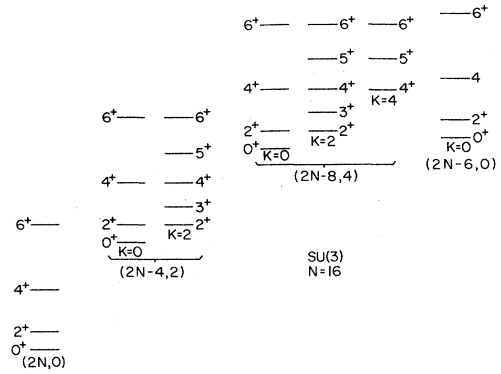


FIG. 5. Low-lying levels of the SU(3) symmetry of the IBA. The intrinsic representations are labeled by the quantum numbers $(\lambda,\mu)$, while individual rotational bands are labeled by their dominant $K$ quantum number.

$$K=0 \text{ for } \mu'=0\ ,$$
$$K=0,2 \text{ for } \mu'=2\ , \tag{2.41}$$
$$K=0,2,4 \text{ for } \mu'=4\ .$$

In general, $K=0,2\ldots,\mu'$. The rule for assigning $L$ values to a given $K$ is familiar from the Bohr-Mottelson treatment of the analogous quantity.

The predicted energy spectrum is shown in Fig. 5 and, not surprisingly, is analogous to that expected from an axially deformed symmetric rotor. Above the ground-state band, the next representation contains two bands that recall the $\beta(K=0)$ and $\gamma(K=2)$ excitations of the rotor. Note, however, that SU(3) is a very specific kind of deformed rotor in which these two bands are degenerate. Other differences from the geometrical model, such as those associated with the adoption of the Vergados scheme, arise because of the finite boson number implicit in the IBA scheme and disappear as $N\rightarrow\infty$. Several of their manifestations remain important for boson numbers typical of deformed nuclei and will be discussed presently.

Since the SU(3) wave functions are complicated linear combinations of U(5) basis states with many $n_d$ values, it is not surprising, first, that $\langle n_d\rangle_{\text{g.s.}}$ is larger than in either U(5) or O(6), or second that it changes little from state to state. Figure 6 illustrates this by showing the values of $\langle n_d\rangle$ for the yrast band calculated for all three limits by diagonalizing the appropriate Hamiltonian. In U(5), changes in the (single) $n_d$ value characterizing each state are reflected directly in the state-dependent behavior of various observables. In contrast, in SU(3), the value of any matrix element normally results from subtle coherent effects, as befits a collective deformed intrinsic state.

Despite this complexity in the structure of SU(3) states, their physical character is clear when discussed in the context of geometrical models. The two bands of the $(\lambda-4,2)$ representation have dominant $K$ values of 0 and 2 and, as noted above, are clearly analogous to the familiar $\beta$ and $\gamma$ bands. The next representation $(\lambda-8,4)$ has three bands, with dominant $K$ components $K=0,2,4$. The $K=4$ excitation is easily interpreted as a double-$\gamma$ vibration, and $K=2$ can only be formed at low energy as a double vibration of $\beta\gamma$ nature. The $K=0$ state is ambiguous, however, since it can be either $\beta\beta$ or $\gamma\gamma$: both are expected at about the same energy. Since the next representation, $(\lambda-6,0)$, also contains a $K=0$ excitation and occurs only slightly higher, the two required $K=0$ modes are indeed both present. It has been shown (Warner and Casten, 1982b), by inspecting the $E2$ matrix

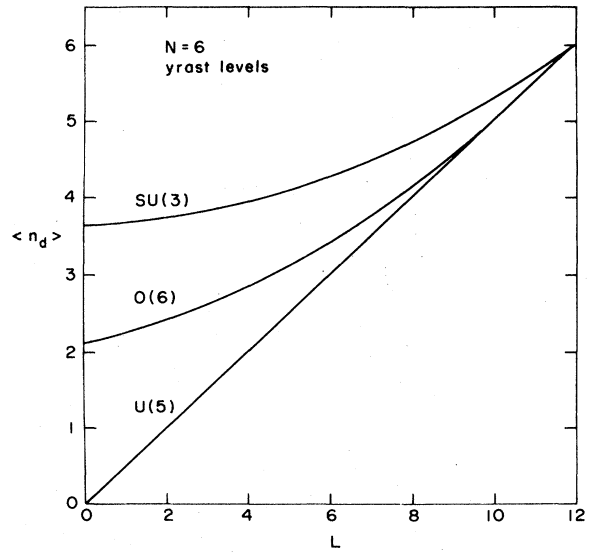


FIG. 6. Expectation values of $\hat{n}_d$ in the yrast states for the three symmetries of the IBA. $N=6$.

elements in the presence of small symmetry breaking, that the $(\lambda-8,4)$ $K=0$ band is $\approx\frac{2}{3}\gamma\gamma$ and $\frac{1}{3}\beta\beta$, while the $(\lambda-6,0)$ $K=0$ band is the orthogonal combination.

The relative energies of different representations are also interesting to consider. The excitation energy of a representation is proportional to the differences in the eigenvalues of $C(\lambda',\mu')$ between it and the ground state. For example (neglecting the $\hat{L}^2$ contribution or, equivalently, considering $0^+$ states or states of the same spin), the energy of the $\beta$ and $\gamma$ bands is proportional to

$$|C(\lambda-4,2)-C(\lambda,0)| = \tfrac{2}{3}6(\lambda-1)=\tfrac{2}{3}6(2N-1)\ . \quad (2.42)$$

From Eq. (2.39), the value of $a_2$ needed to fit a typical SU(3)-like nucleus is

$$a_2=-\frac{E_{2_2^+}-E_{2_1^+}}{3(2N-1)}\ . \quad (2.43)$$

Similarly, $a_1$ is given by $a_1=E_{2_1^+}/6+3a_2/8$.

Note that, in expressions for the differences of the eigenvalues of two $C(\lambda,\mu)$ operators, the $\lambda^2$ terms always cancel, and thus, for *any* representation, the energy is of the form $a_2(AN+B)$. Thus the ratio of the energies of two excited representations is parameter free and of the form

$$\frac{E(\lambda'',\mu'')}{E(\lambda',\mu')}=\frac{AN+B}{CN+D}\underset{N\to\infty}{\to}\frac{A}{C}\ . \quad (2.44)$$

For example,

$$\frac{E(\lambda-8,4)}{E(\lambda-4,2)}\equiv\frac{E(K=0(\gamma\gamma),K=2(\beta\gamma),K=4(\gamma\gamma))}{E(K=0(\beta),K=2(\gamma))}$$
$$=\frac{4N-6}{2N-1}\underset{N\to\infty}{\to}2 \quad (2.45)$$

and

$$\frac{E(\lambda-6,0)}{E(\lambda-4,2)}\equiv\frac{E(K=0(\beta\beta))}{E(K=0(\beta),K=2(\gamma))}$$
$$=\frac{4N-3}{2N-1}\underset{N\to\infty}{\to}2\ , \quad (2.46)$$

where the familiar geometric labels have been given as well. The limiting results are reasonable, since the higher representations are of two-phonon ($\beta\beta$, $\gamma\gamma$, and $\beta\gamma$) character. Finally, note that the first terms in both numerators and denominators rapidly dominate as $N$ increases, so that the asymptotic values are already approximately attained for $N$ values typical of deformed nuclei ($N\approx12-18$). The behavior of the above ratios against $N$ is shown in Fig. 7.

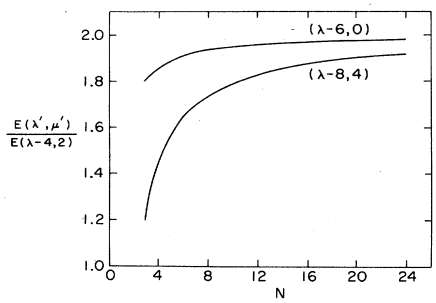


FIG. 7. Ratios of the energies of two higher-lying representations to the $(\lambda-4,2)$ representation containing the $\beta$ and $\gamma$ bands in the SU(3) limit of the IBA as a function of boson number $N$.

### a. E0 transitions

The $E0$ operator is not a generator of SU(3) and hence can connect different representations. In particular, it yields significant matrix elements between the ground band and the $K=0$ band ($\beta$ band) of the $(2N-4,2)$ representation which, for the $0^+$ states, take the values

$$\langle(2N,0),K=0,L=0\,|\,T(E0)\,|\,(2N-4,2)K=0,L=0\rangle$$
$$=e_0\left[\frac{8(N-1)^2(2N+1)N}{9(2N-3)(2N-1)^2}\right]^{1/2}\ , \quad (2.47)$$

where $e_0=\beta/\sqrt{5}$ in the notation of Eq. (2.9). More generally, the operator transforms as $(\lambda,\mu)=(2,0)$ under SU(3) and hence can also connect the $(2N-4,2)$ states with those in the $(2N-6,4)$ and $(2N-8,0)$ representations. (This approach to deducing selection rules will be discussed further in the paragraphs on transfer reactions.) In addition, there is also an effective $K$ selection rule which, while not exact, limits the transitions of significant strength to those with $\Delta K=0$.

### b. E2 transitions

If the specific form of the quadrupole operator

$$Q=(s^\dagger\tilde{d}+d^\dagger s)-\sqrt{7/2}(d^\dagger\tilde{d})^{(2)}$$

is used, then $T(E2)=\alpha Q$ is a generator of SU(3) and hence cannot connect different representations. Thus the selection rule is $\Delta(\lambda,\mu)=(0,0)$, and only *intraband* representation transitions are allowed. Thus $\gamma\to g$ or $\beta\to g$ band transitions are forbidden, in distinct contrast to the harmonic geometrical model. Moreover, the same selection rule permits not only intraband transitions but also transitions between different bands in the *same* representation. For the important $(2N-4,2)$ representation, this leads to collective transitions between the $\beta$ and $\gamma$ bands. This also represents a fundamental and striking difference between the starting points of the IBA and geometrical descriptions of well-deformed nuclei. Interestingly, these $\beta\to\gamma$ collective transitions have now been observed (Greenwood *et al.*, 1978; Davidson *et al.*, 1981a, 1981b; McGowan, 1981; Gelletly *et al.*, 1985; Haque *et al.*, 1986) in a number of nuclei, and their observation constitutes an important confirmation of the IBA description.

Finite boson number effects introduce other

modifications of the $B(E2)$ values, for example, an attenuation of strength as the spins involved approach the cutoff value of $L=2N$, and deviations of interband branching ratios from the Alaga rules, for example, for transitions between $\beta$ and $\gamma$ bands. Since the branching ratios most frequently observed are of $\gamma \rightarrow g$ character, and since these transitions are forbidden in SU(3), it is best to postpone a discussion of this feature until a later section. For the yrast transitions, the $B(E2)$ values are given by

$$B(E2{:}(2N,0);L+2\rightarrow L)=e_B^2\frac{3}{4}\left[\frac{(L+2)(L+1)}{(2L+3)(2L+5)}\right]\times(2N-L)(2N+L+3)\ . \tag{2.48}$$

This gives, for the first $2^+$ state,

$$B(E2{:}2_1^+\rightarrow 0_1^+)=e_B^2\frac{N(2N+3)}{5}\ . \tag{2.49}$$

Note that Eq. (2.48) clearly tends to zero as $L\rightarrow 2N$ and already shows an appreciable falloff at $L\approx\frac{1}{2}L_{\max}$. The predicted falloff is a direct result of finite $N$ and is not very dependent on deviations from SU(3). In most deformed nuclei these falloffs seem *not* to be observed (see, for example, Grosse *et al.*, 1981, and Emling, 1984). Empirical falloffs in $B(E2)$ values have been observed in the Ba and Kr regions (Kaup and Gelberg, 1979; Hanewinkel *et al.*, 1983), but whether or not they can be attributed to boson number effects remains an open question.

Two other interesting results are evident from Eq. (2.48), in the limit $N\gg 1$. First, the spin dependence is given by the factor in large parentheses, which just gives the Alaga rules. For example, in the large-$N$ limit, Eq. (2.48) gives

$$\frac{B(E2{:}4\rightarrow 2)}{B(E2{:}2\rightarrow 0)}=\frac{10}{7}\ . \tag{2.50}$$

However, Eq. (2.48) also shows that deviations from the Alaga rules appear even in the strict SU(3) limit and are a direct reflection of finite-$N$ effects. The second feature of Eq. (2.48) in the large-$N$ limit is a proportionality to $N^2$. It is in fact easy to understand why this arises. In U(5) it can be seen from Eq. (2.29) that $B(E2)$ values (for $N\gg L$, that is, $N\gg n_d$) scale as $N$. This is a direct result of the presence of $n_s\approx N$ $s$ bosons and of the fact that a given state (e.g., $2_1^+$) always contains the same number of $d$ bosons [e.g., $n_d(2_1^+)=1$] independent of $N$. Here, in SU(3) [and, indeed, in O(6); see below], $n_d$ and $n_s$ are both approximately proportional to $N$ (for example, for large $N$, $\langle n_d\rangle_{\text{g.s.}}=\frac{2}{3}N$) and thus, in the derivation of the SU(3) analog of Eq. (2.29), both the $s^\dagger$ and $d$ (or $d^\dagger$ and $s$) operators contribute a factor proportional to $N$, whereas in U(5) only $s^\dagger$ led to such a factor.

*c. Two-nucleon transfer*

The selection rules for the operators $s$ and $s^\dagger$ in the SU(3) limit can be understood by assigning them the SU(3) quantum numbers (2,0) and considering the Young tableaux appropriate to the lowest two SU(3) representations in adjacent nuclei. The existence of a nonzero matrix element is then determined by the ability to connect two representations by the addition or removal of two boxes. The resulting selection rules are shown in Fig. 8 for the situation in which the nuclei involved are below midshell. Above midshell the roles of $(p,t)$ and $(t,p)$ are reversed, since then $(t,p)$ would decrease $N$ and $N_\nu$ by one. In either case, the two-nucleon transfer strengths between ground states are given by

$$S_g(N_\rho\rightarrow N_\rho+1)=\alpha_\rho^2(N_\rho+1)\frac{2N+3}{3(2N+1)}\times\left[\Omega_\rho-N_\rho-\frac{4}{3}\frac{N-1}{2N-1}N_\rho\right],\quad \rho=\pi,\nu\ . \tag{2.51}$$

This expression yields much weaker cross sections than in U(5) and, in particular, predicts a sudden drop in $(t,p)$ cross sections in a U(5)$\rightarrow$SU(3) phase transition (see Sec. III.B.2).

3. Chain III: The O(6) limit

The representation labels appropriate to the O(6) dynamical symmetry (Arima and Iachello, 1978b, 1979) are

$$\begin{array}{ccccccc}\mathrm{U}(6) & \supset & \mathrm{O}(6) & \supset & \mathrm{O}(5) & \supset & \mathrm{O}(3)\ .\\ [N] & & \sigma & & \tau & \nu_\Delta & L\end{array} \tag{2.52}$$

Note that the only difference from chain I is the substitution of the group O(6) for U(5). The corresponding quantum number $\sigma$ takes the values

$$\sigma=N,N-2,\ldots,0 \text{ or } 1\ , \tag{2.53}$$

while the reduction to O(5) gives

$$\tau=\sigma,\sigma-1,\ldots,0 \tag{2.54}$$

for each $\sigma$ representation. For historical reasons, the la-

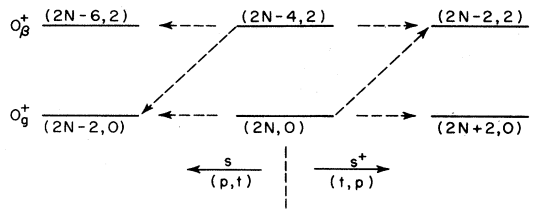


FIG. 8. SU(3) selection rules for two-nucleon transfer for nuclei *below* midshell. The dashed arrows represent allowed matrix elements.

bels $\tau, \nu_\Delta$ have been used for the O(6) scheme, but they are identical to the $v, n_\Delta$ of the U(5) chain. The Hamiltonian $H_{\rm III}$ is obtained by replacing $\alpha C_{1U5}+\beta C_{2U5}$ by $\alpha C_{2O6}$ [Eq. (2.26)], and the eigenvalue expression then becomes

$$E=2\alpha\sigma(\sigma+4)+2\gamma\tau(\tau+3)+2\delta L(L+1)\ . \quad (2.55)$$

Again, the various terms in the Casimir operators can be combined to write $H_{\rm III}$ in the convenient format of the multipole expansion:

$$H_{\rm III}=a_0P^\dagger P+a_1\hat{L}^2+a_3T_3^2\ . \quad (2.56)$$

Here the $P^\dagger P$ term stems from the $C_{2O6}$ Casimir, that is, from the presence of the subgroup O(6). Due to the common use of the multipole Hamiltonian, the form of the (equivalent) eigenvalue expression that has most frequently appeared in the literature is

$$E=A(N-\sigma)(N+\sigma+4)+B\tau(\tau+3)+CL(L+1)\ , \quad (2.57)$$

where $A=a_0/4$, $B=a_3/2$, and $C=a_1-a_3/10$. (Expressions with coefficients $A/4$ and $B/6$ are sometimes also encountered.)

A typical energy spectrum is shown in Fig. 9. In this case the geometrical equivalent, though less familiar, is that of the $\gamma$-unstable rotor of Wilets and Jean (1956). The states are grouped into large families, each characterized by a given value of $\sigma$ and comprising a representation of O(6). Within each family, the states are clustered into $\tau$ multiplets, whose relative energies scale as $\tau(\tau+3)$ and whose degeneracy is split by the $L(L+1)$ term. Note that this term implies that the energies within a $\tau$ multiplet will vary monotonically with spin. Usually $C>0$, so that, for example, as in Fig. 9, $E_{0_2^+}<E_{3_1^+}$. Neglecting the last $L(L+1)$ term, we see that the yrast energies increase more slowly than in a rotational nucleus and more rapidly than in a harmonic vibrator. Thus, for example, to compare the three limits,

$$E_2{:}E_4{:}E_6{:}E_8=\begin{cases}E_{n_d=1}{:}E_{n_d=2}{:}E_{n_d=3}{:}E_{n_d=4}=1{:}2{:}3{:}4, & \text{U(5)}\\ E_{\tau=1}{:}E_{\tau=2}{:}E_{\tau=3}{:}E_{\tau=4}=1{:}2.5{:}4.5{:}7, & \text{O(6)}\\ E_{L=2}{:}E_{L=4}{:}E_{L=6}{:}E_{L=8}=1{:}3.33{:}7{:}12, & \text{SU(3)}\ .\end{cases}$$

In the higher-lying, lower $\sigma$ representations, the sequences of levels are completely identical, except for lower cutoffs, since $\tau_{\max}=\sigma$ in each case.

The structure of the wave functions in the O(6) limit is determined by the $P^\dagger P$ term in Eq. (2.56), which is the only nondiagonal one in a U(5) basis. As pointed out earlier, this operator has $\Delta n_d=0$ and $\pm2$ contributions, and hence can connect states differing by zero-coupled pairs of $d$ bosons. This results in a very distinctive structure for the O(6) wave functions, some examples of which are given in Table II. It can be seen that, for each state, the contributing basis states are determined by a sequential operation of the form $\Delta n_d=2$, $\Delta n_\beta=1$ on the first basis state. Moreover, the specific basis states that contribute are determined by the $\tau$ value: wave functions for states of the same $\tau$ but different $\sigma$ have a different distribution of amplitudes for the same basis states. With this picture in mind, the selection rules again become obvious.

### a. E0 transitions

Since $T(E0)$ is diagonal in the U(5) basis states, it must require $\Delta\tau=0$. Using Eq. (2.9), it is trivial to see that, in addition, $\Delta\sigma=\pm2$ is necessary to avoid a cancellation in the contributing components. Thus the only predicted $E0$ strength to the ground state is from the $\sigma=N-2$, $\tau=0$ state, where the matrix elements take the form

$$\langle\sigma=N,\tau=0,L=0\,|\,T(E0)\,|\,\sigma=N-2,\tau=0,L=0\rangle = e_0\left[\frac{(N-1)(N+3)(2N+4)}{8(N+1)^2}\right]^{1/2}\ . \quad (2.58)$$

### b. E2 transitions

The quadrupole operator that is a generator of the O(6) group consists of only the first part of the most general form, namely,

$$Q=e_B(s^\dagger\tilde{d}+d^\dagger s)\ .$$

By definition, of course, this operator leads to the selection rule $\Delta\sigma=0$. However, inspection of Table II also indicates the existence of a second condition. Since the form of $Q$ given above has the property $\Delta n_d=\pm1$, it is clear that it cannot connect states with the same $\tau$ value, since all the component basis states differ by $\Delta n_d=2$. Moreover, $Q$ does not connect basis states with different values of $n_\beta$ or $n_\Delta$, since it does not contain a term that allows recoupling of the $d$-boson wave functions. Thus the additional selection rule is seen to be $\Delta\tau=\pm1$. This rule, as well as the particular $\tau$ values labeling various states, leads to a characteristic O(6) signature, namely sequences of $0^+$-$2^+$-$2^+$ levels with allowed cascading $E2$ transitions connecting them. Five examples (one truncated to $0^+$-$2^+$) are evident in Fig. 9, namely, those based on the $\tau=0$ and 3, $\sigma=6$ and 4 states, and on the $\tau=0$, $\sigma=2$

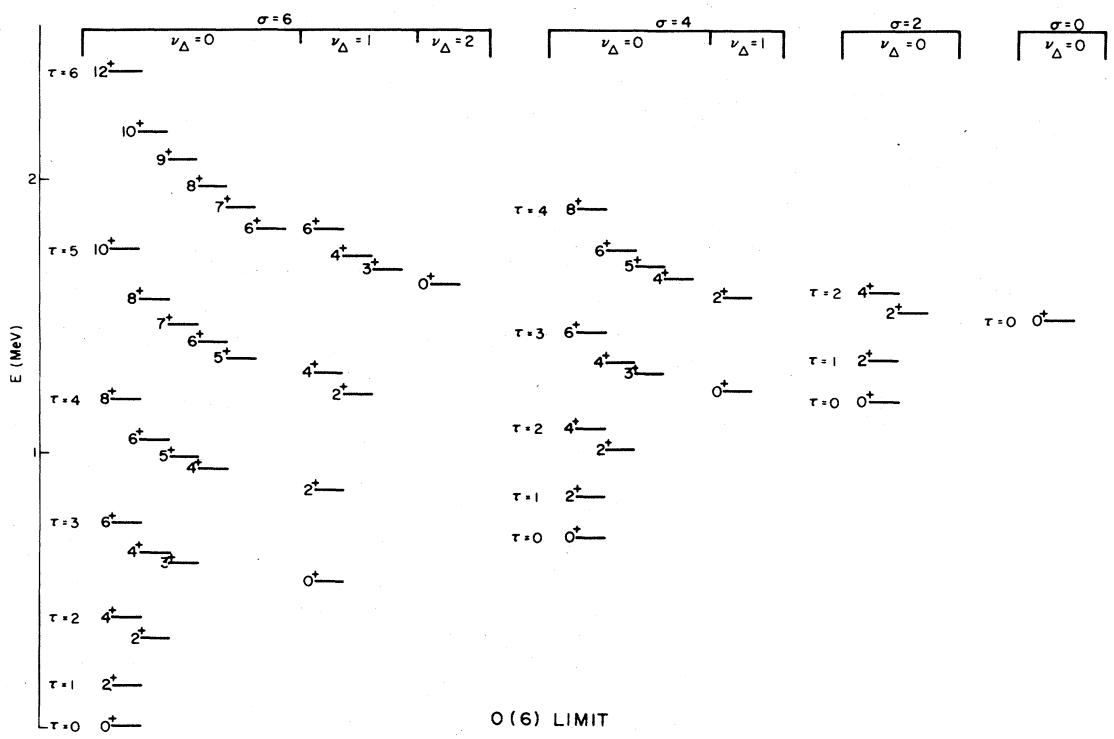


FIG. 9. Low-lying levels of the O(6) limit, for $N=6$.

levels. More such triplets appear for larger $N$ values.

The $\sigma$ selection rule can also be deduced from the form of the wave functions, since for states from different $\sigma$ groups, but with $\tau$ values differing by $\pm 1$, the individual contributions to the $E2$ matrix element exactly cancel. The $E2$ selection rules also imply that the O(6) limit has vanishing quadrupole moments. This has been found to be in disagreement with the data and remains an interesting question, which will be discussed further later.

Since their origins are different, the expected strengths of the $\sigma$ and $\tau$ selection rules differ. If the O(6) symmetry is slightly perturbed by a term of the form $\varepsilon n_d$, the cancellation embodied in the $\sigma$ rule is no longer exact. Thus states with $\sigma < \sigma_{\max}$ will decay, with weak $E2$ matrix elements, to $\sigma=\sigma_{\max}$ levels, while preserving the $\Delta\tau=\pm 1$ selection rule. In particular, the $0^+$ "bandheads" of the $\sigma < \sigma_{\max}$ representations are expected to decay to the $2_1^+$ level rather than to the $2_2^+$ state.

Finally, the expression for the $B(E2)$ values connecting the $\sigma=\sigma_{\max}$, $L=2\tau$ (i.e., yrast) states is given by

$$B(E2{:}\tau+1\rightarrow\tau)=e_B^2(N-\tau)(N+\tau+4)\frac{(\tau+1)}{2\tau+5} . \quad (2.59)$$

Note that, as in SU(3), and for the same reasons, these $B(E2)$ values scale approximately as $N^2$ for large $N$. For the particular case of the $2_1^+\rightarrow 0_1^+$ transition, Eq. (2.59) gives

$$B(E2{:}2_1^+\rightarrow 0_1^+)=e_B^2\frac{N(N+4)}{5} . \quad (2.60)$$

### c. Two-nucleon transfer

The creation or destruction of an $s$ boson obviously requires that the $d$-boson structure of the initial and final wave functions be identical. The $\tau$ selection rule for two-particle transfer is thus $\Delta\tau=0$, while the $\sigma$ rule is $\Delta\sigma=\pm 1$, since the addition or subtraction of an $s$ boson changes $N$ by 1. The result is that population of neighboring ground states of O(6) nuclei is allowed. In addition, for $(t,p)$ [or the analogous ($^3$He,$n$) reaction] below midshell, the $\sigma=\sigma_{\max}-2$, $\tau=0$ excited $0^+$ state has $\sigma=N_t-1$, where $N_t$ is the boson number of the target nucleus, and is an allowed transition, as is the $(p,t)$ transition to the $\sigma<\sigma_{\max}-2$ state above midshell. Once again, because of the different $n_d$ structure of U(5) and O(6), the two-neutron transfer cross sections vary less rapidly with $N$ in O(6) and can serve to identify such regions. The ground-state transfer strengths are given by

$$S_g(N_\rho\rightarrow N_\rho+1)=\alpha_\rho^2(N_\rho+1)\frac{N+4}{2(N+2)}\times\left[\Omega_\rho-N_\rho-\frac{N-1}{2(N+1)}N_\rho\right], \quad \rho=\pi,\nu . \quad (2.61)$$

### d. Differences between U(5) and O(6)

At first sight these two limits appear quite different. One yields a phononlike structure with simple selection

rules, while the other is a $\gamma$-soft deformed rotor with quasi-band-structure and more complex selection rules. Yet both group chains contain the O(5) and O(3) subgroups. As a result, many properties are in fact identical. This point, which is extremely important, has recently been emphasized by Leviatan, Novoselsky, and Talmi (1986).

The most obvious apparent difference between U(5) and O(6) concerns the second group of excited states and in fact is not, rigorously speaking, a difference at all. Reference to Figs. 3 and 9 shows a two-phonon-like triplet, $0^+,2^+,4^+$, in U(5), but only the pair $2^+,4^+$ in O(6). By the $E2$ selection rules ($\Delta n_d=1$ and $\Delta\tau=1$), the first excited $0^+$ state (denoted $0_2^+$ since the ground state is $0_1^+$) decays to the $2_1^+$ level in U(5), but in O(6) the $0_2^+$ state has either $\tau=3$, or $\tau=0$ and $\sigma=\sigma_{\max}-2$, depending on the energy of the second O(6) representation, and thus, in either case, cannot decay to the $2_1^+$ level. However, this contrast implicitly assumes a near-harmonic U(5) spectrum. As noted earlier, the U(5) eigenvalue equation has great flexibility. Thus, for example, in Eq. (2.27), if the coefficients of the terms in $n_d$ are large and positive while that of the $v(\tau)$ term is large and negative, the three-phonon $(n_d,v)\equiv(n_d,\tau)=(3,3)$ $0^+$ state can be brought below the (2,0) $0^+$ level. Then the first excited $0^+$ state in U(5) will be a three-phonon state and will not have allowed transitions to the $2_1^+$ state but rather to the $2_2^+$ level. While this requires very large anharmonicities, and may seem unappealing, it is still within the rigorous philosophy of U(5). More generally, because of the appearance of the O(5) subgroup in both O(6) and U(5), properties having to do only with the $\tau$ structure of the wave functions are, in fact, identical. For example, branching ratios [within the $\sigma=\sigma_{\max}=N$ O(6) representation] such as $B(E2{:}3_1^+(\tau=3)\rightarrow 2_2(\tau=2))/B(E2{:}3_1^+(\tau=3)\rightarrow 4_1^+(\tau=2))$ are the same.

Thus, in principle, as Leviatan, Novoselsky, and Talmi (1986) emphasize, some of the data cited in support of O(6) are really only evidence for O(5) and could be consistent with a very highly anharmonic U(5). However, there do exist many quantities that *can* distinguish between the two. These arise because of the specific $d$-boson structure of the wave functions, which in turn is directly a product either of having the larger group U(5), stemming from $\varepsilon\hat{n}_d$ in the Hamiltonian, with the low-lying states spanning many representations of U(5), or of having O(6), stemming from $a_0P^\dagger P$ in the Hamiltonian, in which case the low-lying states belong to a single representation of O(6).

In going from state to state up the level scheme, for example, in the yrast band, $\langle n_d\rangle$ changes much more rapidly in the U(5) scheme than in O(6) (see Fig. 6). This directly affects absolute $B(E2)$ values, which increase more rapidly in U(5) than in O(6). This is illustrated for the yrast band in Fig. 10.

A particularly important distinguishing characteristic centers on the higher-lying levels: In U(5), these levels have high $n_d$ and are multiphonon states that have allowed $E2$ transitions to many $n_d-1$ levels. In O(6), the states of the $\sigma<\sigma_{\max}$ representations are restricted to decay within those representations by the $\Delta\sigma=0$ selection rule. The data will be inspected later. Suffice it to emphasize here that it is crucial, in potential O(6) regions, to measure absolute $B(E2)$ values and to identify, if possible, extended sequences of $\sigma<\sigma_{\max}$ levels in order fully to discriminate against a possible anharmonic U(5) character.

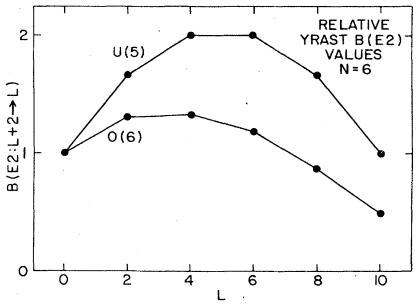


FIG. 10. Yrast $B(E2)$ values in U(5) and O(6) normalized so that $B(E2{:}2_g^+\rightarrow 0_g^+)=1$ in each case. Their differences reflect the different magnitudes of finite-boson-number effects in the two limits.

## 4. Summary

It is evident that each dynamical symmetry limit corresponds to a very specific choice of interactions in the general IBA-1 Hamiltonian. Indeed, each symmetry is characterized by one term in the Hamiltonian that is responsible, by virtue of its effect on the mixing of U(5) basis states, for the characteristic structure of that symmetry's wave functions:

| | Symmetry | Generating term | $\Delta n_d$ structure |
|---|---|---|---|
| I | U(5) | $\hat{n}_d$ | $\Delta n_d=0$ |
| II | SU(3) | $Q^2$ | $\Delta n_d=0,\pm1,\pm2$ |
| III | O(6) | $P^\dagger P$ | $\Delta n_d=0,\pm2$ |

The differences in the structure of the wave functions in each limit were illustrated in Table II. Moreover, it has already been demonstrated that an understanding of the specific structure of each limit allows the role of various operators to be easily deduced. An important point is that the wave functions in a particular symmetry limit are unique (for a given boson number $N$) and *independent* of the parameter values chosen in the symmetry Hamiltonian. This can be seen by the following arguments. For U(5), each multiplet corresponding to the $n$th phonon state always has only one component in the wave function, namely with $n_d=n$. For the other symmetries, the mixing of these basis states is produced by the particular $\Delta n_d$ properties of the single operator [e.g., $Q^2$ for

SU(3)] that produces the characteristic wave functions. Normally, the magnitude of such mixing would depend on the energy separation of the unperturbed basis states, since it is always a function only of the ratio of that separation to the mixing matrix element. However, one notes that the Hamiltonians for SU(3) and O(6) do not contain an $\varepsilon\hat{n}_d$ term. As a consequence, the U(5) basis states on which the nondiagonal operator acts are degenerate. Thus the mixing is already "fully effective" for any value of the coefficient of the characteristic operator, and the wave functions are independent of this strength factor. Clearly, for situations between symmetries, when two or more different nondiagonal operators "compete" in the Hamiltonian, each produces a characteristic mixing, and thus the resultant wave functions depend on their relative strengths (coefficients).

Finally, some comments should be made on the use of the term "symmetry" as applied to the group-theoretical treatment of the IBA, since this term can itself give rise to some confusion. As we have seen, while each group or subgroup in one of the three possible chain decompositions does indeed demand a symmetry in the underlying bosonic degrees of freedom, the entire chain in fact describes a sequential breaking of each symmetry by the next, or lower, subgroup in the chain. Thus, taking the O(6) limit, or chain III, as an example, the symmetry U(6) demands that states be differentiated only by virtue of their total boson number $N$, and hence all states in a specific nucleus are degenerate. The subgroup O(6) then lifts that degeneracy and splits the states into families of multiplets characterized by the quantum number $\sigma$, and so on. This situation is illustrated in Fig. 11. It is for this reason that the more correct definition of these structures is termed *dynamical* symmetry. The Hamiltonian in fact describes a sequence of symmetry structures, each contained within its predecessor, and each of which lifts the degeneracy implied by the earlier group, without mixing its representations. As illustrated above, the simplest example of this is, of course, the $O(3)\supset O(2)$ group. With no term from the O(2) group in the Hamiltonian, the $M$ substates for each state $J$ are degenerate. The addition of the second term proportional to $J_z$ in the Hamiltonian lifts that degeneracy, and this would correspond physically to the introduction of a magnetic field, which breaks the rotational symmetry.

### D. Realistic calculations and symmetry breaking

#### 1. The Hamiltonian

The distinctive structures of the three dynamical symmetries in the IBA provide three clear-cut limits of the general Hamiltonian. Although evidence exists which suggests that some of the features of the pure symmetries are observed empirically in selected nuclei, in general, a

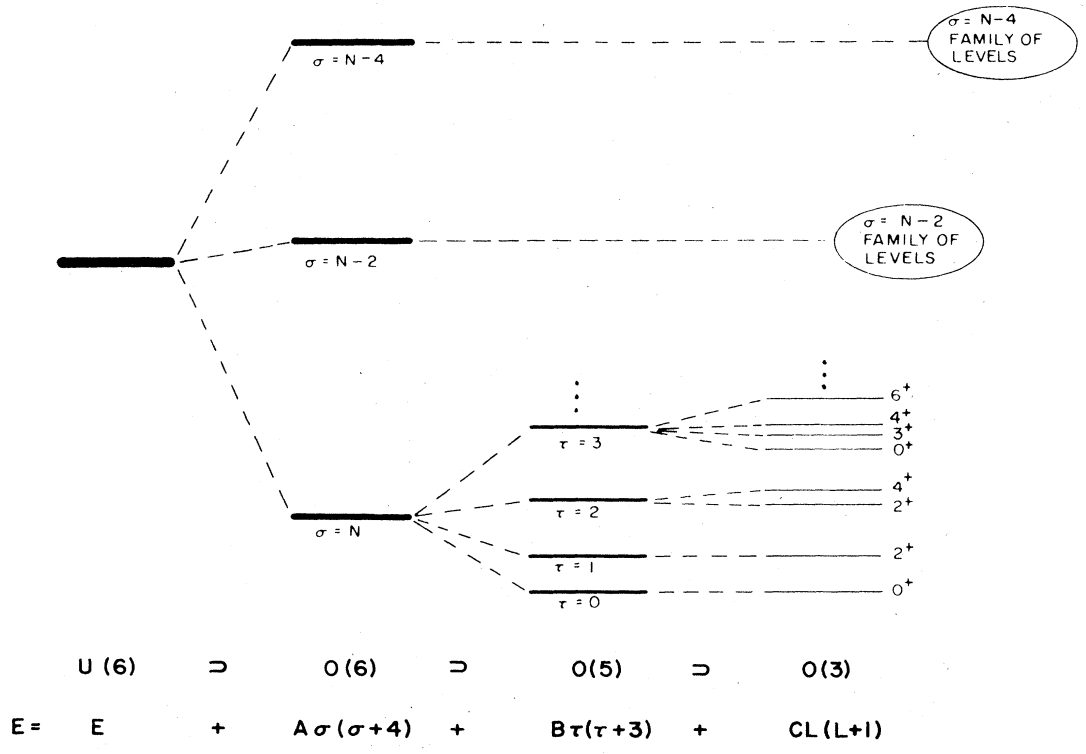


FIG. 11. Illustration of the concept of a dynamical symmetry. Each step in the group chain decomposition breaks a previous degeneracy, introducing new quantum numbers as well as a term in the eigenvalue expression. The example here is for the O(6) limit.

realistic calculation will require a departure from the strict limits or indeed a transition between them. In this context the analytic limits emerging from the group-theoretical treatment of the Hamiltonian can be viewed as "benchmarks" in constructing a more accurate description of the low-lying collective structure of a particular nucleus, or series of nuclei. This approach can be illustrated diagramatically in the form of the symmetry triangle of Fig. 12. The three apexes represent the limits of one of the exact symmetries, while the space enclosed by the three sides denotes the range of more general solutions that can be obtained numerically by diagonalizing the IBA-1 Hamiltonian of Eq. (2.5). A transition between two specific symmetries, without invoking any of the characteristics of the third, would correspond to a path along one of the three sides, but a more complex path between two limiting cases is clearly also possible. For a transition along the sides, the structure at any point will be determined by the ratio of the two parameters [see Eq. (2.5)] that characterize the symmetries in question, and these are also indicated in the figure.

From this discussion, it is clear that one of the most appealing aspects of the IBA-1, aside from the basic symmetries themselves, is the ease with which transition regions can be calculated as a function of a single, physically intuitive, parameter. When it is recalled that such phase-transitional regions have historically been considered the most challenging and complex testing grounds for nuclear models, because of the competition of rival degrees of freedom, it is clear that the group-theoretical structure of the IBA-1 truncation offers a significant simplification. Whether this simplification is physically realistic, of course, can be assessed only by recourse to the data and will be extensively discussed in later sections.

Referring to the multipole expansion of Eq. (2.5), the effect of the various terms and their links with the limiting symmetries have already been discussed, and the latter aspect is contained in the definitions of the various Casimir operators [Eq. (2.24)]. In the context of a general calculation, the first point to note is that the $\hat{L}^2$ term is always diagonal and simply gives a contribution

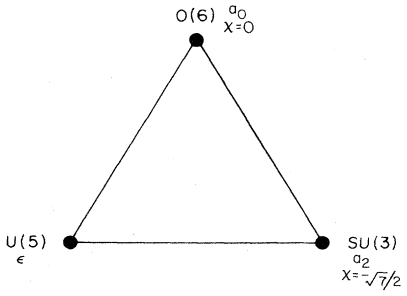


FIG. 12. Symmetry triangle of the IBA indicating the three limiting symmetries on each of the vertices and the transition legs between symmetries. The $\chi$ labels are discussed in Sec. II. D.3.

$L(L+1)$ to each level of spin $L$, for any Hamiltonian. Thus it has no effect on state wave functions, and also none on energy differences of states of the same spin. The term in $T_4^2$ has seldom been found necessary in actual applications. It will therefore be ignored in the discussion that follows. The terms in $\varepsilon\hat{n}_d$, $P^\dagger P$, and $Q^2$ produce the characteristics of the U(5), O(6), and SU(3) structures, respectively, while $T_3^2$ stems from the O(5) subgroup, which is common to both the U(5) and O(6) chains.

The first step in an IBA-1 calculation is thus to determine the approximate position of the nucleus under study with regard to the three limiting symmetries. This can be done phenomenologically by reference to some of the characteristic energy and $B(E2)$ ratios that distinguish the symmetries (discussed above) or by virtue of a theoretical understanding of the underlying microscopic shell-model basis of the IBA and the geometrical approach. Thus nuclei in which both neutrons and protons are near their respective closed shells can be expected to show U(5) or vibrational behavior, while $Z$ and $N$ values near midshell would suggest rotational structure and hence SU(3) as a starting point. The occurrence of axially asymmetric features can be expected in cases where the neutrons are particles and the protons holes, or vice versa, and suggests the use of the O(6) symmetry. Care must be taken in using these qualitative arguments, however, since the particles or holes character of the bosons can be influenced by significant subshell effects (see Sec. III.C). Moreover, since in practice the O(6) symmetry frequently occurs near the end of major shells, and since many of its predictions are very similar to those of U(5), it is sometimes difficult initially to distinguish between the two. It is therefore particularly important to consider both energies and $B(E2)$ values in this case.

### *a. O(6) and U(5) nuclei*

Traditionally, the most characteristic and easily recognizable signature of O(6) has been the appearance of nearly degenerate $2_2^+$ and $4_1^+$ states at an energy of roughly 2.5 times that of the $2_1^+$ level, with the $0_2^+$ state (assigned $\tau=3$) lying significantly higher and decaying to the $\tau=2$ second $2^+$ state rather than to the $2_1^+$ level. However, as noted earlier, these O(6) features actually arise from the O(5) structure, and hence are equally characteristic, in principle, of a U(5) symmetry. Since a near-harmonic U(5) spectrum has $E_{2_2^+} \approx E_{0_2^+} \approx E_{4_1^+} \approx 2.0 E_{2_1^+}$, it should be reemphasized here that to reproduce an O(6)-like spectrum with U(5) requires a highly anharmonic structure in which the three-phonon $0^+$ state lies below the two-phonon $0^+$ state. While this is, in principle, allowed, experience has shown (see Sec. III.A) that the empirical observation of the O(6) characteristics cited above usually coincides with additional, and unique, signatures of O(6). Therefore, pending the discovery of counterexamples, this traditional set of O(6) characteristics is best taken as at least an initial indica-

tion of likely O(6) character, to be tested by other empirical information. In addition, it is interesting to note that, working within a very different framework, Kumar (1970, 1972) and Cline (1971) pointed out many years ago that the descent of the $2^+$ quasi-$\gamma$ bandhead near or below the $4_1^+$ state is the signature of a $\gamma$-soft potential whose prolate and oblate minima are of roughly equal depth. Thus, at least as initial starting points, U(5)- and O(6)-like spectra are easily recognizable.

### b. Deformed nuclei

The first important feature of deformed nuclei to note in the context of the IBA is that, in general, they cannot be described by the SU(3) limit, which, as pointed out earlier, corresponds to a very specific type of deformed rotor with degenerate $\beta$ and $\gamma$ bands and vanishing $\gamma \rightarrow g$ and $\beta \rightarrow g$ $B(E2)$ values. Clearly, therefore, it is necessary to introduce considerable SU(3) symmetry breaking. In most deformed nuclei the $\beta$ band is above the $\gamma$ band. Comparison of Figs. 5 and 9 suggests that this can be produced by introducing a perturbation to SU(3) in the direction of O(6). An example of part of a practical calculation for the well deformed nucleus $^{168}$Er is shown in Fig. 13. The final calculated spectrum of the ground, $\beta$, and $\gamma$ bands is shown on the right, while on the left the SU(3) "starting point" is shown. In the SU(3) limit the parameters $a_1$ and $a_2$ of the $\hat{L}^2$ and $Q^2$ terms, respectively, have been determined according to the eigenvalue expression (2.39). Thus, as given earlier, this yields

$$a_2 = -\frac{E_{2_2^+} - E_{2_1^+}}{3(2N-1)} \tag{2.62}$$

and

$$a_1 = \frac{E_{2_1^+}}{6} + \frac{3}{8}a_2 \ . \tag{2.63}$$

The resulting SU(3) spectrum fits the $2_1^+$ and $2_2^+$ states by definition, has an exact $L(L+1)$ rotational band structure, and has degenerate $\beta$ and $\gamma$ bands. The next step is to break this latter degeneracy, without losing the rotational energy spacing. The terms in $\varepsilon \hat{n}_d$ or $T_3^2$ will tend to decrease the ratio $E_{4_2^+}/E_{2_1^+}$ and thus must be kept small for well deformed nuclei. As can be seen in Fig. 13, however, the $P^\dagger P$ term has very little effect on this feature, but does raise the $\beta$ band, since it represents a symmetry breaking in the direction of O(6), whose higher

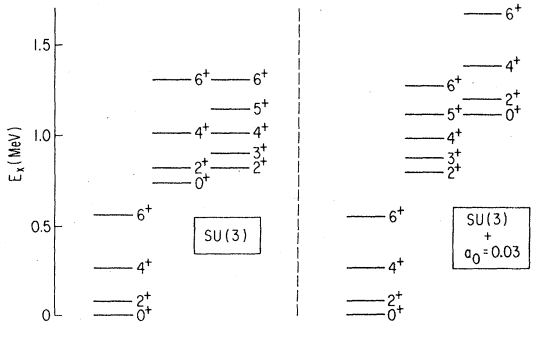


FIG. 13. Example of the effect of adding a term $a_0 P^\dagger P$ to an SU(3) Hamiltonian with $a_1 = 0.0105$ MeV, $a_2 = -0.008$ MeV, and $N = 16$. $a_0$ is in MeV.

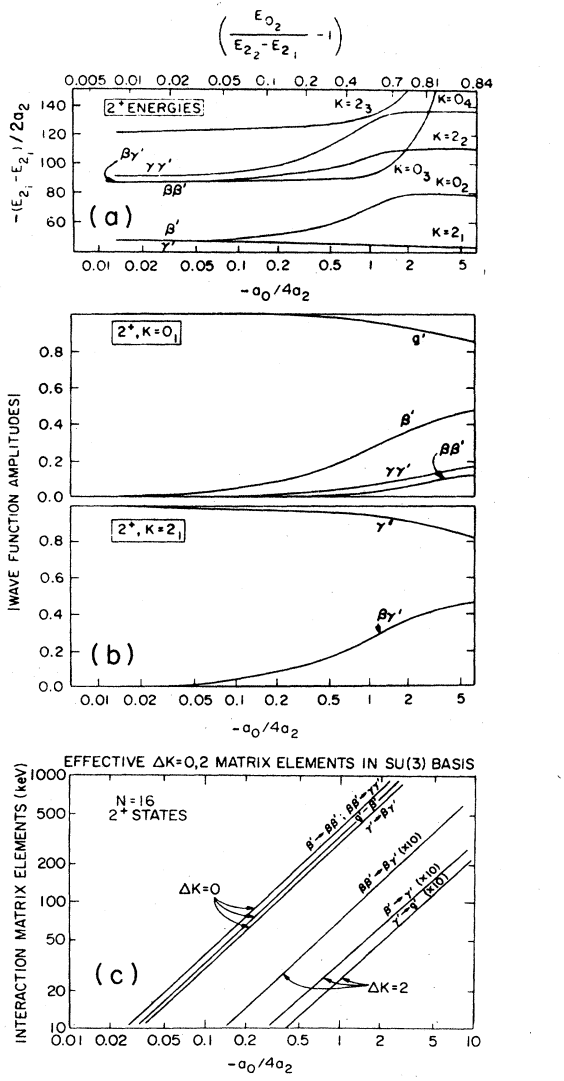


FIG. 14. The effects of SU(3) symmetry breaking in the IBA. The scale on the abscissa is such that 0 corresponds to SU(3), while the O(6) limit is approached when the abscissa tends toward large values. (a) $2^+$ energies of various rotational bands relative to $E_{2_1^+}$; (b) principal wave-function components expressed in an SU(3) basis; [the primed labels refer to the various SU(3) intrinsic excitations] (c) matrix elements that mix different SU(3) basis states. Note the sharp separation into $\Delta K = 0$ and 2 matrix elements.

representations each begin with a $0^+$ state. The effects of this term can be understood rather easily if the Hamiltonian is written as

$$H=a_2Q^2+a_0P^\dagger P+a_1\hat{L}^2\ , \tag{2.64}$$

with $Q$ and $P$ defined following Eq. (2.5). Then, as noted earlier, the $\hat{L}^2$ term is diagonal and can be dropped for our present considerations. Thus

$$H=a_2\left[Q^2+\frac{a_0}{a_2}P^\dagger P\right]\ , \tag{2.65}$$

from which it is clear that $a_2$ is now only a scale factor on the energies and that the structure is fully specified by the ratio $a_0/a_2$. The energies of the $\beta$ and $\gamma$, and the next $K=0$ and 2 bands, are shown in Fig. 14. Typically, one finds values of $a_0/4a_2\approx -1$ for most deformed nuclei. The behavior is easy to understand by considering the matrix elements that mix SU(3) representations in this Hamiltonian. The perturbation is proportional to $a_0/4a_2$ and therefore so must be the matrix elements that mix SU(3) representations. These matrix elements may be easily calculated by transforming the symmetry-breaking Hamiltonian to an SU(3) basis. Typical results (Casten and Warner, 1983) are shown for $N=16$ in Fig. 14. Clearly, they must lie on parallel straight lines in a log-log plot. The interesting point is the overwhelming dominance of $\Delta K=0$ over $\Delta K=2$ mixing. Moreover, these $\Delta K=0$ matrix elements easily attain several hundred keV. Given that typical separations of $\beta$ and $g$ bands are $\approx 1$ MeV, this is a substantial mixing, whose most obvious effect is a repulsion of the $g$ and $\beta$ bands. The $\beta\gamma$ and $\gamma$ bands, whose mixing matrix elements and unperturbed SU(3) separation [see Eq. (2.45)] are comparable to those for the SU(3) $\beta$ and $g$ bands, also repel. The net effect, as shown in Fig. 14, is a nearly unchanged $\gamma$-$g$ separation and a rising $\beta$ (and $\beta\gamma$) band energy. For values of $a_0/4a_2$ appropriate (Warner, Casten, and Davidson, 1981) to deformed rare-earth nuclei, the ground-band wave functions are thus a substantially mixed combination of $g$, $\beta$, $\gamma\gamma$, and $\beta\beta$ SU(3) excitations, while the $\gamma$ band is largely the SU(3) $\gamma$ and $\beta\gamma$ modes. The dependence (Casten and Warner, 1982, 1983) of the wave functions on the SU(3) symmetry-breaking parameter is also illustrated in Fig. 14. The important consequences of a large amplitude for the SU(3) $\beta$ mode in the calculated ground state will be discussed later. In any case, the key point for the moment is that the parameter $a_0$ can be varied to fit the $\beta$ bandhead, leaving the ground and $\gamma$ bands virtually unchanged.

### c. Transitional regions

As noted earlier, the three transitional regions O(6)→SU(3), U(5)→SU(3), and U(5)→O(6) are particularly easy to treat in the IBA, generally in terms of a single parameter reflecting the position along a leg of the symmetry triangle of Fig. 12. Nuclei in a transitional region between SU(3) and O(6) may be treated by breaking the SU(3) symmetry with the same terms just discussed [Eq. (2.64)] except with much larger magnitudes, so that, when the $a_0P^\dagger P$ term begins to dominate, an O(6) structure develops. Such SU(3)→O(6) transitional nuclei have been extensively studied (Casten and Cizewski, 1978) and will be further discussed in Sec. III.

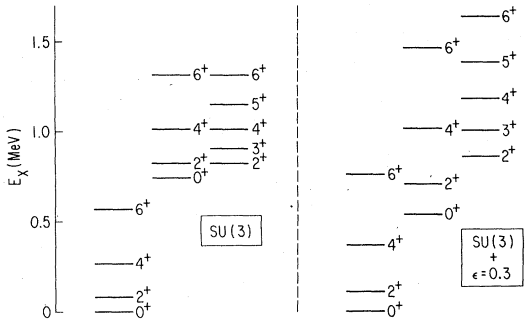


FIG. 15. Example of the effect of adding a term $\varepsilon\hat{n}_d$ to an SU(3) Hamiltonian with $a_1=0.0087$ MeV, $a_2=-0.013$ MeV, and $N=10$. $\varepsilon$ is in MeV.

An analogous example for the case of a nucleus that is transitional between U(5) and SU(3) is shown in Fig. 15. Again, the SU(3) limit has been used as the starting point, but, in this case, the boson number has been chosen as $N=10$, since this is more typical of this type of transitional region. The appropriate Hamiltonian is

$$H=\varepsilon\hat{n}_d+a_2Q^2+a_1\hat{L}^2\ . \tag{2.66}$$

There is a clear reduction in the ratio $E(4_1^+)/E(2_1^+)$, an increase in both $E(2_1^+)$ and $E(4_1^+)$ separately, and the excited $0^+$ band is now below the $\gamma$ band, in contrast to the situation for the $P^\dagger P$ symmetry breaking in Fig. 13. The introduction of a term in $\varepsilon\hat{n}_d$ to an SU(3) Hamiltonian must usually be accompanied by a concomitant adjustment of the $Q^2$ and $\hat{L}^2$ terms to maintain the required energies for the $2_1^+$ and $2_2^+$ states, since the presence of a nonzero $d$-boson energy will raise both. The relative magnitude required for the $\varepsilon\hat{n}_d$ and $Q^2$ terms will depend on the boson number, since the effects of the former scale roughly as $N$, while the latter is a function of $N^2$. Thus, near closed shells, the $\varepsilon\hat{n}_d$ term is relatively more important, while near midshell the calculations are largely insensitive even to rather large $\varepsilon$ values.

Nuclei in a U(5)→O(6) transitional region can be calculated with a Hamiltonian containing $\varepsilon\hat{n}_d$ and $a_0P^\dagger P$ terms. This type of transition region has been less studied than the other two and is dealt with below in the context of the alternative consistent-$Q$ formalism (CQF) and the extended CQF (ECQF).

## 2. Electromagnetic transitions

### a. E2 transitions

The most general form, Eq. (2.8), of the $E2$ operator is repeated here,

$$T(E2)=e_B[(s^\dagger\tilde{d}+d^\dagger s)+\chi(d^\dagger\tilde{d})^{(2)}] ,$$

where $e_B$ is the boson effective charge that determines the absolute $B(E2)$ scale. In fact, its value has been found to be remarkably constant in virtually all applications of the IBA-1, and in the range 0.12–0.16 eb. As pointed out earlier, the first term in $T(E2)$ is a generator of O(6), and the second is a generator of U(5). However, in practice, the first term is employed in both these symmetry limits to generate the characteristic selection rules. Thus, in a transitional region involving U(5) and O(6) terms in the Hamiltonian, the first choice for $T(E2)$ would be with $\chi=0$. However, for SU(3) symmetry, $\chi$ takes the value $-\sqrt{7}/2$, so that, in transitional Hamiltonians incorporating a $Q^2$ term, the corresponding $E2$ operators might be expected to involve $\chi$ values in the range 0 to $-\sqrt{7}/2$. Of course, it must be emphasized that the above arguments only serve to suggest an initial value for $\chi$ with which to compare experiment and theory. $\chi$ can simply be treated as a free parameter with no *a priori* restrictions.

The first extensive studies of the $E2$ operator in realistic calculations were performed for the well-deformed nuclei in the rare-earth region, and it is instructive to summarize some of the results of that work here, although the reader is referred to the original paper (Warner and Casten, 1982b) for details. The Hamiltonian employed was of the form discussed in the context of Fig. 13, namely,

$$H=a_1\hat{L}^2+a_2Q^2+a_0P^\dagger P ,$$

with $Q$ taking the SU(3) form of Eq. (2.8) with $\chi\equiv-\sqrt{7}/2$. Thus the perturbation to the pure SU(3) limit is supplied by the last term and can describe nuclei in which the $\beta$ band lies above the $\gamma$ band in energy, which in fact is the case for the majority of the well-deformed rare-earth nuclei.

The characteristic empirical feature, and indeed signature, of these nuclei is the remarkable stability of many of the $B(E2)$ systematics across the entire region, as illustrated in Fig. 16 for the ground and $\gamma$ bands. However, Fig. 16 also reveals the far greater fluctuations in the $\beta\rightarrow g$ $B(E2)$ strengths, as well as their significantly reduced magnitude, relative to $\gamma\rightarrow g$ strengths. The most obvious conclusion from these systematics, in the context of the IBA, is that the finite $\gamma\rightarrow g$ and $\beta\rightarrow g$ $B(E2)$ values both require departures from the strict SU(3) limit, as they involve transitions between representations that cannot occur as long as $a_0=0$ and $T(E2)$ utilizes a $Q$ operator with $\chi=-\sqrt{7}/2$. Nevertheless, decades of familiarity with the geometrical model render the weak $\beta\rightarrow g$, rather than the strong $\gamma\rightarrow g$, transition rates the more intriguing, since, given our well-established understanding of the intrinsic excitations in geometrical terms as involving simply a different orientation of the vibrational quanta with respect to the symmetry axis of the nucleus, the naive expectation would be that the $E2$ properties should be similar. It is, of course, true that

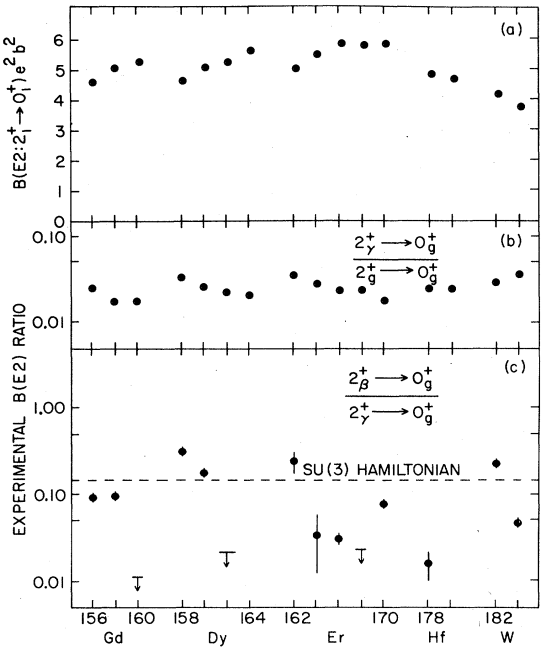


FIG. 16. Empirical values of some important $B(E2)$ values and $B(E2)$ ratios in deformed nuclei.

microscopic calculations (Bes, 1963), using, for example, the random-phase approximation in a deformed basis, reproduce the low $\beta\rightarrow g$ $B(E2)$ values, but it is not intuitively clear how the IBA-1 could incorporate such information.

The $B(E2)$ strengths that result from the SU(3) Hamiltonian and from a broken-symmetry calculation with a typical ratio $a_0/4a_2=-0.94$ are shown in Fig. 17 as a function of the parameter $\chi$ in $T(E2)$. The intrarepresentation transitions are very little affected by $\chi$, while the interrepresentation transitions, which must trend to zero in the SU(3) limit as $\chi\rightarrow-\sqrt{7}/2$, grow rapidly as $|\chi|$ decreases. For a given $\chi$, the dominant effect of the $a_0P^\dagger P$ symmetry-breaking term (for $\chi$ values to the left of the dashed line) is to decrease the magnitude of the $\beta\rightarrow g$ transitions, relative to other transition rates. These results can be easily seen in the ratios plotted in Fig. 18, which also shows an additional striking feature, namely, the rigorous constancy of the ratio $2_\beta\rightarrow 0_g/2_\gamma\rightarrow 0_g$ in SU(3).

The latter behavior can be understood simply in terms of the contributions from the two parts of the $E2$ operator. The vanishing of the interrepresentation transitions, for $\chi=-\sqrt{7}/2$, implies that, of necessity, the $\Delta n_d=0$ and $\Delta n_d=\pm1$ matrix elements interfere destructively and cancel exactly. Thus their magnitudes must be in the ratio $\sqrt{7}/2$ and their signs the same. This feature in turn implies the more general result that the ratio of *any* two interrepresentation transitions will be a constant, independent of $\chi$, for the SU(3) Hamiltonian. For the specific example of $\beta\rightarrow g/\gamma\rightarrow g$ cited in Fig. 18 this ratio

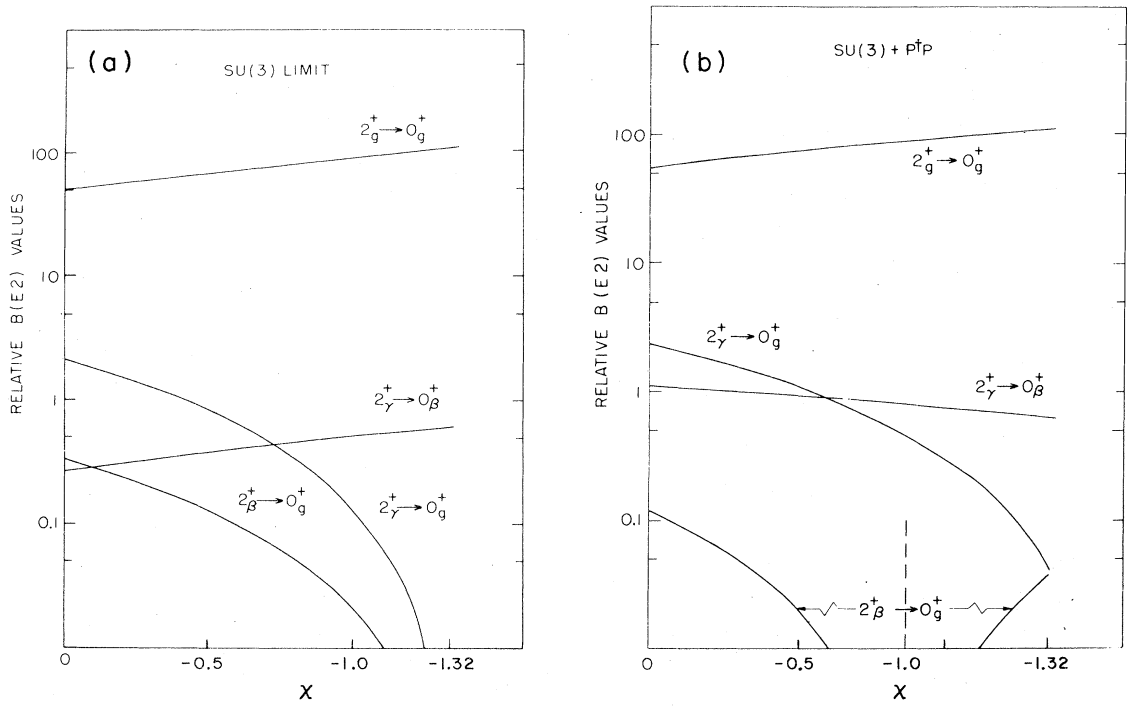


FIG. 17. Relative $B(E2)$ values involving the $\beta$, $\gamma$, and ground bands plotted as a function of the constant $\chi$. (a) For the SU(3) Hamiltonian with $N=16$; (b) similar except with a $P^\dagger P$ perturbation to SU(3). The broken SU(3) predictions depend only on the ratio $a_0/a_2$ and on $\chi$. Here, a typical value $a_0/a_2=-0.94$ is used. From Warner and Casten (1982b).

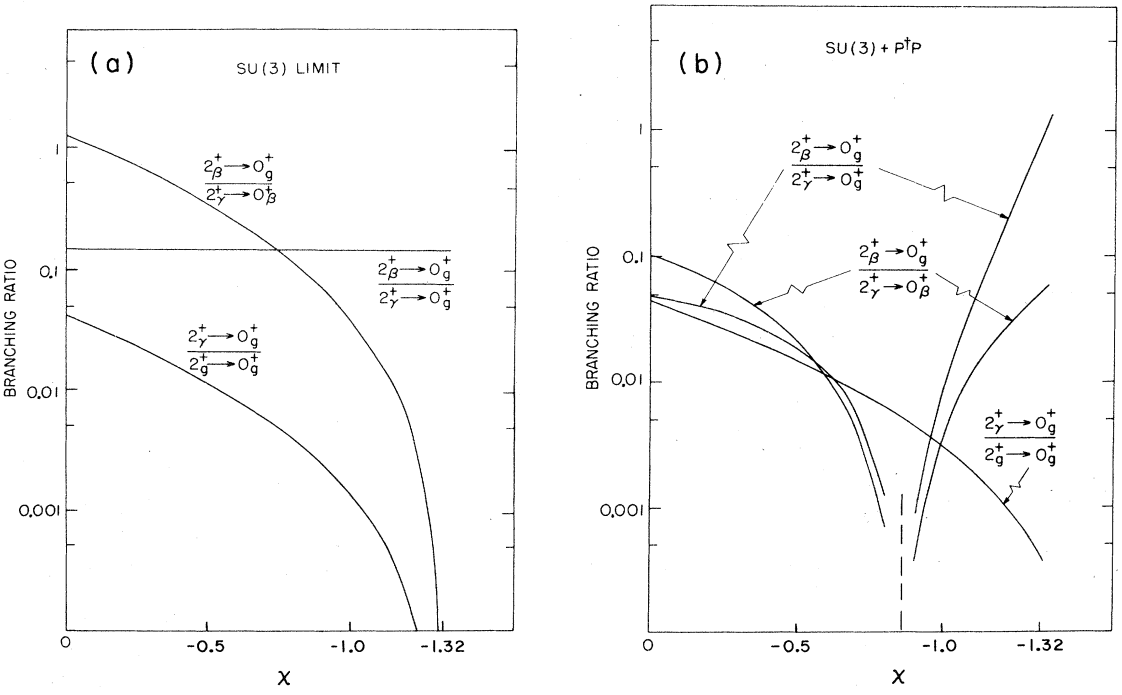


FIG. 18. $B(E2)$ ratios based on the $B(E2)$ values in Fig. 17. From Warner and Casten (1982b).

takes the value of $\approx\frac{1}{6}$. For intrarepresentation transitions the contribution from the first term in $T(E2)$ ($\Delta n_d=\pm 1$) dominates and hence $\chi$ has very little effect on their magnitude.

The empirical data for the $\gamma\rightarrow g/g\rightarrow g$ $B(E2)$ ratios (see Fig. 16) can now be combined with the results of Fig. 18 to extract (Warner and Casten, 1982b) a range of $\chi$ values capable of reproducing these $B(E2)$ data in the rare-earth region. Note that this step is possible because of the very small effect of the $P^\dagger P$ perturbation on both the $\gamma\rightarrow g$ and $g\rightarrow g$ $B(E2)$ strengths. The result is

$$-0.54<\chi<-0.22 \tag{2.67}$$

and immediately shows that the SU(3) form of the $E2$ operator cannot reproduce the observed data. Moreover, one notes that, for most deformed nuclei, $\chi$ falls in a rather narrow range, as pointed out by McGowan and Milner (1981) and Warner and Casten (1982b). Indeed, Fig. 18 shows that, even with symmetry breaking in the Hamiltonian, for $\chi=-\sqrt{7}/2$, the predicted magnitude of $\gamma\rightarrow g$ strengths would be 2 orders of magnitude too low. Thus the SU(3) symmetry must always be broken in the $E2$ operator. In addition, the results of Fig. 18 and Eq. (2.67) give rise to two important predictions concerning the decay of the $\beta$ band,

$$\frac{B(E2{:}\beta\rightarrow g)}{B(E2{:}\gamma\rightarrow g)}\simeq\frac{B(E2{:}\beta\rightarrow g)}{B(E2{:}\beta\rightarrow\gamma)}\approx 0.04\ . \tag{2.68}$$

(The specific values all refer to $2^+\rightarrow 0^+$ transitions.) We shall see similar results below in the discussion of the consistent-$Q$ formalism. It is interesting to note (see Fig. 17) that while the $\beta\rightarrow g$ transitions are very weak, the $\beta\rightarrow\gamma$ transitions are comparable in strength to $\gamma\rightarrow g$ transitions. Thus, while it must be noted that the specific range quoted in Eq. (2.68) is rather sensitive to the chosen value of the $P^\dagger P$ perturbation, it is nevertheless clear that, even in the presence of large SU(3) symmetry breaking, the $\beta$ band of an IBA deformed nucleus is characterized by a collective transition to the $\gamma$ band, rather than to the ground band. Moreover, the data in Fig. 16 and the recently observed collective $\beta\rightarrow\gamma$ $E2$ matrix elements confirm at least semiquantitatively this crucial characteristic.

The origin of the $\beta\rightarrow\gamma$ transitions provides an interesting contrast to geometrical models. In the latter, they are, of course, forbidden in the harmonic limit but can be introduced if $\beta$-$\gamma$ band mixing is introduced. In the IBA, this latter element also appears, since $K$ is not a rigorously good quantum number in the Vergados basis. However, the principal source of $\beta\rightarrow\gamma$ $E2$ matrix elements is a *direct* $\Delta K=2$ amplitude. [This can be seen, for example, from the finite intercept on a Mikhailov plot (Mikhailov, 1966) of calculated $B(E2{:}L_\beta\rightarrow L_\gamma)$ values (e.g., Warner, Casten, and Davidson, 1981).] The implication is that, even if $\beta-\gamma$ band mixing is introduced in the geometric model to produce $B(E2{:}L_\beta\rightarrow L_\gamma)$ values comparable to those of the IBA, the spin dependence of these and their branching ratios will differ considerably from the IBA for finite $N$. This has been discussed at length by Casten and Warner (1983).

The data of Fig. 16 on absolute $B(E2)$ strengths for $2_g^+\rightarrow 0_g^+$ transitions can now be used, in conjunction with the deduced range of $\chi$ values, to ascertain a corresponding range for the boson effective charge. The outcome is a phenomenologically defined form for $T(E2)$ in well-deformed, rare-earth nuclei:

$$T(E2)=0.145(15)[(s^\dagger\tilde{d}+d^\dagger s)-0.38(16)(d^\dagger\tilde{d})^{(2)}]\ . \tag{2.69}$$

The situation in the actinides is much less clear. The ratio of $B(E2{:}\gamma\rightarrow g)$ to $B(E2{:}g\rightarrow g)$ values seems to be less than for the rare-earth region, and widely different $E2$ operators have been tried (Maino *et al.*, 1981; Zhang *et al.*, 1985). A systematic study here would be well worthwhile. In any case, this equation can be used as an initial guide to calculations and as a reasonable estimate. For detailed fits to a given nucleus it may be best to fine-tune the coefficients $e_B$ and $\chi$.

Another prominent feature of the IBA for deformed nuclei is the prediction of interband $E2$ branching ratios that deviate from the Alaga rules, for finite $N$. These deviations actually appear in the exact SU(3) limit as well [e.g., in ratios of $B(E2{:}\beta\rightarrow\gamma)$ strengths] but are more pronounced in broken SU(3) calculations. This is consistent with a large body of data on deformed nuclei, particularly for $\gamma\rightarrow g$ transitions. Such effects can be introduced in geometric models via $\Delta K=2$, $\gamma$-$g$ band mixing and have traditionally been parametrized in terms of a band mixing parameter $Z_\gamma$ (or $Z_\beta$ for $\beta\rightarrow g$ transitions). For detailed discussions see Lipas (1962), Riedinger, Johnson, and Hamilton (1969), and Bohr and Mottelson (1975). In realistic IBA calculations for deformed nuclei, there are *two* distinct mechanisms for deviations of $\gamma\rightarrow g$ transition strengths from the Alaga rules (Casten, Warner, and Aprahamian, 1983). One is similar to the geometrical model, namely $\Delta K=2$ mixing of the SU(3) $\gamma$ and $g$ intrinsic states when SU(3) is broken. These matrix elements are, however, rather small, as reference to Fig. 14 shows. A more important source stems in an interesting indirect way from the allowed $\beta\rightarrow\gamma$ SU(3) $E2$ transitions. When SU(3) is broken, large $\Delta K=0$ matrix elements mix substantial amplitudes of the SU(3) $\beta$ band into the SU(3) $g$ band, as discussed above. Therefore, in the resultant $\gamma\rightarrow g$ $E2$ matrix elements, there will be important components of the type $\langle\beta_{\mathrm{SU(3)}}\,|\,E2\,|\,\gamma_{\mathrm{SU(3)}}\rangle$. But this allowed matrix element itself deviates from the Alaga rules because, as just noted, there is $K$ mixing in the $(2N-4,2)$ representation even in the strict SU(3) limit. Thus the deviation from the Alaga rules arises, ultimately, from two distinct sources of $\Delta K=2$ mixing, both dependent on the breaking of SU(3), but one, the more important, originating in an inherent characteristic of SU(3) itself. In both cases, but particularly the latter, the $\Delta K=2$ mixing has a strong $N$ dependence, decreasing as $N\rightarrow\infty$. Indeed, since the amplitude of $K=0$ in the

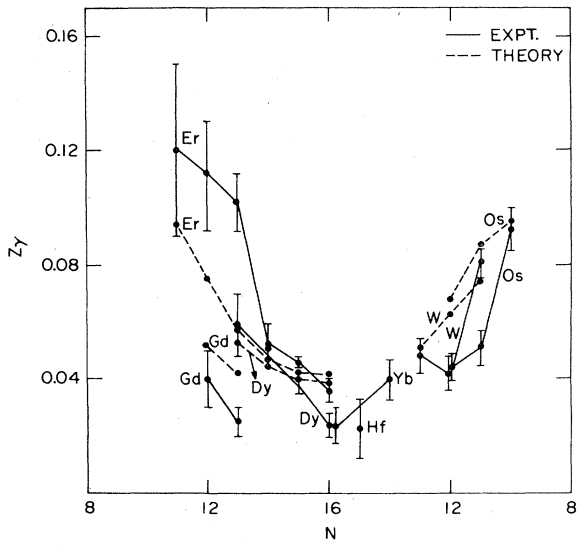


FIG. 19. Calculated and empirical values of $Z_\gamma$ in the rare-earth nuclei. From Casten, Warner, and Aprahamian (1983).

SU(3) $\gamma$ band for large $N$ goes as $1/N^2$, the geometrical concept of independent $\gamma$ and $\beta$ modes is recovered for large $N$. Thus the effective $Z_\gamma$ values that characterize the IBA predictions have a parabolic variation throughout the rare-earth region, minimizing at midshell (Casten, Warner, and Aprahamian, 1983; see also Van Isacker, 1987). Most remarkably, the data, shown in Fig. 19 along with some calculated values, disclose exactly this behavior.

This point is important for three reasons. It is typical of many "automatic" predictions of the IBA for deformed nuclei which cannot be avoided by reasonable parameter choices and which therefore are telling tests of the basic structure of the model. (Collective $\beta \rightarrow \gamma$ transitions are the most obvious other example.) Second, it is perhaps the most obvious example of the observable effects of finite $N$ in the IBA; interestingly, it does not concern high-spin states, nor small $N$ values. [For further discussion of this point, see Casten, Warner, and Aprahamian (1983) and Dieperink and Wenes (1985).] Finally, it is an excellent example of an apparent microscopic aspect of the phenomenlogical IBA-1 since, even with constant parameters, the model predicts a very specific valence nucleon number dependence of structure.

### b. *M*1 transitions

As pointed out in Sec. II.B, the lowest-order description of the $M1$ operator is proportional to the total angular momentum and hence does not give rise to transitions. It is therefore necessary to consider higher-order terms in a realistic calculation, and, rather surprisingly, it is then in fact possible to extract some simple predictions for the behavior of $E2/M1$ mixing ratios in a variety of cases. Of course, these predictions must be tempered by the realization that, *a priori,* an explicit recognition of neutron and proton degrees of freedom would seem to be appropriate to the description of magnetic properties in general. Indeed, $M1$ transitions have recently taken on high importance in the context of the IBA-2 with the discovery (Berg *et al.*, 1984; Bohle, Kuchler *et al.*, 1984; Bohle, Richter *et al.*, 1984; Richter, 1985) of a new collective mode, the so-called isovector $M1$ excitation (Loludice and Palumbo, 1978; Dieperink, 1981, 1983; Iachello, 1981b, 1984; Pittel and Dukelsky, 1985), which is characterized by collective $M1$ matrix elements connecting the ground state of deformed nuclei to $1^+$ levels near 3 MeV. There have also been a number of recent IBA-2 studies of the relation of $M1$ transition rates between low-lying states to $F$-spin purity in deformed and O(6) nuclei (Harter *et al.*, 1986, 1987; Novoselsky and Talmi, 1986; Warner, 1986; and Gelletly, Van Isacker *et al.*, 1987). On account of the interest in this mode, it is important to understand, first, the role of possible $M1$ transitions even in the IBA-1. Interestingly, several studies (Warner, 1981; Lipas, Hammarén, and Toivonen, 1984; Wood and Morrison, 1985; Lipas, Toivonen, and Hammarén, 1987) have shown that a number of features emerge from an IBA-1 treatment that are, in fact, observed.

The expanded $M1$ operator (Arima and Iachello, 1978a; Warner, 1981) becomes

$$T(M1)=(g_B+A\hat{N})\hat{L}+B(Q\hat{L})^{(1)}+C\hat{n}_d\hat{L} \ . \quad (2.70)$$

The first term remains diagonal and can be discarded in a discussion of transition properties. The quadrupole operator in the second term has the same structure as that defined in Eq. (2.8) and can connect states that differ by $\Delta L=0$ or $\pm 1$, while the third term contains $\hat{n}_d$ and hence is proportional to the $E0$ operator and can only connect states with $\Delta L=0$. In general the parameter $\chi$ in the quadrupole operator of the second term can be varied freely, and a number of fits (Lipas, Hammarén, and Toivonen, 1984; Lipas, Toivonen, and Hammarén, 1987) to $M1$ properties in collective nuclei have been attempted in this fashion with varying degrees of success. However, no well-defined or systematic behavior of the fitted parameters in the $M1$ operator seems to emerge naturally from this procedure, nor does it give rise to any clear-cut predictions concerning the behavior of $M1$ transitions in different regions. On the other hand, a number of simple predictions do result if the quadrupole operator in Eq. (2.70) is constrained to take the same form as that used to describe $E2$ transitions.

The matrix element of the $M1$ operator can be written as

$$\begin{aligned}\langle \varphi' L_f \| T(M1) \| \varphi L_i \rangle = &-Bf(L_i L_f)\langle \varphi' L_f \| Q \| \varphi L_i \rangle \\ &+C[L_i(L_i+1)(2L_i+1)]^{1/2} \\ &\times \langle \varphi L_f \mid \hat{n}_d \mid \varphi L_i \rangle \delta_{L_i L_f} \ ,\end{aligned} \quad (2.71)$$

where $\varphi',\varphi$ denote additional quantum numbers. The spin dependence of the first term is contained in the factor

$$f(L_iL_f)=[(\tfrac{1}{40})(L_i+L_f+3)(L_f-L_i+2)\times(L_i-L_f+2)(L_i+L_f-1)]^{1/2} . \quad (2.72)$$

In fact, for $L\rightarrow L\pm1$ transitions, it is only this first term that contributes, and, with the assumption that the quadrupole operator has the same $\chi$ value as used in the $E2$ operator, the expression for the reduced mixing ratio then becomes

$$\Delta(E2/M1)=\frac{\langle\varphi' L_f\|T(E2)\|\varphi L_i\rangle}{\langle\varphi' L_f\|T(M1)\|\varphi L_i\rangle}=\frac{-1}{Bf(L_iL_f)} . \quad (2.73)$$

The reduced mixing ratio is related to the quantity normally measured, $\delta(E2/M1)$, by

$$\delta(E2/M1)=0.835E_\gamma\Delta(E2/M1) ,$$

with $E_\gamma$ in MeV. The second term in Eq. (2.71) is proportional to the $E0$ operator and hence in vibrational nuclei, or in deformed nuclei for the $\gamma\rightarrow\gamma$ and $\gamma\rightarrow g$ transitions, will be negligible, and the $E2/M1$ mixing ratio will simply have the form of Eq. (2.73). This immediately leads to a prediction for the spin dependence of $M1$ $\gamma\rightarrow g$ transitions that in fact is the same as emerges from many other approaches (Grechukhin, 1963, Greiner, 1966; Kumar, 1975). Moreover, the fact that the same spin dependence holds true for transitions within the $\gamma$ band results in the additional prediction of a link between the reduced mixing ratios for $\gamma\rightarrow g$ transitions and $\gamma\rightarrow\gamma$ transitions, namely, that they should be identical for the same values of the initial- and final-state spins. In addition, the sign of the mixing ratios should be constant throughout the deformed region. In fact, all three predictions seem to be reasonably well borne out by the data (Warner, 1981), although some very recent results (Gelletly, Van Isacker *et al.*, 1987) for $\gamma\rightarrow g$ transitions in $^{169}$Er seem to show a factor-of-2 disagreement with the corresponding mixing ratio values within the $\gamma$ band. For the case of $\beta\rightarrow g$ transitions in deformed nuclei it will be the second term in Eq. (2.71) that dominates, since, while the $E0$ transitions are strong, the equivalent $E2$ transitions are weak, as discussed in the previous section. In fact, in this case, the spin dependence remains the same but, of course, the constant can change. Thus the sign of mixing ratios in $\beta\rightarrow g$ transitions may be different from those involving the $\gamma$ band. The data on mixing ratios for $\beta\rightarrow g$ transitions are rather sparse, and as yet no comparison has been made with the predictions of this simple framework. However, the data that exist (Lange, Kumar, and Hamilton, 1982) do seem to support the idea that the sign of the mixing ratios for these transitions is constant across the rare-earth region and opposite to that observed for $\gamma\rightarrow g$ transitions (Krane, 1973).

In the O(6) limit, the selection rules associated with the $E2$ and $E0$ operators, respectively, lead to the specific prediction that the $\Delta\tau=0$ transitions from the $\sigma=N-2$ to the $\sigma=N$ group of levels should be dominated by $M1$ transitions, since, while these are allowed by the second term of Eq. (2.71), the $E2$ operator is forbidden.

### 3. The consistent-*Q* formalism (CQF)

In the previous section it was demonstrated that the empirical data on $E2$ transitions in the rare-earth region mandate a rather well-defined structure for the $E2$ operator, which is not consistent with the SU(3) form of $Q$ assumed in the Hamiltonian. Thus different forms of the quadrupole operator are needed in $H$ and $T(E2)$ in order to describe the data. It is clearly of interest to ask whether a comparable description can be obtained within a framework where *consistent* forms of the quadrupole operator are used. This approach is referred to as the consistent-$Q$ formalism (CQF; Warner and Casten, 1982a, 1983) and, in its simplest form, utilizes a Hamiltonian

$$H=a_2Q^2+a_1\hat{L}^2 , \quad (2.74)$$

where

$$Q=(s^\dagger\tilde{d}+d^\dagger s)^{(2)}+\chi(d^\dagger\tilde{d})^{(2)} \quad (2.75)$$

and

$$T(E2)=e_BQ . \quad (2.76)$$

The result of changing the absolute magnitude of $\chi$ in the Hamiltonian can easily be inferred from the consequent changes in the $d$-boson seniority changing terms generated by the $Q^2$ interaction. The earlier study of the $E2$ operator suggests that a reduction in the absolute magnitude of $\chi$ might be required, which in turn would generate a reduction in the $\Delta n_d=\pm1,0$ terms relative to the $\Delta n_d=\pm2$ terms. It will be recalled that the former are important in the $Q^2$ [SU(3)] interaction, while the $P^\dagger P$ term does not involve $\Delta n_d=1$ terms. Hence the CQF approach would seem likely to generate the same type of perturbation to the SU(3) spectrum as the $P^\dagger P$ symmetry-breaking term considered earlier. This is indeed the case, and it has now become clear that the CQF framework outlined above, which involves one *less* parameter than the Hamiltonian and $E2$ operator of Eqs. (2.64) and (2.8), in fact produces equivalent or better agreement with the data.

More specifically, a reduction in the absolute magnitude of $\chi$ produces the same effect as the $P^\dagger P$ term in pushing the $\beta$ band above the $\gamma$ band in energy. Indeed, the resulting matrix elements between SU(3) states behave similarly against $|\chi|$ to those of the original formalism against $a_0/4a_2$ shown in Fig. 14. The higher excitations ($\beta\beta$, $\gamma\gamma$, $\beta\gamma$ bands) are also pushed higher in energy relative to the $\gamma$ band. The ratios of their energies as a function of $\chi$ are shown in Fig. 20 and are seen to be

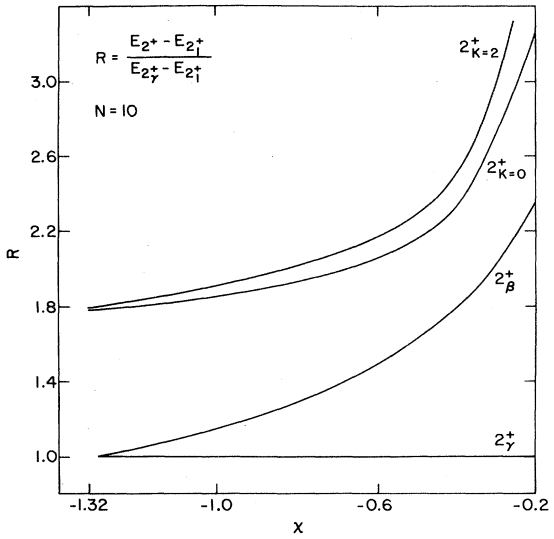


FIG. 20. Energy ratios in the consistent-$Q$ formalism for the transition from SU(3) (left-hand side) towards O(6) ($\chi=0$). The subtraction of $E_{2_1^+}$ in both numerator and denominator is performed simply to remove the effects of any $\hat{L}^2$ term.

very similar to those against $a_0/4a_2$ in Fig. 14 (up to $a_0/4a_2\approx -1$) discussed earlier. Note that Fig. 14 showed energies and not ratios, but the relative behavior of the higher excitations can be compared with the present Fig. 20, since $E_\gamma$ was nearly constant. However, the important difference in the CQF approach is that the $\gamma$ band itself is strongly lowered in energy as $|\chi|$ decreases. That is, in contrast to Fig. 14, the increase in such ratios as $E_\beta/E_\gamma$ occurs because of the more rapid

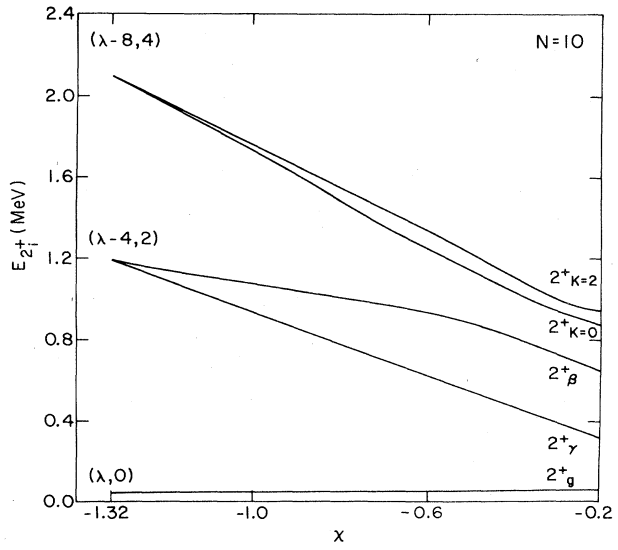


FIG. 21. Energies of various $2^+$ states in the consistent-$Q$ formalism for the transition from SU(3) (left-hand side) towards O(6) ($\chi=0$). For $N=10$, with $a_2=-0.02$ MeV.

decrease of $E_\gamma$ than $E_\beta$ and not because of an increase in the latter. This is illustrated, for $N=10$, in Fig. 21. The compression of the entire level scheme is apparent. Of course, in practical calculations, this can be compensated by larger absolute values of $a_2$.

### a. O(6) nuclei in the CQF

Just as the dominance of the $a_0\,P^\dagger P$ term in the original form of the multipole Hamiltonian results in an O(6) spectrum, here too, in the CQF, when $\chi\to 0$, the quadrupole operator of Eq. (2.8) becomes a generator of O(6), so that a spectrum with O(6) symmetry must be produced. However, inspection of the original O(6) Hamiltonian of Eq. (2.56) shows that the CQF version, Eq. (2.74), involves one less parameter and therefore must produce a more constrained form of the O(6) symmetry than Eq. (2.57). In fact, the resulting O(6) eigenvalue expression is (Warner and Casten, 1982a, 1983)

$$E\approx A[(N-\sigma)(N+\sigma+4)+\tau(\tau+3)]+CL(L+1)\ , \tag{2.77}$$

showing that the constraint that emerges is an equality of the O(6) and O(5) contributions, so that $A=B$ in Eq. (2.57). Note that in the original O(6) limit there is no constraint whatsoever of this type, and $A$ and $B$ may take on any values. It is therefore very encouraging to note (see below for further details) that empirical fits using the more general eigenvalue expression do indeed seem to result in a near equality of $A$ and $B$. This feature has now been noted in both the $A=130$ Xe,Ba region (Casten and von Brentano, 1985) and the $A=196$ Pt region. Moreover, it has recently, been shown (Casten *et al.*, 1986) that the fermion dynamical symmetry model of Wu, Feng, Guidry, Ginocchio, and co-workers (Wu *et al.*, 1986; see also Ginocchio, 1980) also gives this result.

### b. Deformed and transitional nuclei in the CQF

From this discussion it is apparent that the transition from O(6) to SU(3) can be accomplished in the CQF simply by varying $\chi$ between the values (0 and $-\sqrt{7}/2$) appropriate to each limit. As will be seen below, this treatment, which again is simpler than the earlier formalism and involves one less parameter, works at least as well.

It is interesting to understand the physical effect of varying $\chi$. This was first worked out numerically (Casten, Aprahamian, and Warner, 1984) and, subsequently, analytically by Castanos, Frank, and Van Isacker (1984). the basic idea is that SU(3) is a symmetric rotor, while O(6) is an asymmetric, $\gamma$-soft rotor with a mean or rms $\gamma$ value of 30°. Thus changes in $\chi$ should correspond somehow to the introduction of (dynamic) axial asymmetry. On the other hand, studies of the classical limit (see Sec. II.E) of the IBA-1 show that all $\gamma$ dependence in the equivalent geometrical potential,

$V(\beta,\gamma)$, enters through terms of the form $\cos 3\gamma$ so that $V(\beta,\gamma)$ can have a minimum only at $\gamma=0°$ or 60° (prolate, oblate limits) but never for intermediate axially asymmetric values. Thus the question arises as to how the IBA goes from the axially symmetric SU(3) limit to the $\gamma$-soft ($\gamma_{\rm rms}=30°$) O(6) case. In Casten, Aprahamian, and Warner (1984) calculations in the Davydov and Filippov (1958) model as a function of $\gamma$ were compared to those of the IBA in the CQF, and a one-to-one relationship between $\gamma$ and $\chi$ was deduced. The results are shown in Fig. 22. By comparing results for different observables it is apparent that similar $\gamma$-$\chi$ relationships occur and thus that an effective $\gamma$ value can be defined to within a few degrees. Thus the O(6)→SU(3) transition corresponds to a potential changing from completely $\gamma$ flat to one whose minimum value is at $\gamma=0°$ but which has a finite slope as a function of $\gamma$. The slope becomes steeper (but remains finite) as $\chi$ approaches the SU(3) value. It becomes infinitely steep only if $N\to\infty$. Thus, for finite $N$, $\gamma_{\rm rms}$ never vanishes. This potential is shown for several $\chi$ values in Fig. 23. The $\gamma$ values and the asymmetry that characterize the IBA, even in SU(3), but more so with deviations toward O(6), are thus dynamic, resulting from zero-point motion in a finite potential, $V(\beta,\gamma)$. The above procedure is subject to the criticism that it compares the Davydov-Filippov model of rigid $\gamma$ asymmetry with one of substantial $\gamma$ softness. There have been a number of subsequent studies that explored this question with different approaches. Dobeš (1985) has employed the Hartree method with angular momentum projection and obtained similar results. This approach is sensitive, not so much to $\gamma_{\rm rms}$ as to $\gamma_{\rm min}$, the value of $\gamma$ at which the finite potential $V(\beta,\gamma)$ is minimized. He therefore obtained $\gamma_{\rm min}=0°$ in SU(3), but this is not inconsistent with the results just discussed. Castanos, Frank, and Van Isacker (1984), on the other hand, expressed the wave functions of the Hamiltonian for arbitrary $\chi$ in a U(5) basis and then used the Holstein-Primakoff representation to map this basis onto the explicit wave functions $\Psi(\beta,\gamma,\Omega)$ of a truncated quadrupole phonon space. However, this procedure implies the specific choice $\chi=0$ in the operator determining $\gamma$, and hence their results, though very similar to those described above, are not strictly relevant to the case of an $E2$ operator with $\chi\neq 0$. Elliott, Evans, and Van Isacker (1986) used a different method, based on calculating the expectation values of the quadrupole and cubic invariants $Q^2, Q^3$ in the ground state. Here, the general trend is the same, but the deduced values of $\langle\gamma\rangle$ are smaller and go to essentially zero at the SU(3) limit even for finite $N$ values.

The nature of the transition induced by changing $\chi$ from its SU(3) to O(6) value can be investigated in a different sense by rewriting the CQF Hamiltonian in terms of the Casimir operators of the various symmetry groups. This yields the surprising feature that the transi-

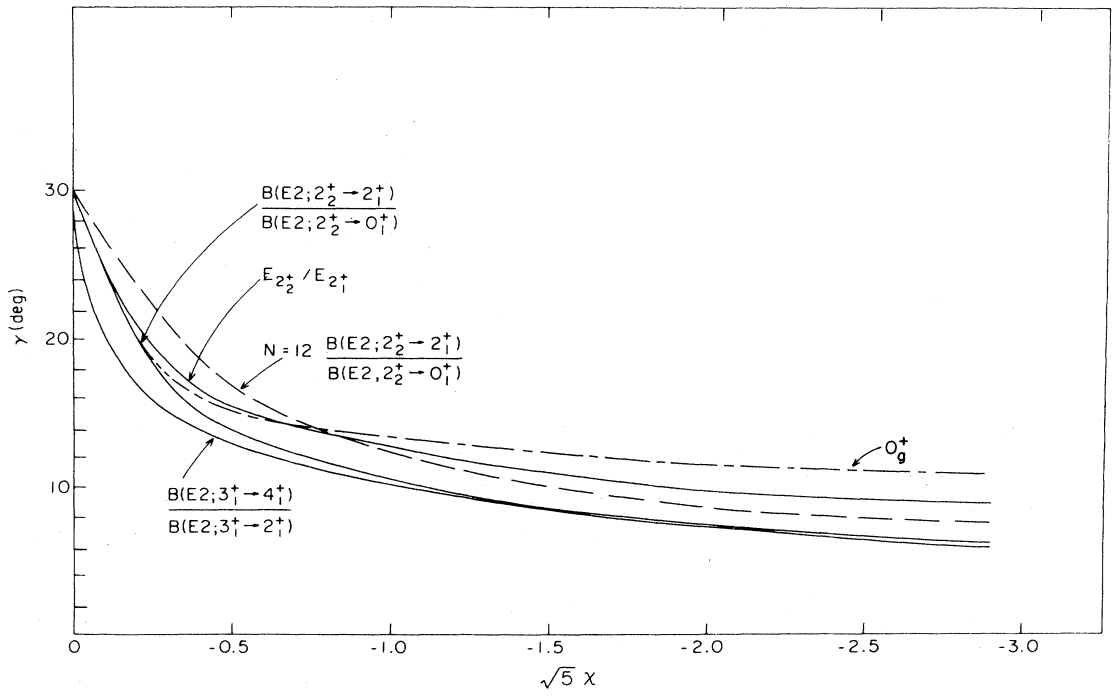


FIG. 22. $\gamma\leftrightarrow\chi$ relationship in the SU(3)↔O(6) transition, for various observables in the IBA. For one observable the results for two different $N$ values are shown. From Casten, Aprahamian, and Warner (1984). The curve marked $0_g^+$ was obtained analytically by Castanos, Frank, and Van Isacker (1984).

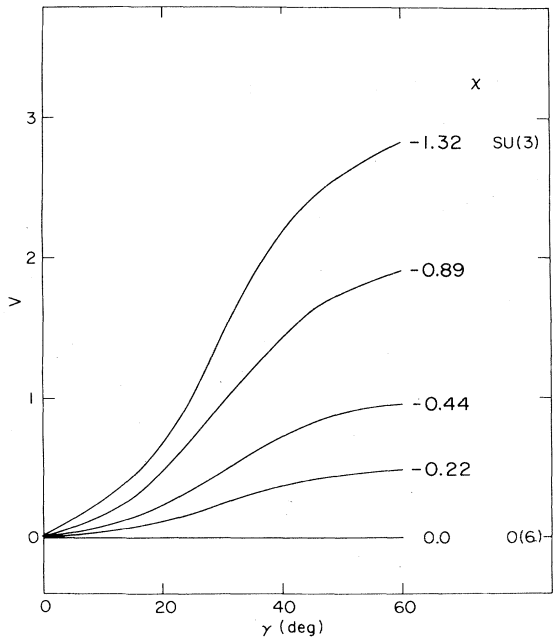


FIG. 23. The dependence of the classical potential corresponding to the IBA as a function of $\gamma$ for several values of $\chi$, ranging from the SU(3) limit ($\chi=-1.32$) to O(6) ($\chi=0$). From Casten, Aprahamian, and Warner (1984).

tion does not correspond exactly to the SU(3)-O(6) leg of the symmetry triangle but rather to a path of the type indicated schematically in Fig. 24, which involves a contribution from the U(5) Casimirs also. In fact, the coefficients of the linear and quadratic U(5) contributions are equal and related to the parameters of the quadrupole interaction by (A. Frank, 1986)

$$C_{1U5}=C_{2U5}=a_2\frac{\chi}{\sqrt{7}}\left[1+\frac{2\chi}{\sqrt{7}}\right]. \tag{2.78}$$

Note that, as evident from Fig. 24, both vanish for the SU(3) value of $\chi=-\sqrt{7}/2$ and for the O(6) value of $\chi=0$. The largest contribution arises for $\chi=-\sqrt{7}/4$ and yields a value for $\varepsilon$ of $-a_2/8$. In practice, therefore, in realistic calculations, the U(5) contribution is rather small.

The principal advantage of the CQF approach lies in its considerable simplicity. Since the $\hat{L}^2$ term in Eq. (2.74) is always diagonal, the wave functions of the CQF Hamiltonian are uniquely specified by $\chi$ (and the boson number $N$). The parameters $a_2$ and $e_B$ both act only as scaling factors on the absolute energies and $B(E2)$ values, so that relative values of these observables are also uniquely specified only by $\chi$ and $N$. Thus, in this framework, the energy and $E2$ properties are inexorably linked, so that, if the $\chi$ value is determined from one, the other is determined (at least on a relative scale). In fact, ratios of energies or $B(E2)$ values can be predicted in this framework as a function of $\chi$ and $N$ and displayed in the form of contour plots, as illustrated in Figs. 25 and 26. (The dots on these figures serve to emphasize the fact that the predictions are valid only for integral values of $N$.) The ratio $R_\gamma=B(E2{:}2^+_\gamma\rightarrow 0^+_g)/B(E2{:}2^+_g\rightarrow 0^+_g)$ displayed in Fig. 25 can now be used, as before, to determine the permissible range of $\chi$ values appropriate to the well-deformed nuclei in the rare-earth region using the data of Fig. 16. The result is the hatched rectangle in the upper center of Fig. 25, which can then be transposed to other contour plots to provide predictions for other $B(E2)$ ratios and for the relative energy spectrum. [The other hatched area corresponds to O(6)-like nuclei.] The relatively narrow range of $\chi$ values appropriate to deformed nuclei reflects the relatively constant values of $R_\gamma$ seen empirically in Fig. 16. Note that in the upper part of Fig. 26 the energy ratio plotted is effectively the ratio of the intrinsic excitation energies of the $\beta$ and $\gamma$ bands, since the form of the denominator is designed to remove the $L(L+1)$ dependence. The contour plot involving $\beta\rightarrow\gamma$ transitions in Fig. 26 shows that, as stated earlier, these remain collective for large ranges of $\chi$ and $N$. Finally, the CQF, in the context of an SU(3)$\rightarrow$O(6) transition, gives simple results not only for ratios of energies and $B(E2)$ values but for their actual values. Figure 21 gave some of these results for energy levels.

In Eqs. (2.32), (2.49), and (2.60) we gave analytic expressions for the $B(E2{:}2^+_1\rightarrow 0^+_1)$ value in each of the three limits. Of course, an analytic expression in intermediate situations is not possible, but the simplicity of

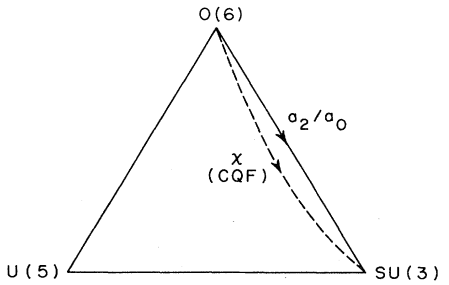


FIG. 24. Symmetry triangle of the IBA with an indication of the path corresponding to the O(6)$\leftrightarrow$SU(3) transition in the consistent-$Q$ formalism (CQF).

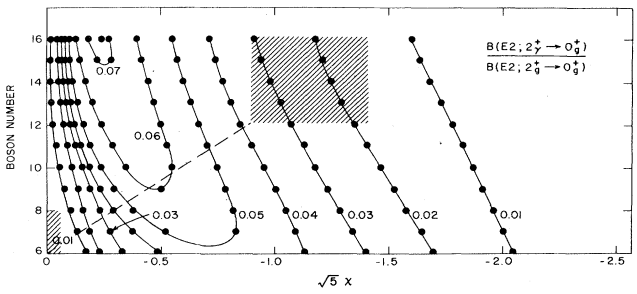


FIG. 25. Contour plot of the indicated $B(E2)$ ratio in the CQF as a function of $N$ and $\chi$. From Warner and Casten (1983).

the CQF may be exploited to develop the following approximate expression (Casten and Wolf, 1987):

$$B(E2{:}2_1^+ \rightarrow 0_1^+) \approx e_B^2 (N+1)^2 (1-0.1\chi)/2 \ . \qquad (2.79)$$

[Note that $\chi$ is generally negative, so the coefficient of $(N+1)$ is slightly greater than 0.5.] This expression is valid to better than $\pm 12\%$ for $\chi = 0 \rightarrow -1$, thus covering nearly all deformed and transitional nuclei. It may be used either to estimate absolute $E2$ transition rates or to extract boson effective charges for nuclei not satisfying a limiting symmetry. For the $\chi$ value of $-0.5$, approximately valid for most rare-earth deformed nuclei, one has, simply, $B(E2{:}2_1^+ \rightarrow 0_1^+) \approx 0.525(N+1)^2 e_B^2$.

While a more detailed comparison of the predictions of the CQF approach with specific nuclei will be made in subsequent sections, it is instructive at this stage to use the $\chi$ and $N$ values corresponding to the empirically determined rectangle on the contour plot of Fig. 25 in conjunction with the other contour plots to construct the predicted structure of a deformed nucleus in this framework. The result is shown in Fig. 27 for the lowest three rotational bands. Note again that the three distinctive features that characterize this description are the $\beta$ band lying above the $\gamma$ band, a $\beta \rightarrow \gamma$ $E2$ strength roughly equivalent to the $\gamma \rightarrow g$ strength, and a much weaker $\beta \rightarrow g$ strength. All of these features are predictions that arise automatically for $\chi$ values defined by the ratio in Fig. 25, and hence the fact that they are at least qualitatively in agreement with the large body of data in this region speaks very strongly in favor of the underlying basis of this approach. In addition it raises some interesting questions concerning the nature and relationship of the $\beta$ and $\gamma$ intrinsic modes in deformed nuclei; this point will be returned to in the next section.

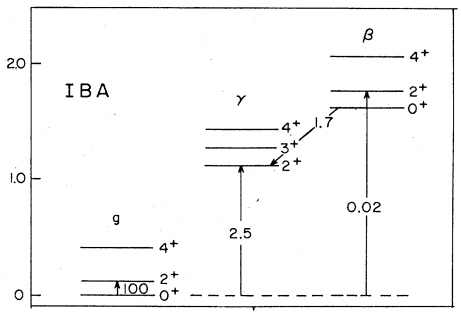


FIG. 27. Typical structure of a deformed nucleus in the IBA. The numbers on the transition arrows indicate typical relative $B(E2)$ values. From Warner and Casten (1983).

In an O(6)-SU(3) transitional region there are obviously many routes that could be taken from the crosshatched area in the center of Fig. 25 to the bottom left-hand corner, which represents the O(6) limit. However, some predictions are independent of the route. For example, it is clear that it is impossible to pass between the crosshatched regions, in both of which $R_\gamma$ is small, without going through a maximum. This prediction, though qualitative, is parameter independent and inescapable (within the CQF framework). Similar results characterize other $B(E2)$ ratios, such as the quantity $B(E2{:}3_\gamma \rightarrow 2_\gamma^+)/B(E2{:}3_\gamma^+ \rightarrow 2_g^+)$.

It is also interesting to consider the simplest route, namely a straight line as indicated in Fig. 25. Some results are illustrated in Figs. 28 and 29, where the predicted behavior is compared with the experimental data for the relevant nuclei. The agreement is in general good, although for specific nuclei in the transitional region it is no better than a factor of 2. On the left-hand side of Fig. 29, the predicted behavior of the quadrupole moment of the first $2^+$ state is shown. Since this prediction does not involve a ratio of quantities, a value for the effective charge in the $E2$ operator must be chosen, and the results of two such choices are indicated in the figure, both falling within the previously determined range for this parameter and, between them, encompassing essentially all of the data. The value for $^{196}$Pt is not shown and remains, as discussed earlier, in marked disagreement with the pure O(6) symmetry prediction. It is also interesting to observe that the quadrupole moment data in the deformed region appear to separate according to element, possibly suggesting a small $Z$ dependence of the effective charge in this region. More striking is the clear tendency of the values to saturate at larger boson num-

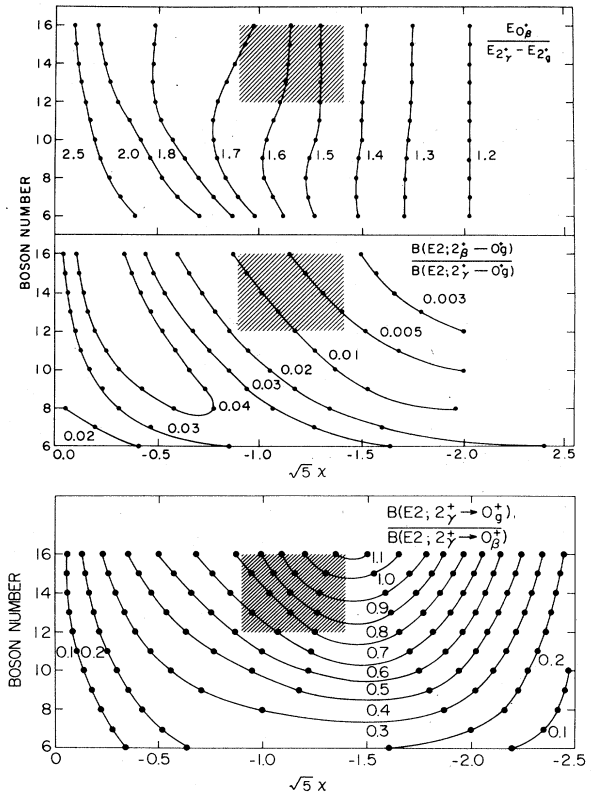


FIG. 26. Contour plot of the indicated ratios in the CQF as a function of $N$ and $\chi$. From Warner and Casten (1983).

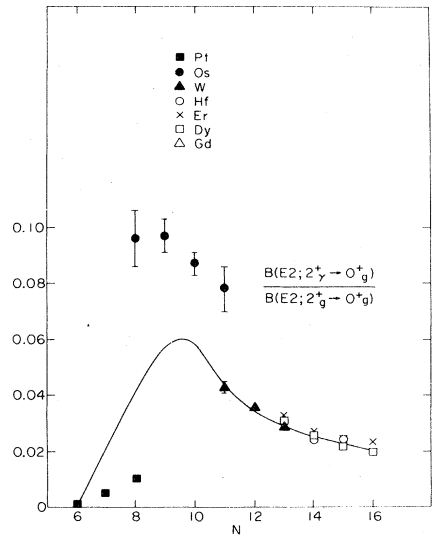


FIG. 28. Comparison of calculated (CQF) and empirical $B(E2{:}2^+_\gamma \rightarrow 0^+_g)$ values normalized to the $2^+_1 \rightarrow 0^+_1$ transition. The calculations utilized $\chi$ values corresponding to the dashed straight line trajectory in Fig. 25. From Warner and Casten (1983).

bers, indicating that the empirical dependence on $N$ is weaker than the predicted one. Of course this feature could also be explained by an $N$ dependence in the effective charge or by effective $N$ values in the IBA-1 itself, since qualitatively $Q_{2^+_1} \propto N$. Finally, the right-hand side of Fig. 29 shows the dependence on $\chi$ of a $\gamma \rightarrow g$ branching ratio. The interesting feature here is that, while the calculated curve clearly approaches the rotational value of 0.7 as $N$ increases, it never attains it for realistic values of the boson number. This behavior simply reflects the automatic incorporation of band mixing effects within the IBA framework alluded to earlier and discussed in considerably more detail in Sec. III.

It is clear, therefore, that the CQF can give a reasonably good and extremely simple description of the main characteristics of the nuclei spanning the deformed-O(6) region. Of course it must be emphasized that the results shown above should not be expected to provide detailed agreement with specific nuclei throughout the deformed rare-earth region. Rather they may be conceived as a (much improved) starting point in such a calculation, relative to the pure SU(3) limit.

For an SU(3)→U(5) transition, the above procedure is inadequate, since the $\varepsilon\hat{n}_d$ term is essential for U(5). Although it has been pointed out that the transitional CQF Hamiltonian implicitly contains such a term, in fact, the contributions of $C_{1U5}$ and $C_{2U5}$ reach a maximum for $\chi = -\sqrt{7}/4$, the magnitude at this point being $\frac{1}{8}$ that of the $a_2$ coefficient of $Q^2$. In practice this is totally insufficient to describe the specific onset of vibrational structure, and hence an additional term in $\varepsilon\hat{n}_d$ (at least) must be introduced into the Hamiltonian of Eq. (2.74) to give (Lipas, Toivonen, and Warner, 1985)

$$H = \varepsilon\hat{n}_d + a_2 Q^2 + a_1 \hat{L}^2 \,. \tag{2.80}$$

This approach has been called the extended consistent-$Q$

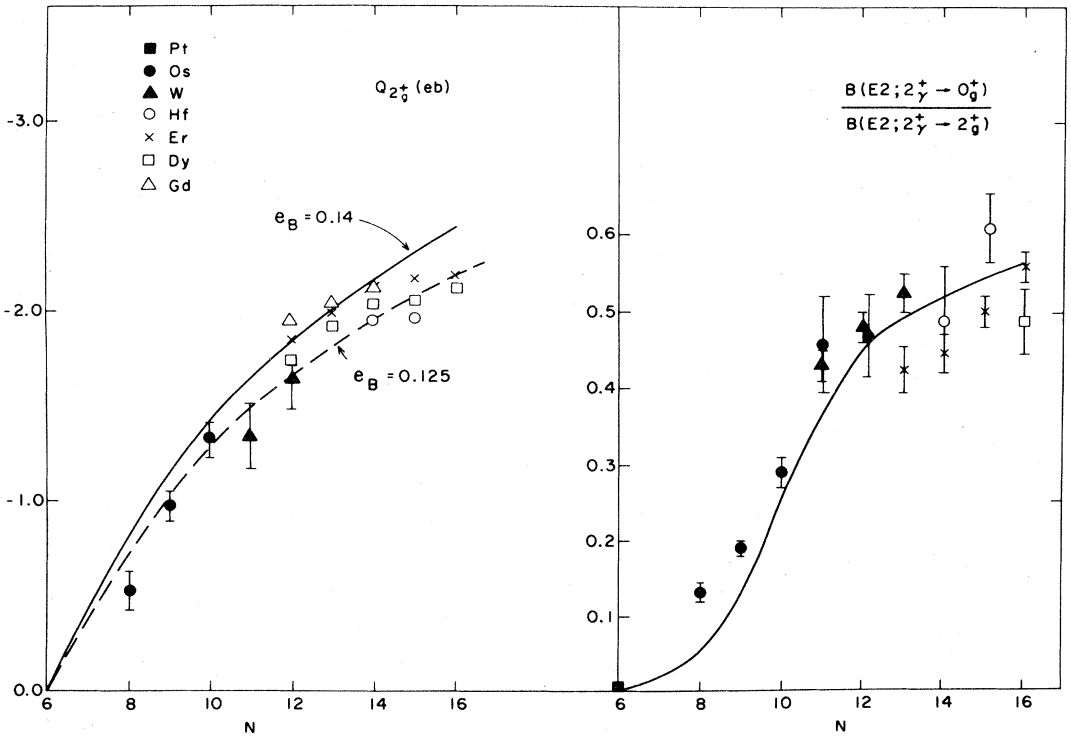


FIG. 29. Further IBA predictions in the CQF. From Warner and Casten (1983).

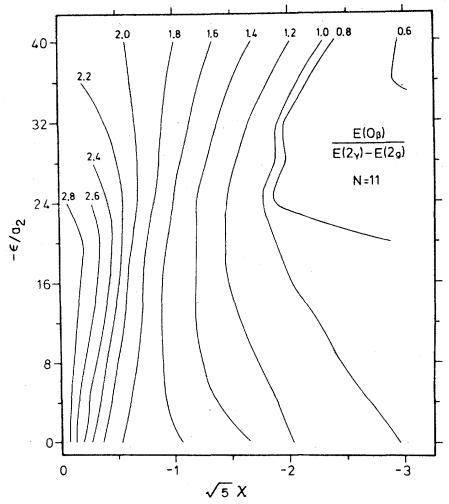


FIG. 30. Contour plot relating $\beta$ and $\gamma$ band energies in the ECQF for $N=11$. From Lipas, Toivonen, and Warner (1985).

formalism or ECQF. This step sacrifices some of the simplicity inherent in the original CQF Hamiltonian since, now, for a given boson number $N$, the wave functions will depend on both $\chi$ and $\varepsilon/a_2$ rather than on $\chi$ alone. Nevertheless, it is still possible to construct contour plots for energy and $B(E2)$ ratios as functions of $\chi$ and $\varepsilon/a_2$, albeit now for a specific $N$ value. Some examples are shown in Figs. 30 and 31. Clearly these figures are considerably more complex than their SU(3)→O(6) counterparts, and of course two of them must be used in order to determine both $\chi$ and $\varepsilon/a_2$ uniquely. There are still, however, a number of interesting signatures that can be discerned, which together emulate the known characteristics of a rotational-vibrational transition. One such signature is a lowering of the $\beta$ bandhead below the $\gamma$ bandhead and an accompanying increase in the strength of the $\beta\rightarrow g$ $B(E2)$ transitions. This lowering of the $\beta$ band immediately places the calculation outside of the scope of the normal CQF, but reference to Fig. 30 shows that the addition of the $\varepsilon\hat{n}_d$ term indeed generates a region in the $\chi$-$\varepsilon/a_2$ plane where this occurs. Specifically, it involves the upper right-hand corner, where the energy ratio $E_{0_\beta}/(E_{2_\gamma}-E_{2_g})$ falls below unity. Then Fig. 31 shows that, in the same quadrant, the $\beta\rightarrow g$ strength maximizes while the $\gamma\rightarrow g$ strength remains largely unaffected.

A U(5)→O(6) transition region is even simpler than SU(3)→U(5), since $\chi=0$ is used in both these limits and therefore may plausibly be kept constant throughout the transition region. Thus the appropriate Hamiltonian is simply that of Eq. (2.80) with $\chi=0$. Once again, simple contour plots, of the type possible in SU(3)→O(6) transition regions, are possible, since the structure depends only on $\varepsilon/a_2$ and $N$. Some typical predictions (for $N=11$) are discernible in Figs. 30 and 31 by setting $\chi=0$. The predicted energy and $B(E2)$ ratios are clearly seen to reflect the expected trends between U(5) and O(6). It is interesting to note that, as in the SU(3)→O(6) case, a number of branching ratios such as those shown in Fig. 31 vanish in both limits and are finite only in the transition region.

Thus the use of a consistent form of the quadrupole operator in the description of both energies and $B(E2)$ strengths seems to succeed in characterizing the major structural changes in both across an entire major shell. The question of which additional terms are necessary in

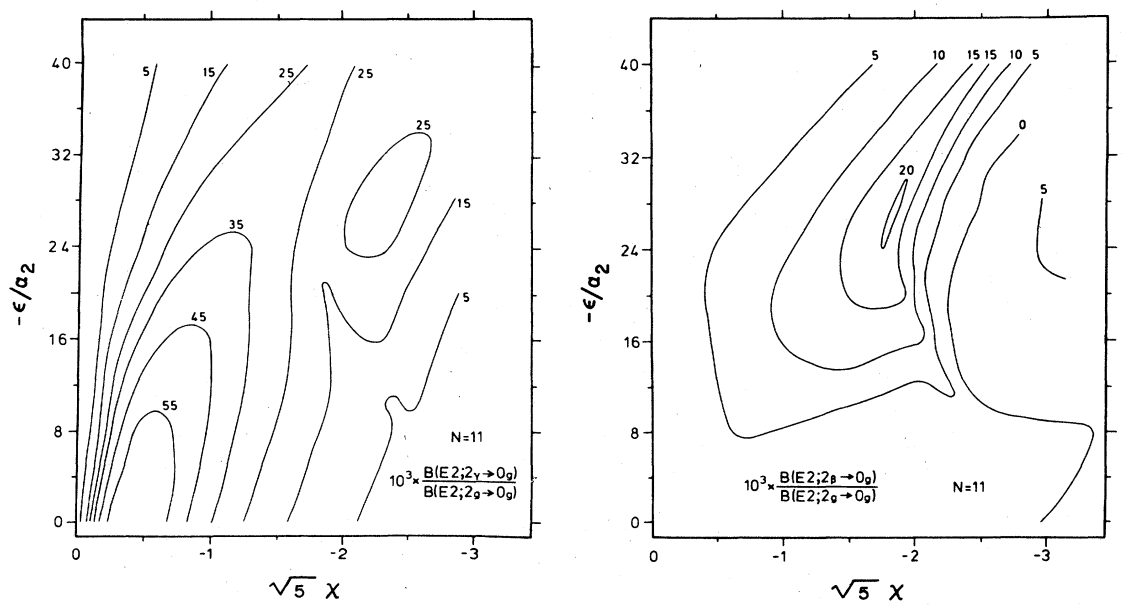


FIG. 31. Contour plots of $B(E2)$ ratios in the ECQF for $N=11$. From Lipas, Toivonen, and Warner (1985).

specific regions to improve the agreement between theory and experiment is still an open one and requires further study. A further advantage of this approach that has not yet been mentioned is its rather direct connection to the parameters of the IBA-2 Hamiltonian, which in turn can be linked to the underlying shell-model basis. Indeed, there have been attempts (Xu, 1984) to derive the CQF from a microscopic approach. This connection implies that the constraints extracted from the data in the IBA-1 basis for parameters such as $\chi$ can be used as direct input to the problem of developing a fermion-boson mapping procedure.

A final comment on terminology is useful here. In recent years the term "CQF" has come to denote two somewhat different ideas. In one, which is the formalism presented here, $Q$ takes on the same form in $H$ and $T(E2)$, and an O(6)→SU(3) transition can be obtained simply by varying $\chi$. In the other, the CQF (variable-$\chi$) form of the Hamiltonian [$H \approx Q^2(\chi)$] alone is used (see, for example, Faessler *et al.*, 1985) to study nuclei between the U(6) symmetries, but without constraining $\chi$ to be the same in $T(E2)$. We would prefer to use the term "CQF" for the former and "CQF Hamiltonian" for the latter.

### 4. Summary

To conclude and summarize this section, it is useful to recapitulate some basic guidelines for practical IBA-1 calculations. This is most easily done by reference to the symmetry triangle of Fig. 12. Calculations involving a large $\varepsilon$ will tend towards a U(5) structure, while those with a large $a_2$ term will give deformed nuclei with deviations from SU(3) depending on the size of the symmetry breaking [e.g., $\varepsilon$ or deviations of $\chi$ from $\chi_{\mathrm{SU(3)}}$]. O(6)-like spectra are produced either by a large $P^\dagger P$ term or, in the CQF, by small $|\chi|$ values. As general guidance, it is also useful to recall that the $N$ dependence of the $Q^2$ term is $\approx N^2$, while the effects of $\varepsilon \hat{n}_d$ go as $N$, so that, even for constant $\varepsilon/a_2$, a monotonic tendency towards deformation will ensue as $N$ increases. How far it goes depends on the actual values of $\varepsilon/a_2$. In an SU(3)-O(6) region, it is useful to note that, while deviations from SU(3) grow approximately linearly with $a_0 P^\dagger P$, or with $|\chi - \chi_{\mathrm{SU(3)}}|$, a good deformed structure nevertheless persists until these latter terms are quite large: for example, as the contour plots of Figs. 25 and 26 show, deformed character remains more or less intact for $N > 10$ even for $|\chi|$ values as small as 0.4.

## E. The intrinsic-state formalism: geometric interpretation of the IBA

We have made numerous allusions and some brief comments from time to time concerning the physical or geometrical interpretation of the IBA. In fact, the problem of constructing a quantitative link between the algebraic and geometric frameworks has produced a wealth of literature over recent years. The motivation for such studies is, of course, to understand the successes and failures of the purely algebraic IBA in terms of the more familiar and physically intuitive concept of a nuclear shape. In this short section we shall develop some of these ideas a little more formally and present some basic results in simple form.

The association of a geometrical shape with a given IBA Hamiltonian or wave function involves taking the classical limit of a quantum system. This is a nontrivial problem, and in general the correspondence is ambiguous. However, Gilmore and co-workers (Gilmore, Bowden, and Narducci, 1975; Gilmore, 1979) have shown that an unambiguous definition is possible whenever the quantum system has the group structure of a Lie algebra, such as U(6). For a system of $N$ bosons, described by the group U($r$), there are $r-1$ independent associated classical variables. For U(6) the sixth variable is fixed by a normalization condition determined by the fact that the boson number $N$ is conserved. That is, all states belong to a single representation [$N$] of U(6). For the IBA-1, then, there are five classical variables, and these may be chosen to be the familiar geometrical quantities $\beta$, $\gamma$, and the three Euler angles. The algorithm of Gilmore (1979) depends on the concept of intrinsic or coherent states in terms of which one calculates upper and lower bounds of the expectation values of any operator. These bounds converge, in the $N \to \infty$ limit, to the exact classical limit (Gilmore and Feng, 1978a, 1978b; Gilmore, 1979). We refer the reader to the primary literature for the details of this formalism and its conditions of applicability (Gilmore, 1979; Dieperink and Scholten, 1980; Dieperink, Scholten, and Iachello, 1980; Ginocchio and Kirson, 1980a, 1980b; Arima and Iachello, 1981; Van Isacker and Chen, 1981; Bijker and Dieperink, 1982; Iachello and Arima, 1987). For related approaches, see Castanos, Frank, Hess, and Moshinsky (1981), Hatch and Levit (1982), Balantekin, Barrett, and Levit (1983), Chen and Arima (1983), and Leviatan (1984, 1986). Here we outline the basic ideas and the results. As recently discussed by Kirson and Leviatan (1985), a general IBA Hamiltonian can be separated into collective and intrinsic parts: $H = H_{\mathrm{coll}} + H_{\mathrm{int}}$. The $H_{\mathrm{coll}}$ is the "rotational" part, while $H_{\mathrm{int}}$ depends on $\beta$ and $\gamma$. The concept of an intrinsic state is applicable if the fluctuations in $\beta, \gamma$ are small compared to their mean values. Then one can write an intrinsic state for the IBA ground-state condensate as follows:

$$|N,\beta,\gamma\rangle = \frac{1}{\sqrt{N!}}(b_c^\dagger)^N |0\rangle \ , \tag{2.81}$$

where the operator $b_c^\dagger$ acts in the intrinsic system and is given by

$$\begin{aligned} b_c^\dagger &= (1+\beta^2)^{-1/2}\{s^\dagger + \beta[\cos\gamma(d_0^\dagger) \\ &\qquad + \sqrt{1}/2 \sin\gamma(d_2^\dagger + d_{-2}^\dagger)]\} \\ &= (1+\beta^2)^{-1/2}(s^\dagger + \beta d_0^\dagger) \quad \text{for } \gamma = 0 \ . \end{aligned} \tag{2.82}$$

The origin of the factorial in the denominator on the right-hand side of Eq. (2.81) can be seen by considering the result of repeated applications of Eq. (2.16), namely,

$$(b_N^\dagger)^N \mid 0\rangle = \sqrt{N!}\mid N\beta\gamma\rangle \ ,$$

while the factor $(1+\beta^2)^{-1/2}$ in Eq. (2.82) arises from the requirement that the states be properly normalized. Ginocchio and Kirson (1980a, 1980b) have shown that this is indeed an intrinsic state for the IBA, valid for all $N$ values, in the sense that the entire basis spanned by the IBA can be projected out from it.

The form of this intrinsic state, and the use of the notation $\beta$ for the coefficient of the $d_0$ term, can be made plausible by noting that the IBA ground state in U(5) has $n_d=0$, while $\langle n_d\rangle \gg 0$ in the deformed SU(3) limit. For $\gamma=0$ the number of $d$ bosons in the intrinsic state, and hence, by analogy, the deformation, is clearly controlled by the magnitude of the coefficient of $d_0$. This coefficient is then reasonably called $\beta$. It has been shown that the quantity $\beta$, in an intrinsic state that has a well-defined quadrupole moment and that minimizes the quadrupole-quadrupole interaction (i.e., the ground-state energy of a CQF Hamiltonian), is given by the condition (Ginocchio and Kirson, 1980b)

$$\beta=\beta_0=\tfrac{1}{2}(-\sqrt{2/7}\chi\pm\sqrt{(2/7)\chi^2+4}) \ , \tag{2.83}$$

where the $\pm$ signs are for $\chi>0$ and $\chi<0$, respectively. The minimum occurs for $\gamma=0$ (prolate) if $\chi<0$ and $\gamma=\pi/3$ (oblate) if $\chi>0$. For $\chi=0$, the interaction energy is independent of $\gamma$. These results are valid to order $1/N$ for any CQF Hamiltonian and thus include the O(6) and SU(3) limits, as well as intermediate situations. In particular, for SU(3), $\chi=-\sqrt{7}/2$ and $\beta_0=\sqrt{2}$, and, for O(6), where $\chi=0$, Eq. (2.83) gives $\beta_0=1$. It is evident that $\beta_0$ is much larger than the typical $\beta$ values of the Bohr-Mottelson (BM) model. However, in the latter approach $\beta$ refers to the deformation of all $A$ nucleons, while the IBA describes only the $2N$ valence nucleons. Ginocchio and Kirson (1980b) have obtained the approximate relationship $\beta_{\rm BM}\approx 1.18(2N/A)\beta_{\rm IBA}$. The fact that $\beta_{\rm IBA}\gg\beta_{\rm geom}$ has the important consequence that the role of anharmonic terms in the Hamiltonian is far more critical in the IBA than in the Bohr-Mottelson approach.

The expression for the minimization condition for $\chi<0$, $\gamma=0$ to next order in $N$ is (Ginocchio and Kirson, 1980b)

$$\beta_1=\beta_0-\frac{(\chi^2-4)(\sqrt{2/7}\chi\beta_0-2)}{2N\beta_0(\frac{2}{7}\chi^2+4)}+O(1/N^2) \ , \tag{2.84}$$

where $\beta_0$ is given by Eq. (2.83). Clearly, $\beta_1\to\beta_0$ for $N\to\infty$, but contains significant correction terms for realistic $N$ values. Specifically one has

$$\beta_1({\rm O}(6))\approx 1-1/N \ , \tag{2.85}$$

$$\beta_1({\rm SU}(3))\approx\sqrt{2}(1-3/8N) \ . \tag{2.86}$$

Thus far, the analysis has concerned an IBA Hamiltonian which contains only a $Q^2$ term. In the more general case, of course, the intrinsic state will not be an eigenstate of the quadrupole operator, and thus a different approach is necessary. Dieperink, Scholten, and Iachello (1980), Ginocchio and Kirson (1980a, 1980b), and Van Isacker and Chen (1981) have all approached this question by constructing an energy surface corresponding to a general IBA Hamiltonian. By Gilmore's algorithm this gives an upper bound to the exact ground-state energy and approaches it as $N\to\infty$. By studying the minima in this energy surface as functions of the parameters of the IBA Hamiltonian, one can derive the associated geometrical shape. A general expression for this energy surface, as a function of $\beta$ and $\gamma$, stated in terms of the Hamiltonian of Eq. (2.4), is given by (Van Isacker and Chen, 1981; Iachello and Arima, 1987)

$$E(N,\beta,\gamma)=\frac{N\varepsilon_d\beta^2}{1+\beta^2}+\frac{N(N-1)}{(1+\beta^2)^2}(\alpha_1\beta^4+\alpha_2\beta^3\cos3\gamma+\alpha_3\beta^2+\alpha_4) \ , \tag{2.87}$$

where the $\alpha_i$'s are simply related to the coefficients $C_2$, $v_2$, $v_0$, $u_2$, and $u_0$. One notes that $\gamma$ occurs only in the term in $\cos3\gamma$, and thus, as before, the energy surface has minima only at $\gamma=0°$ and 60°. No asymmetric minima occur; for these one would need to introduce higher-order interactions such as cubic terms. By choosing coefficients corresponding to the different IBA symmetries one can display energy surfaces for each. The situation is unfortunately rather confusing at this point because, as we have noted, different authors use different definitions of the coefficients in the IBA Hamiltonian and because it is possible to construct the three IBA limits with different Hamiltonians. For example, the O(6) limit may be obtained with a Hamiltonian $H=a_0P^\dagger P$ or with the CQF Hamiltonian, $H=a_2Q^2$ with $\chi=0$. Similarly, in each limit one may also include an $\hat{L}^2$ term. Rather general forms for the energy expressions in the three limits have been given by Arima and Iachello (1981) using the Hamiltonian of Van Isacker and Chen (1981). Simpler expressions, which display the essential dependence on $\beta$ and $\gamma$, have been given by Dieperink, Scholten, and Iachello (1980), who obtain

$$E(N,\beta,\gamma)=\varepsilon_d N\frac{\beta^2}{1+\beta^2}, \quad {\rm U}(5) \ , \tag{2.88}$$

$$E(N,\beta,\gamma)=\kappa N(N-1)\frac{1+\frac{3}{4}\beta^4-\sqrt{2}\beta^3\cos3\gamma}{(1+\beta^2)^2}, \quad {\rm SU}(3) \ , \tag{2.89}$$

$$E(N,\beta,\gamma)=\kappa' N(N-1)\left[\frac{1-\beta^2}{1+\beta^2}\right]^2, \quad {\rm O}(6) \ , \tag{2.90}$$

where $\kappa\propto a_2$ and $\kappa'\propto a_0$ in Eq. (2.5). These expressions give (for large $N$) $\beta_{\rm min}=0$, $\sqrt{2}$, and 1 for U(5), SU(3), and O(6), respectively, as was found previously.

Finally, another way of seeing the same results is by considering the structure of the wave functions themselves in the three limits. These have been obtained by Ginocchio and Kirson (1980a) and are given by the following expressions (for large $N$):

$$\Psi \approx \beta^{n_d} e^{-1/2N\beta^2}, \quad \mathrm{U}(5)\ , \tag{2.91}$$

$$\Psi \approx e^{-1/2N[(\sqrt{2}-\beta)^2+\gamma^2]}, \quad \mathrm{SU}(3)\ , \tag{2.92}$$

$$\Psi \approx e^{-N(1-\beta)^2}, \quad \mathrm{O}(6)\ . \tag{2.93}$$

Clearly, in U(5) the energy minimum for the ground state, where $n_d=0$, corresponds to $\beta=0$, while in O(6) the minimum is at $\beta=1$, and in SU(3) at $\beta=\sqrt{2}$. It is also clear that, as $N$ increases, the wave functions become more and more localized in $\beta$ and, for SU(3), in $\gamma$. These features are illustrated in Fig. 32, in which $|\Psi|$ is plotted against $\beta$ for each limit for $N$ values of 6 and 16.

Thus, to recapitulate, via the intrinsic-state formalism, one obtains a geometrical picture of the IBA in which U(5) corresponds to a spherical anharmonic vibrator [note that it is also trivially $\gamma$ independent, thus reflecting the earlier discussion of some similarities to O(6)], SU(3) is a deformed, axially symmetric rotor, and O(6) is also deformed but is completely $\gamma$ soft. Thus we recover exactly the geometrical picture, discussed often above, that is also apparent by analogy between the level schemes of the geometrical and IBA models.

Using the intrinsic-state formalism, one can also derive (Dieperink and Scholten, 1980) a result obtained numerically earlier and illustrated in Fig. 6, namely the expectation value $\langle n_d \rangle$ in the ground state for the different limits. The result is

$$\langle n_d \rangle = \frac{N\beta^2}{1+\beta^2}\ , \tag{2.94}$$

where $\beta$ is the equilibrium deformation value. This gives $\langle n_d \rangle = 0$ in U(5), where the ground state is the $s$-boson condensate. In O(6) and SU(3), the limiting values of $n_d/N$, as $N\to\infty$, are $\frac{1}{2}$ and $\frac{2}{3}$. Reference to the earlier result in Fig. 6 shows that the actual calculated expectation values of $n_d$ are reasonably close to these limiting values for typical $N$ values.

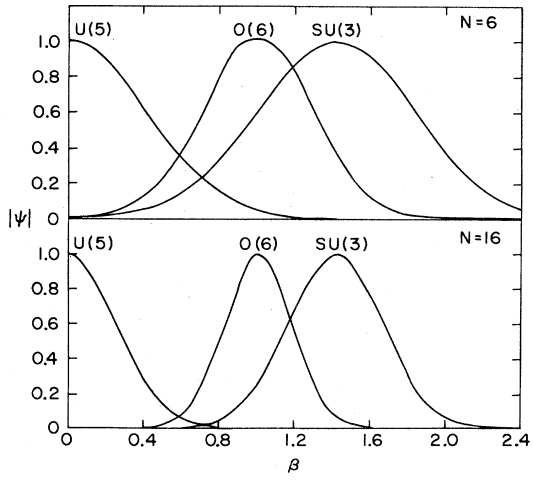


FIG. 32. Plots of $|\Psi|$ vs $\beta$ for $N=6$ and 16 for each of the three IBA-1 symmetries. From Eqs. (2.91)–(2.93).

The intrinsic-state formalism may also be used to study excited states and $E2$ transition rates. Such work has been discussed by Bijker and Dieperink (1982). Starting with the intrinsic ground-state wave function of Eq. (2.81) in the limit of large $N$, one may create $\beta$ and $\gamma$ vibrations by employing the operators (Bohr and Mottelson, 1982)

$$b_\beta^\dagger = \frac{1}{\sqrt{1+\beta^2}}(-\beta s^\dagger + d_0^\dagger)\ , \tag{2.95}$$

$$b_\gamma^\dagger = \frac{1}{\sqrt{2}}(d_2^\dagger + d_{-2}^\dagger)\ , \tag{2.96}$$

so that one of the bosons of the ground-state condensate is replaced by an appropriate combination of $s$ and $d$ bosons for the $\beta$ and $\gamma$ vibrations. It may be seen that these expressions are plausible by noting, for example, for the $\beta$ vibration, that the replacement of one condensate boson of the ground state by an orthogonal combination is analogous to the geometrical picture in which the $\beta$ vibration is formed from an orthogonal combination of the same microscopic components that comprise the ground state. Thus the $\beta$ and $\gamma$ vibrational states become (for large $N$)

$$b_\beta^\dagger b_c\,|\,g\rangle = N^{1/2}\,|\,\beta\rangle, \quad b_\gamma^\dagger b_c\,|\,g\rangle = N^{1/2}\,|\,\gamma\rangle\ , \tag{2.97}$$

$$|\,\beta\rangle = N^{-1/2} b_\beta^\dagger b_c\,|\,g\rangle\ , \tag{2.98}$$

$$|\,\gamma\rangle = N^{-1/2} b_\gamma^\dagger b_c\,|\,g\rangle\ . \tag{2.99}$$

The value of $\langle n_d \rangle$ in the $\beta$ band, for example, then is given by

$$\langle n_d \rangle_\beta = \frac{N-1}{N}\langle n_d \rangle_g + (1+\beta^2)^{-1}\ , \tag{2.100}$$

reflecting the separate contributions of the $N-1$ condensate bosons and the one $\beta$ boson. Similarly, the quadrupole moments are related by

$$Q_\beta = \frac{N-1}{N} Q_g - (1-\beta^2)^{-1}(2\beta + \sqrt{2/7}\chi)\ . \tag{2.101}$$

The dominant characteristics of the two-particle transfer operator [see Eq. (2.12)] can also be easily deduced by noting that the operator $s^\dagger$ can now be rewritten as

$$s^\dagger = (1+\beta^2)^{-1/2}(b_c^\dagger - \beta b_\beta^\dagger)\ . \tag{2.102}$$

This then yields immediately

$$\langle g, N+1\,|\,s^\dagger\,|\,g, N\rangle = \frac{(N+1)^{1/2}}{(1+\beta^2)^{1/2}}\ , \tag{2.103}$$

$$\langle \beta, N+1\,|\,s^\dagger\,|\,g, N\rangle = \frac{-\beta}{(1+\beta^2)^{1/2}}\ , \tag{2.104}$$

and hence, for the simplest form of the operator (2.12), the ratio of transfer strengths is given by

$$\frac{S_\beta}{S_g}=\frac{\beta^2}{N+1} . \tag{2.105}$$

Thus the cross section of the $\beta$ band, relative to the ground band, vanishes as $N\to\infty$, in accordance with its geometrical equivalent. Moreover, the ratio of ground-state transfer strengths in the three symmetry limits of the IBA is simply

$$\text{U(5):SU(3):O(6)}=3:1:1.5 . \tag{2.106}$$

The factor-of-3 difference between U(5) and SU(3) in Eq. (2.106) also appears in the exact expressions found in Eqs. (2.35) and (2.51).

Finally, using Eqs. (2.95) and (2.96), Bijker and Dieperink (1982) obtained the following analytic expressions, valid for large $N$, for intraband and interband $E2$ transitions involving the ground and $\beta$ and $\gamma$ bands:

$$\langle g \mid T(E2) \mid g \rangle = e_B N(1+\beta^2)^{-1}(2\beta-\sqrt{2/7}\chi\beta^2) , \tag{2.107}$$

$$\langle \beta \mid T(E2) \mid g \rangle = e_B N^{1/2}(1+\beta^2)^{-1}(1-\sqrt{2/7}\chi\beta-\beta^2) , \tag{2.108}$$

$$\langle \gamma \mid T(E2) \mid g \rangle = e_B N^{1/2}\frac{(1+\beta^2)^{-1/2}}{\sqrt{2}}(2+2\sqrt{2/7}\chi) , \tag{2.109}$$

$$\langle \gamma \mid T(E2) \mid \beta \rangle = e_B \frac{(1+\beta^2)^{-1/2}}{\sqrt{2}}(-2\beta+2\sqrt{2/7}\chi) , \tag{2.110}$$

where $\chi$ is the parameter contained in $T(E2)$. For large $N$, the relative magnitudes of these matrix elements follow the sequence $g\to g \gg \gamma\to g \gg \beta\to\gamma$, thus recovering the predictions of the Bohr-Mottelson picture in which transitions between $\beta$ and $\gamma$ bands are forbidden while intraband transitions are strongest. However, for finite $N$ and typical values of $\chi$ for deformed nuclei, these expressions also yield the important result discussed earlier that $\beta\to\gamma$ band transitions dominate $\beta\to g$ and are comparable to $\gamma\to g$ band transitions. In fact, using these expressions, one may reproduce Fig. 18, and, in particular, the interesting result is that the ratio of $\beta\to g$ transitions to $\gamma\to g$ transitions, for large $N$, equals $\frac{1}{6}$, which is very similar to the numerical value obtained by Warner and Casten (1982b). One last interesting result is that if one inserts the expression for $\beta$, in Eq. (2.83), into the expression (2.108) for the $\beta\to g$ band transitions, one finds (Warner and Casten, 1982c) that $\beta\to g$ band transitions vanish identically. This result corresponds to the CQF formalism in which $\chi$ in $T(E2)$ is made identical to $\chi$ in $Q^2$ of the Hamiltonian. In numerical calculations, small but nonzero values of the $\beta\to g$ matrix element emerge, corresponding to the neglected terms of order $1/N$ or higher in the intrinsic-state formulas.

## III. COMPARISON WITH EMPIRICAL DATA

In the above sections the basic concepts, structure, and physical interpretation of the IBA have been outlined, along with a discussion of its application to practical calculations and its relation to geometrical models. Although some comparisons with data were presented above, the purpose of the present section is a more systematic and thorough assessment of where the model stands *vis-à-vis* the experimental facts of low-energy nuclear excitations. A convenient way to view this comparison is in terms of the symmetry triangle of Fig. 12, the essential features of which are the three symmetries or limits and three transition legs linking them. Each of these six features has been discussed above in terms of the parametrization of the IBA-1 Hamiltonian and in terms of the appropriate geometrical analogs.

### A. Symmetries

When the IBA was first proposed it was thought that many examples of the U(5) and SU(3) limits were known, since these describe vibrational and rotational spectra. As discussed above and as will be seen below, however, the situation with respect to these two limits is more complicated than was at first appreciated. The U(5) limit is a very general anharmonic vibrator, while, in contrast, the SU(3) limit is a very specific kind of deformed rotor. The O(6) limit, on the other hand, when first presented theoretically, was viewed as a major new prediction of the model, although it has since been understood to correspond to a $\gamma$-soft potential and hence to an extension of the model of Wilets and Jean (1956). In any case, the subsequent empirical discovery of nuclei approximating an O(6) description in several regions of the nuclear chart has shown that it represents the third commonly occurring form of collective behavior in nuclei. It therefore seems appropriate to start with this limit.

#### 1. O(6)

The level structure and $E2$ selection rules for the O(6) limit were discussed earlier. The first nucleus to be identified as manifesting the O(6) symmetry was $^{196}$Pt. Its level scheme is compared to the O(6) limit for $N=6$ in Fig. 33 (Cizewski *et al.*, 1978). The eigenvalue expression for the O(6) limit, Eq. (2.57), contains three parameters denoted $A$, $B$, and $C$. $A$ controls the separation between states belonging to different $\sigma$ families, $B$ controls the spacing between different $\tau$ values, and $C$ relates to the degeneracy splitting within a $\tau$ multiplet. There are several ways of choosing these parameters in fitting actual spectra. In Fig. 33, a fit that optimizes the overall comparison is shown, although it will become apparent later than an alternate one in which $B$ is chosen to fit the $0^+$ $\tau=3^+$ level at 1422 keV may be more useful. The figure shows, first, that there is a one-to-one correspondence between predicted and empirical levels. This ex-

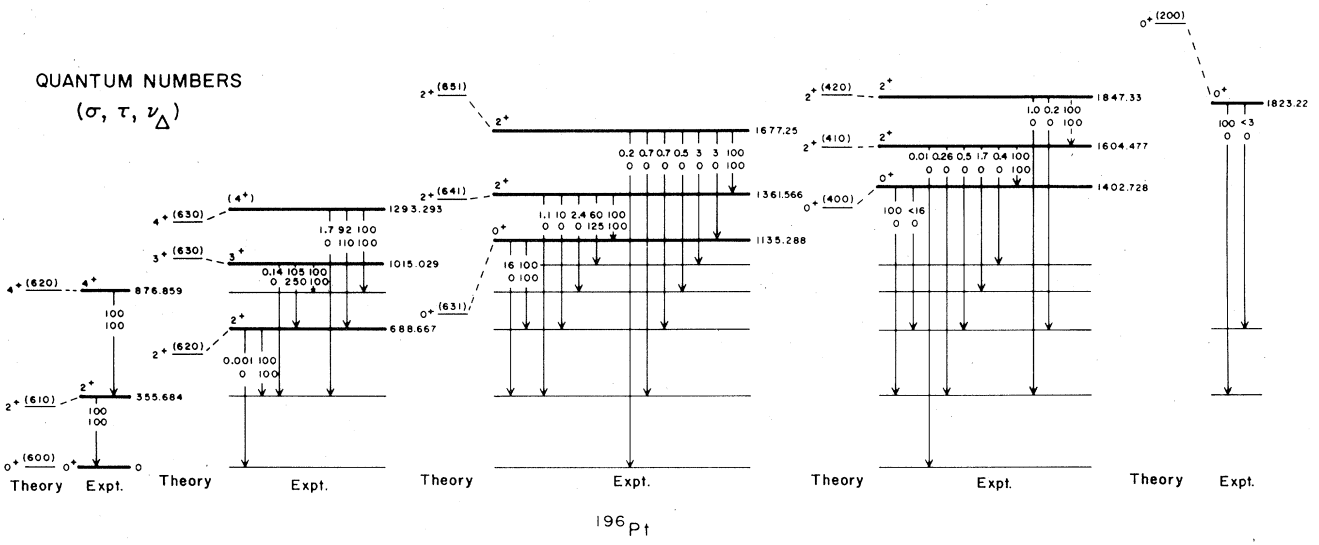


FIG. 33. Comparison of the predictions of the O(6) limit with the empirical level scheme for $^{196}$Pt. The upper numbers on the transition arrows are the empirical relative $B(E2)$ values, and the lower set gives the O(6) predictions. From Cizewski *et al.* (1978).

tends through the complete $\tau=3$ multiplet for the $\sigma=N$ family and includes levels of two $\sigma<N$ families as well. This latter result is particularly crucial, as will be seen, and, among known O(6)-like nuclei, is still unique. Three examples of the characteristic O(6) sequences of $0^+$-$2^+$-$2^+$ levels with cascading connecting $E2$ transitions are seen in Fig. 33, namely, for the quasi-ground-band, for the levels related to the $0^+(\tau=3)$ level, and for the lowest levels of the $\sigma=N-2=4$ representation.

As noted, the O(6) limit is analogous to the geometric model of a $\gamma$-unstable rotor, and thus has the typical $2^+$, $(3^+,4^+)$, $(5^+,6^+)$, ... $\gamma$-band energy staggering of a $\gamma$-soft potential. This is opposite to the staggering in the rigidly asymmetric rotor model of Davydov and Filippov (1958) for $\gamma=30°$, and this is in fact one of the few practical empirical distinctions between these two types of asymmetric rotors. The levels of $^{196}$Pt display the predicted staggering, as can be seen by comparing Figs. 8 and 33, although, as discussed in more detail below, not to the extent predicted by a completely $\gamma$-flat potential.

It will be noted that, despite the one-to-one correspondence of theoretical and empirical levels, there are severe energy discrepancies. Of particular note is the large predicted spacing between high $\tau$ states [due to the $\tau(\tau+3)$ dependence], which is contrary to experiment, as well as the fact that, empirically, $E_{0_2^+}$ is not less than $E_{3_1^+}$ as is mandated in O(6) by the monotonic dependence of energies on spin within a $\tau$ multiplet. These discrepancies are also related to the question of $\gamma$ softness and will be dealt with below. First, it is important to test further the basic O(6) predictions, since the one-to-one level correspondence, in the absence of other data, does not necessarily imply a structural correspondence.

The most crucial available structure indicators are $E2$ branching ratios and absolute $B(E2)$ values. In Fig. 33, the relative $B(E2)$ values are indicated on the transition arrows and compared with the predictions of the O(6) limit. It is seen that all allowed transitions are observed and represent strong branches and that all forbidden transitions are either weak or unobserved. In addition many of the detailed branching ratios are close to the predicted values. A comment on the decay of the $0^+$ bandheads of the $\sigma<N$ families is necessary. According to the $\Delta\sigma=0$ selection rule these levels cannot, in principle, decay by $E2$ transitions. Of course, they must decay, and do so by a small amount of symmetry breaking. As mentioned earlier, the $\sigma$ selection rule arises from an exact cancellation of the many nonzero terms contributing to the total $E2$ matrix element. This rule is therefore in principle expected to be weaker than the $\tau$ selection rule, for which each individual term vanishes. Thus the $0^+$ bandheads of the $\sigma<N$ groups would be expected, *a priori,* to decay to the $2_1^+$, $\tau=1$ member of the ground-state band rather than the $2_2^+$, $\tau=2$ state. Empirically, this is indeed the case.

While the agreement with the O(6) predictions shown in Fig. 33 is impressive, the earlier caveats about U(5) are relevant and, indeed, have been the object of recent studies (Fewell *et al.*, 1985; Fewell, 1986; Casten and Cizewski, 1987). It is therefore worthwhile to compare specifically both symmetries with the data for $^{196}$Pt for the two most crucial observables, absolute $B(E2)$ values and $E2$ branching ratios from $\sigma<\sigma_{\max}$ states. The data (Bolotin *et al.*, 1981; Raman *et al.*, 1987) for the former are shown in Table IV. The effects of the different $\langle n_d \rangle$ values in U(5) and O(6) discussed earlier clearly show up in the different predicted $B(E2)$ values, and the O(6) set is equally clearly in better agreement with the data in

TABLE IV. Comparison of absolute $B(E2)$ values in $^{196}$Pt with O(6) and U(5) predictions. All values are $e^2b^2$. From Casten and Cizewski (1987).

| $I_i \rightarrow I_f$ | Expt.[a] | O(6)[b] | U(5)[b] |
|---|---|---|---|
| $2_1 \rightarrow 0_1$ | 0.276±0.001 | 0.276 | 0.276 |
| $2_2 \rightarrow 0_1$ | $<2\times10^{-6}$ | 0 | 0 |
| $2_2 \rightarrow 2_1$ | 0.34 ±0.03 | 0.36 | 0.46 |
| $4_1 \rightarrow 2_1$ | 0.38 ±0.03 | 0.36 | 0.46 |
| $0_2 \rightarrow 2_1$ | 0.021±0.01 | 0 | 0 |
| $0_2 \rightarrow 2_2$ | 0.14 ±0.07 | 0.36 | 0.56 |
| $4_2 \rightarrow 2_1$ | 0.003±0.001 | 0 | 0 |
| $4_2 \rightarrow 2_2$ | 0.17 ±0.03 | 0.19 | 0.29 |
| $4_2 \rightarrow 3_1$ | <0.06 | 0 | 0 |
| $4_2 \rightarrow 4_1$ | 0.18 ±0.09 | 0.18 | 0.26 |
| $6_1 \rightarrow 4_1$ | 0.40 ±0.11 | 0.36 | 0.56 |

[a]Taken from Cizewski *et al.* (1978) and Bolotin *et al.* (1981) with a normalization to the recent, highly accurate, $B(E2{:}2_1^+ \rightarrow 0_1^+)$ value of Fewell (1986) and Fewell *et al.* (1985).
[b]Normalized to the $2_1^+ \rightarrow 0_1^+$ transition.

every case where O(6) and U(5) differ.

For $E2$ branching ratios, there are two $\sigma < \sigma_{max}$ states, the $2^+$ levels at 1604 and 1847 keV, that can be used. The results for the former are shown in Fig. 34. The preference for the O(6) scheme is clear.

There is, however, a major discrepancy. The O(6) symmetry predicts vanishing quadrupole moments (they correspond to $\Delta\tau=0$ $E2$ matrix elements). Fairly large values, however, have been reported (Fewell *et al.*, 1985) for $^{196}$Pt. This is clearly a current failing of the model, which, though improved, is not satisfactorily overcome by resorting to IBA-2 calculations.

The data for the other even Pt isotopes is substantial (but less complete than for $^{196}$Pt) and fully supports the O(6) interpretation. Of particular interest, since it links the region, is the sequence of $(p,t)$ and $(t,p)$ ground-state cross sections whose $N$ dependence was shown earlier also to be a clear reflection of the different structure of U(5) and O(6) wave functions. The data are compared to these predictions in Fig. 34 and, again, support the O(6) scheme.

For many years it was suspected (Arima and Iachello, 1979), both on microscopic grounds and from the sparse data that did exist, that the proton-particle, neutron-hole nuclei around $A=130$, especially the Ba isotopes, might be another O(6) region. The possibility of O(6) structure in this region has also been discussed by Maino and Ventura (1982a) for Nd and, less convincingly, for $^{124}$Te, by Robinson, Hamilton, and Snelling (1983). Recently, however, extensive new $(\alpha,n\gamma)$ and heavy-ion data, taken by the Köln group of von Brentano and co-workers, has been used to show (Casten and von Brentano, 1985) that there is indeed a very extensive region of near-O(6) nuclei in the Ba and Xe isotopes. In its extent this region is in fact a better example of O(6) than the Pt isotopes. In addition, a number of $\tau=4$ states are identified (indeed the complete multiplet in $^{128}$Xe). On the other hand, fewer $\sigma < N$ levels are assigned. A summary of the comparison of these nuclei with the O(6) limit is shown in Fig. 35. As with $^{196}$Pt, it has also recently been shown (Gelberg and von Brentano, 1987) that absolute $B(E2)$ values in this region favor O(6) over U(5).

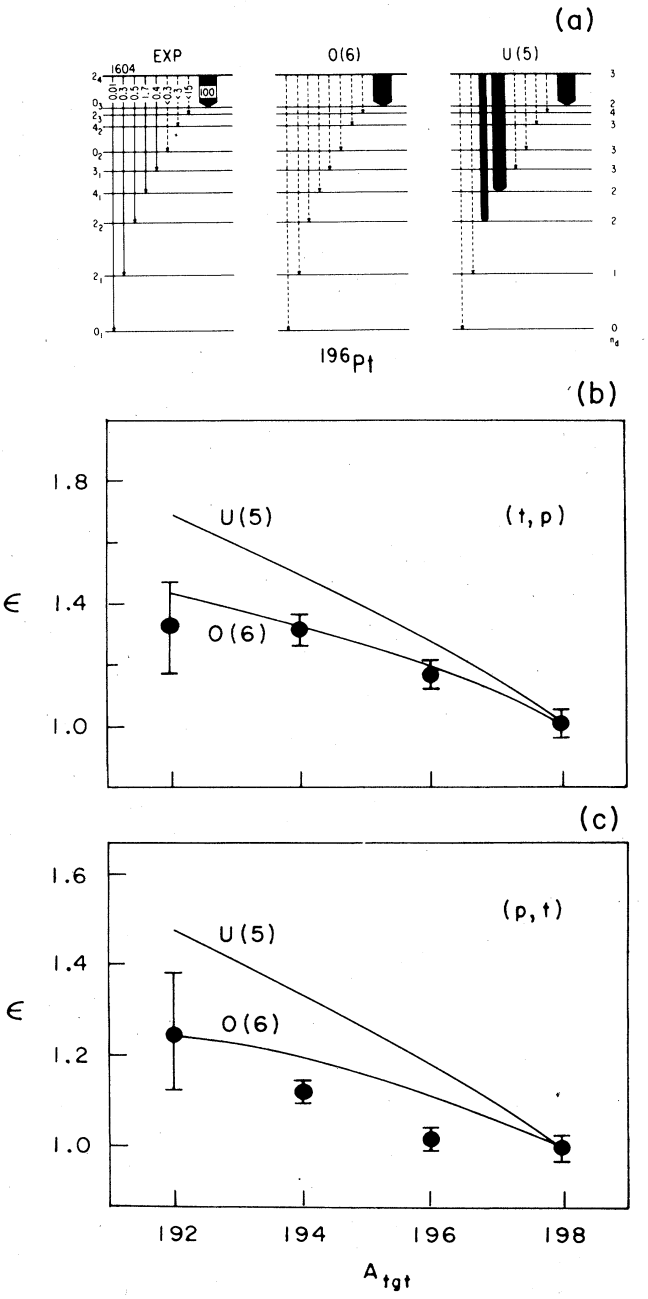


FIG. 34. Comparison of O(6) and U(5) predictions. (a) Branching ratios for the decay of a $\sigma < N$ level in $^{196}$Pt compared with O(6) and U(5) predictions. The widths of the transition arrows are relative $B(E2)$ values. Forbidden or experimentally unobserved transitions are dashed. From Casten and Cizewski (1987). (b) and (c) Enhancement factors for $(t,p)$ and $(p,t)$ in the U(5) and O(6) limits compared to the empirical data. Based on Cizewski *et al.* (1979, 1981).

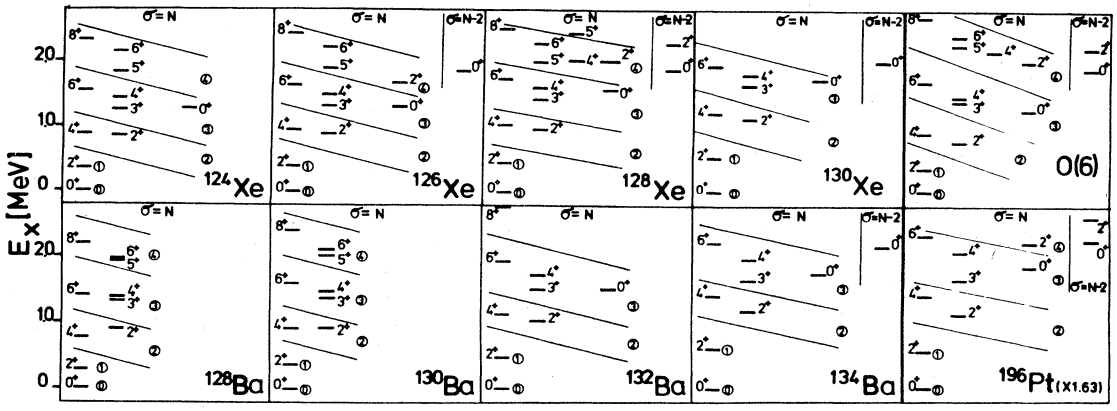


FIG. 35. Comparison of the low-lying levels of several Xe and Ba nuclei with the O(6) limit and also with a scaled level scheme for $^{196}$Pt. The O(6) parameters for Eq. (2.57) are $A=67$ keV, $B=70$ keV, and $c=10$ keV for $N=6$. From Casten, von Brentano, and Haque (1985).

The quadrupole moment problem in $^{196}$Pt and the observation of weak but finite strengths for some forbidden $\Delta\tau=0,2$ transitions, both in $^{196}$Pt and in the $A=130$ region, has led Van Isacker (1987) to consider the effects of a generalized $E2$ operator for O(6)-like nuclei in which the $\chi(d^\dagger d)^{(2)}$ term is nonzero. Such an operator permits at least small values for such normally forbidden moments. Since the two terms in $T(E2)$ connect different basis states, the predictions for the forbidden transitions form a completely independent set. Indeed, ratios of these, such as $Q_{2_1^+}/B(E2{:}2_2^+\rightarrow 0_1^+)$, are parameter independent (including $\chi$). Van Isacker compares these predictions with the data for $^{196}$Pt and $^{134}$Ba. Rather good agreement for several transitions and the above ratio are obtained for $^{134}$Ba. For $^{196}$Pt, some improvement also occurs, but discrepancies for some of the detailed strengths of these forbidden but weakly observed transitions remain.

It is interesting to note the striking similarities between the $A=130$ region and $^{196}$Pt, which is also shown in Fig. 35, with energies scaled by a factor 1.63 to make them comparable. (This factor is roughly consistent with the expected dependence of energy scales on mass.) One finds nearly identical $B$ and $C$ parameters. The ratio $A/B$ is also particularly interesting. It may be recalled that the CQF predicts a specific form of the O(6) limit in which there is an inherent relation between the degeneracy splitting of the O(6) and O(5) steps in the U(6) chain decomposition such that $A=B$. The ratio $A/B$ can be extracted from the empirical spacings by using the relation

$$R=\frac{A}{B}=\left[\frac{E_{0^+}(\sigma=N-2)}{E_{2_2^+}(\tau=2)-E_{2_1^+}(\tau=1)}\right]\frac{3}{2(N+1)}\ , \qquad (3.1)$$

which follows from Eq. (2.57). The $A/B$ values for $^{196}$Pt and the $A=130$ region are listed in Table V. Recalling that this ratio may take on any value whatsoever in the O(6) symmetry, the observed near constancy of $A/B$ for nuclei far separated in mass and occupying different major shells, as well as the closeness to the CQF value, suggests a deeper underlying significance.

The table shows another interesting result. Suppose that nuclei actually tending toward SU(3) were misassigned an O(6) character. The energy ratio $E_{0_2^+}/(E_{2_2^+}-E_{2_1^+})$ in Eq. (3.1), which is given by $\frac{2}{3}(N+1)$ in the CQF for the O(6) limit, is unity in SU(3), where the $0_2^+$ level is the $\beta$ bandhead. This gives the result $R=1.5/(N+1)$, which yields, for example, a value of 0.17 for $N=8$. The beginning of a decrease towards such values is apparent in the table and reflects an incipient trend toward deformed character in the lighter nuclei. Recent Daresbury data (Varley *et al.*, 1985) on the extremely neutron-deficient Nd and Ce nuclei in this same region have indeed confirmed the onset of such a phase transition.

The similarity of the $A=130$ and Pt regions runs even

TABLE V. Empirical and theoretical values of the ratio $R=A/B$ as given in Eq. (3.1).

| Nucleus | CQF[a] | $^{196}$Pt | $^{134}$Ba | $^{130}$Xe | $^{128}$Xe | $^{126}$Xe |
|---|---|---|---|---|---|---|
| $A/B$ | 1.0 | 0.90 | 0.96 | 0.86 | 0.76 | 0.67 |

[a]This ratio may take any value whatsoever in the general O(6) limit of the IBA, but is always unity in the consistent-$Q$ formalism (CQF).

deeper than noted above, extending even to the discrepancies with the O(6) limit. As noted earlier, the energies of states within a $\tau$ multiplet must be monotonic with $L$. Thus, if $E_{4_2^+} < E_{6_1^+}$ (as is common), then $E_{0_2^+}$ must be $< E_{3_1^+}$. In both Pt and the $A=130$ region this prediction is violated. Moreover, in both regions the energy staggering in the $\gamma$ band is less extreme than is predicted by the O(6) limit if $C$ is fixed from other spacings that are insensitive to the details of the potential in the $\gamma$ degree of freedom. Finally, the smaller-than-predicted spacing between high $\tau$ states (e.g., the $\tau=3$-4-5, $0^+$-$2^+$-$2^+$ sequence in Fig. 33) is also observed in the $A=130$ region.

It will be recalled that the rigid triaxial rotor model of Davydov and co-workers (Davydov and Filippov, 1958) also displays a $\gamma$-band staggering, but of exactly the opposite sequencing: in the O(6) limit the $\gamma$-band levels are grouped as $2^+,(3^+,4^+),(5^+,6^+),\ldots$ whereas in the rigid triaxial rotor model for $\gamma=30°$ the sequence for low $L$ is $(2^+,3^+)(4^+,5^+),\ldots$ (the staggering changes sign for higher spins). The empirical spectra of Pt and the $A=130$ nuclei show an intermediate situation between these two extremes, with little staggering suggesting that the addition of a small triaxial term to the completely $\gamma$-independent potential of the O(6) limit might induce an appropriate correction to the energy staggering. This can be conveniently done with a term, introduced by Heyde, Van Isacker *et al.* (1984), which is cubic in $d$-boson creation and destruction operators and, geometrically, introduces a minimum in the potential at $\gamma=30°$. Such an approach is appealing, since it does not change the mean $\gamma$ characteristic of the O(6) limit, namely $\gamma_{\rm rms}=30°$, but only avoids the extreme complete $\gamma$ softness of the O(6) limit. In effect, it reduces the extent of zero-point motion around $\gamma=30°$. Such calculations have been performed (Casten, von Brentano, Heyde *et al.*, 1985), and the results, exemplified by $^{128}$Xe in Fig. 36, are in fact rather surprising. Of course, they correct the energy staggering in the $\gamma$ band as they were designed to do. However, at the same time and with the same parameter values, they also now predict that the first excited $0^+$ state is above the $3^+$ member of the $\gamma$ band, in agreement with the data. [It is interesting that this difficulty with the O(6) limit had always been ascribed to the $0^+$ level, but is now seen to be probably a secondary effect of the $\gamma$-band staggering problem itself.] More importantly, these same calculations also greatly reduce the spacing among the high $\tau$ states, in particular the $0^+$-$2^+$-$2^+$ sequence with $\tau=3$, 4, and 5. Finally, the $\tau=4$ $4^+$ level in $^{128}$Xe now falls at the correct energy as well. It should be commented that a similar calculation has also been carried out in an analytic way by Sun, Zhang, and Feng (1985), who present a diagrammatic construction of the O(6) wave functions that vividly displays their structure. It is now evident why the alternate set of initial O(6) parameter values of Fig. 36, in which the predicted and observed $0_2^+$ energies agree, may be a more appropriate choice for the $\sigma=N$ levels in $^{196}$Pt than that in Fig. 33. While this new set does not give the best fit in the pure O(6) limit, it leads to predicted energy levels in close agreement with the data when a cubic or triaxial term is added to the Hamiltonian.

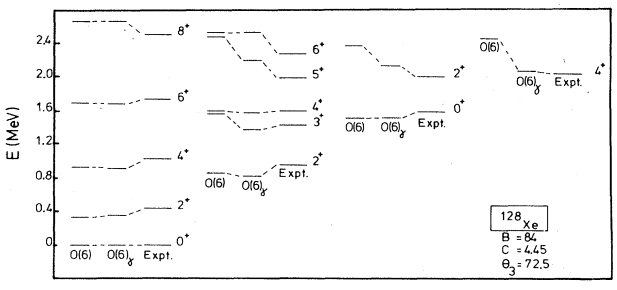


FIG. 36. Comparison of the empirical levels of $^{128}$Xe with the O(6) limit [O(6)] and with the incorporation of a cubic (triaxial) term [$O(6)_\gamma$]. The coefficients $B$, $C$, and $\theta_3$ (the coefficient of the cubic term) are in keV. From Casten *et al.* (1985).

It is interesting that the degree of triaxiality introduced into the nuclear potential is extremely small. At $\gamma=30°$, where the effect is a maximum, it amounts to only a 3–5 % change. Thus these nuclei, while not rigorously $\gamma$ independent, are nevertheless well described by potentials that are extremely $\gamma$ soft.

Finally, other regions may also display O(6) character or at least systematic tendencies toward it. Kaup and Gelberg (1979) have suggested that the Kr nuclei undergo a U(5)→O(6) transition with decreasing mass such that the lighter isotopes may well approximate O(6) character.

## 2. SU(3)

The other two limits of the IBA, and SU(3) and U(5) limits, are not nearly so well identified in actual nuclear spectra. The reasons for this will be evident shortly. We shall consider here both the SU(3) limit and the more common and general case of deformed nuclei. These are not identical, since SU(3) structure is a particular case of the deformed symmetric rotor, and, although deformed nuclei abound, the exact limiting case envisioned by this limit is not observed. Figure 37 summarizes four important signatures of the SU(3) limit and illustrates clearly why typical deformed nuclei cannot be described as SU(3) nuclei.

The first, and most striking, criterion for SU(3) stems from the fact that the $\gamma$ and $\beta$ vibrational modes belong to a different SU(3) representation than the ground band, and hence $\gamma\rightarrow g$ and $\beta\rightarrow g$ $E2$ transitions are strictly forbidden. While $\beta\rightarrow g$ transition strengths are often rather small in deformed nuclei, Fig. 16 shows that $\gamma\rightarrow g$ transitions are always significantly stronger than single-particle estimates for deformed nuclei. Hence it is clear that an exact SU(3) symmetry is never realized. Second, levels of

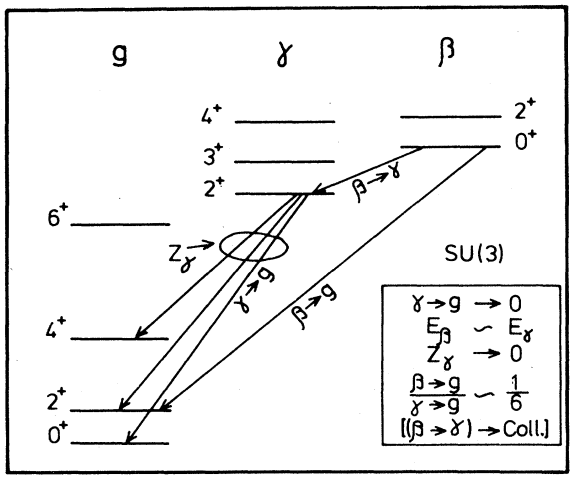


FIG. 37. Principal signatures of the SU(3) limit of the IBA. Note that the last indicated, namely, collective $\beta \rightarrow \gamma$ transitions, is preserved in the presence of considerable SU(3) symmetry breaking and thus is not specifically a signature of the rigorous SU(3) limit. From Casten, von Brentano, and Haque (1985).

equal spins in the $\beta$ and $\gamma$ rotational bands must be degenerate. Of course, in actual deformed nuclei the most common situation is $E_\beta > E_\gamma$. A third criterion is related to the fact that, empirically, $\gamma \rightarrow g$ $E2$ branching ratios usually deviate from the Alaga rules. As discussed above, it has been traditional (Lipas, 1962; Bohr and Mottelson, 1975) to describe such deviations in terms of band mixing, whose strength is specified by a band mixing parameter $Z_\gamma$. In the pure SU(3) limit there is no interaction, and no mixing, between the $\beta$ or $\gamma$ bands and the ground-state band. Thus, in SU(3), $Z_\gamma \rightarrow 0$. The fourth criterion for identifying the SU(3) symmetry stems from a peculiarity of the $E2$ matrix elements connecting $\beta$ and $\gamma$ bands to the ground-state band, which was first identified numerically by Warner and Casten (1982b) and subsequently derived analytically in a coherent-state formalism approach by Bijker and Dieperink (1982). $\beta \rightarrow g$ and $\gamma \rightarrow g$ intrinsic $E2$ matrix elements both vanish in the SU(3) limit. However, for any $\chi$ value in the $E2$ operator, including the case in which $\chi$ is arbitrarily close to $\chi_{SU(3)}$, the ratio $R_{\beta\gamma} = B(E2{:}2^+_\beta \rightarrow 0^+_g)/B(E2{:}2^+_\gamma \rightarrow 0^+_g)$ is finite and constant at a value $\approx \frac{1}{6}$. In general, most deformed nuclei do not display any of these particular SU(3) features. Occasionally, and presumably as a fortuitous consequence of evolving systematic trends, $\beta$ and $\gamma$ bands may lie close to each other or $\beta \rightarrow g / \gamma \rightarrow g$ $B(E2)$ values may approximate $\frac{1}{6}$.

It is worth noting, however, that there is one region that comes closest to displaying the four signatures cited above, namely, the rare-earth nuclei near $N = 106$, especially Yb and Hf. The data are illustrated in Fig. 38, where it is seen that, near $N = 104, 106$, the systematics of each of these four observables passes near or through the SU(3) predictions. A further expectation for an SU(3) region is that the $\beta$ and $\gamma$ bands will be rather high lying in energy since, assuming a constant coefficient $a_2$ of the $Q^2$ term in the Hamiltonian, their energies [see Eq. (2.42)] scale as $(2N-1)$, thus reaching a maximum at midshell ($N = 104$ in this case). The systematics (Sakai, 1984) of $\gamma$ vibrational energies in the second half of the rare-earth region are compared to this expected dependence in Fig. 39. The empirical trend is consistent with SU(3), although exaggerated.

Nevertheless, even in this region an unambiguous interpretation is difficult, since some of the SU(3)-like features could also occur if the quadrupole collectivity were low in this region, as has been previously suggested (Bes *et al.*, 1965; Soloviev, 1965). Then the $\beta$ and $\gamma$ bands would be rather high lying, and consequently $Z_\gamma$

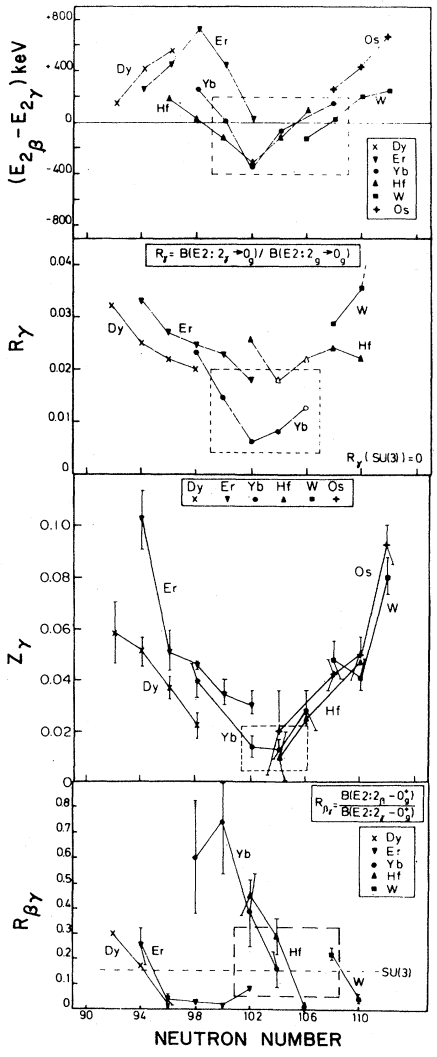


FIG. 38. Comparison of the data in the rare-earth region with the four signatures of the SU(3) limit summarized in Fig. 37. From Casten, von Brentano, and Haque (1985).

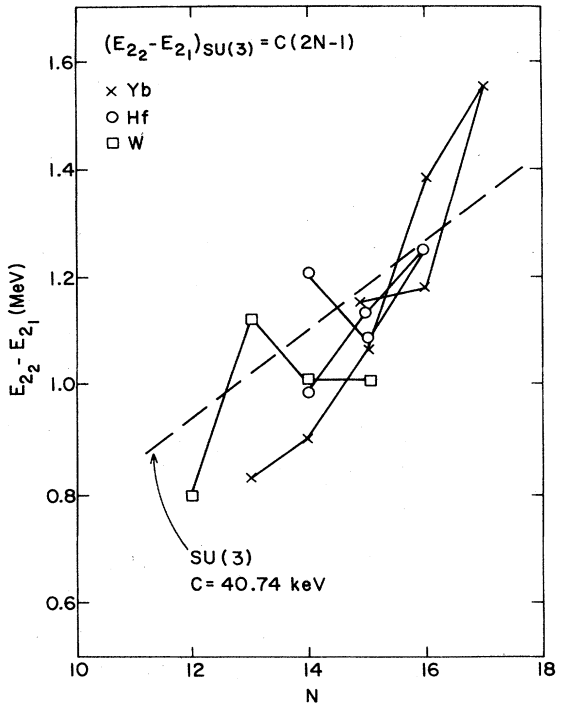


FIG. 39. Energy levels of the $\gamma$ band (relative to $E_{2_1^+}$) for nuclei in the $A=170$ region. The dashed line is the SU(3) prediction.

would be apt to be small and $\beta \rightarrow g$ and $\gamma \rightarrow g$ $B(E2)$ values would also decrease. The degeneracy of $\beta$ and $\gamma$ bands and the approximate $\frac{1}{6}$ ratio of their ground-state band $B(E2)$ values is occasionally seen elsewhere and could arise fortuitously. It is perhaps best to conclude that the status of the SU(3) symmetry in this region is not yet settled. (Indeed, the two authors of this review have rather different opinions on this issue: the phrasing above represents a major diplomatic achievement between them.) The possible applicability of the SU(3) symmetry to the actinides has also been discussed (Zhang *et al.*, 1985).

### 3. Deformed nuclei

As pointed out above, most deformed nuclei are by no means good examples of SU(3). Many of the properties of broken SU(3) calculations were discussed earlier. Here we shall confront these with some of the pertinent data, with special emphasis on the well-studied nucleus $^{168}$Er. The original IBA calculations (Warner, Casten, and Davidson, 1980, 1981) for $^{168}$Er were carried out prior to the development of the CQF and used a Hamiltonian consisting of the quadrupole, $\hat{L}^2$, and $P^\dagger P$ terms of Eq. (2.5). [Subsequent calculations (to be discussed below) in the CQF utilized the Hamiltonian of Eq. (2.74). This latter approach has one less parameter and in fact results in better agreement with the data.] The predicted and measured levels for $^{168}$Er are compared in Fig. 40. There are several essential points that should be noted. First, it is evident that the overall agreement between experiment and theory is satisfactory: the ground, $\gamma$-band, and $\beta$-band energies are well reproduced, as is the experimental sequence of higher-lying bands. However, the associated comparison of branching ratios indicates that the apparent agreement for the higher-lying $K=2$ bands is probably largely fortuitous and that, even for the second excited $K=0$ band, the IBA description gives only a semiquantitative interpretation. There is also, one clear disagreement (pointed out by Bohr and Mottelson, 1982) from the energy levels themselves. Since they are complete for low-spin states below about 1900 keV, due to the use of the $(n,\gamma)$ average resonance capture (ARC) technique, it is clear that there is no $K=4$ band below $\approx 2$ MeV, while the calculations predict a $K=4$ double $\gamma$ vibration at $\approx 1600-1700$ keV. There is no easy way to repair the IBA predictions for this band since, just as in geometrical models, where the $\gamma\gamma$ vibration is expected at $\approx 2E_\gamma$, it is difficult (Dumitrescu and Hamamoto, 1982) to introduce sufficient anharmonicity to obtain $E_{4^+} \approx 2.5E_\gamma$. It now appears likely that one must include a $g$ boson to ameliorate the situation. Further discussion of the effects of incorporating a $g$ boson into the *sd* IBA-1 formalism will be presented in Sec. IV.

This discussion raises the general issue of multiphonon states in the IBA, especially in deformed nuclei where the $(\lambda,-8,4)$ and $(\lambda-6,0)$ representations with $K=0,2,4$ and $K=0$ bands, respectively, contain intrinsic states approximating the $\gamma\gamma(K=0,4)$, $\beta\beta(K=0)$, and $\beta\gamma(K=2)$ two-phonon geometrical modes. In this respect the IBA and the Bohr-Mottelson picture are very similar, and difficulties (Dumitrescu and Hamamoto, 1982) such as those concerning the high empirical energy and implied anharmonicity of the $K=4$ band in $^{168}$Er apply equally to both. On the other hand, for years, the low-lying states of deformed nuclei have been the subject of extensive investigations in the quasiparticle phonon model of Soloviev and co-workers (see, for example, Gallagher and Soloviev, 1962; Soloviev, 1965; Soloviev and Shirikova, 1981; and, especially, Soloviev, 1986, and references therein). The basic ingredients in this model are a Woods-Saxon mean-field potential with pairing and multipole interactions treated in the random-phase approximation along with a quasiparticle-phonon coupling interaction. The predicted wave functions for nonrotational (i.e., vibrational) modes can be written in terms of linear combinations of phonon amplitudes and two-quasiparticle components. Moreover, the phonon structure itself can be expressed in terms of its two-quasiparticle components. A key result is that, because of Pauli principle effects, the model predicts that multiphonon states will not survive intact but will be highly fragmented and that the low-lying intrinsic states of deformed nuclei can be adequately described in terms of various one-phonon excitations and two-quasiparticle

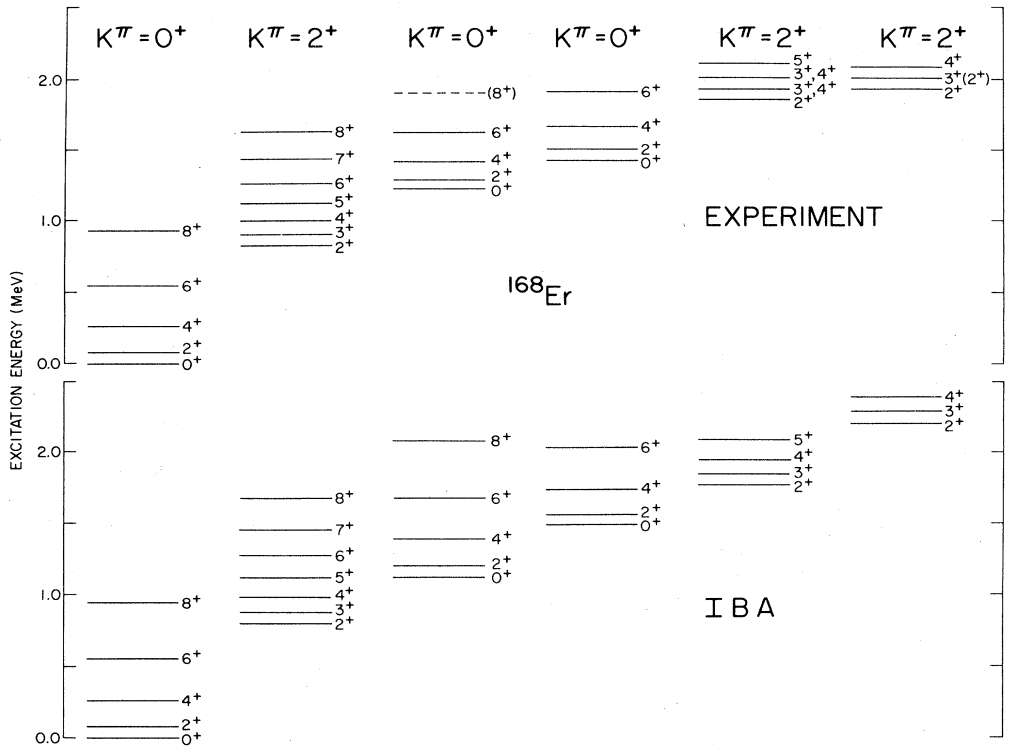


FIG. 40. Comparison of the experimental low-lying levels of $^{168}$Er with the predictions of the IBA calculations of Warner, Casten, and Davidson (1980). Note that, while all experimental levels of the low-lying $K=0,2$ bands are shown, the IBA also predicts an unobserved $K=4$ band at approximately two times the energy of the $\gamma$ band.

states. Soloviev (1986) draws out these distinctions, stressing the point that the IBA-1 includes only that portion of the full two-quasiparticle space that enters into the $\beta$ and $\gamma$ modes. Moreover, he cites qualitative arguments (mostly from single-nucleon transfer data) in support of the major predicted two-quasiparticle components throughout the rare-earth deformed region.

As assessment of this claim is difficult at present, partly because the data themselves are fragmentary (possibly this is in fact an argument in Soloviev's favor), partly because the single-nucleon transfer data that do exist can, even in principle, provide information only on certain very specific two-quasiparticle amplitudes (those in which one component is that of the odd fermion ground-state orbital in the target nucleus for the relevant reaction), and partly because recent studies by Piepenbring (1986, 1987) suggest that, in calculations incorporating a much larger multiphonon space, the two-phonon excitations can emerge more or less intact, being lowered in energy by interactions with three-phonon and higher levels. Even here, however, their predicted energies seem to be $\geq 2.5E_{2^+_\gamma}$, and thus an association with the $0^+_2$ and $2^+_2$ levels in deformed nuclei is uncertain. In any case, it is clear that any success to date in the IBA-1 description of multiphonon levels is at best qualitative and that much more work, especially experimental, in this area is needed.

As noted above, the energy levels shown in Fig. 40 were calculated using the Hamiltonian of Eq. (2.5). In the original $^{168}$Er calculations the $E2$ transition rates were calculated with an $E2$ operator of Eq. (2.8) in which $\chi$ was separately varied to fit the branching ratio $B(E2{:}2^+_\gamma \rightarrow 2^+_g)/B(E2{:}2^+_\gamma \rightarrow 0^+_g)$. The results were rather good but, as pointed out by Bohr and Mottelson (1982), there were systematic discrepancies in predicted and empirical deviations from the Alaga rules. However, the importance of these discrepancies became a moot point with the development of the CQF formalism, in which calculations of energy levels and transition rates involve one fewer parameter than the earlier calculation and yet achieve better agreement with the data. In particular, for transition rates, the $\gamma \rightarrow g$ $E2$ branching ratios are now in essentially exact agreement with the data, as shown in Table VI and, in the form of a Mikhailov plot (Mikhailov, 1966, Riedinger *et al.*, 1969), in Fig. 41. In such a plot, if data or calculations for interband transitions lie on a straight line, it implies that the deviations from the Alaga rules can be explained by simple two-band mixing whose strength is proportional to the slope. The earlier discrepancies (dashed line) are apparent, as is the fact that the newer calculations (dotted-dashed line) agree with the data to well within the experimental uncertainties. It is important to emphasize that these $\gamma \rightarrow g$ band mixing effects in the IBA are inherent in the model.

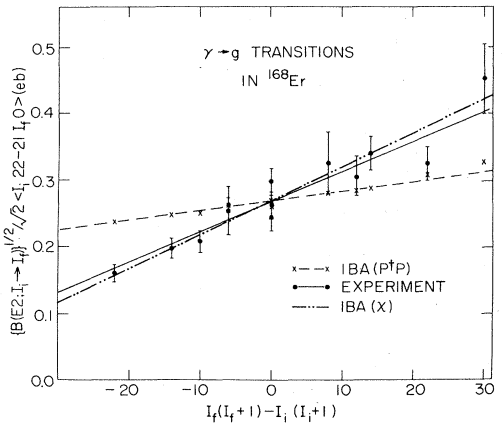


FIG. 41. Mikhailov plot for the decay of the $\gamma$ band in $^{168}$Er. The solid line is a linear least-squares fit to the data. The dashed line is the prediction of the original IBA calculations (Warner, Casten, and Davidson, 1980), while the dotted-dashed line is the CQF prediction of Warner and Casten (1982a).

The origin of $\gamma$-$g$ band mixing was discussed earlier. As shown in Fig. 19, the predicted $N$ dependence across the deformed rare-earth region can be easily reproduced by the IBA and represents, in fact, the clearest evidence for finite-$N$ effects.

It will be recalled that another central result of IBA calculations in deformed nuclei is the automatic prediction that $\beta\rightarrow g$ $B(E2)$ values are much less than $\gamma\rightarrow g$ strengths. Of course, this is also a well-known empirical feature (see Fig. 16) about which geometrical models cannot make a statement without input from microscopy.

A key feature of both the earlier and the CQF calculations, referred to on several occasions above, is the characteristic IBA prediction in deformed nuclei of strong transitions *between* the $\beta$ and $\gamma$ bands. Such transitions are forbidden in traditional harmonic models, because they violate the phonon selection rule, but are allowed and collective in the IBA because, in the parent SU(3) scheme, the $\beta$ and $\gamma$ bands occur within the same $(\lambda,\mu)$ representation. Of course, $\beta\rightarrow\gamma$ transitions can be introduced into geometrical models by $\beta$-$\gamma$ band mixing. However, as described earlier, even then, the two models are still not equivalent. The *origin* of the $\beta\rightarrow\gamma$ transitions in the IBA can be dissected with a Mikhailov plot. Such an analysis shows that they arise primarily from a direct $\Delta K=2$ $\beta\rightarrow\gamma$ matrix element and, to a much lesser extent, from $\beta$-$\gamma$ band mixing. A Mikhailov plot analysis (see the extensive discussion of this in Warner, Casten, and Davidson, 1981, and in Casten and Warner, 1983) of the empirical $B(E2{:}\beta\rightarrow\gamma)$ values shows that a direct $\Delta K=2$ matrix element dominates here as well, in agreement with the IBA prediction. It is important to emphasize that this prediction, which is inherent to the model, arises specifically as an effect of finite boson number: in the $N\rightarrow\infty$ limit $\beta\rightarrow\gamma$ transitions become negligible relative to intraband and $\beta\rightarrow g$ and $\gamma\rightarrow g$ transitions, and the IBA predictions go over into those of the traditional geometrical model.

To summarize, there are several aspects of the IBA in deformed nuclei that agree with empirical observations and that are important because they are inherent features of the model, namely, the dominance of $\gamma\rightarrow g$ over $\beta\rightarrow g$ $B(E2)$ values, the dominance of $\beta\rightarrow\gamma$ transitions over $\beta\rightarrow g$ transitions, and the automatic inclusion of an $N$ dependence of the effective band mixing and therefore of deviations from the Alaga rules.

Since the $^{168}$Er results appeared, there has been extensive study of many deformed nuclei in the IBA. These include studies of $^{178}$Hf (Haque *et al.*, 1986), $^{172,174}$Yb (Gelletly *et al.*, 1985; Gelletly, Larysz *et al.*, 1987), $^{162}$Dy (Warner *et al.*, 1987), and others. In general, they result in comparable and reasonable agreement with the data and confirm the characteristic IBA predictions discussed above. Discrepancies, of course, do occur. As a general rule the properties of $\gamma$ bands are predicted remarkably well, but significant deviations in detail (although not in gross features) appear for lowest $K=0^+$ bands. Such excitations have always been more enigmatic than their simple descriptions as $\beta$ bands would indicate. It seems that, although the IBA offers an improved characterization, there remain significant structural aspects of these states that are not understood. Mixing with nearby quasiparticle excitations may be involved in some cases (e.g., near Yb where $E_\beta$ is particularly high), but an IBA formalism that simply includes such degrees of freedom is not yet available, although initial efforts in this direction have been made and will be mentioned in Sec. IV.

TABLE VI. Relative $B(E2)$ values from the $\gamma$ band in $^{168}$Er. The IBA calculations utilized the consistent-$Q$ formalism and correspond to the dotted-dashed line in the Mikhailov plot of Fig. 41. Based on Warner and Casten (1982a, 1983).

| $I_i$ | $I_f,K_f$ | Expt. | IBA |
|---|---|---|---|
| 2 | 0,0 | 54.0 | 54 |
| | 2,0 | 100 | 100 |
| | 4,0 | 6.8 | 7.6 |
| 3 | 2,0 | 2.6 | 2.6 |
| | 4,0 | 1.7 | 1.8 |
| | 2,2 | 100 | 100 |
| 4 | 2,0 | 1.6 | 1.7 |
| | 4,0 | 8.1 | 9.6 |
| | 6,0 | 1.1 | 1.5 |
| | 2,2 | 100 | 100 |
| 5 | 4,0 | 2.9 | 3.5 |
| | 6,0 | 3.6 | 4.4 |
| | 3,2 | 100 | 100 |
| | 4,2 | 122 | 95 |
| 6 | 4,0 | 0.44 | 0.44 |
| | 6,0 | 3.8 | 4.9 |
| | 8,0 | 1.4 | 1.0 |
| | 4,2 | 100 | 100 |
| | 5,2 | 69 | 57 |
| 7 | 6,0 | 0.7 | 1.9 |
| | 5,2 | 100 | 100 |
| | 6,2 | 59 | 36 |

### 4. U(5)

The U(5) symmetry offers a description of a vibrational nucleus that can encompass an extremely broad range of anharmonicities. This has been alluded to above in commenting that the U(5) eigenvalue expression is even capable of generating O(6)-like sequences, at least for the $\sigma = N$ family of states. It is therefore a little difficult to discuss whether or not true U(5) nuclei have indeed been observed. In this review such considerations will be limited to the question of whether or not nuclei have been observed that are relatively harmonic expressions of U(5) resembling the traditional vibrational spectra.

Since the energy spacings in typical vibrational-like nuclei lying close to closed shells are larger than those of deformed nuclei, there is a difficulty in identifying unperturbed two- and three-phonon levels. The $2_1^+$ level in such nuclei is typically at 500–800 keV, and thus the two- and three-phonon states will be between 1 and 2.5 MeV, which is well into the region of single-particle or two-quasiparticle excitations. Moreover, in regions where vibrational character is expected, so-called intruder states, which can be described (Wenes *et al.*, 1981; Heyde *et al.*, 1982, 1985; Wood, 1984) in terms of excitations crossing a major shell gap, may descend into the low-lying region.

The Cd nuclei have long been considered (Scharff-Goldhaber and Weneser, 1955) archetypical vibrational nuclei. Unfortunately, in recent years, the above-mentioned intruder levels have been discussed and studied in considerable detail in several isotopes near $^{114}$Cd (see Mheemeed *et al.*, 1984, for the most thorough study). Indeed, at the energy of levels supposedly representing the two-phonon triplet, a set of five levels is observed with strong interconnecting $B(E2)$ values. Mheemeed *et al.* (1984) and Schreckenbach *et al.* (1982) have carried out explicit intruder-state calculations here and are able to account rather well for most of the observed properties. As a consequence of the proton-neutron interaction, the intruder levels are expected to descend in energy toward midshell (which occurs at $^{114}$Cd) and rise thereafter. Thus the heavier Cd isotopes

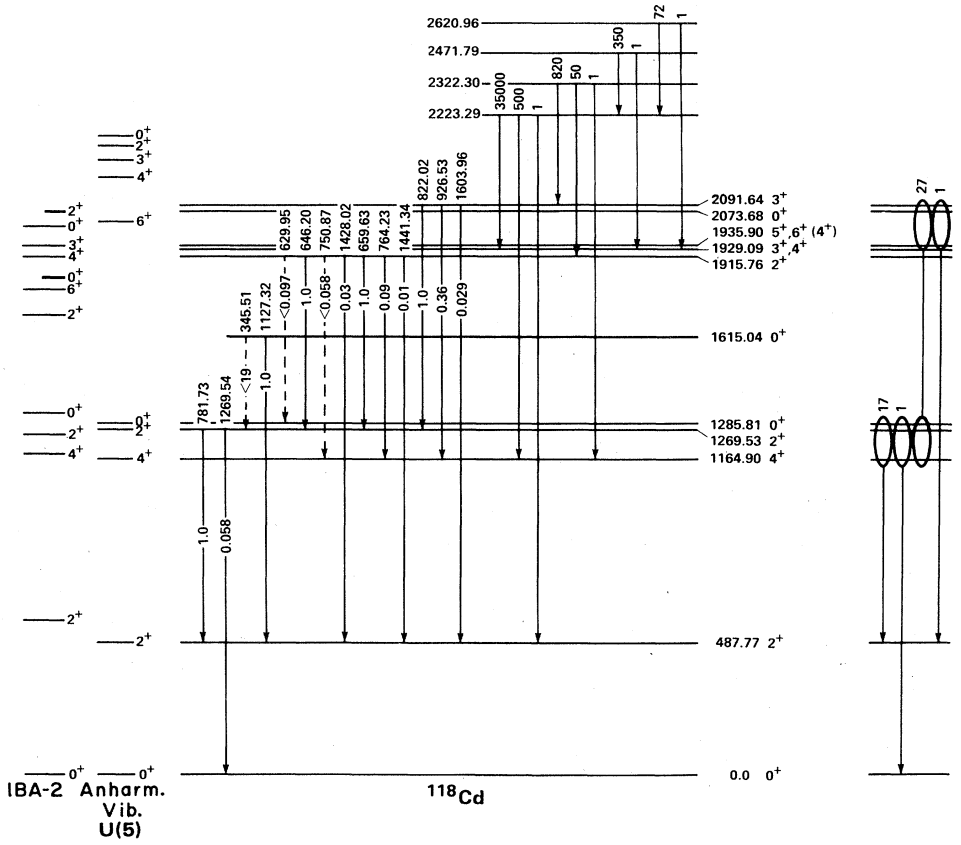


FIG. 42. Low-lying levels of $^{118}$Cd. The numbers of the transition arrows are relative $B(E2)$ values. On the far right are the averaged relative empirical $E2$ branching ratios for transitions changing the phonon number by one and two. The $0^+$ level at 1615 keV has been assigned to the intruder configuration. On the left is a comparison with the U(5) limit of the IBA, which gives the same predictions as the anharmonic vibrator model of Brink, de Toledo Piza, and Kerman (1965). IBA-2 calculations are also shown: the short horizontal bars indicate levels with calculated dominant intruder amplitudes. From Aprahamian *et al.* (1987).

might be expected to display relatively higher-lying intruder states and a more intact phonon spectrum. This has recently been confirmed in experiments by Aprahamian *et al.* 1984, 1987) on $^{118}$Cd, whose level scheme is shown in Fig. 42, where an isolated $0^+$ intruder state can be seen lying rather far from the other groupings of levels. These latter seem to represent a nearly degenerate two-phonon triplet and five levels that represent candidates for the three-phonon quintuplet. The data, however, still allow two possible spin choices for two of these latter levels, one choice of which in each case is consistent with that expected for the three-phonon quintuplet. The interesting aspect of this level scheme is the extremely close spacing among the levels assigned to both the two-phonon triplet and the three-phonon quintuplet.

The decay properties of these levels may also exhibit the selectivity expected in the vibrator: if one assumes pure $E2$ transitions, and $\chi=0$ is adopted in $T(E2)$ so that the U(5) selection rules are the same as those of the geometric vibrator model, the dominance of allowed ($\Delta N_{\rm ph}=1$) over forbidden ($\Delta N_{\rm ph}=2$) $B(E2)$ values is more than an order of magnitude for both the two-phonon triplet and the three-phonon quintuplet. The one disturbing aspect of this scheme is that no $2^+$ level decaying to the $0^+$ intruder level has been located at an appropriate energy. Based on the $0^+$-$2^+$ intruder spacings in the lighter Cd isotope, one would expect such a level near 2.1 MeV. The lowest known $2^+$ state that decays to the $0^+$ intruder level is at 2518 keV. While it is therefore possible that there is an undetected intruder level near 2 MeV, it would not appear from the decay properties to be one of those already known.

There is another feature worth noting in the level scheme of $^{118}$Cd. Above 2 MeV there is a sequence of levels extending up to 2.8 MeV which decay by a cascading set of transitions that terminate in one or another of the members of the three-phonon quintuplet. The possibility of their representing an even higher-lying multiplet structure has recently been discussed (Aprahamian *et al.*, 1987).

## B. Transition regions

An important aspect of symmetry concepts is that pairs of symmetries act as termini for nuclear transition regions, as illustrated in Fig. 12 and described earlier. Sequences of nuclei in such a phase transition can be very simply calculated, generally by the variation of a single parameter, which specifies their location along the appropriate leg of the symmetry triangle. This parameter can usually be taken as the ratio of the coefficients in the Hamiltonian characteristic of the two symmetries occupying the vertices of the triangle at the termini of the transition leg. Thus, for example, for a U(5)→SU(3) transition the relative parameter is $\varepsilon/a_2$, while for an O(6)→SU(3) transition it is the ratio of the coefficients $a_2$ and $a_0$ of the $Q^2$ and $P^\dagger P$ terms in the Hamiltonian of Eq. (2.5) or the value of $\chi$ in the CQF formalism. The first two regions to be discussed in this way were Pt-Os, which undergoes an O(6)→SU(3) transition, and Sm-Gd, which undergoes a U(5)→SU(3) transition.

### 1. O(6)→SU(3) or deformed rotor

In an O(6)→rotor transition the levels of the deformed asymmetric $\gamma$-soft rotor evolve into those of the deformed symmetric rotor, as illustrated schematically for a few levels in Fig. 43. The states of maximum spin in each $\tau$ multiplet combine to form the ground-state rotational band. The states of next lower spin become the $\gamma$ band, while the states of maximum spin for each $\tau$ value in the $\sigma=N-2$ multiplet become the $\beta$ vibrational band. The $0^+$ ($\tau=3$) state in the $\sigma=N$ representation, and the quasiband built on it, become predominantly the two-phonon $\gamma$ vibrational band with $K=0$. In the $\sigma=N$ group there is a $4^+$ state with $\tau=4$ which, in the deformed rotor, becomes the bandhead of a $K=4$ band. This band also has the properties of a double $\gamma$ vibration.

Obviously, the Pt-Os region is ideal for testing the IBA in this regard. In calculations of this transition region the pre-CQF Hamiltonian of Eq. (2.5) was used. Some results (Casten and Cizewski, 1978, 1984) are shown in Figs. 44 and 45. The essential structural changes depend only on $a_2/a_0$. It will be observed that the agreement is rather remarkable, especially considering the extreme simplicity of the calculations. One interesting feature is that they reproduce the enigmatic decay of the excited $0^+$ states where, in Pt, some decay predominantly to the $2_1^+$ state but others decay to the $2_2^+$ state, while in Os, all decay predominantly to the $2_2^+$ states. These calculations also show the gradual emergence with decreasing $A$ of branching ratios close to the Alaga rules, as opposed to those characteristic of the O(5) symmetry observed in the Pt region. The development of the quasi-$\gamma$-bands accurately reflects the empirical systematics. Careful inspec-

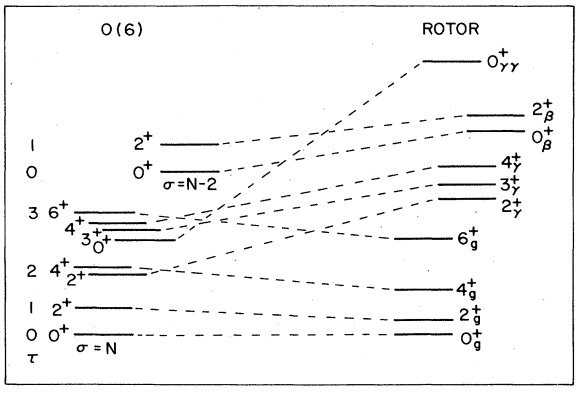


FIG. 43. Schematic indication of the relation of levels in the O(6) limit and in the deformed rotor. Note that the association of excited $0^+$ states is ambiguous and can be reversed.

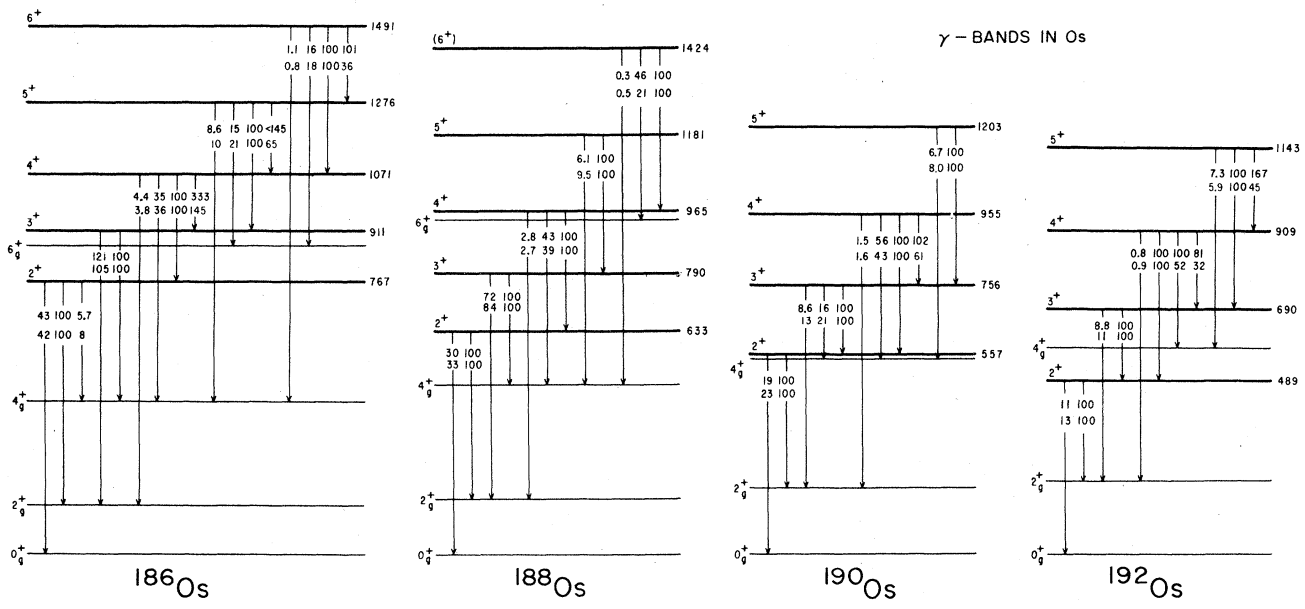


FIG. 44. Comparison of calculated and empirical relative $B(E2)$ values for the $\gamma$ bands in an O(6)→SU(3) transition region, the Os isotopes. The upper rows of numbers are the empirical relative $B(E2)$ values, while the lower rows are the calculated ones. From Casten and Cizewski (1978, 1984).

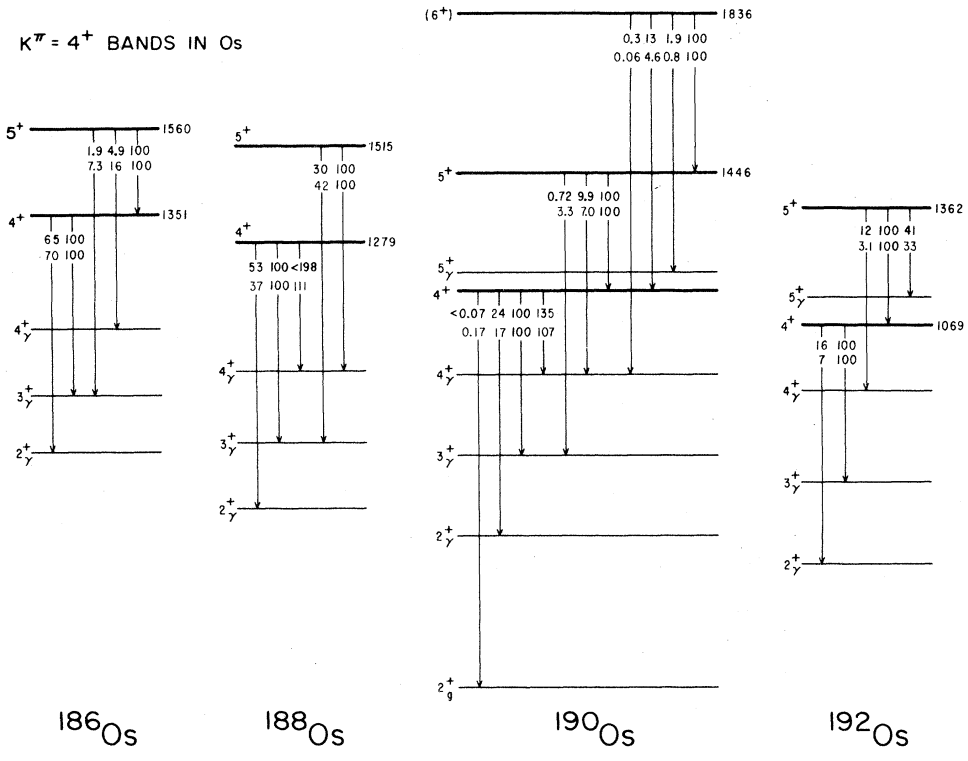


FIG. 45. Same as Fig. 44, except $K=4$ bands in Os.

tion reveals many examples of detailed agreement and few, if any, significant disagreements. The properties of the $K=4$ bands in Os are particularly important. They are a characteristic feature of all the even-even Os isotopes and occur consistently near 1.1 MeV. Their observed properties are extremely well reproduced.

An interesting and as yet unresolved point arises here. There has long been much discussion of the possible role of a $g$ boson in the IBA (see Sec. IV). If such a higher-angular-momentum boson is important, its effects should be revealed, among other places, in the presence of collective $K=4$ excitations in deformed nuclei. They would be analogous to hexadecapole vibrations in traditional geometrical models. Bagnell *et al.* (1977, 1979) have indeed shown that the dominant two-quasiparticle amplitudes observed in $(t,\alpha)$ transfer reactions leading to the relevant $4^+$ states in Os nuclei are exactly those which would be important in such a hexadecapole vibration. They concluded that these states were admixtures both of double $\gamma$ vibrational excitations (that is, in IBA language, $K=4$ bands in the $s$-$d$ boson space) and hexadecapole vibrations and, moreover, that the collective $E2$ properties of these levels are dominated by their double $\gamma$ vibrational character, while the transfer reaction properties were dominated by the two-quasiparticle hexadecapole amplitudes. Very recently, Baker (1985) has shown that a consistent calculation of all the electromagnetic properties ($E2$ and $E4$) can be obtained by carrying out an IBA calculation involving $s$, $d$, and $g$ bosons. While these results look convincing, Morrison (1986) has pointed out that a proper accounting of the effects of the Pauli principle on the mass dependence of the $T(E4)$ operator itself is at least as significant as the introduction of a $g$ boson in reproducing the systematic trends in $E4$ excitation modes. While the issue thus remains unresolved, the agreement shown in Figs. 44 and 45 for the $E2$ decay properties calculated in the IBA-1 remains undeniable.

The further development of the collective aspects of the deformed symmetric rotor as one goes to the $W$ isotopes has not been calculated in detail in the IBA-1 (but see the IBA-2 calculations of Duval and Barrett, 1981b), but the CQF calculations discussed in Sec. II indicate that this phase transition continues smoothly into the region near midshell.

Another O(6)→SU(3) phase transition has been discussed by Kaup and Gelberg (1979) in the Kr isotopes, although the less extensive data preclude definitive conclusions. Finally, in the $A=130$ region, an O(6)→rotor transition clearly characterizes the Xe and Ba isotopes: near $N=74$ an O(6) character predominates, while recent heavy-ion reaction data from Daresbury (Varley *et al.*, 1985) discloses a developing rotational character near $N=68$ and 70. A detailed calculation of the phase transition in this region would be highly interesting but has not yet been carried out; early treatments by Castanos *et al.*, (1982) and the recent study of $^{120}$Xe (Loewenich *et al.*, 1986; see below) treat some aspects of this region.

### 2. U(5)→SU(3)

The vibrator→rotor transition region near $A=150$ was treated very early by Scholten, Iachello, and Arima (1978), using the schematic Hamiltonian

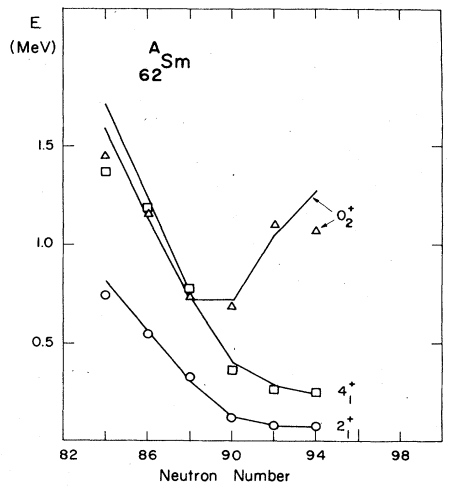


FIG. 46. Comparison of calculated (lines) and empirical (points) energies of low-lying states in the Sm isotopes spanning a U(5)→SU(3) transition region. From Scholten, Iachello, and Arima (1978).

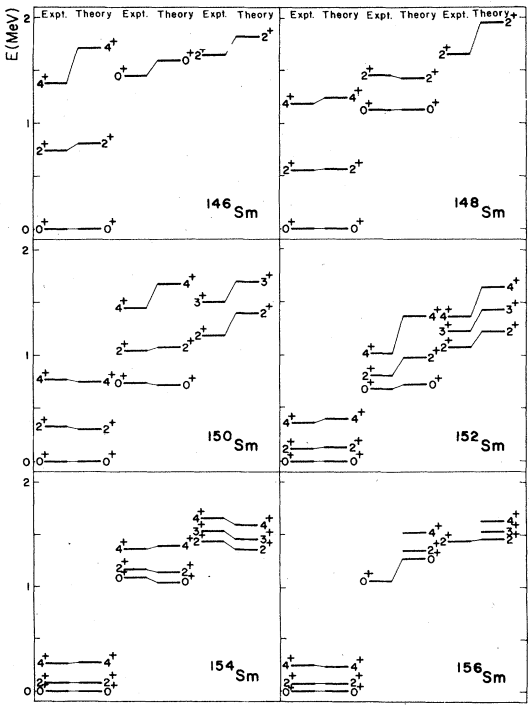


FIG. 47. Comparison of calculated and empirical energy levels in the Sm isotopes for the same calculations as shown in Fig. 46.

$$H=\varepsilon\hat{n}_d+a_2Q^2+a_1\hat{L}^2\ . \tag{3.2}$$

The parameter ε was constrained to decrease linearly with increasing boson number in going from nuclei close to the $N=82$ closed shell towards the deformed nuclei with $N>90$. That is, ε was written $\varepsilon=\varepsilon_0-\theta\hat{N}$. This decreases the ratio of $\varepsilon/a_2$ and induces a U(5)→SU(3) phase transition. They achieved good agreement with a wide variety of data. Examples of predicted energies are given in Figs. 46 and 47. As the phase transition develops (as ε decreases), the $2_2^+$ state first decreases along with the compression of the entire scheme including, particularly, the first excited $0^+$ state, which later evolves into the $\beta$ band. Near the phase transitional point around $N=90$, the $Q^2$ interaction, which depends on $N^2$, begins to dominate. It will be recalled that the energy of the $(\lambda-4,2)=(2N-4,2)$ representation behaves as $2N-1$ in SU(3). In accord with this, one sees that both the $\beta$ and $\gamma$ bands begin to increase in energy once deformation has set in. The $0^+$ band, however, remains below the $\gamma$ band because of the ε term. Although the quadrupole operator used by Scholten, Iachello, and Arima (1978) in the Hamiltonian is of the SU(3) form, rather than one with a variable $\chi$, this feature of a low-lying $0^+$ band is also common to the ECQF formalism (Lipas, Toivonen, and Warner, 1985), as was noted in discussing the contour plot of Fig. 30.

$E2$ transition rates were also calculated by Scholten, Iachello, and Arima (1978), and some results are shown in Figs. 48 and 49 for transitions within the ground band and for those involving the interband transitions from the $\beta$ and $\gamma$ bands. The results are in good agreement with experiment and are typical of what is expected in a U(5)→SU(3) transition. The ground band $B(E2)$ values increase rapidly, changing from a proportionality to $N$ in the U(5) limit toward one going as $N^2$ in SU(3). At the same time the ground-state transitions from the second and third $2^+$ levels, which are forbidden in U(5), become finite around $N=90$, where the structure is intermediate between U(5) and SU(3). As expected from the earlier discussion, the predicted and experimental ground-state transitions from the $2_3^+$ $\gamma$ bandhead state are stronger than those from the $\beta$ band $2_2^+$ level. Both of these calculated $B(E2)$ values must vanish when the $Q^2$ term dominates, since the quadrupole operator in the Hamiltonian is, again, the SU(3) form, and the Hamiltonian then yields the SU(3) limit. This is seen in the figures. While there are no data in this regard for Sm, it is well known (see Fig. 16) that the $\gamma\rightarrow g$ $B(E2)$ values do not vanish in the rare-earth region. This simply reflects the fact that the SU(3) symmetry must be broken either by the addition of a $P^\dagger P$ term throughout the rare-earth region or by $|\chi|<|\chi_{SU(3)}|$ in the CQF. Finally, the branching ratios shown in Fig. 49 increase from near 0 towards the rotational limit given by the appropriate Alaga rule as the deformed region sets in. This agrees reasonably well with the empirical trends. Some other branching ratios are not reproduced as well. The Sm nuclei have also been

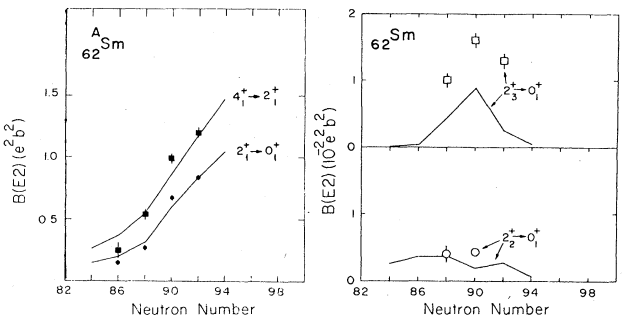


FIG. 48. Comparison of calculated and empirical $B(E2)$ values in the Sm isotopes. See caption to Fig. 46.

treated in a similar manner by Yen *et al.* (1984).

One additional feature of the calculations of Scholten, Iachello, and Arima (1978) concerns two-nucleon transfer reaction strengths, in particular $(p,t)$ and $(t,p)$ reactions. Expressions for the ground-state transfer strengths in the three limits were given previously in Eqs. (2.35), (2.51), and (2.61). The structure of all three expressions is similar, namely, a product of a factor de-

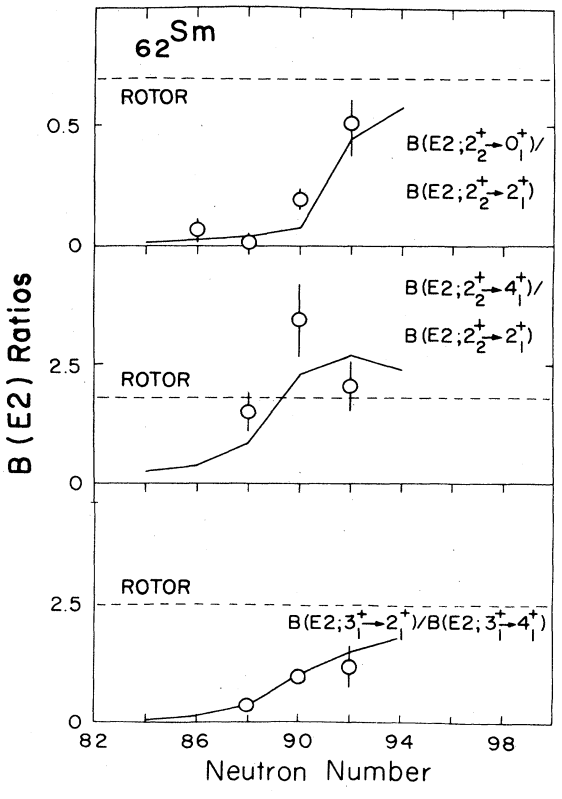


FIG. 49. Comparison of calculated and experimental $B(E2)$ ratios in the Sm isotopes. The labels ROTOR denote the Alaga values. See caption to Fig. 46.

pending on the number of neutron bosons $N_\nu$ and the total number of bosons $N$ times a correction factor, which depends on $(\Omega_\nu - N_\nu)$. It is interesting to compare the U(5) and SU(3) expressions in the limit of large $N$. The SU(3) value is substantially smaller than that in U(5): in particular, besides having a different $(\Omega_\nu - N_\nu)$ dependence, the two expressions [Eqs. (2.35) and (2.51)] differ by a factor of one-third, a result which also emerged [Eq. (2.106)] from the intrinsic-state approach discussed in the previous section. Part of the reason for the lower ground-state cross section in SU(3) is that, as noted earlier, the strength is now shared with an excited $0^+$ state. In any case, one therefore expects the $(p,t)$ and $(t,p)$ ground-state cross sections to decrease upon entry into a deformed region. The results of these calculations are compared with experiment in Fig. 50: for both $(p,t)$ and $(t,p)$ the sudden drop near $N=90$ in the ground-state cross-section strength is evident and is accompanied by an increase in the excited $0^+$ state cross section. The results are in qualitative agreement with experiment.

An alternate set of calculations for this region, specifically for the Gd isotopes, is that of Lipas *et al.* (1983) and Lipas (1983). They utilize a slightly more general Hamiltonian incorporating a $P^\dagger P$ term as well, and they also allow full freedom of the $(s^\dagger\tilde{d}+d^\dagger s)$ and $(d^\dagger\tilde{d})^{(2)}$ parts of the $T(E2)$ operator. They fit extensive data in the Gd isotopes spanning the transition region. An interesting aspect of their approach is that the Hamiltonian parameters are unconstrained and unmodeled, so that they are free to obtain best fits. The results show reasonable agreement with most of the energy and $B(E2)$ data, but it is worth highlighting one specific discrepancy which they emphasize. In the well-deformed isotopes, the IBA is incapable of reproducing the fine structure of intraband energy staggering effects in the $g$, $\beta$, and $\gamma$ bands: the IBA spacing is always fixed essentially at rigid rotor patterns. This limitation of the IBA was also pointed out by Bohr and Mottelson (1982) and is inherent unless higher-order terms in the Hamiltonian are introduced.

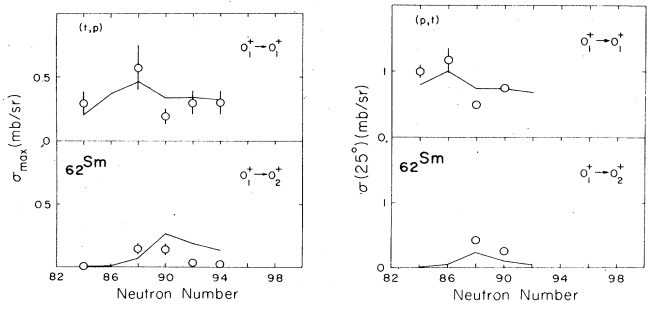


FIG. 50. Comparison of calculated and empirical two-nucleon transfer cross sections to $0^+$ states in the Sm isotopes. See caption to Fig. 46.

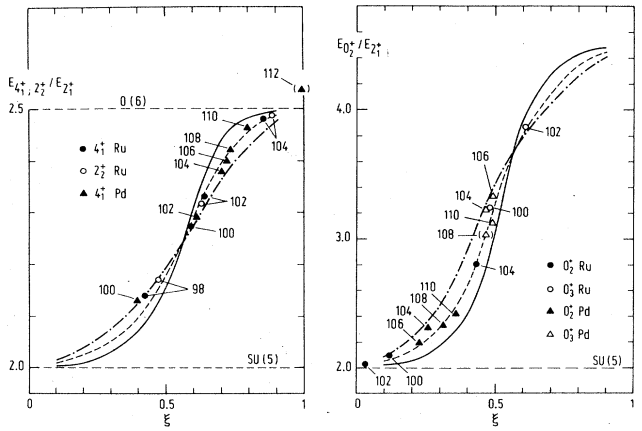


FIG. 51. Calculated energy ratios for the Ru and Pd isotopes spanning a U(5)→O(6) transition region. The quantity $\xi$ measures the position along this transition leg. $\xi=0$ in U(5) and 1 for O(6). The different curves correspond to different boson numbers. Each nucleus is placed in the figure according to its known empirical ratio from which the appropriate value of $\xi$ can be deduced. If different observables for a given nucleus point to similar values of $\xi$ then a consistent interpretation of that nucleus in this transition region is indicated. From Stachel, Van Isacker, and Heyde (1982).

### 3. U(5)→O(6)

There remains the question of the third leg of the symmetry triangle, namely, a U(5)→O(6) phase transition. The nuclei near $^{104}$Ru have been extensively studied in recent multiple-Coulomb-excitation experiments and it has been suggested (Stachel *et al.*, 1982, 1984) that these nuclei occupy an intermediate position along this transition leg. Stachel and collaborators (Stachel, Van Isacker, and Heyde, 1982; Stachel *et al.* 1984) have carried out calculations for such a phase transition and obtained reasonably good agreement with empirical systematics in the

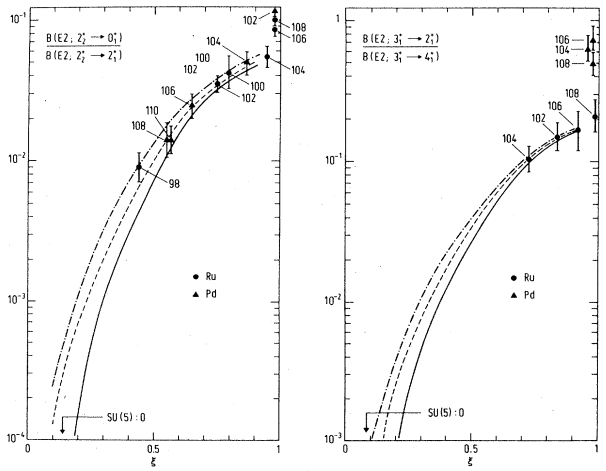


FIG. 52. Similar to Fig. 51, for a pair of $B(E2)$ ratios.

Ru-Pd region. Those calculations utilized a different form for the $E2$ transition operator than has been traditional and are somewhat difficult to interpret physically in the scheme discussed in this paper. The phase transition is defined in terms of a parameter $\xi$, which varies from 0 to 1 in a U(5)→O(6) transition. As a result of the specific $E2$ operator used, however, $B(E2)$ ratios do not necessarily reproduce the expected O(6) values with $\xi=1$. Rather than presenting fits to each nucleus for a specific $\xi$ value, each observable is separately used to extract a $\xi$ value. The success in describing the phase transition is tested and inspected by the constancy in extracted $\xi$ values for different observables in a given nucleus and by the variation in $\xi$ across the region. Some results are shown in Figs. 51 and 52. Although there is some evidence for an evolution in $\xi$ with mass, it is not very consistent nor can a single $\xi$ value generally be assigned to a given nucleus.

There have been other interesting IBA-1 calculations of this region. Very recently, Bucurescu *et al.* (1986, 1987) have applied the ECQF formalism of Lipas, Toivonen, and Warner (1985) to the Ru and Pd isotopes using the Hamiltonian of Eq. (2.80), in which the structural characteristics depend only on $\varepsilon/a_2$ and on $\chi$. Two $E2$ branching ratios are used to fix these parameters for each nucleus. Note that, since $\chi\neq 0$, these calculations are not strictly of the simple U(5)→O(6) type but also involve some components of SU(3). These authors obtain good agreement with the data, as exemplified for $B(E2)$ values in Ru in Fig. 53.

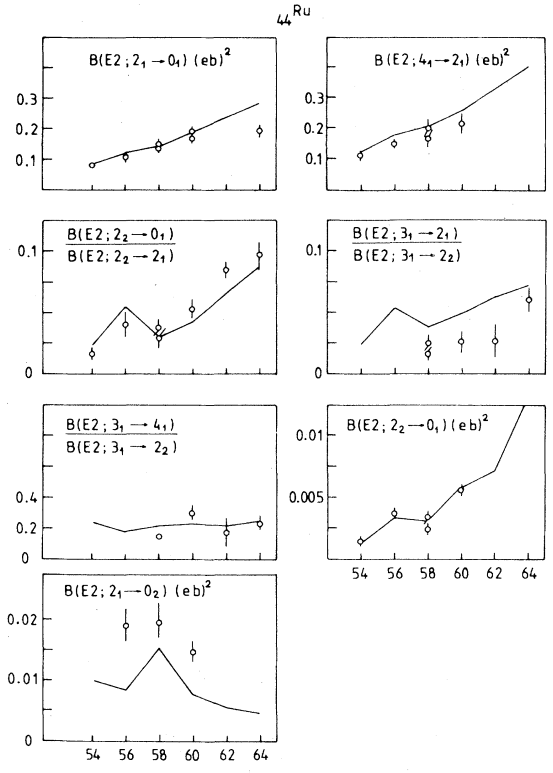


FIG. 53. A comparison of calculated and empirical values for certain $B(E2)$ values and ratios in Ru. From Bucurescu *et al.* (1986).

Finally, it should be commented that similar ECQF calculations have been carried out (Aprahamian, 1984; Shi *et al.* 1985) for $^{102,104}$Ru (with identical parameters for the two nuclei) and achieved good accord with experiment, including the energies and $B(E2)$ values associated with the first excited $0^+$ state and the quasiband built on it. This is significant, since earlier discrepancies with IBA calculations for these levels had motivated suggestions that they were intruder states. In fact, while low-lying intruder $0^+$ states have been observed in a few isotopes (especially in Zr and Pd) in this region, they seem not to be among the low-lying states in Ru.

## 4. Calculations for extended series of nuclei

### a. The $N_pN_n$ approach

An important feature of the IBA is the simplicity it offers in treating extensive ranges of nuclei within a consistent unified framework. In principle, of course, whatever Hamiltonian is used involves several unknown parameters, which must be chosen for each nucleus. In order to reduce the total number of parameters for a large set of nuclei, various models for the parameter variations are usually involved. We have seen several examples (Casten and Cizewski, 1978; Scholten, Iachello, and Arima, 1978; Stachel *et al.*, 1984) above. Nevertheless one is usually left with an uncomfortably large parameter set.

Recently, a different approach (Casten, Frank, and von Brentano, 1985) has been suggested that drastically reduces the number of free parameters. It exploits the empirically discovered (Casten, 1985a, 1985b) simple dependence of many collective observables on the valence nucleon product $N_pN_n$ (or the boson product $N_\pi N_\nu=\frac{1}{4}N_pN_n$) by writing the parameter variations of the IBA Hamiltonian in terms of $N_\pi N_\nu$. Two calculations have been carried out, one (Casten, 1985a), for the U(5)→O(6)→SU(3) transition region near $A=130$ and a second (Casten, Frank, and von Brentano, 1985) encompassing about 100 nuclei in a U(5)→SU(3) transition consisting of about 70 in the $A\approx 150-180$ region and about 30 near $A=100$. The U(5)→SU(3) calculations utilized the Hamiltonian

$$H=\varepsilon\hat{n}_d+a_2Q^2$$

in the CQF formalism, with $T(E2)=e_BQ$. A U(5)→SU(3) transition is obtained if the ratio $\varepsilon/a_2$ decreases with increasing $N$. To achieve this, $\varepsilon$ was parametrized according to

$$\varepsilon=\varepsilon_0 e^{-\theta(N_\pi N_\nu-N_0)}=(\varepsilon_0 e^{\theta N_0})e^{-\theta N_\pi N_\nu}\ .$$

Here, $\varepsilon_0$ is a general scale factor, $\theta$ describes the rate of

change of $\varepsilon$ with $N_\pi N_\nu$, and $N_0$ is an offset in $N_\pi N_\nu$ that varies from region to region. The second form above eliminates one parameter. In order to carry out the simplest possible set of calculations, an extreme simplifying constraint was imposed, namely, that $\varepsilon_0$, $\theta$, $a_2$, and $\chi$ were *held constant* for *all* 100 nuclei. Three values were assigned to $N_0$, one for the $A=100$ region and two in the rare earths, namely, one for protons below midshell and one for the second half of the region. Thus a total of only six constants ($\varepsilon_0$, $a_2$, $\chi$, and three values of $\theta N_0$) were used to describe the 100 nuclei (or five for the rare-earth region). A particular feature of these calculations is that the counting of valence nucleons (hence $N_\pi N_\nu$) takes account of the appearance and disappearance of important subshell effects, specifically that of $Z=64$ for neutron numbers from $N=84-88$ and its assumed disappearance for $N>90$. Though this aspect of the calculations is a key element in their success, it is not inherent in the methodology of the $N_\pi N_\nu$ parametrization, and further discussion of it will be postponed to the next section.

Some results for energy levels in the rare-earth region and $B(E2)$ values near $A=100$ are shown in Fig. 54. Given the highly simplified and constrained nature of the calculations, the agreement is remarkable. As noted, similar calculations, with comparable results, have been carried out for the $A=130$ region.

Thus this simple approach yields rather good results, which, if not the best obtainable for a given nucleus, at least provide an apt starting point, and which are the only ones to date to tackle the systematic evolution of such extensive sets of nuclei.

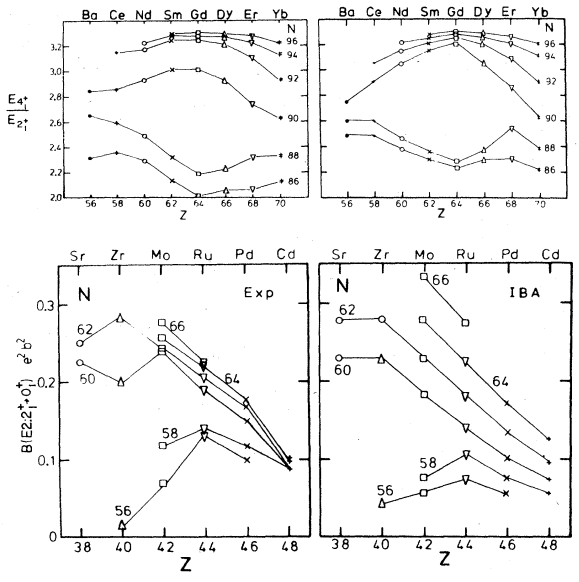


FIG. 54. Comparison of calculated and empirical energy ratios and $B(E2)$ values for two large groups of nuclei in the rare-earth and $A=100$ regions. The IBA calculations, carried out in the CQF, were parametrized using the $N_pN_n$ scheme. From Casten, Frank, and von Brentano (1985).

*b. The general Hamiltonian*

An alternative to the above approaches, in which the Hamiltonian is tailored to the perceived transitional character of a given region, is one in which the most general IBA-1 Hamiltonian is used to fit a large number of data comprising extended sequences of nuclei. One such study is the early one by Castanos and co-workers (Castanos, Frank, and Federman, 1979; Castanos, Federman, and Frank, 1981; Castanos *et al.*, 1982). It is also of interest as one of the few detailed calculations carried out explicitly with the Casimir operator form of the Hamiltonian. These authors treated three groups of isotopes, the Xe,Ba region below $N=82$ [an O(6)$\rightarrow$SU(3) region], the Sm,Gd isotopes centering on $N=90$ [U(5)$\rightarrow$SU(3)], and the U nuclei (stably deformed). In each region the parameters were allowed to run free, and for each element typically 50 individual level energies were fit to an average deviation of 70–100 keV (except for U, where the average discrepancy was 27 keV). An example of the results is given for Xe in Fig. 55. The agreement is rather impressive. Up to $\approx$2.0 MeV essentially every empirical level has a theoretical counterpart, while a few extra predicted levels occur. Since these calculations were carried out, in fact, some of these predicted states have been identified experimentally, such as the $3_1^+$, $4_1^+$, and $6_1^+$ levels in $^{126}$Ba (Schiffer *et al.*, 1986) and the $4_2^+$ level in $^{128}$Xe (Goetting *et al.*, 1981). In many cases these are in reasonable accord with the prior calculations. Although this work was carried out before recent data permitted a full appreciation of the O(6) character of the heavier Xe isotopes, it is interesting that Castanos *et al.* (1982) comment that the $O_3^+$ level in $^{130}$Xe (now assigned as the $\sigma=\sigma_{\max}-2$ bandhead) was instrumental in fixing the $P^\dagger P$ term in assuring a convergent solution.

The results for Sm and Gd are also interesting. The general form of the Hamiltonian contains a term in $\hat{n}_d\hat{N}$ that automatically gives a correction to the $\varepsilon\hat{n}_d$ term, which is identical in first order to the phenomenological-

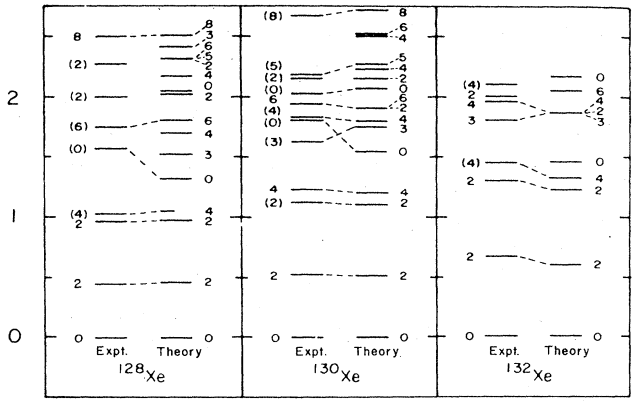


FIG. 55. Comparison of calculated and empirical energy levels for some Xe isotopes using the global fit parameters of Castanos *et al.* (1982).

ly parametrized form for $\varepsilon$, namely $\varepsilon=(\varepsilon_0-\theta\hat{N})$, used by Scholten, Iachello, and Arima (1978). Castanos, Frank, and Federman (1979) in fact get almost exactly the same predictions for the energy levels as were shown in Fig. 47. Another interesting aspect of this study in this region arises in light of the discussion in Sec. IV of the calculations of Van Isacker *et al.* (1982). Castanos *et al.* (1982) point out that their calculations fail to reproduce one low-lying $0^+$ level in $^{154}$Sm and $^{156}$Gd. The missing excitations are exactly the states described by Van Isacker *et al.* (1982) as due to the $s'$ "intruder" boson.

### 5. Specific nuclei

There have been innumerable IBA-1 calculations of specific nuclei or small groups of nuclei. It is not our purpose here to discuss all of these, although many are important contributions to the testing and understanding of the IBA. The reader who encounters these (or future ones) should by now have the requisite tools and feeling for the IBA-1 to place them easily in the context of what has been discussed here.

Having said this, however, there are two specific calculations that are worthwhile to cite. One, by Maino and Ventura (1982a), treats all the Nd isotopes, even crossing the $N=82$ shell closure. They choose the same effective $N_\pi$ values used by Casten, Frank, and von Brentano (1985). By breaching the $N=82$ gap they gain access, in one systematic calculation, to Nd isotopes close to each of the U(6) symmetries: O(6) below $N=82$, U(5) just above, and SU(3) for $N>90$.

A second study of the Se isotopes by Erokhina *et al.* (1985) is of interest since these nuclei are among the lightest yet studied with the IBA-1. They obtain the interesting result that some states in a given isotopes have high overlaps with U(5) wave functions, while others (e.g., some excited $0^+$ states) have near-SU(3) character.

## C. Subshell effects in IBA calculations and effective boson numbers

The above discussion (Secs. II.B.2 and II.B.4) of three sets of comparably successful calculations (Scholten, Iachello, and Arima, 1978; Lipas *et al.*, 1983; Lipas, 1983; Casten, Frank, and von Brentano, 1985) for the $A\approx150$ transition region highlights alternative viewpoints on the role and choice of boson numbers and Hamiltonian parameters in IBA calculations.

It is by now generally agreed that the Federman and Pittel interpretation (Federman and Pittel, 1977, 1978, 1979; Federman, Pittel, and Campos, 1979) of the sudden onset of deformation near $A=100$ in fact provides a general scheme for interpreting many transitional regions in heavy nuclei. In particular, it has been argued (Casten *et al.* 1981) that the phase transition near $A=150$ is due not simply to an abundance of valence nucleons but to the obliteration of the $Z=64$ proton gap when neutrons begin to fill the $1h_{9/2}$ orbit near $N=90$. The strong $1h_{11/2\pi}$-$1h_{9/2\nu}$ monopole $p$-$n$ interaction (Heyde *et al.*, 1985) depresses the effective single-particle energy of the $1h_{11/2\pi}$ orbit, closing the $Z=64$ gap, and allowing the quadrupole component of the $p$-$n$ interaction to act upon a much larger number of valence $p$-$n$ pairs (Casten, Brenner, and Haustein, 1987).

In the context of IBA calculations with normal boson numbers in this region, the above effects will be manifested as discontinuities (Lipas, 1983) in the parameters around $N=88-90$. However, it was pointed out by Scott *et al.* (1980) that the subshell gap can also be regarded as resulting in a reduction in the effective number of active protons. Following the development of a detailed understanding of the changing proton shell structure in this region (Casten *et al.* 1981), it was realized that an alternative approach can be adopted in which such changes are reflected in a neutron number dependence of the proton-boson number $N_\pi$. This approach has been investigated by Gill *et al.* (1982), Maino and Ventura (1982a, 1982b), Wolf *et al.* (1983), Warner (1984), Casten, Frank, and von Brentano (1985), Wolf, Warner, and Benczer-Koller (1985), Hsieh *et al.* (1986), and Passoja *et al.* (1986). In such calculations, for example, for $N<90$, $_{62}$Sm would be viewed as having an effective $N_\pi=1$ instead of $N_\pi=6$, but would revert to the latter value for $N\geq90$. Of course, this is an extreme simplification and, indeed, it has now been shown, first by Wolf, Warner, and Benczer-Koller (1985), and subsequently by Menzen *et al.* (1985), Gill *et al.* (1986), Wolf, Casten, and Warner (1987), and Wolf and Casten (1987) that the gap dissipation is more gradual. These studies utilize a nearly-parameter-free interpretation (Wolf, Warner, and Benczer-Koller, 1985) of $g(2_1^+)$ factors in the IBA-2. Recently, such data have been combined with $B(E2{:}2_1^+\rightarrow0_1^+)$ results in the $Z=64$ region to obtain both $N_{\pi\text{eff}}$ and $N_{\nu\text{eff}}$ values (Wolf and Casten, 1987). These are shown in Fig. 56 and demonstrate the normal sequence of $N_\nu$ values and the sharply changing $N_\pi$ values when the $Z=64$ shell gap vanishes near $N=90$. It has also been pointed out (Iachello, 1983a) that isotope shift data disclose the presence of the kind of monopole polarizability just referred to. A very recent example of this in lighter nuclei is a study of the charge radii of neutron-deficient Sr nuclei (Eastham *et al.*, 1987).

Equally compelling but even simpler evidence for the dynamic behavior of shell structure stems from the energies of the first excited $2_1^+$ levels. It is a well-known feature of the generalized seniority scheme (Talmi, 1971, 1983) that $E_{2_1^+}$ is constant for singly magic nuclei independent of the number of valence nucleons in the open shell. This result is empirically exhibited, for example, by the Sn isotopes. Moreover, a decrease in $E_{2_1^+}$ has long been associated with an increase in collectivity. The $E_{2_1^+}$ data for Xe-Ge for $N=84-90$ are shown in Fig. 57. Despite the expectations based on normal magic numbers, it is immediately apparent that, for $N=84$, 86, and

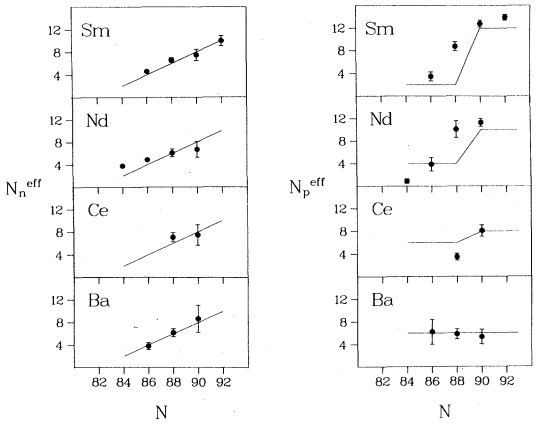


FIG. 56. Effective values of valence neutron ($N_n^{\rm eff}$) and proton ($N_p^{\rm eff}$) numbers for nuclei near the $N=90$ transition region extracted from $g(2_1^+)$ and $B(E2)$ data. From Wolf and Casten (1987).

88, Sm and Gd are actually less collective, less deformed, than Ba and Ce, despite their apparently larger number of valence protons. If, however, a $Z=64$ gap is introduced, the systematics is immediately understandable. In contrast, for $N=90$, the lack of any influence of a gap at $Z=64$ is apparent. Finally, Scholten (1983) has carried out microscopic calculations that suggest the relevance of effective boson numbers. His results for $N_\pi$, obtained in a generalized seniority calculation with $N=82$, are shown in Fig. 58 and are intermediate between the normal values and the extreme assumptions of a sudden disappearance of the $Z=64$ gap at $N=90$.

This discussion highlights two alternate approaches to phase transition regions in the IBA-1. One may use the traditional approach with "normal" $N$ values, obtaining good fits but with substantial parameter variations (even in IBA-2; see Sec. IV.F), or one may incorporate subshell effects in the boson counting (effective $N$ values), keeping the parameters constant or their variations to a minimum.

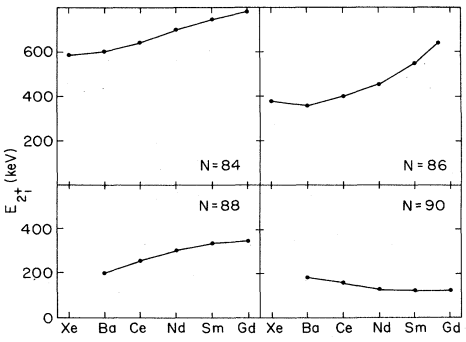


FIG. 57. $E_{2_1^+}$ energies for isotones with $N=84$, 86, 88, and 90.

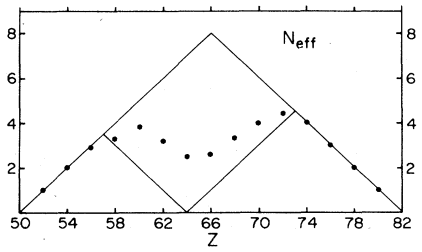


FIG. 58. Effective values of the proton-boson number $N_\pi$ in the region near $Z=64$, calculated for neutron number $N=82$. The dots are the calculations of Scholten (1983), and the solid lines illustrate the simple predictions of the normal counting scheme and of one in which a subshell closure at $Z=64$ is assumed.

It is interesting to remark that, in terms of the mathematics of the Hamiltonian matrix, the two approaches are essentially equivalent. Consider the Hamiltonian

$$H=\varepsilon\hat{n}_d+a_2Q^2=\varepsilon\left[\hat{n}_d+\frac{a_2}{\varepsilon}Q^2\right].$$

The transition U(5)→SU(3) requires the eventual dominance of the second term. This can be achieved either by increasing $a_2/\varepsilon$ or by increasing $N$ (since $Q^2\approx N^2$, while $\hat{n}_d\approx N$).

The use of an approach in terms of a Hamiltonian $H=H(N_{\rm eff})$ is physically appealing and highlights the subshell effects. Yet it must be remembered that, in any given nucleus, comparable predictions can be obtained with "normal" boson numbers and other values for the parameters. While further study of the question and role of $N_{\rm eff}$ values in IBA calculations would be worthwhile, it is pertinent to caution against invoking a proliferation of subshell effects to account for every deviation of IBA calculations from empirical results or to remove all rapid changes in parameter values.

## IV. EXTENSIONS TO THE IBA

### A. The need for extensions

Overall it is fair to say that the IBA has been rather successful within the original boundaries where it was intended to apply, namely the low-lying collective excitations of even-even nuclei. Of course, there have been discrepancies, but overall the model has provided a simple yet flexible approach to individual nuclei and, especially, to the systematic trends in the behavior of nuclei over extended sequences. In a number of cases it has yielded surprising predictions [e.g., a new symmetry, the O(6) limit, $\beta\rightarrow\gamma$ collective transitions in deformed nuclei], which have subsequently been verified. Moreover, and interestingly, as a result of the inherent properties of its group structure, particularly the SU(3) limit, the IBA

automatically yields many well-known features of collective nuclei which, in earlier approaches, had to be fitted separately as perturbations to a basic model. Finally, due to the emphasis on the valence space, which becomes explicit through the use of finite boson numbers, the predictions of the IBA exhibit a characteristic mass dependence that, in most cases, is reflected in the data.

On the other hand, the enormous truncation involved in the IBA restricts its scope, and there are many observed features in collective nuclei that have not proved amenable to a successful interpretation in terms of the IBA-1 with $s$ and $d$ bosons. In many of these cases it is the geometrical models that naturally predict the observed results and the IBA which must be extended. The purpose of this section is to describe some of these extensions and the results obtained so far.

There are two major developments of the IBA-1, namely, the IBA-2 which distinguishes proton and neutron degrees of freedom, and the IBFA which treats odd-mass nuclei by incorporating fermion states coupled to the boson basis, which can be considered as extensions of the IBA-1. However, each of these areas has become a large and active field of study in its own right, and it would be a disservice even to attempt a brief summary in the present context. Thus, while they will not be discussed further here, it is important to remember that they are both indeed outgrowths of the IBA-1, and their motivation, philosophy, background, and methodology are similar to those of the IBA-1.

Most work on extensions to the IBA to date has been motivated by difficulties with particular nuclei in the *sd* IBA-1 framework. However, it is possible to take a more global view and to show that there is *systematic* evidence for the need for extra degrees of freedom. This is most evident in deformed nuclei because the data are more extensive and because there are more excitations below the pairing gap.

It will be recalled that, in SU(3), there are simple relationships between the energies of different representations. These were illustrated in Fig. 7 for the lowest intrinsic states above the $\beta$ and $\gamma$ bands, in terms of ratios to the $\gamma$ band energy. If now the data for the lowest $K=0$ or 2 bands above the $\beta$ and $\gamma$ bands are added to this figure, the results shown in Fig. 59 are obtained. It is clear that the vast majority of points fall well below either of the possible SU(3) representations. Of course, it can be countered that deformed nuclei are not SU(3) and that perhaps lower predictions for the energies of these intrinsic states could be obtained with either an $\varepsilon\hat{n}_d$ or $\chi$ breaking [towards U(5) and O(6), respectively] of SU(3). It turns out that this hardly changes the picture. Figure 20 earlier showed that as $\chi$ deviates from $\chi_{SU(3)}$ the higher bands move still higher relative to the $\gamma$ band. While an $\varepsilon\hat{n}_d$ term does lower some states, their energies have a minimum against $\varepsilon$ and then rise again relative to the $\gamma$ band. This minimum is shown in Fig. 59 as a dashed line, which was calculated for $\chi=-1.0$. Since this is a large $|\chi|$ (nearly all deformed nuclei are

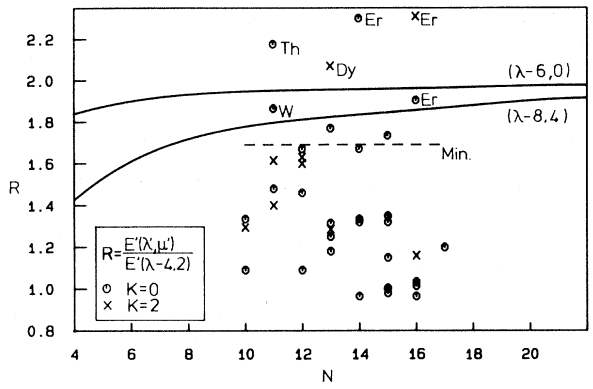


FIG. 59. Ratios of higher-lying levels to the $\gamma$ band. The solid curves are the SU(3) predictions as given in Fig. 7. The dashed line labeled Min. is the minimum energy ratio obtainable with an IBA Hamiltonian that reproduces the low-lying energy levels of deformed nuclei. The symbols represent the empirical values for all nuclei in the deformed rare-earth and actinide regions. Where the empirical ratios are at or above the predictions of the SU(3) limit, the specific nuclei are indicated. The highest Er point is actually off scale at the top.

characterized by $\chi$ values closer to $\chi=-0.5$), the minima given by the dashed line should give a conservative lower limit on the possible energies of intrinsic excitations above the $\beta$ and $\gamma$ bands. Thus the principal conclusion remains intact, namely, that the higher excitations of most deformed nuclei cannot be described within the *sd* IBA with reasonable Hamiltonians that fit the properties of lower-lying bands. This exercise tells us nothing about the nature of these extra states, only that they are beyond the *sd* IBA. Of course, this does not necessarily mean that all such states are purely excitations outside the *sd* space. One possible explanation is obviously that the pure *sd* states are mixed with and pushed down by interactions with higher-lying excitations that are outside the basis. In any case, we shall see below various attempts to account for this wealth of structure that is beyond the *sd* IBA horizon, as well as other empirical features (e.g., backbending) never intended to be encompassed by the IBA.

### B. *g* bosons

The most obvious extension of the *sd* IBA-1 is, of course, to incorporate a $g$ boson. The original truncation to an *sd* space was justified by the fact that, in a simple shell-model calculation, it is these pairs which come lowest in energy. Nevertheless, it was always recognized that, at some energy, higher-$l$ pairs would become important. Several experimental facts also suggest the need for $l=4$ bosons, the most prominent of which is the fact that $B(E2)$ values in the ground bands of deformed nuclei do not show the falloffs and cutoff effects expected as a result of finite $N$ (see, for example, Grosse *et al.*, 1981;

Ower *et al.*, 1982; Emling, 1984). Another motivation for the introduction of the $g$ boson is the presence, in a number of deformed nuclei, of relatively low-lying $K^\pi=3^+$ bands and the systematic appearance in the Os isotopes of very low-lying ($\approx 1$ MeV) $K^\pi=4^+$ bands. In addition, it has long been speculated (Bohr and Mottelson, 1982) that the difficulty with the $K=4$ band in $^{168}$Er might be resolved by the introduction of $g$ bosons.

The possible need for $g$ bosons was, in fact, argued very early in the history of IBA studies by Sage and Barrett (1980) and Otsuka (1981). Chakraborty, Kota, and Parikh (1981) found that the energy spectra and intrinsic quadrupole moments calculated for deformed nuclei could be interpreted in terms of effective boson numbers significantly larger than those normally defined in the IBA, but consistent with the definitions obtained in an *sdg* version of this model. They concluded that $g$ bosons are essential for a natural description of the deformation-producing properties. McGrory (1978, 1979) has carried out shell-model calculations for deformed nuclei and found that $l=0$ and 2 coupled fermion pairs exhaust only about 70% of the wave functions even for low-spin states. Similar results have also been obtained by Dukelsky, Dussel, and Sofia (1981) and Otsuka, Arima, and Yoshinaga (1982). Although the latter note that many collective properties obtained by inclusion of $g$ bosons can be reproduced by a renormalization of the parameters of the *sd* IBA, it is clear from their calculated amplitudes for $l=4$ fermion pairs that the explicit inclusion of $g$ bosons is necessary at least for the treatment of high-spin states. Other studies of $g$-boson amplitudes and renormalization effects include those of Sage, Goode, and Barrett (1982), Maglione *et al.* (1983), and Arima (1983, 1984). Dukelsky *et al.* (1983) have advanced an interesting argument for the need for $g$ bosons from $E1$ transitions between high-spin states in parity doublet rotational bands in the light actinides ($^{218}$Ra). Their argument, framed in a near-U(5) context, points out that yrast states of spin $L$ have $n_d=L/2$, while the negative-parity yrast state of spin $L-1$ is viewed as consisting of a fully aligned coupling of an octupole excitation or $f$ boson and the positive-parity yrast band. For example, a $6^+$ state has $n_d=3$, while the $5^-$ level is viewed as a fully aligned level of structure $\Psi(3^-)\times\Psi(2^+)$ and therefore has $n_d=1$ and $n_f=1$ (or one octupole phonon). The $L=7^-$ state has $n_d=2$. Clearly, then, while the latter may deexcite to the $6^+$ level by an $E1$ transition, the $6^+\rightarrow 5^-$ $E1$ transition is forbidden. This contradicts the experimental situation. If, however, a fully aligned $g$ boson is introduced, the $6^+$ state has structure $n_d=1$, $n_g=1$, and an $E1$ transition to the $5^-$ level can occur via the transition operator $f^\dagger g$. Finally, Pittel *et al.* (1984) in the framework of IBA-2 have argued for the particular importance of a $g$ boson at higher energies in the region of the isovector $1^+$ states, where an *sdg* model may account for the fragmentation of $1^+$ $B(M1)$ strength.

Basically, two ways have been explored to introduce a $g$ boson into the *sd* IBA-1, by diagonalization of a Hamiltonian with $N=n_s+n_d+n_g$ where $n_g$ is limited to values 0 and 1, and group-theoretically by expanding U(6) to U(15). The latter assumes a zero $g$-boson energy $\varepsilon_g$ at least in the SU(3) limit, and the wave functions for the low-lying levels can have reasonably large values of $n_g$. The former procedure of numerical diagonalization is motivated by the presumption that the intrinsic energy of a $g$ boson should be substantially larger than $\varepsilon_d$.

### 1. Numerical treatments

We consider the numerical approach (Van Isacker *et al.*, 1981, 1982; Heyde, Van Isacker, Waroquier *et al.*, 1983) first. In it, the Hamiltonian is of the form

$$H=H_{sd}+\varepsilon_g g^\dagger\cdot\tilde{g}+H_g+H_{\rm int}\ , \tag{4.1}$$

where $H_{sd}$ is the normal IBA-1 Hamiltonian, acting on the *sd* space (sometimes called the $\Sigma$ space) only, the second term (with $\langle n_g\rangle=0$ or 1) accounts for the $g$-boson energy, the third term acts on the $g$-boson (or $\Gamma$) space, and the last term mixes the $\Sigma$ and $\Gamma$ spaces. $H_g$ is often taken simply to be of the form $H_g\approx\kappa_g Q_{sd}\cdot Q_g$ with $Q_g=(g^\dagger\tilde{g})^{(2)}$. Since it independently conserves $n_s+n_d$ and $n_g$, $H_g$ merely splits the energies of states with $n_g=1$ but does not mix them. $H_{\rm int}$ can, in principle, be rather complex but is usually truncated to simple terms such as

$$H_{\rm int}\approx(g^\dagger s^\dagger)^{(4)}\cdot(\tilde{d}\tilde{d})^{(4)}+\text{H.c.} \tag{4.2}$$

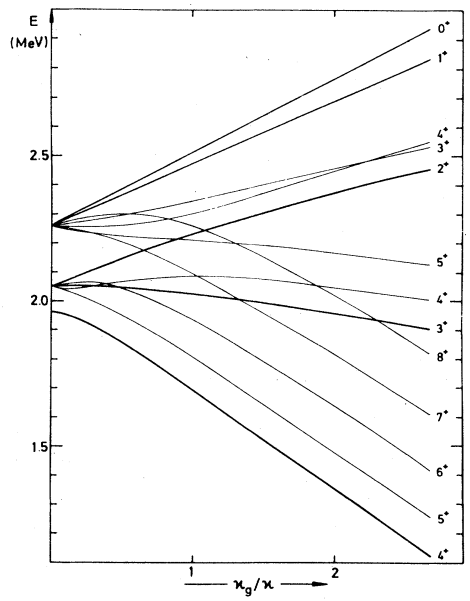


FIG. 60. Energy spectrum resulting from the coupling of a $g$ boson to an SU(3) core as a function of the ratio $\kappa_g/\kappa$ for $N=12$. The degenerate multiplets arising in the absence of a $g$-boson quadrupole interaction term in the Hamiltonian are seen at the left, while rotational bands with $K=0$, 1, 2, 3, and 4 are seen to emerge for large values of $\kappa_g$ on the right. From Van Isacker *et al.* (1982).

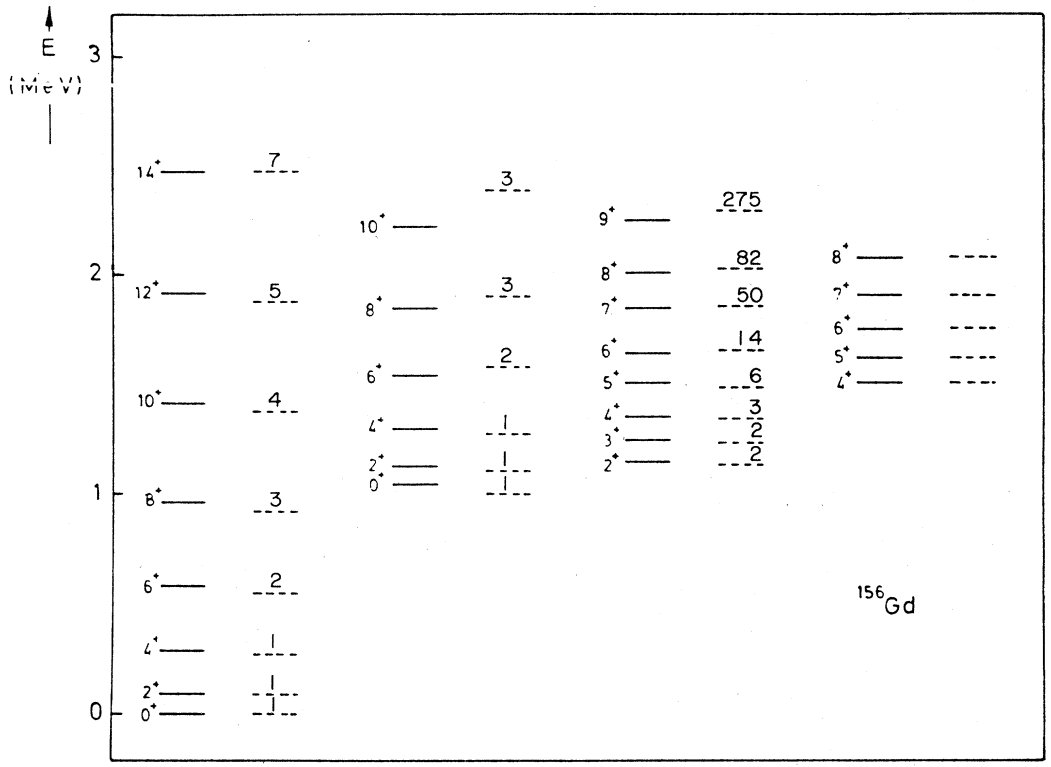


FIG. 61. Calculated (dashed lines) and empirical (solid lines) energy levels of $^{156}$Gd. The numbers on the theoretical levels of the ground, $\beta$, and $\gamma$ bands represent the expectation value of the $g$-boson number in each state in units of 0.1%. From Van Isacker *et al.* (1981).

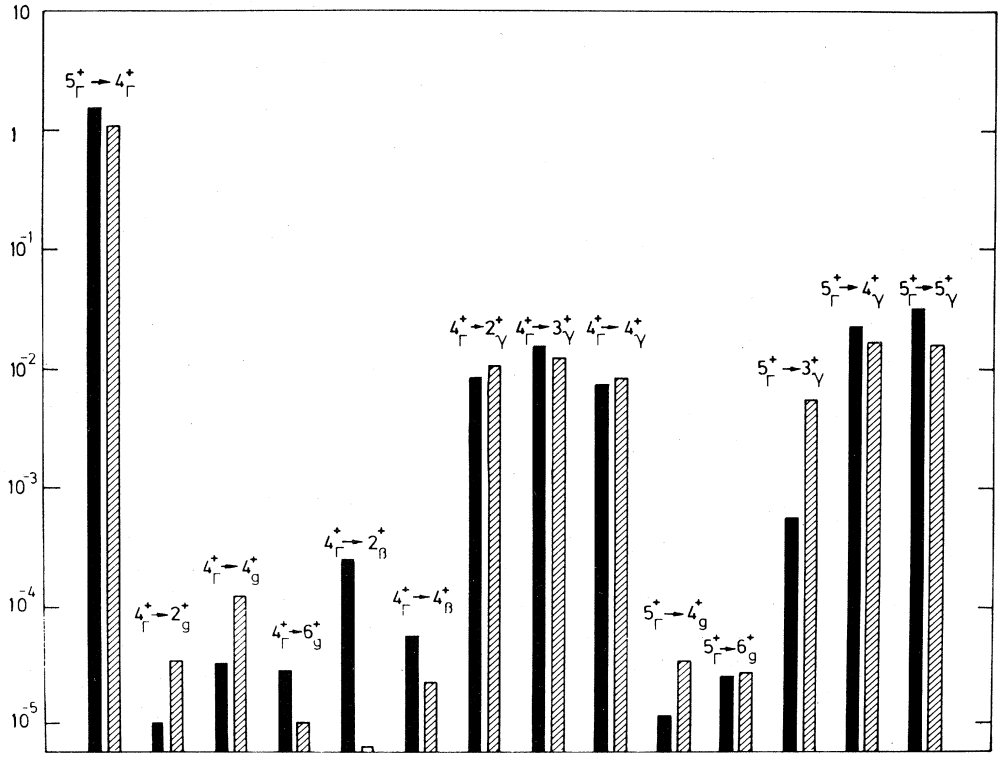


FIG. 62. Comparison of calculated (hatched) and empirical (black) $B(E2)$ values for transitions from the $L^\pi K = 4^+4$ and $5^+5$ states to the members of the ground, $\beta$, and $\gamma$ bands in $^{156}$Gd. From Van Isacker *et al.* (1981).

in order to minimize the number of additional parameters.

Heyde, Van Isacker, and co-workers (Van Isacker *et al.*, 1982; Heyde, Van Isacker, Waroquier *et al.*, 1983) have systematically studied the cases in which $H_{sd}$ satisfies or approximates one of the U(6) symmetries, and the reader is referred to those studies for details. Here, it is useful to highlight some general results. First of all, in deformed nuclei, where $H_{sd}$ is close to the SU(3) Hamiltonian, a $K=4$ band, which is largely $g$ boson in character, appears in the low-lying spectrum. Bands of similar structure but with $K=0,1,2,3$ are substantially higher lying, the splitting between bands being generated by the $Q_{sd}\cdot Q_g$ term. This is seen in Fig. 60, which shows the evolution of the spectrum of $g$-boson bands as a function of $\kappa_g/\kappa$ ($\kappa \propto a_2$) as a concrete example of a calculation for a deformed nucleus. The calculated (Van Isacker *et al.* 1982) and experimental energy spectra of $^{156}$Gd, as well as the $B(E2)$ values from the $K=4$ band, are shown in Figs. 61 and 62. Several interesting features may be noted. The energies and wave functions of the $g$, $\beta$, and $\gamma$ bands are little affected by the addition of a $g$ boson: the expectation value of the $g$-boson number $\langle n_g \rangle$ (in units of 0.1%) is given for each level of the $\beta$ and $\gamma$ bands in Fig. 61, and only for the $8^+_\gamma$ and higher levels does it approach or exceed 1%. Of course, this conclusion might change if $n_g > 1$ values were allowed in the calculations. The $B(E2)$ values are also in excellent agreement with the data. Note particularly the relative scales of branching to various bands. In obvious band notation, the $B(E2)$ values from the $K=4$ band go as $4\rightarrow 4 \gg 4\rightarrow\gamma \gg 4\rightarrow\beta \gg 4\rightarrow g$, in agreement with experiment. Further discussion of these calculations for $^{156}$Gd will be given in Sec. IV.D below, since they also incorporate intruder bosons and thus include a second extension to the IBA-1 as well.

The coupling of a $g$ boson to U(5) or O(6) cores (Heyde, Van Isacker, Waroquier *et al.*, 1983) is also interesting. A significant difference from the SU(3) case above is that, here, the $Q_{sd}\cdot Q_g$ term is much less effective in splitting the $g$-boson states, since the matrix elements of $Q_{sd}$ are much smaller. Thus predictions closer to those of a weak-coupling calculation result. However, the effects on $B(E2)$ values are important. Some of these are related to simple changes in boson cutoff effects and are best discussed below in the more general U(15) frame-

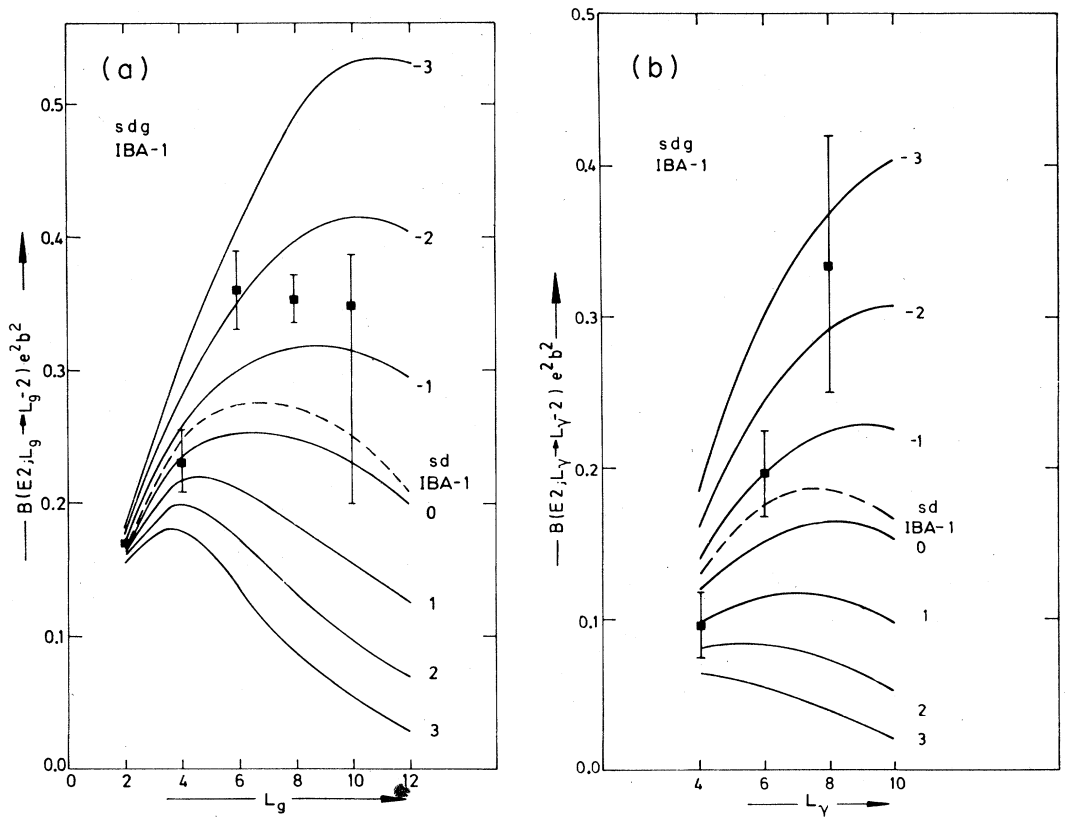


FIG. 63. Comparison of empirical and calculated intraband $B(E2)$ values for (a) ground band and (b) $\gamma$ band in $^{104}$Ru. The calculations utilize an IBA-1 Hamiltonian incorporating $g$-boson excitations. The different solid curves correspond to different strengths of the boson effective charge $e^{(2)}_{gd}$ and are labeled in units of 0.1 eb. The empirical results are roughly consistent with the calculations corresponding to $e^{(2)}_{gd} \simeq -1.5$. The dashed curve corresponds to the *sd* IBA-1. From Heyde, Van Isacker, Waroquier *et al.* (1983).

work, but it is interesting that some very specific empirical features can be reproduced. A nice example is provided by the nucleus $^{104}$Ru, which is intermediate between U(5) and O(6) and in which the yrast $B(E2)$ values show a large jump at the $6^+ \rightarrow 4^+$ point. As shown in Fig. 63, it is possible (qualitatively) to reproduce this effect for an appropriate sign and value of $g$-boson effective charge $e_{gd}$ in the $E2$ transition operator,

$$T(E2)=e_{sd}T(E2)_{sd}+e_{gd}(g^{\dagger}\tilde{d}+d^{\dagger}\tilde{g})^{(2)} + e_{gg}(g^{\dagger}\tilde{g})^{(2)} . \quad (4.3)$$

The same figure also shows reasonable agreement (considering the large experimental uncertainties) with the intra-$\gamma$-band transitions.

### 2. U(15)

The effects of a $g$ boson can also be studied by exploiting the symmetry properties of U(15). Such an approach is not limited to $\langle n_g \rangle \leq 1$, and was explored several years ago by Ratna Raju (1981, 1982), Wu (1982), and others and more recently in a renewed burst of interest (see, for example, Akiyama, 1985; Borghols *et al.*, 1985; Akiyama *et al.*, 1986; Yoshinga, Akiyama, and Arima, 1986; Akiyama, von Brentano, and Gelberg, 1987). Most of the work thus far has been carried out in an SU(3) chain, and we shall therefore treat only this case. [For a discussion of the U(5) case, see Sun *et al.*, 1983.]

There are, basically, two effects of going from U(6) to U(15). First, the effective value of $N$ is changed to $2N$. Thus all falloffs in $B(E2)$ values are postponed to much higher spins. Related to this, rotational bands also extend now to $L=4N$ and thus cutoffs are effectively eliminated. Second, the number of SU(3) representations in U(15) increases dramatically compared to U(6) and thus new possibilities for intrinsic excitations appear.

The eigenvalue equation is given by (Akiyama, 1985)

$$E=\alpha C(\lambda,\mu)+\beta L(L+1)+\gamma S , \quad (4.4)$$

where the first two terms are exactly as in the *sd* SU(3) limit except that the values of $(\lambda,\mu)$ are based on $\lambda_{\max}=4N$ rather than $2N$. Thus, for example, the ground state is characterized by $(4N,0)$, and the $\beta$ and $\gamma$ bands by $(4N-4,2)$. Now, however, as noted, new representations appear. These are of two types, those containing odd $K$ rotational bands, and those stemming from multiple appearances of representations with the same $(\lambda,\mu)$ values. The lowest-lying of the former is $(\lambda-6,3)=(4N-6,3)$ and contains $K=1$ and 3 bands. The latter are typified by representations such as $(\lambda-8,4)=(4N-8,4)$ which now occur twice, each time containing $K=0$, 2, and 4 bands. These two occurrences can be distinguished by a new quantum number $w$, which takes on the values 0 and 1 for the $(\lambda'\mu')=(4N-8,4)$ representation. Thus for $w=0$ the states occur at the same energies (after substitution of $4N$ for $2N$) as those of the $(\lambda-8,4)$ representation in the *sd* IBA (but now have wave functions containing components with a $g$ boson) while, for $w=1$, a second set of $K=0$, 2, and 4 bands appears with shifted energies. This shift in energy is provided by the $\gamma S$ term in Eq. (4.4), which represents the eigenvalue of an SU(3) scalar operator and is given by (Akiyama, 1985)

$$S=w(2N-2w+3) , \quad (4.5)$$

thus splitting the $w=0$ and 1 representations. Hence, the level energies are given by

$$E=\alpha C(\lambda,\mu)+\beta L(L+1)+\gamma w(2N-2w+3) . \quad (4.6)$$

The quantity $w$ is akin to a seniority quantum number, which counts the number of $(\lambda,\mu)=04$ coupled pairs. Here, the value of $w$ will be distinguished by a subscript on the values of $(\lambda',\mu')$. Thus one has now the representations $(\lambda-8,4)_0$ and $(\lambda-8,4)_1$.

The states of $(\lambda-8,4)_0$ have a double phonon (e.g., $\gamma\gamma$ or $\gamma\beta$) vibrational character. In contrast, the $(\lambda-8,4)_1$ representation has been shown (Akiyama *et al.*, 1986) to resemble a one-phonon excitation. This geometric interpretation helps account for the differences in predictions of, for example, $(t,p)$ cross sections discussed below.

An example of a fit of this model to the data is shown for $^{178}$Hf in Fig. 64. Note that, above the $\beta$ and $\gamma$ bands, the next representation has $w=1$. In a fit without $g$ bosons, these empirical states are predicted too high. The odd $K$ bands on the right should also be noted. Since these states have $w=0$ they are not separately parametrized and their predicted energies are fixed by the $g$, $\beta$, and $\gamma$ band energies. Empirically, the band with $K=3$ is in good agreement with the data. The predicted $1^+$ band, however, is not observed experimentally.

It is clear that realistic applications of an *sdg* model to most deformed nuclei must allow for some symmetry breaking. Akiyama (1985) has introduced several operators that achieve this result without destroying the band structure. When such a scheme is applied to $^{168}$Er, the fit in Fig. 65 is obtained (Yoshinaga, Akiyama, and Arima, 1986). The agreement with the data is excellent, but this may simply reflect the much larger number of parameters. In particular, compared to the SU(3) case, the $K=1^+$ band is pushed much higher (to 2.7 MeV) than the $K=3$ band and the $K=4$ band of the $(\lambda-8,4)_1$ representation is separated off from the lower $K$ bands. Indeed, the lowest $K=4$ band now has a dominant component $(\lambda-8,4)_0$ and reproduces the observed energy of the $K=4$ band at 2.055 MeV, thus accounting for the earlier $K=4$ anharmonicity problem.

While there are indeed a larger number of parameters than in the *sd* case, several other predictions are also obtained in agreement with the data. A number of these center on cross sections for two-neutron transfer (Akiyama *et al.*, 1986), especially $(t,p)$, which are very different in the *sdg* IBA-1 model. The $(t,p)$ transfer operator now transforms as (4,0) under SU(3) instead of (2,0). Thus, starting from a target with $(\lambda,\mu)=(4(N-1),0)$, the

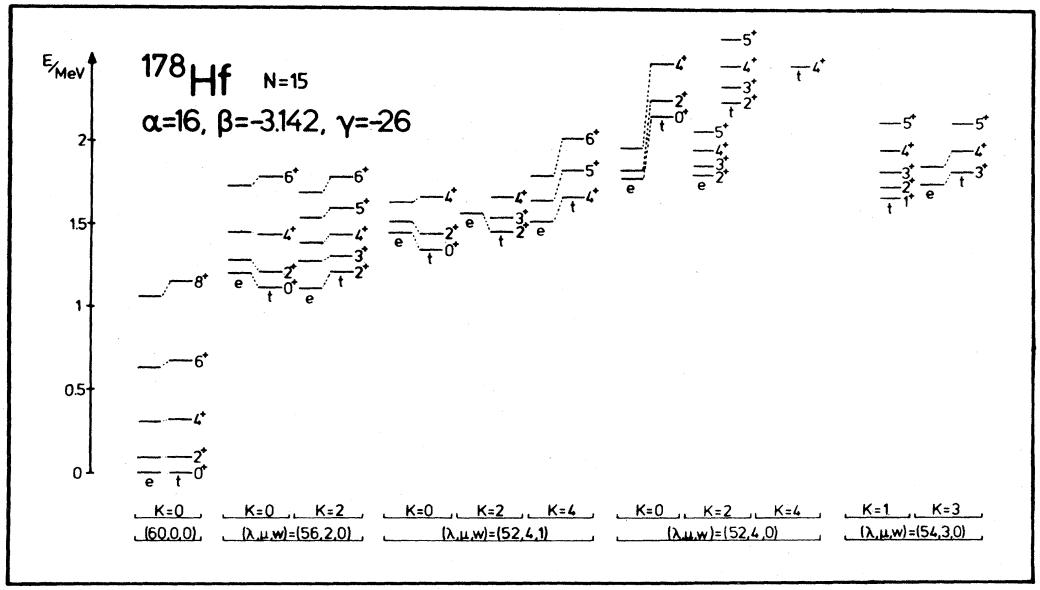


FIG. 64. Comparison of empirical levels of $^{178}$Hf with calculations including a $g$ boson. The symbols $e$ and $t$ denote experimental and theoretical levels, respectively. $\alpha$, $\beta$, and $\gamma$ are in keV. From Akiyama, von Brentano, and Gelberg (1987).

selection rule in $(t,p)$ (below midshell) allows population of the representations $(4N,0)$, $(4N-4,2)$, $(4N-8,4)$. However, the last of these occurs with both $w=0$ and 1, and there is a strong theoretical preference for population of the "one-phonon" $w=1$ states over the $w=0$ "two-phonon" levels. In $^{168}$Er, the second excited $K=0$ band in the $sdg$ model has $w=1$ and thus can be significantly populated in $(t,p)$. A comparison of predicted and observed $0^+$ $(t,p)$ strengths in $^{168}$Er is shown in Table VII. While the comparison still lacks detailed agreement, the experimental values fall in between those of the SU(3) limit of U(15) and the broken-symmetry case. Moreover, the $2^+$ state of the second $K=2$ band also has a large amplitude for $w=1$ and can be populated in $(t,p)$. In contrast, in the $sd$ model, both these bands ($K^\pi=0_2^+$ and $2_2^+$) belong predominantly to the $(\lambda-8,4)$ ("two-phonon") representation. The $sdg$ model calculations of Akiyama *et al.* (1986) predict that the ratio of relative spectroscopic strengths $S(2^+,K=2_2^+)/S(2^+,K=2_1^+)\approx 6$ compared to an experimental value of 5. Finally, the $K=4$ band at 2.055 MeV, as noted just above, has $w=0$ and therefore, again, is of two-phonon character and will only be populated very weakly. The calculated ratio $S(4^+,K=4_1^+)/S(4^+,K=0_1^+)\approx 0.034$ is consistent with the upper limit obtained by Burke *et al.* (1985). In general, the $sdg$ model allows more states to be successfully populated than the $sd$ model and is in better agreement with experiment.

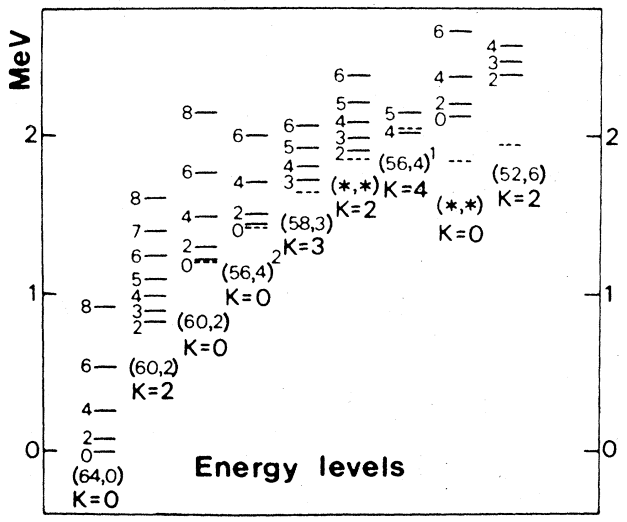


FIG. 65. Calculated energy levels of all positive-parity levels below 2.4 MeV in $^{168}$Er with the inclusion of a $g$ boson. The empirical bandhead energies are indicated by the dashed lines. The labels below each bandhead represent the dominant SU(3) representation and $K$ quantum number. States with asterisks cannot be assigned definite SU(3) representations. From Yoshinaga, Akiyama, and Arima (1986).

As described in the earlier discussion of the O(6)→rotor transition in the Os isotopes, a set of $K=4$ bands develops in each of the even-even Os isotopes near 1 MeV. Their properties, in particular their $\gamma$ decay, and the evolution in $E2$ branching ratios, are extremely well reproduced by the simple $sd$ IBA-1 calculations. Nevertheless, these low-lying bands and their direct $E4$ population in Coulomb excitation are suggestive of $g$-boson components. Baker (1985) has argued that a consistent interpretation of all the data ($E2$ and $E4$ properties) could be obtained by the inclusion of a $g$ boson. His cal-

TABLE VII. Relative $(t,p)$ strengths for $0^+$ states in $^{168}$Er (from Akiyama *et al.*, 1986).

| Band $K_i^\pi$ | Level energy (keV) | Relative strength | | | |
|---|---|---|---|---|---|
| | | Experimental cross section[a] | IBA prediction | | |
| | | | *sd* IBA[a] | *sdg* IBA | |
| | | | | SU(3) | Band mixing |
| $0_1^+$ | 0 | 100 | 100 | 100 | 100 |
| $0_2^+$ | 1217 | 15 | 11 | 8.3 | 21.6 |
| $0_3^+$ | 1422 | 10 | 2 | 14.7 | 3.6 |
| $0_4^+$ | 1833 | 2.4 | 0.05 | | 7.6 |

[a]Burke *et al.* (1985).

culations succeed rather well. However, as noted earlier, Morrison (1986) has recently shown that, while a $g$ boson may aid in accounting for a given nucleus, the systematic behavior of $E4$ properties arises mostly from the effects of the Pauli principle on the mass dependence of the $E4$ transition operator itself. Clearly, further study is in order.

Kuyucak and Morrison (1987) have recently suggested another area where an *sdg* space may significantly ameliorate a recent perplexing problem. All $g$ factors are constant in the IBA-1, independent of spin or intrinsic excitation. However, recent work (Doran *et al.*, 1986) has disclosed evidence for falloffs in measured $g$ factors along the yrast band, for example, in $^{166}$Er. With the inclusion of a $g$ boson, Kuyucak and Morrison find that the $g$ factors are spin dependent and given by

$$g(L)=g_0+g_2L(L+1)\ . \tag{4.7}$$

A fit to the measured $g$ factors (Doran *et al.* 1986) in $^{166}$Er is shown in Fig. 66. The agreement is good, although the empirical uncertainties are large. Clearly, the fit relies on a negative $g_2$, and it remains to be seen whether this is microscopically reasonable and whether it also leads to consistent results for $M1$ transition rates.

Finally, and perhaps most importantly, the $g$ boson, of course, significantly diminishes the problem of the predicted falloff in yrast $B(E2)$ values characteristic of the *sd* model, since finite-$N$ effects are much weaker when $N$ is replaced by $2N$ in all $B(E2)$ expressions. The basic problem is nicely exemplified by the data shown at the left in Fig. 67, which compares the empirical values for yrast band $E2$ reduced matrix elements for $^{236}$U with rigid-rotor and IBA [SU(3)] calculations. The discrepancies for the latter starting at $I\approx N_{\max}$ are readily apparent. The effects of a $g$ boson on the high-spin behavior of the IBA have been studied by Ratna Raju (1981, 1982) and Wu (1982). For example, Ratna Raju (1982) has shown that in the yrast band,

$$B(E2{:}L+2\rightarrow L) = e_B^2\frac{3}{4}\frac{(L+2)(L+1)(\eta N-L)(\eta N+L+3)}{(2L+3)(2L+5)}\ . \tag{4.8}$$

This formula is actually written for the general case of a set of bosons with angular momenta $0,2,4,\ldots,\eta$ and where the total degeneracy is $1/2(\eta+1)(\eta+2)$. (For a $g$ boson $\eta=4$, and this gives the familiar result 15.) Equation (4.8) clearly shows that falloff effects, which stem only from the last two factors in the numerator, are much less severe [compare the *sd* SU(3) result of Eq. (2.48), which is obtained from Eq. (4.8), by substituting $\eta=2$]. On account of this result, Ratna Raju (1982) has argued that the reduction in $B(E2)$ values at high spin predicted by the *sd* IBA is not at all a reflection of finite boson number effects but of insufficient collectivity, a difficulty that is greatly reduced by the addition of an $l=4$ boson.

An example of this effect is shown at the right in Fig. 67, The improvement over the *sd* case is substantial. It is also evident that the introduction of $l=6,8,\ldots$ bosons leads to little further change, since the $g$-boson results are already quite close to the rigid-rotor result. It is the clear need for $g$ bosons in this context, perhaps more than any other factor, that suggests that the improved agreement obtained for other observables is also physically significant and not just an exercise in parameter proliferation.

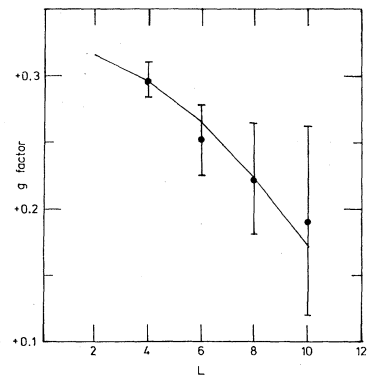


FIG. 66. Comparison of empirical and calculated values of $g$ factors for yrast states in $^{168}$Er. The calculated values would be constant in the absence of a $g$ boson. From Kuyucak and Morrison (1987).

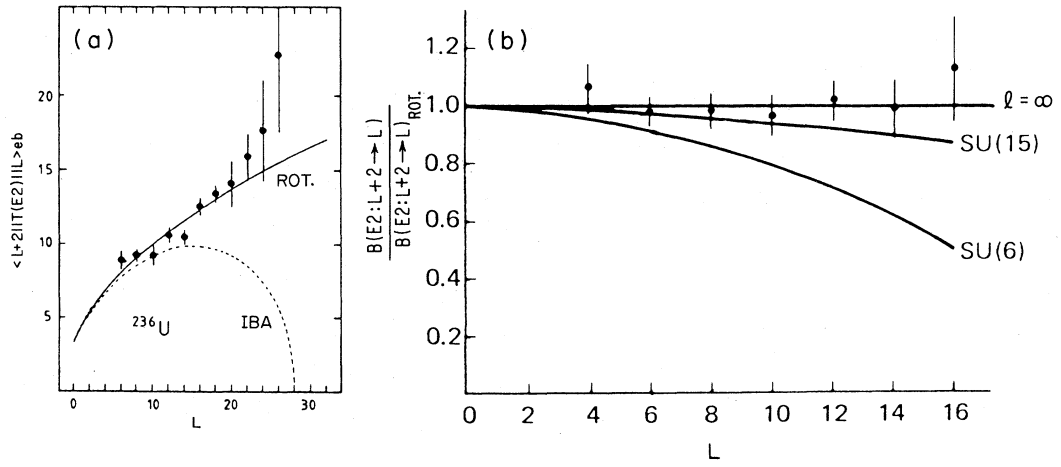


FIG. 67. Comparison of models for yrast band $E2$ transitions: (a) Empirical reduced $E2$ matrix elements for the yrast band in $^{236}$U compared to rigid-rotor (solid line) and IBA [SU(3)] (dashed line) predictions. From Ower *et al.* (1982). (b) Ratios of yrast $B(E2)$ values to rotational values for $^{232}$Th. The line labeled $l=\infty$ corresponds to the pure rotor model predictions, while the SU(15) and SU(6) lines correspond to the IBA with $s$, $d$, and $g$ bosons and $s$ and $d$ bosons, respectively. From Wu (1982).

### C. Higher-order terms

Another obvious extension of the IBA-1 is the introduction of higher-order terms either in the Hamiltonian or in the transition operators. An example of the latter was already discussed earlier for the $M1$ operator whose first-order term is diagonal in the IBA-1 basis, and therefore leads to no $M1$ transitions, while a second-order term leads to predictions of the signs and magnitudes of mixing ratios in deformed nuclei that seem capable of reflecting the experimental situation. There are of course many higher-order terms that can be included in the IBA-1 Hamiltonian, and there has been little systematic study of them. One must therefore be cautious when the choice of a particular one enhances agreement with the data. Nevertheless, one that has proved particularly useful is the addition of a cubic interaction term (Heyde, Van Isacker *et al.*, 1984). This has already been discussed rather extensively above in connection with the addition of a small component to the O(6) potential (see Sec. III.A.1). Here we wish to discuss one additional calculation of this type, since it concerns the more general situation in which no particular symmetry applies. Loewenich *et al.* (1986) have studied $^{120}$Xe with the ($^{13}$C,$2n_\gamma$) and ($^{12}$C,$3n_\gamma$) reactions and have developed an extensive level scheme including several sidebands. This nucleus is intermediate in character between O(6) and SU(3). Calculations with the Hamiltonian

$$H=\varepsilon\hat{n}_d+a_2Q^2+a_1\hat{L}^2 \tag{4.9}$$

with $\chi\approx-0.527$, that is, intermediate between its O(6) and SU(3) values, give generally good results for both energies and relative $B(E2)$ values. However, just as in the case of the heavier, O(6)-like Xe isotopes, it was found that the energy staggering in the $\gamma$ band was poorly reproduced and that the spacing of higher-lying levels was too large. Naturally this suggested the introduction of a cubic term. Here, however, its effects are somewhat different, since it is now superimposed on an SU(3)-like potential with a minimum at $\gamma=0°$ rather than on a deformed $\gamma$-soft O(6) one. Nevertheless, a similar improvement in predictions occurs, as can be seen in Fig. 68. In both the present case and that of the O(6)-like Xe and Ba nuclei, it is important to note that the amount of triaxiality thus introduced represents a very small correction to the potential obtained without this term. This is evident

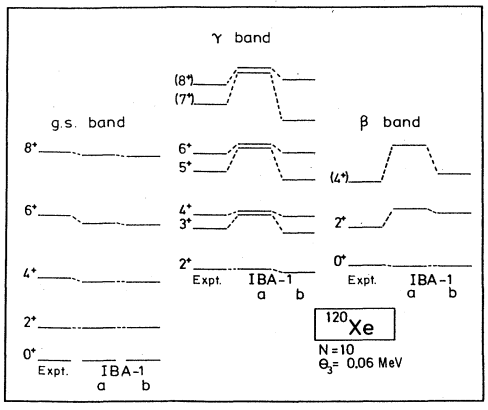


FIG. 68. Comparison of the experimental levels of the ground, $\gamma$, and $\beta$, bands of $^{120}$Xe with predictions of the simple IBA-1 model (a) and with the IBA-1 model with the inclusion of a cubic (triaxial) term ($\propto\theta_3$) (b). For a detailed specification of the parameters see Loewenich *et al.* (1986), from which this figure is taken.

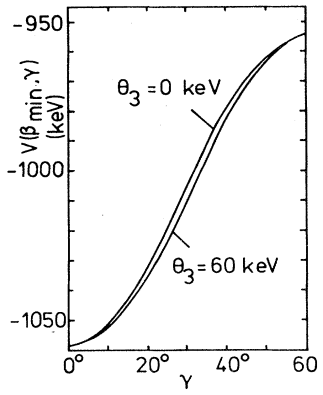


FIG. 69. Dependence of the IBA potential on $\gamma$ in the classical limit for the Hamiltonian of Loewenich *et al.* (1986) with and without a cubic term whose magnitude is specified by the coefficient $\theta_3$.

from Fig. 69, which shows the corresponding classical potential with and without the cubic term.

While the choice to introduce a single third-order term, to the exclusion of others, may seem rather *ad hoc* it has an appealing physical interpretation and appears to be a relatively simple way of significantly improving some of the IBA-1 predictions.

### D. The IBA-1 with configuration mixing

The presence of intruder states as a common feature (Wood, 1984; Heyde *et al.*, 1982) throughout heavy nuclei has motivated another extension to the IBA, namely, the incorporation of multiple systems of $s$ and $d$ bosons. The most common application of this idea utilizes the so-called Duval-Barrett (1981a, 1981b) formalism, in the framework of the IBA-2, in which intruder states are viewed as two-particle two-hole excitations from the valence shell into the next higher shell or major subshell. If the structural differences between particle and hole bosons in two different shells are ignored, the creation of two additional holes in the valence shell and two particles in the next shell increases the total number of bosons by two. Reasonable results have been obtained (Duval and Barrett, 1981a, 1982; Sambataro and Molnar, 1982; Schreckenbach *et al.*, 1982; Duval, Goutte, and Vergnes, 1983) using this approach in several widely separated mass regions (e.g., Hg, Mo, Cd, and Ge). The Hamiltonian consists of the normal one, containing $N_\pi$ and $N_\nu$ $s$ and $d$ bosons, plus a second Hamiltonian for the intruder system in which $N_{\pi'}=N_\pi+2$ or $N_{\nu'}=N_\nu+2$ (depending on whether the intruders are proton or neutron excitations) and a term that mixes these two configurations. It is also possible to develop a similar idea in the framework

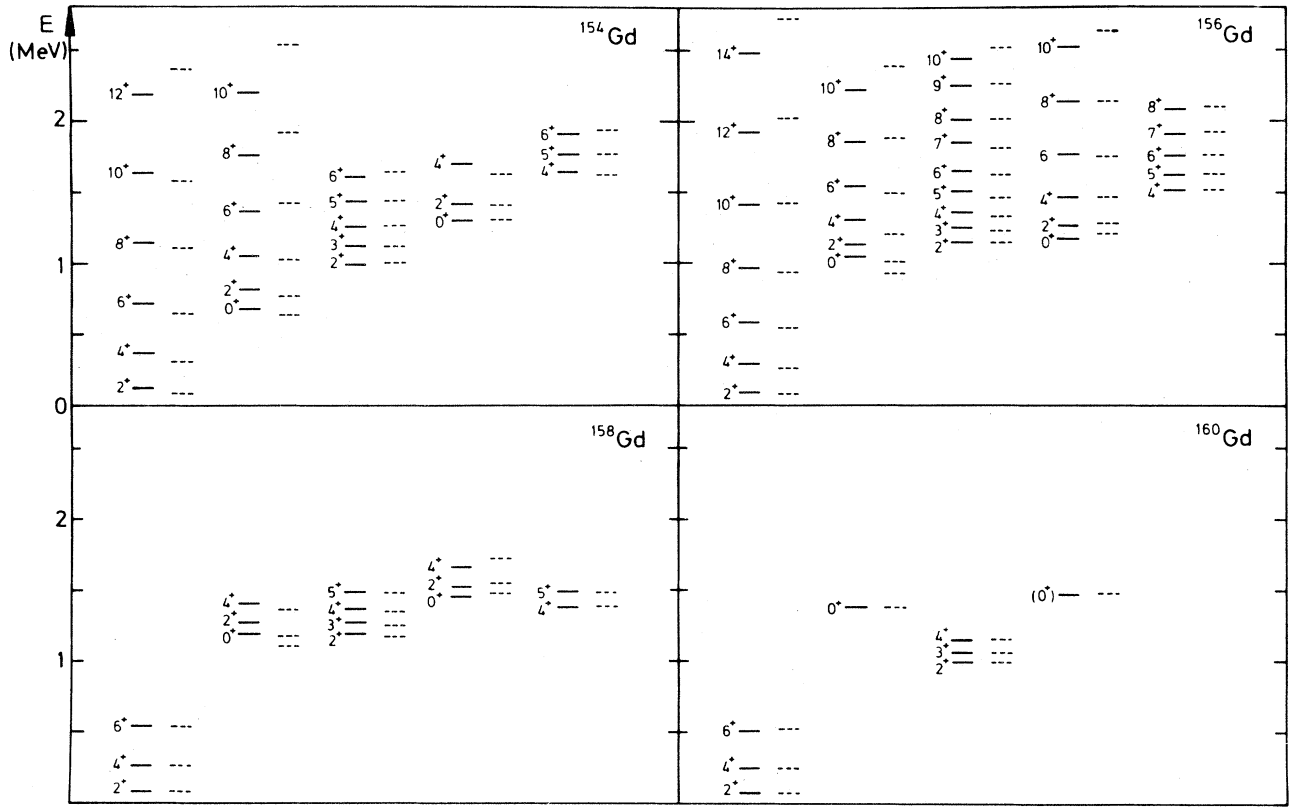


FIG. 70. Comparison of empirical (solid lines) and calculated (dashed lines) energy levels for several Gd isotopes. The calculations include both a $g$ boson and an $s'd'$ system of bosons. From Van Isacker *et al.* (1982).

of the IBA-1, and this has been done and used by Van Isacker *et al.* (1982) in calculations for the Gd isotopes, in particular $^{156}$Gd. It is useful to consider this, since it is both an interesting extension of the IBA-1 and an illustration of many of the main effects arising in the full IBA-2 Duval-Barrett approach.

The difficulty in the deformed Gd isotopes is that, if one attempts to apply the SU(3) limit, it is easy to reproduce the ground $\beta$ and $\gamma$ bands but there is another $K=0$ band lying just above the first excited $K=0$ band and there is also a low-lying $K=4$ band. It is impossible to reproduce these within the standard framework of the IBA. Motivated by this, Van Isacker *et al.* (1982) proposed a Hamiltonian of the following form:

$$H=H_{sd}+H_{s'd'}+H_g+H_{\rm int}\ , \tag{4.10}$$

where the meaning of the terms is clear. Some results of this work were described earlier in the discussion of $g$ bosons. Here we concentrate on the $s'd'$ excitations, which in practice are negligibly mixed with $g$-boson amplitudes. In order to simplify the calculations, the following assumptions were made: First, $H_{sd}$ was taken in SU(3) form. Second, it was assumed that there were either $N$ bosons of $sd$ type or $(N-1)$ $s$ and $d$ bosons with one boson allowed to occupy *either* an $s'd'$ state or a $g$-boson state. Furthermore, in practice the effects of the $d'$ boson were found to be small and were ignored. Therefore $H_{s'd'}$ is simply $\varepsilon_{s'}s'^{\dagger}s'$. The Hamiltonian for the $g$ boson was also taken in a simple form, namely, $H_g=\varepsilon_g g^{\dagger}\cdot\tilde{g}-\kappa_g Q_{sd}\cdot Q_g$. Finally, $H_{\rm int}$ describes an interaction (very weak) between the $sd$ states and the $s'd'$ levels or between the $sd$ states and the $g$-boson states. With this Hamiltonian, and with smoothly varying values for the parameters, the systematics of the level schemes of the even-even Gd isotopes for $N\geq 90$ were well reproduced, in particular, the energy of the second excited $K=0$ band, which appears experimentally in $^{156}$Gd at 1.17 MeV (whereas the $K=0_2$ band from the $sd$ system is calculated at 1.7 MeV).

Some of the results of the calculation are shown in Fig. 70. In addition, a large number of $B(E2)$ values were calculated which, in general, are in very reasonable agreement with the data. A particularly interesting feature is that experimental Mikhailov plots of $\gamma\rightarrow g$ and $\beta\rightarrow g$ transitions in the Gd isotopes deviate sharply from straight lines. The calculations (Van Isacker *et al.*, 1982), while not achieving detailed agreement with the complex empirical plots, nevertheless show similar curvatures and, at least in $^{158}$Gd, reproduce well the minima and maxima in the curved Mikhailov plot contours.

### E. Backbending and particle alignment effects in the IBA-1

The study of high-spin phenomena in nuclear physics has developed over the past decade into a widespread field of activity abounding in interesting phenomena. Most of these, at present, are outside the scope of the IBA. However, a simple extension of this model is capable of describing at least the most basic phenomena, namely backbending and the accompanying changes in yrast band $B(E2)$ values. The basic idea is rather simple. The Hamiltonian is written as

$$H=H_{sd}(N)+H_{sd}(N-1)+\varepsilon_{2\rm qp}+H_{\rm mix}\ , \tag{4.11}$$

where the IBA Hamiltonians in the first two terms are solved for $N$ and $N-1$ bosons, respectively. In the latter case one boson has been destroyed to create an aligned two-quasiparticle state at excitation energy $\varepsilon_{2\rm qp}$. $H_{\rm mix}$ provides for mixing of these two basic configurations (but also contains nonmixing interactions). The calculations are usually carried out in two steps: first, energies and wave functions for the $N$ and $N-1$ boson systems are obtained by diagonalization of the appropriate IBA Hamiltonians, and then a mixing calculation is carried out. As efforts in this direction have developed, they have come to center on the addition of two-quasiparticle configurations to a core described by the IBA-2. For example, quite reasonable agreement has been obtained (Yoshida, Arima, and Otsuka, 1982) for the backbending observed in such nuclei as the Ba and Ce isotopes, as well as for the observed decreases in yrast $B(E2)$ values near the backbend.

In earlier tests of the inclusion of quasiparticle excitations in the IBA, however, the IBA-1 was used, and thus a brief summary of these efforts is appropriate here. An early initiative in this direction was taken by Gelberg and Zemel (1980), who simplified their task by adopting the particularly restrictive assumption that for the $N$-boson system only the ground band core states were included, so that $H_{sd}(N)=\alpha\hat{L}^2$. With this simplification, the calculations depend on four parameters, $\alpha$, $\varepsilon_{2\rm qp}$, one related to the two-quasiparticle level system, and one to mixing with the normal one. Results for the energies of the yrast band in $^{126}$Ba are shown in Fig. 71. Clearly, the backbend, which occurs around spin 12, is reasonably well reproduced. With an $E2$ transition operator consisting solely of a boson part there would, of course, be no transitions connecting states above and below the backbend in the absence of the mixing term in the Hamiltonian. With that mixing term, finite, though small, $B(E2)$ values are obtained as shown on the right in Fig. 71. While the empirical $B(E2)$ values for $L=12^+$ and $14^+$ in the region of the backbend are indeed below the rotational model predictions, there is actually a more severe drop in observed $B(E2)$ values below the band crossing, and the IBA calculations qualitatively reproduce this feature, now known as the prealignment anomaly (Hanewinkel *et al.* 1983). The predicted results arise from the interplay of a boson cutoff effect and a band crossing. Although no pretense to an accurate description of the empirical results can really be made in such a simplified model, this example highlights two effects: the ability to incorporate particle alignment in a rather simple extension of the IBA-1 and the ability to investigate

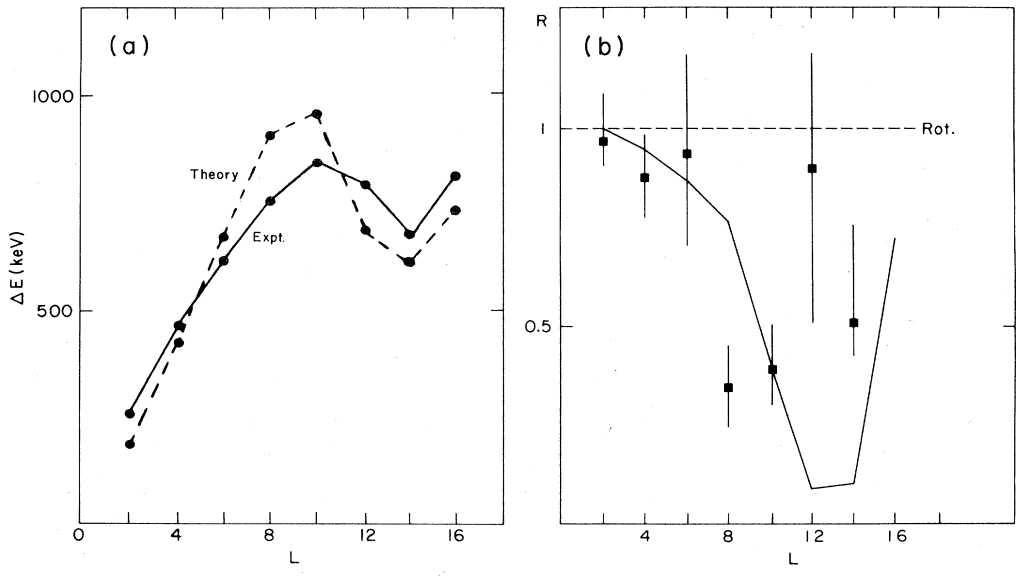


FIG. 71. (a) Empirical (solid line) and calculated (dashed line) energy intervals vs spin in $^{126}$Ba. (b) Ratios of yrast $B(E2)$ values for $^{126}$Ba. $R$ is defined as $R=[B(E2{:}L\rightarrow L-2)/B(E2{:}2\rightarrow 0)]/[B(E2{:}L\rightarrow L-2)/B(E2{:}2\rightarrow 0)]_{\rm rot}$. The solid line represents a calculation including a schematic model incorporating the possibility of two-quasiparticle excitations. From Gelberg and Zemel (1980).

possible $B(E2)$ falloffs, even in the presence of backbending.

A more ambitious approach for the inclusion of two quasiparticles in the IBA has been developed by Morrison, Faessler, and Lima (1981). It has recently been applied by Faessler and co-workers (1985) to the Ba and Ce nuclei. In this more general approach, the entire $N$-boson core structure is included. Moreover, the core structure is allowed to undergo an O(6)→SU(3) transition across these isotopes by using a CQF *sd* Hamiltonian [$\chi$ is fixed in $T(E2)$]. Additionally, $H_{\rm mix}$ is allowed to be spin dependent, and includes exchange terms, and $\varepsilon_{2qp}$ is replaced by a more realistic fermion Hamiltonian allowing for a surface delta residual interaction. Both neutron and proton alignments are considered. In fact, the results for both alignments are used to test which is operative. Reasonable agreement for Ba and Ce isotopes is achieved: an example, Fig. 72, shows results for $^{130}$Ba and includes rotor plus two-quasiparticle calculations as well. These IBA calculations, however, do not explain the prealignment anomaly discussed above, which, it seems, is very sensitive to the alignment energy and assumed mixing of aligned and core states. In the more phenomenological calculations of Gelberg and Zemel (1980) described above, this effect was specifically parametrized to test the capability of the calculational framework, while the philosophy of the calculations of Faessler *et al.* (1985) is substantially more *ab initio* and therefore misses this particular empirical detail.

Finally, a rather different approach to backbending in the IBA-1 has been taken by Heyde and co-workers (Heyde, Van Isacker, Jolie *et al.*, 1983; Heyde, Jolie *et al.*, 1984). It is reminiscent of the Duval-Barrett (1981a) technique for inclusion of intruder states with different effective boson numbers $N$, but utilizes the IBA-1 and generalizes it to include subsystems of states with $N_0, N_0+2, \ldots, N_{\rm max}=N_0+6$. The Hamiltonian is simply

$$H=H_{\rm mult}+\Delta(\hat{N}-N_0)+H_{\rm mix}\ , \tag{4.12}$$

where $N_0=N_{\rm normal}$ and $H_{\rm mult}$ is the normal multipole Hamiltonian such as $\varepsilon(N)\hat{n}_d+a_2Q^2$, $2\Delta$ is the energy

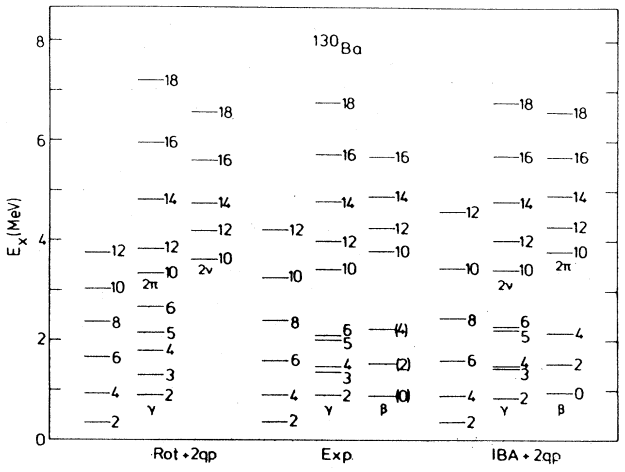


FIG. 72. Energy levels of $^{130}$Ba compared to predictions of IBA and rotor models with the inclusion of two-quasiparticle excitations. From Faessler *et al.* (1985).

needed to create a $2p$-$2h$ excitation, that is, the energy separation of families of levels with $\Delta N=2$, and $H_{\rm mix}$ has $\Delta N=\pm 2$ matrix elements only. The first two parts of the Hamiltonian are separately calculated for each boson number. The key ingredient specifically incorporated in order to achieve the desired result (backbending) is that the parameter $\varepsilon$ in $H_{\rm mult}$ is $N$ dependent. It is written as

$$\varepsilon=\theta(N_{\rm max}-\hat{N}) , \tag{4.13}$$

so that states with *larger* $N$ have *smaller* $\varepsilon$ and therefore smaller inertial parameters. Moreover, the $Q^2$ term in $H_{\rm mult}$ dominates to a greater extent. Thus the yrast band with $N=N_{\rm max}-6$ will have the largest spacings and will eventually be crossed by the more collective higher-lying bands, leading to backbending. Whether this happens before the spin cutoff is a question of detailed parameter values. Clearly, a large $\theta$ will lead to backbending at smaller $L$ values and to a more significant change in the falloff effects in $B(E2)$ values relative to a standard IBA-1 calculation with fixed $N$.

Calculations in this scheme for the six nuclei from $^{154-164}$Dy reproduce the empirical systematics of sharp backbending at low frequency in $^{154}$Dy and no backbend in the heavier isotopes.

This picture describes a backbending phenomenon completely within a (multi-$N$) collective framework. Although it succeeds reasonably well, its success is, in a sense, built in, and its relation to more traditional approaches is not yet clear.

### F. IBA-1 as a projected IBA-2

As noted above, the IBA-2 is an important extension of the IBA-1, not only for calculational purposes, where the distinction between protons and neutrons is essential, but also because of its closer relationship to the underlying shell structure and its prediction of new collective modes. A particularly important property of the IBA-2 is that the proton-neutron symmetry character of each state is specified in terms of a new quantum number called $F$ spin (Van Isacker *et al.*, 1986; Arima *et al.*, 1977). A given nucleus has a fixed value of the projection of $F$ spin, $F_0\equiv 1/2(N_\pi-N_\nu)$, but, in analogy with isospin, can have states with different values of $F$. Moreover, there are terms in the IBA-2 Hamiltonian that can mix $F$ spin, although in most IBA-2 calculations, with certain notable recent exceptions (Novoselsky and Talmi, 1986), the low-lying states are rather pure $F=F_{\rm max}=1/2(N_\pi+N_\nu)$ states. To the extent that this is a good approximation one can then make use of projection formulae (Scholten, 1980; Harter, Gelberg, and von Brentano, 1985; Frank, Harter, and von Brentano, 1987) that, for a particular set of IBA-2 parameters, give the IBA-1 parameters that produce exactly the same predictions for the $F_{\rm max}$ states as the original IBA-2 calculation. An approximate method, applicable for states with $F$ values close to $F_{\rm max}$ has also recently been discussed by Dobeš (1987).

We shall not specify the projection formulas explicitly here. However, their existence is very useful and appealing, since IBA-1 calculations are much simpler and more economical to carry out and since it is generally easier to understand the character of the resulting IBA-1 wave functions in the context of dynamical symmetries and geometrical analogs. Several uses have been made of this approach, primarily by the Köln group of von Brentano, Gelberg, and co-authors. Besides the references cited above they have studied (Sala, Gelberg, and von Brentano, 1986) the systematics of boson effective charges in the rare-earth region by carrying out a set of IBA-2 projected into IBA-1 calculations in the CQF and relating the calculated $B(E2)$ values to the quantity $F_0/F$. Another use of the projection idea which can be of quite general applicability is found in their recent study of $M1$ transitions and $F$-spin purity in $^{128}$Xe, in which an IBA-1 Hamiltonian was inversely projected to give a "starting point" IBA-2 Hamiltonian to fit the near-O(6) spectrum of $^{128}$Xe (Harter, von Brentano, and Gelberg, 1986). However, it should be recognized that, in general, the process of inverse projection from IBA-1 to IBA-2 is not

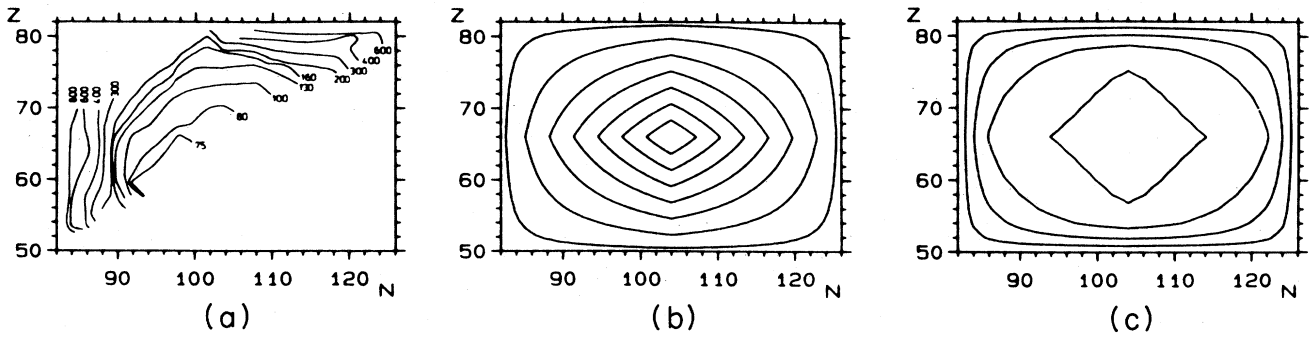


FIG. 73. Contours in the $N$-$Z$ plane. (a) Empirical $E_{2_1^+}$ energies in the rare-earth region (labels are in keV); (b) hyperbolic contours of constant $N_pN_n$; (c) predictions of projected IBA-2 calculations with constant parameters. The contours start at 100 keV (innermost) and increase in 100-keV steps. From Theuerkauf *et al.* (1987).

unique. In fact, in principle, there are an infinite number of IBA-2 Hamiltonians that can give rise to the same projected IBA-1 Hamiltonian.

A final application of this approach starts from the observation that in many phenomenological fits to extended sequences of nuclei with the IBA-1, one must generally vary the IBA-1 parameters, but in some cases (Casten, Frank, and von Brentano, 1985) these variations can be written as simple functions of $N_\pi N_\nu$. Since this factor frequently enters in the projection equations just discussed, it might then be possible to use constant IBA-2 parameters, with the variation in IBA-1 parameters coming naturally through the projection. With the aim of testing this idea, Theuerkauf and co-workers (1987) have carried out extensive series of IBA-2 calculations within the IBA-1 framework with constant IBA-2 parameters. In regions of little structural change, these projected IBA-1 calculations can indeed describe the empirical systematics. Moreover, in general, most observables are predicted to be smooth functions of $N_\pi N_\nu$. Despite this, as illustrated in Fig. 73, in transition regions, the changes in IBA-1 parameters arising simply from the projection formulas are *not* sufficient to account for the systematics. While both theory and experiment follow $N_\pi N_\nu$ systematics, the predicted strength of the dependence on $N_\pi N_\nu$ is insufficient. The point here in all these diverse examples is not the detailed agreement or disagreement of a particular choice of IBA-2 parameters with the data, but rather the use of a simple approximate method to utilize the IBA-1 in a way that this capable of recognizing effects of the separate variation of proton and neutron boson numbers.

### G. *f* bosons and negative-parity states

Clearly, the *sd*-boson IBA-1 model cannot account for negative-parity states at all. Yet numerous examples of such states are known in heavy even-even nuclei, and, in particular, negative-parity rotational bands are a common feature of deformed nuclei. Many of these intrinsic excitations are identified experimentally by enhanced $E3$ transition rates to the ground state. Although they may not be extremely collective, frequently being populated rather strongly (see, for example, Burke, Maddock, and Davidson, 1985) in single-nucleon transfer reactions as well, many have been interpreted in terms of octupole degrees of freedom coupled to the ground state. Microscopic arguments for negative-parity nucleon pairs have recently been given by Catara *et al.* (1986). It is a natural extension of the IBA-1, therefore, to incorporate an $f$ boson. Indeed, a rather extensive discussion of $f$-boson properties appeared as early as the fundamental paper on the U(5)→SU(3) transition by Scholten, Iachello, and Arima (1978), who considered a simple Hamiltonian of the form

$$H=H_{sd}+\varepsilon_f f^\dagger\cdot\tilde{f}+\theta_f\hat{N}-Z_2[Q_f\times Q_{sd}]^{(0)}\ , \qquad (4.14)$$

where $\varepsilon_f$ is the $f$-boson energy and $\theta_f$ and $Z_2$ describe the interaction of the octupole bosons with the *sd*-boson system. The quadrupole boson operator $Q_f$ is defined as $Q_f=2(7)^{1/2}(f^\dagger\tilde{f})^{(2)}$. The system is constrained so that the wave functions either contain $N$ $s$ and $d$ bosons or $(N-1)$ $s$ and $d$ bosons along with one $f$ boson. To simplify the treatment, Scholten, Iachello, and Arima (1978) carry out a series of calculations in which the parameters $\varepsilon_f$, $\theta_f$, and $Z_2$ are constant as a function of $N$.

If $H_{sd}$ is taken in the harmonic U(5) limit and the interaction term in $Z_2$ is neglected, the energies of the negative-parity states are simply given by $E=\varepsilon n_d+E_3$, where $E_3=\varepsilon_f+\theta_f N$. This produces a spectrum with a series of multiplets in which an octupole boson is coupled to each positive-parity state. The low-lying levels of such a system are shown on the left of Fig. 74. In the SU(3) limit another simple level scheme results, also shown in the same figure, in which a series of excited octupole bands with $K=0^- - 3^-$ appear. The energies are given in simplified form by $E(K_f)=AL(L+1)+\alpha_f K_f^2+\beta_f$, where $\alpha_f$ and $\beta_f$ are appropriate combinations of the parameters of the Hamiltonian. Depending on the sign of $\alpha_f$, negative-parity bands result whose energies are either monotonically increasing or monotonically decreasing as a function of $K_f$. Scholten, Iachello, and Arima (1978) also calculate the U(5)→SU(3) transition including an $f$ boson. The calculation simply consists of diagonalizing the Hamiltonian given in Eq. (4.14), where $H_{sd}$ is allowed to undergo a transition from U(5) to SU(3). Typical examples of the results are shown in Fig. 75. The most interesting feature is the evolution of the sequence of negative-parity states. Near the closed shell at $N=82$, where a vibrational spectrum is obtained, the lowest negative-parity state is $3^-$, followed by groupings of other negative-parity states at higher energies. This is reminiscent of the U(5) scheme shown on the left in Fig. 74. As the spherical-deformed transition region sets in, so does the development of rotational bands. In particular, the lowest levels are seen to evolve into a $K=0^-$ band.

Finally, Scholten, Iachello, and Arima (1978) also calculate $B(E3)$ values connecting the ground state with

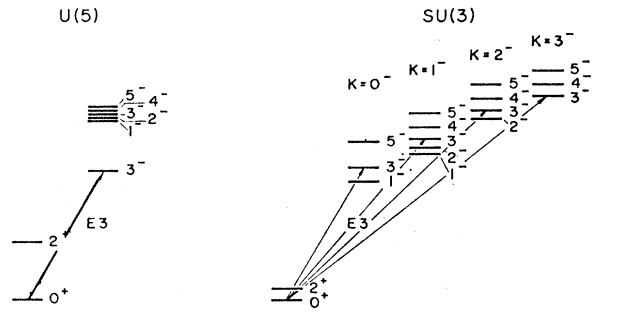


FIG. 74. Schematic representation of the octupole ($\pi=-$) spectrum in the U(5) and SU(3) limits. From Scholten, Iachello, and Arima (1978).

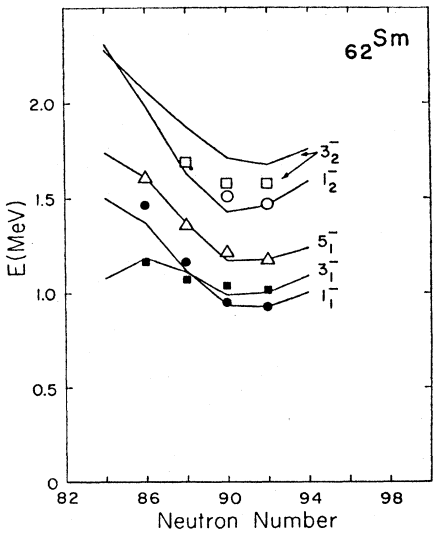


FIG. 75. Comparison of calculated (lines) and empirical (points) energy levels of negative-parity states in the Sm isotopes. From Scholten, Iachello, and Arima (1978).

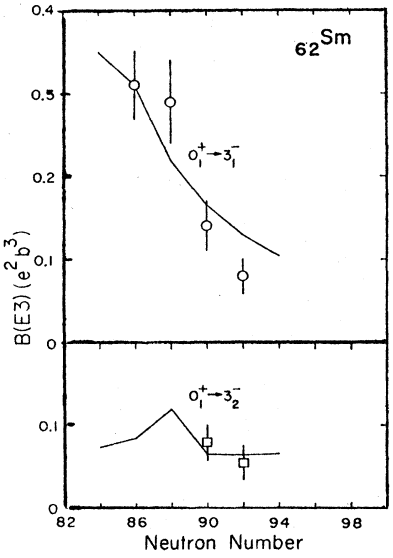


FIG. 76. Comparison of calculated and empirical $B(E3)$ values for $E3$ transitions in the Sm isotopes. From Scholten, Iachello, and Arima (1978).

the various octupole levels. Assuming the simple $E3$ operator $T(E3)\approx(s^\dagger\tilde{f}+f^\dagger s)^{(3)}$, then, in the U(5) limit, only the first excited $3^-$ state with $n_s=N-1$, $n_d=0$ and $n_f=1$ is connected to the ground state by an $E3$ transition. On the other hand, in SU(3), the $3^-$ states of all four octupole bands have $E3$ ground-state transitions. In fact, the relative $B(E3)$ values from these states are in the ratios 1:2:2:2, for the deexcitation of the $K=0^-$, $1^-$, $2^-$, and $3^-$ bands, respectively. The larger $B(E3)$ values in the case of $K\neq0$ stem simply from the fact that the antisymmetrized wave functions in these cases contain two terms, while that for $K=0$ contains only a single one. Due to this fragmentation of $E3$ strength, the conspicuous feature of the transition from U(5) to SU(3) will be decreasing $B(E3)$ values. These results are empirically observed, as illustrated in Fig. 76.

The neutron-rich nuclei $^{140-146}$Ba were also described with the Hamiltonian of Eq. (4.14) by Scott *et al.* (1980). For $H_{sd}$, the authors employed constant coefficients of the $Q^2$ and $\hat{L}^2$ terms, and a simple linear dependence on boson number for the boson energy and pairing terms. The low-lying $1^-$ and $3^-$ states in each nucleus were described by a single constant interaction strength $Z_2$. The $f$-boson energy was adjusted to normalize the $3^-$ energy in each case. (Note that $\varepsilon_f$ does not affect the relative spacing of the negative-parity states, but merely shifts them with respect to the positive-parity states.) The results of the fit are shown in Fig. 77. The striking feature of interest here is the correct reproduction of the crossing of the $1^-$ and $3^-$ levels between neutron numbers 86 and 88, which is a characteristic signature of the onset of deformation (Scott *et al.*, 1979).

Another approach to negative-parity states in this region is a calculation of the $N=88$ isotopes by Han *et al.* (1985), who use a Hamiltonian of the form of Eq. (4.14) but without the $\theta_f$ $N$ term. $H_{sd}$ is taken from previous calculations (Chuu *et al.*, 1984) of the positive-parity states and is $Z$ independent from Nd to Dy. Good agreement is obtained except for the lowest $1^-$ levels (predicted too high) and the predicted $E1$ strengths. Both of

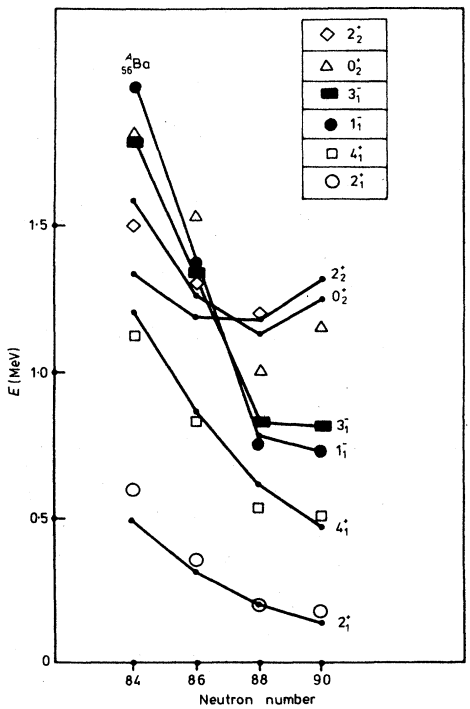


FIG. 77. Comparison between the calculated (solid lines) and experimental (points) energies of the low-lying states in the neutron-rich Ba isotopes. From Scott *et al.* (1980).

these difficulties are corrected (however, at a substantial cost in the number of parameters) by adding a $p(l=1)$ boson. There have been several other studies that explored the need for $p$ bosons. The introduction of a $p$ boson helps compensate for the shift in the center of mass when an octupole or $f$ boson is introduced and may also be useful in accounting for the decay of higher-spin $\pi=-$ states. Engel and Iachello (1985) studied the effects of $p$ and $f$ bosons in the case of a U(16)$\supset\cdots\supset$SU(3) dynamical symmetry. More recently, Otsuka and Sugita (1987) have incorporated both $p$ and $f$ bosons into an IBA-1 study of negative-parity states in the actinide region.

At the same time additional studies with only an $f$ boson have been carried out. The coupling of an $f$ boson to an O(6) core has recently been considered by Engel (1986) and applied to the negative-parity states of $^{190-196}$Pt. The Hamiltonian is similar to that in the work of Han *et al.* (1985) but with $H_{sd}$ in the O(6) limit. Reasonable agreement for $J^\pi \leq 4^-$ states is obtained, but the facts that the lowest negative-parity states in Pt have $J^\pi=5^-$ and that the $J^\pi \geq 6^-$ states are not well fit are illustrative of strong nonoctupole character in these states.

More recently, an extensive set of calculations including the $f$ boson have been carried out by Barfield (1986) and Barfield, Wood, and Barrett (1986). Their formalism is rather similar to that of Scholten, Iachello, and Arima (1978), except that they also include an exchange term (proportional to a coefficient $A_3$) in the Hamiltonian, which arises from an octupole-octupole interaction. This term plays a particularly crucial role, and the competition between it and the quadrupole-quadrupole interaction term, denoted $A_2 Q_{sd}\cdot Q_f$, determines the relative ordering of the octupole bands. This feature is illustrated in Fig. 78, where it can be seen that a variety of relative orderings can be obtained and it becomes possible to go naturally from the $0^-1^-2^-3^-$ sequence for prolate shape at the beginning of a shell towards the inverse situation expected at the end of a shell.

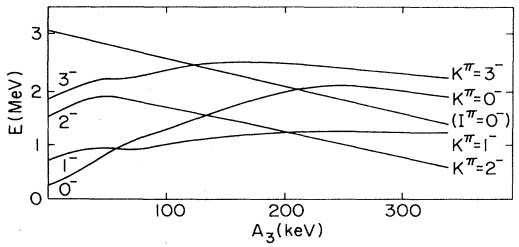


FIG. 78. Schematic calculation of the relative ordering of the different negative-parity $K$ bands with a Hamiltonian incorporating $s$, $d$, and $f$ bosons. $A_3$ is the strength of the exchange term. The parameter $A_2$ in the Hamiltonian was set at $-50$ keV. The full specification of the Hamiltonian and the values for the other parameter values are given in Barfield (1986) [Eq. (8.43)] on which this figure is based. The $I^\pi=0^-$ line gives the energy of the lowest $I^\pi=0^-$ state.

In this work, $H_{sd}$ is treated in the CQF formalism. The $E3$ operator is generalized, relative to earlier studies, to the form

$$T(E3)=e_3[(s^\dagger\tilde{f}+f^\dagger s)+\chi_3(d^\dagger\tilde{f}+f^\dagger\tilde{d})^{(3)}]\,. \quad (4.15)$$

This study is particularly interesting because it covers a broad range of nuclei stretching from $^{154}$Sm to $^{182}$W. The calculation has a rather large number of free parameters, and it is not the purpose of this review to discuss the detailed variations in each except to note that the $B(E3)$ values are primarily determined by $\chi_3$. The most detailed results are presented for the nucleus $^{168}$Er; the fit to the negative-parity energy levels is shown in Fig. 79. (The fit to the positive-parity energy levels is essentially the same as obtained in earlier studies.) As can be seen, four negative-parity bands below 2 MeV are well fitted by the calculations. Several other empirical low-lying negative-parity bands, indicated in the box at the left, are also known, but at least several, the low-lying $4^-$, $3^-$, and $6^-$ bands, are considered (Davidson *et al.*, 1981a) to be two quasiparticle in character and therefore outside the space of these calculations.

Finally, a related approach that has been introduced by Iachello and Jackson (1982) is the $\alpha$-clustering model, which is designed to account simultaneously for low-lying negative-parity states, large $\alpha$-transfer cross sections, and small $\alpha$-decay hindrance factors, and has been applied in the actinides and elsewhere. The model envisages a normal IBA set of states coupled to another set described by $s'$ and $p$ $(l=1)$ bosons. The basic idea is that, although the simultaneous excitation of both proton and neutron pairs might seem to require a large energy, the attractive $p$-$n$ interaction in an $\alpha$ cluster can significantly lower the energy required, and such states may play a role in the low-lying spectrum. The group structure of this second set of states is then determined by the space spanned by $s'$ and $p$ bosons, or $U(4)\times$U(2). The U(2) group here allows for both proton and neutron $s'$ and $p$ bosons. In the IBA-1 this reduces to U(4) (but

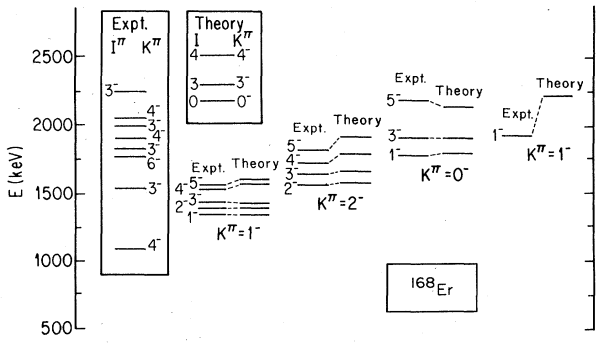


FIG. 79. Comparison of calculated and empirical negative-parity states in $^{168}$Er. The boxes contain experimental bandheads thought to represent dominantly two-quasiparticle excitations, and the next-higher-lying theoretical bands. From Barfield, Wood, and Barrett (1986).

note that this may be a risky simplification because, then, a $4p$ or $4n$ state is at the same energy as the $\alpha$ cluster). In any case, this subset of states is then coupled to the normal *sd* space with appropriate mixing terms. Depending on the *p*-boson energy and the interaction terms (and the group chain describing the *sd* system), such a model can account for many low-lying negative-parity states, for large $\alpha$ decay probabilities, and for enhanced $E1$ transitions (since the center of charge and mass do not coincide when the $\alpha$ cluster is present). However, despite extensive comparisons to the data, in both the rare earths and the actinides, and with models of stable octupole deformation, dynamic octupole vibrations, and $f$ bosons, there is not as yet a clear picture of the relative merits or areas of validity of each approach.

While the above discussion illustrates a few results of incorporating an $f$ boson into the IBA, it is clear that this is a field that has barely been touched. The data in deformed rare-earth and actinide nuclei on negative-parity states are very extensive, while only a few initial theoretical probes of the $f$-boson structure and of the coupling of the $f$ boson to the *sd*-boson space have been published. This entire area and its relation to other approaches, such as that of the $\alpha$-clustering model, would seem to be ripe for much more extensive and systematic theoretical investigation.

### H. Other applications of the IBA

A generic kind of extension of the IBA-1 consists, not in introducing new degrees of freedom, but in exploiting the normal IBA structure of low-lying collective excitations in conjunction with the description of other states or, more commonly, of various nuclear reaction processes. Examples of this are electron scattering, the decay of giant resonances, and medium-energy proton scattering.

#### 1. Electron scattering

Electron scattering has been the most extensively studied of these three, and we begin with it. It offers, in principle, a much more detailed and sensitive probe than electromagnetic decay (or $\gamma$ scattering), since it is sensitive to the radial wave-function structure: electron scattering at different angles samples different momentum transfer and therefore different radial regions.

The formalism is extremely simple and was first discussed at a very early stage (Dieperink *et al.*, 1978; Dieperink, 1979) and subsequently by Dieperink (1981) as well as in many specific articles exploiting the formalism. In $E2$ excitations in electron scattering, the transition operator of Eq. (2.8) is modified as follows:

$$T_r(E2)=\alpha(r)(s^\dagger\tilde{d}+d^\dagger s)^{(2)}+\beta(r)(d^\dagger\tilde{d})^{(2)} , \qquad (4.16)$$

where the boson densities $\alpha$ and $\beta$ have now been expressed as radial functions $\alpha(r)$ and $\beta(r)$. It is then clear that an arbitrary $E2$ matrix element can be expressed as

$$\langle i\|T_r(E2)\|f\rangle=\alpha(r)A+\beta(r)B , \qquad (4.17)$$

where $A$ and $B$ are the normal IBA matrix elements, connecting states $i$ and $f$, of the operators $(s^\dagger\tilde{d}+d^\dagger s)$ and $(d^\dagger\tilde{d})^{(2)}$, respectively. $A$ and $B$ can be calculated trivially once an IBA calculation for a given nucleus has been performed. Then a standard distorted-wave Born approximation calculation of the electron scattering cross sections can be parametrized in terms of $\alpha(r)$ and $\beta(r)$, and the data as a function of momentum transfer $q$ can be used to deduce $\alpha(r)$ and $\beta(r)$ for each value of $r$.

Such experimental studies are difficult, and the analysis time consuming, and therefore only a few results have appeared as yet although it is clear that this is an exciting field that offers much promise. See, for example, the work of Moinester *et al.* (1982), Hersman *et al.* (1983), Goutte (1984), Borghols *et al.* (1985), de Leo *et al.* (1985), and van der Laan *et al.* (1985). Some of these utilize the IBA-2, while others either use the IBA-1 or incorporate approximations that essentially reduce the calculations to IBA-1.

Several complementary approaches may be taken. In one the boson densities $\alpha(r)$ and $\beta(r)$ are extracted from measured transition charge densities to two states, say $2_1^+$ and $2_2^+$, and then used to predict the transition densities for the $2_3^+$ level. Alternatively, if $\alpha(r)$ and $\beta(r)$ are known, $A$ and $B$ can be extracted and compared with results obtained with more conventional techniques. Finally, $\alpha(r)$ and $\beta(r)$ could be calculated from a microscopic theory.

An interesting point concerns the general structure of $\alpha(r)$ and $\beta(r)$. Despite the differences between geometric, particle-hole or quasiparticle phonons and the particle-particle (or hole-hole) IBA bosons, it is tempting to identify the creation of a $d$ boson with a one-phonon operator. Then, by analogy with the geometric model, it has been argued (Dieperink *et al.*, 1978; Borghols *et al.*, 1985) that boson densities involving one $d$-boson operator

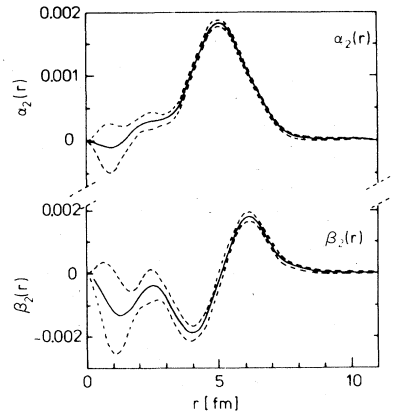


FIG. 80. Boson densities $\alpha(r)$ and $\beta(r)$ for $^{110}$Pd deduced from the charge densities of the $2_1^+$ and $2_2^+$ states. From van der Laan *et al.* (1985).

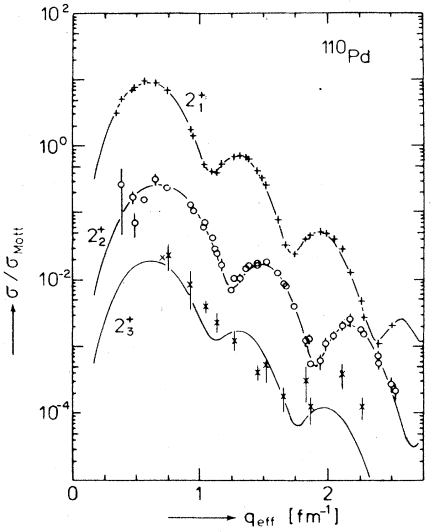


FIG. 81. Form-factor data for the $2^+$ states at 274, 814, and 1470 keV in $^{110}$Pd. The curves for the $2_1^+$ and $2_2^+$ states are Fourier-Bessel fits, while that for the $2_3^+$ level is the IBA prediction. From van der Laan *et al.* (1985).

should be surface peaked (first derivative of the charge density), while a second derivative form would apply to an operator with two $d$ bosons. Thus, crudely, $\alpha(r)$ should have the former character and $\beta(r)$ the latter.

Applications of these ideas have been carried out for the Pd, Sm, and other isotopes. The $^{110}$Pd results from the NIKEFF group (van der Laan *et al.*, 1985) are a good example of the technique. Although they employ the IBA-2, their approximation that $\alpha_\pi(r)=\alpha_\nu(r)$ and $\beta_\pi(r)=\beta_\nu(r)$ simulates some of the reduction to IBA-1. Figure 80 shows the boson densities $\alpha(r)$ and $\beta(r)$ deduced from the transition charge densities for the $2_1^+$ and $2_2^+$ states. Note that $\alpha(r)$ is indeed of first derivative form and that $\beta(r)$ is more complex. Using these results, the fit to the scattering cross section for the $2_4^+$ level (the $2_3^+$ level is considered to be an intruder state) shown in Fig. 81 is obtained. The agreement is rather encouraging.

De Leo *et al.* (1985) have expanded on this work by studying inelastic proton scattering and by using the form factors deduced from the electron scattering data. They also obtain results for $\alpha(r)$ and $\beta(r)$ that closely resemble first and second derivative shapes, respectively.

A particularly beautiful application of electron scattering to test the IBA concerns the Ge isotopes in which an intruder configuration forms an excited band in the light isotopes, $^{68,70}$Ge, and the ground state in the heavier ones, $^{74,76}$Ge. This work has been discussed by Goutte (1984) and, although it utilizes the IBA-2 in the Duval-Barrett formalism, it is still worth illustrating the results here, since it so well demonstrates the power of this technique. The data from $^{72,76}$Ge are used to extract $\alpha(r)$ and $\beta(r)$ boson densities for each configuration of levels. Then the $2_1^+$ and $2_2^+$ form factors for $^{70,74}$Ge are predicted. The results are shown in Fig. 82 and show remarkably good agreement with the data. In particular, the strikingly different behavior of the $2_2^+$ state in $^{70}$Ge is well reproduced. Careful interpretation (see also Duval, Goutte, and Vergnes, 1983) allows one to assign this $2^+$

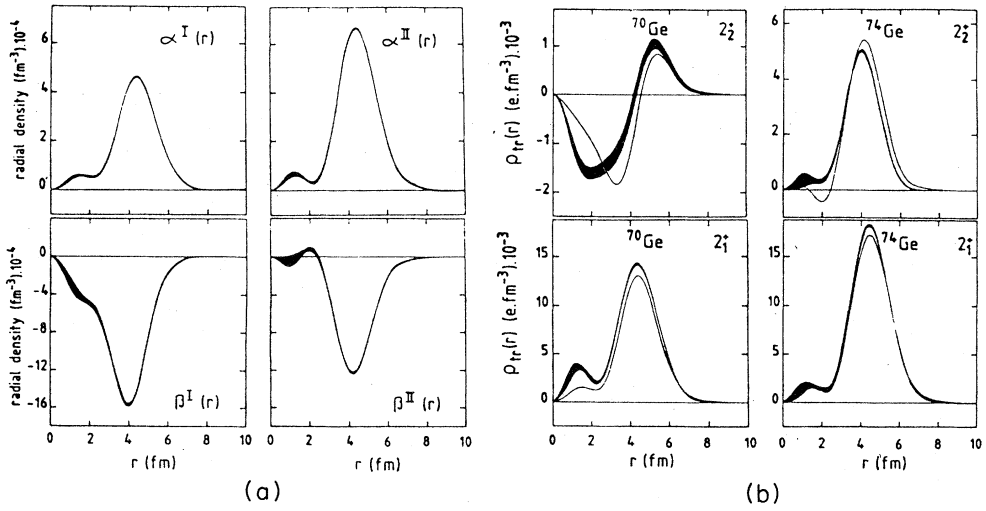


FIG. 82. Boson densities and transition charge densities. (a) The four boson densities appearing in the $T(E2)$ operator. The superscripts I and II refer to the two intrinsic configurations (Duval, Goutte, and Vergnes, 1983) present in the Ge isotopes, and the widths of the curves indicate the uncertainties in the extracted values of $\alpha(r)$ and $\beta(r)$. These were obtained from four of the eight low-lying $2^+$ states in the four even-even isotopes $^{68-74}$Ge. These densities are then used to obtain predicted transition charge densities (thin lines) for the other four, as shown in (b), where the dark curves are the experimental transition charge densities. From Goutte (1984).

level to a normal configuration and the others to an intruder $2p$-$2h$ configuration and thereby to map out the evolution and mixing of the interacting configurations as a function of $A$.

The approach of using the data from some states to determine $\alpha(r)$ and $\beta(r)$ and then predicting others has also been taken by Hersman *et al.* (1983), in this case for $^{154}$Gd, in order to test the IBA description of the lowest excited $K=0$ ($\beta$) band. They fit the scattering data to the $2_g^+$ and $2_\gamma^+$ levels and then found rather serious disagreements for the $2_\beta^+$ state. The results are shown in Fig. 83. Several different parameter sets were used to describe the $2_3^+$ levels, but none succeeded.

Moinester *et al.* (1982) have tackled a particularly tough problem, namely, the entire set of Sm isotopes from $A=144-154$. Their approach consists of first calculating these isotopes in the IBA. (The calculations were entirely done in the IBA-2, but the resultant wave functions turned out to be nearly totally symmetric in proton and neutron degrees of freedom and thus the calculation corresponds closely to the IBA-1.) Then, boson densities deduced from the scattering to lower states are used to predict the higher ones. Here these authors extracted a single set of boson structure functions, $\alpha(r)$ and $\beta(r)$, for the entire isotopic chain, which, notably, spans a transition region. The transition charge densities for the $2_1^+$ states are shown in Fig. 84 where they are compared to IBA-1 predictions. The observed variations in these densities are well reproduced. Another interesting feature of this study is that monopole densities $\alpha_0(r)$ and $\beta_0(r)$ are extracted from $0^+\rightarrow 0^+$ transitions and are used to interpret isotope shift and other monopole data in Sm as well. Figure 85 shows one of the resulting predictions, namely, for the $E0$ excitation of the $0_2^+$ level in $^{152}$Sm.

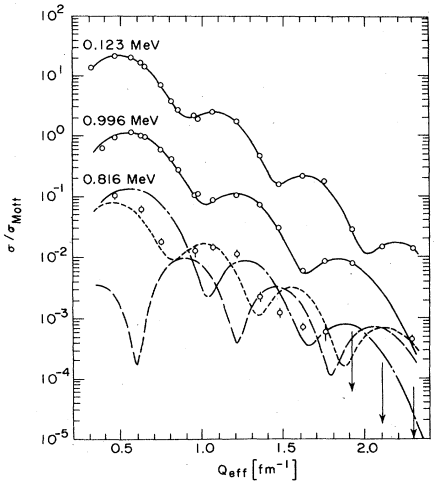


FIG. 83. Comparison of calculated and empirical electron scattering cross sections for $2^+$ states in $^{154}$Gd. The parameters of the fits were determined from the 123- and 966-keV states, and the three lines for the 816-keV $2^+$ state are different IBA fits. From Hersman *et al.* (1983).

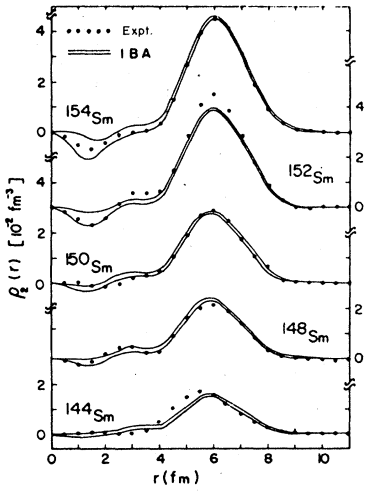


FIG. 84. Comparison of calculated and empirical transition charge densities for $2_1^+$ states in Sm isotopes using the same overall best fit $\alpha(r)$ and $\beta(r)$ densities for all isotopes. The uncertainties in $\alpha(r)$ and $\beta(r)$ are reflected by the envelope of predictions for the IBA model. From Moinester *et al.* (1982).

While the empirical uncertainties are large, the agreement is nevertheless apparent.

A final interesting application (Borghols *et al.*, 1985) of these ideas concerns excitation of the $4^+$ levels in $^{196}$Pt. These should proceed by double $E2$ excitation $(d^\dagger\times\tilde{d})^{(4)}$ and therefore the form factors should be of second derivative form. However, the electron scattering data for three $4^+$ states, shown in Fig. 86, are clearly surface peaked. Furthermore, in O(6), only the first $4^+$ level should be excited, which is clearly not the case here. If, on the other hand, a $g$ boson is important in the excita-

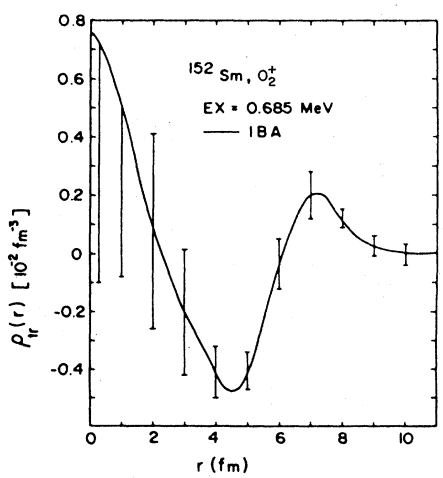


FIG. 85. Calculated and empirical transition charge densities for the $E0$ excitation of the $0_2^+$ state in $^{152}$Sm. From Moinester *et al.* (1982).

tion of the $4^+$ states, the operator is just $\beta'(r)g^\dagger s$ and the boson density should be of first derivative form as observed. This is an interesting, albeit roundabout, argument for $g$-boson effects that could prove extremely useful in other regions.

### 2. Giant resonances

The application of the IBA to giant resonances is a relatively untouched field in which the first efforts also look encouraging. The basic idea (Morrison and Weise, 1982; Rowe and Iachello, 1983; Scholtz and Hahne, 1983; Maino *et al.*, 1984) is simply to describe the low-lying collective states with the IBA-1 and use their structure to calculate photoabsorption and photon inelastic scattering cross sections. The giant dipole resonance (GDR) is incorporated via a $p(l=1)$ boson, and a Hamiltonian

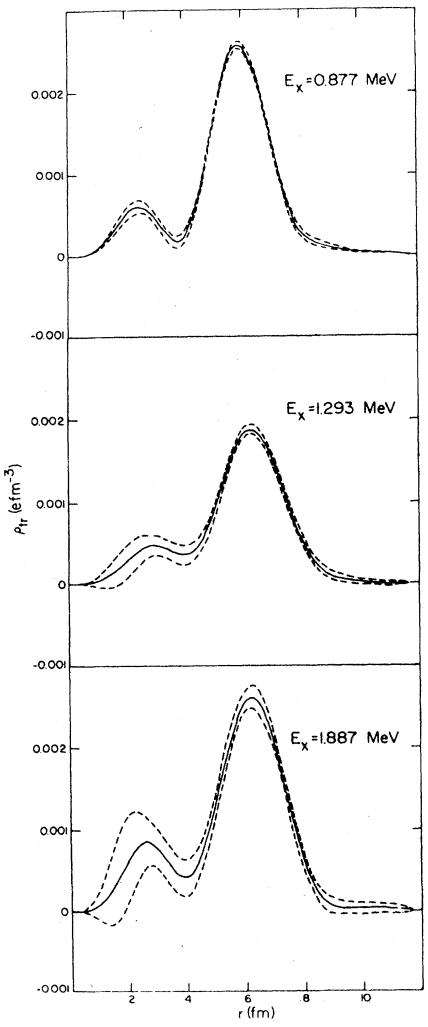


FIG. 86. Experimental transition densities for the $4^+$ states of 0.877, 1.293, and 1887 MeV in $^{196}$Pt. From Borghols *et al.* (1985).

$$H = H_{sd} + H_p + H_{\text{int}} \tag{4.18}$$

is used where the notation is obvious. The energy and spreading of the GDR is separately parametrized. Thus the calculations trivially predict the energy and rough shape of the photoabsorption cross section as a function of $E_\gamma$: this is not really a test of the model. However, an interesting result, exemplified by the transitional Nd and Sm isotopes, is shown in Fig. 87, namely, that the calculations reproduce the fine structure involved in the development of a double-humped distribution as deformation sets in. The origin of this, geometrically, is well known: in the deformed field, the GDR splits into $K=0$ and 1 components. The latter is higher in energy because it represents a vibration along the minor axis of the nucleus, and also has nearly twice the total cross section because of the presence of both $K=+1$ and $-1$ amplitudes. The calculations reproduce this, as well as the larger width of the $K=1$ part, because of the larger number of $K^\pi=1^-$ states than $K=0^-$ levels.

While most of the basic physics is inserted into these results *a priori*, it turns out that, without additional parameters, this type of calculation also predicts (Maino *et al.*, 1985) inelastic photon scattering to excited states, with the difference relative to other models that coupling of the GDR to *all* core states (not just the ground state or ground-state band) is automatically included. Figure 88 shows the differential cross sections for elastic and inelastic $(2_1^+)$ photon scattering for $^{232}$Th and $^{238}$U. The agreement is clearly rather good and did not require the assumption of extra amplitudes outside the model framework.

The above results are for deformed nuclei or transitional nuclei in a U(5)→SU(3) region (e.g., the Nd isotopes). Recently, Maino *et al.* (1986) have considered the SU(3)→O(6) region spanned by the Os isotopes. They obtain excellent agreement with the data for the photoabsorption cross sections and generate predictions for photon scattering cross sections to the $2_1^+$, $2_2^+$, and $0_2^+$ levels. These results have all been obtained by numerical diagonalization of the Hamiltonian of Eq. (4.18). Also, recently, Zuffi *et al.* (1987) have developed analytic formulas to describe both photoabsorption and scattering in the SU(3) and SU*(3) (triaxial) limits in the framework of the IBA-2.

### 3. Medium-energy proton scattering

Lastly, one can exploit the simplicity of group and symmetry structure to study scattering processes. As just one example, Ginocchio *et al.* (1986) have applied the IBA-1 to medium-energy proton scattering at 800 MeV. By combining the IBA-1 description of the low-lying states with the Glauber approximation treatment of the scattering process, they utilize the known IBA matrix elements of an eikonal phase operator to evaluate the scattering, obtaining analytic results in all three IBA-1 limits. Again, because the IBA basis provides a simple

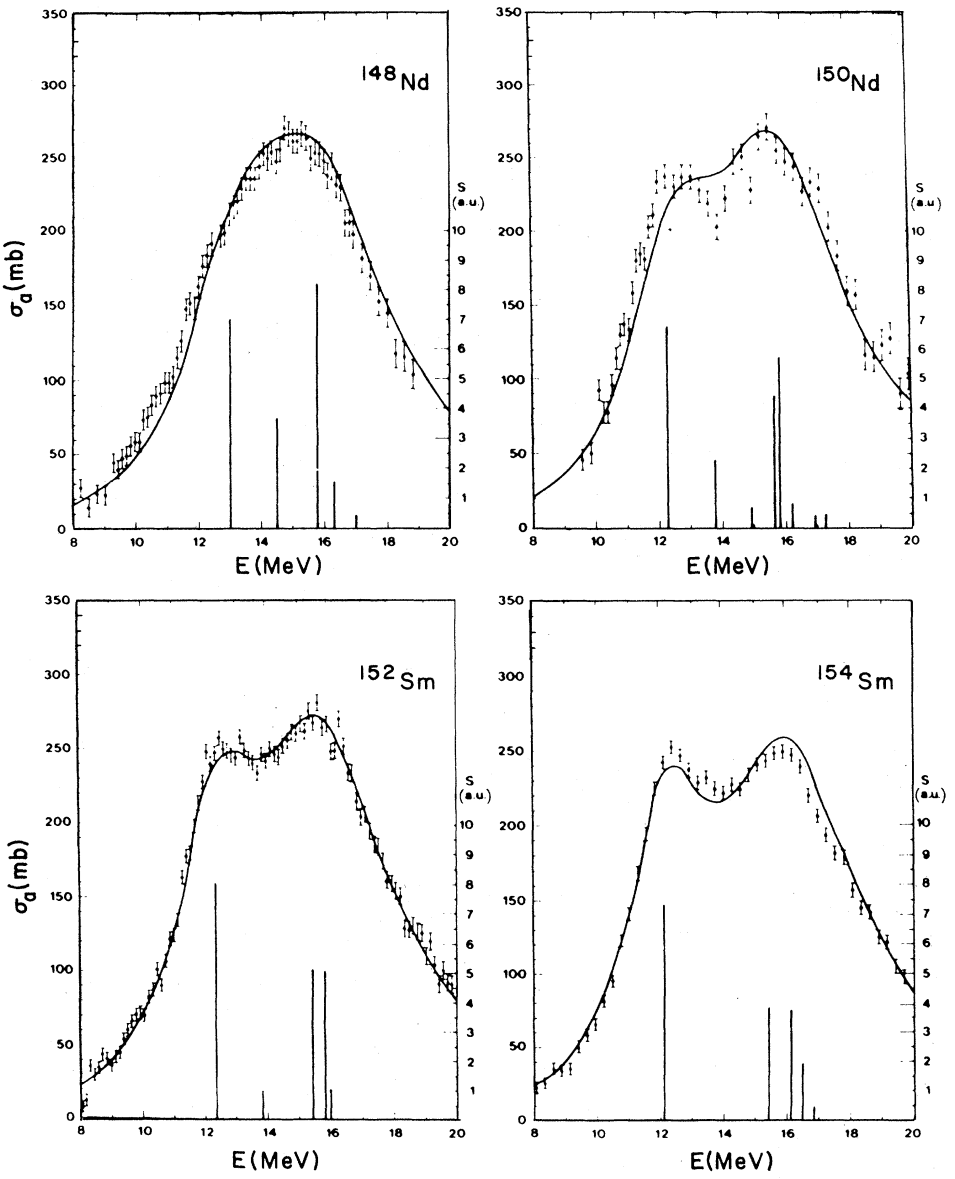


FIG. 87. Comparison of calculated and empirical total photoabsorption cross sections in the Nd and Sm isotopes. The fragmentation of $E1$ strength is shown in arbitrary units at the bottom. From Maino *et al.* (1984).

framework to include all low-lying states, the calculations automatically include coupling to all inelastic channels. In this way one is able to investigate the dependence of these on the low-lying structure, finding, for example, that such effects are only important for high-$q$ ($>2.5$ fm$^{-1}$) scattering in U(5) and O(6), but are first-order effects (at $q \gtrsim 1$ fm$^{-1}$) in SU(3). For elastic scattering, channel coupling effects again are largest in SU(3) and are directly related to $B(E2)$ values. Third-order effects in SU(3) appear at $q \gtrsim 2.5$ fm$^{-1}$ and can distinguish oblate and prolate deformations. Figure 89 illustrates some of these results. Once again, this is a new field in which only the first ventures have been made.

## V. SUMMARY AND CONCLUSIONS

We have tried in this review to discuss the IBA-1 model and some of its more significant extensions. The basic model was outlined and discussed from the standpoints both of its central group-theoretical structure, leading to analytic dynamical symmetries with clear physical interpretations, and of its numerical diagonalizations. The importance of its emphasis on the valence space, and the consequent appearance of the boson number $N$ in the formalism, was stressed. The essential element here is not the specific values of $N$ used, and indeed some calculations have employed choices differing from the tradition-

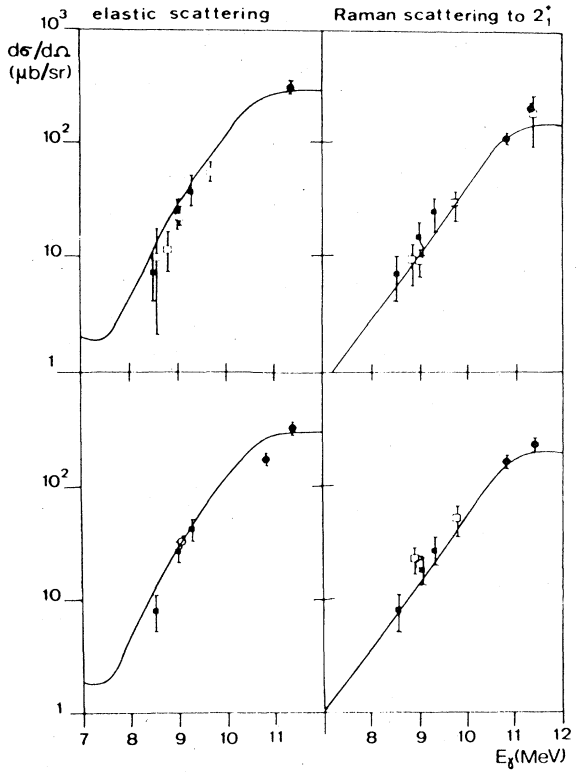


FIG. 88. Cross sections for elastic and inelastic photon scattering (to the $2_1^+$ state). Top, $^{232}$Th; bottom, $^{238}$U. From Maino *et al.* (1985).

al ones, but the fact that $N$ is finite and varies from nucleus to nucleus. Both these features distinguish the IBA from geometrical models.

Throughout the review a substantial effort has been made to demystify many aspects of the model by way of specific examples and by attempting to provide a simple and intuitive understanding of the underlying physics. A number of important tests of the model have been discussed, some in passing and others in some detail. Many other important contributions have been made that have barely, if at all, been mentioned.

We hope that, in addition to an appreciation and understanding of the formal structure of the model, the reader will have acquired a physical feeling for the IBA as well, so that, when faced with a particular application, he or she will have a grasp of where to start and, moreover, a prior feeling of what will be the likely outcome of an IBA calculation or of a series of calculations for a sequence of isotopes.

In sum, we think it is reasonable to state that the IBA has been a very successful model which correlates a large body of data, and which, though phenomenological, has predictive power, even in the microscopic sense. It has led to a much deeper understanding of many collective phenomena in heavy nuclei as well as of the systematics of the evolution of nuclear structure over broad ranges of nuclei. On the other hand, the model is manifestly phenomenological and remains in need of additional work directed towards its microscopic justification and foundations. Moreover, even at the phenomenological level, the model has obvious shortcomings, some of which are inherent to the basic truncation scheme involved in its formulation, and, naturally, numerous extensions of the model have been developed over the last years to overcome these shortcomings.

It may be appropriate in these final paragraphs to summarize where, following the work of the last decade, the IBA sits with respect to the pantheon of nuclear models available for medium and heavy nuclei. After much initial excitement over the model and its predictions, as well as considerable controversy, the situation today seems to be one in which the IBA has become one of a triad of approaches to nuclear structure, each with different advan-

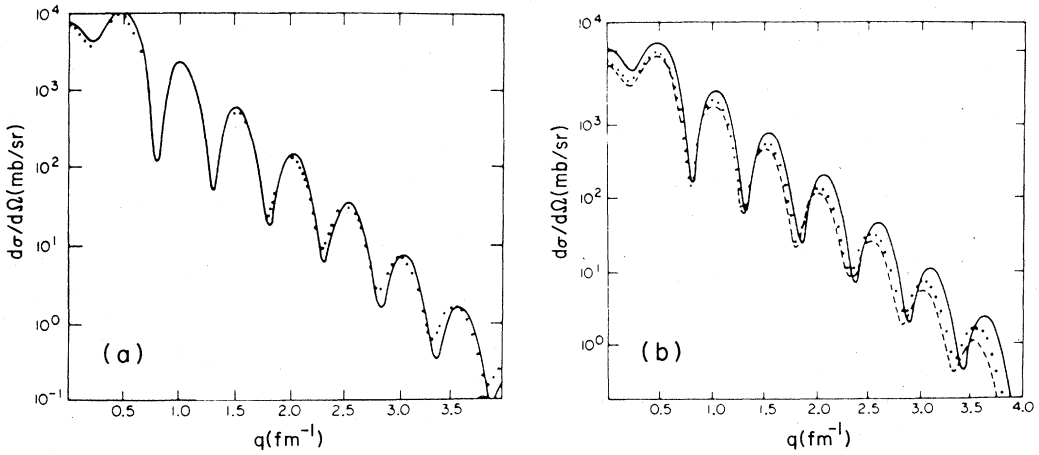


FIG. 89. Calculated cross sections for 800-MeV proton excitation of the $2_1^+$ state in a schematic Sm isotope: (a) assuming the structure to be O(6) or U(5); (b) assuming SU(3) symmetry. The solid lines are the full calculation [with the assumption of prolate shape for the SU(3) case]. The dashed line in (b) is the SU(3) prediction for an oblate shape. The dots are the results without coupled-channel effects. From Ginocchio *et al.* (1986).

tages and disadvantages: this triad consists of a microscopic shell-model approach, a geometrical approach, and an algebraic approach. Each of these starts with simple concepts of approximate validity, namely the spherical single-particle shell model (including pairing), often truncated in practical calculations, the spherical phonon and deformed symmetric rotor geometric models for collective nuclei, and the *s*- and *d*-boson IBA-1 model. Each of these parent models has in turn spawned generations of offshoots: the shell model has been extended to a multiparticle situation, and deformed nuclei can be described with the Nilsson model. Geometrical models have been developed that include other degrees of freedom, such as axial asymmetry or hexadecapole deformations, as well as versions that include rotation-vibration coupling or quasiparticle excitations. As regards the IBA, extensions such as the IBA-2 or those discussed in the previous section, which include *g* bosons, coupling to the quasiparticle spectrum, and, of course, coupling to odd-mass nuclei, are being actively studied. In both their simplest and their more complex forms, the IBA-1 and its extensions, as well as the other algebraic techniques they have fostered, thus provide an important alternative to existing approaches to the modeling of heavy nuclei.

## ACKNOWLEDGMENTS

Each of the authors would like to take this opportunity to express his deep appreciation to the other for years of stimulating discussions and fruitful collaborations and to wish the other success in the years ahead. In addition, we are very grateful to many of our colleagues (and often collaborators) who through their publications and, especially, through innumerable discussions, have helped us enormously in developing our own understanding of the IBA and in carrying out our own research in this field. First, it is fitting to single out for special thanks A. Arima and F. Iachello, who, besides having initiated and inspired the entire field of research described here, have been for us personally an invaluable source of advice, expertise, and guidance. It is clearly impossible to mention all the others who have also been of so much help, but we cannot close without specifically thanking A. Aprahamian, B. Barrett, R. Bijker, A. Bohr, P. von Brentano, A. Bruce, J. A. Cizewski, A. E. L. Dieperink, D. H. Feng, A. Frank, A. Gelberg, J. N. Ginocchio, K. Heyde, P. Lipas, I. Morrison, B. R. Mottelson, T. Otsuka, S. Pittel, O. Scholten, I. Talmi, P. Van Isacker, and A. Wolf. We also thank J. Winger and D. Brenner for technical help in the preparation of this manuscript. Finally, we are greatly indebted to J. Mooney, without whose dedicated help and unrivalled expertise neither this project nor much of the work of the last eight years would have been completed. Research has been supported under Contract No. DE-AC02-76CH00016 with the United States Department of Energy and by the Bundesministerium für Forschung und Technologie.

## REFERENCES

Akiyama, Y., 1985, Nucl. Phys. A **433**, 369.
Akiyama, Y., K. Heyde, A. Arima, and N. Yoshinaga, 1986, Phys. Lett. B **173**, 1.
Akiyama, Y., P. von Brentano, and A. Gelberg, 1987, Z. Phys. A **326**, 517.
Alaga, G., K. Alder, A. Bohr, and B. R. Mottelson, 1955, K. Dan. Vidensk. Selsk. Mat. Fys. Medd. **29**, No. 9.
Aprahamian, A., 1984, private communication.
Aprahamian, A., D. S. Brenner, R. F. Casten, R. L. Gill, and A. Piotrowski, 1987, Phys. Rev. Lett. **59**, 535.
Aprahamian, A., D. S. Brenner, R. F. Casten, R. L. Gill, A. Piotrowski, and K. Heyde, 1984, Phys. Lett. B **140**, 22.
Arima, A., 1983, in *Progress in Particle and Nuclear Physics, Vol. 9, Collective Bands in Nuclei,* edited by D. Wilkinson (Pergamon, Oxford), p. 51.
Arima, A., 1984, in *Proceedings of the International Workshop on Collective States in Nuclei,* Suzhou, PRC . . ., edited by Li-Ming Yang, Xiao-Qian Zhou, Gong-Ou Xu, Shi-Shu Wu, and Da Hsuan Feng (Nucl. Phys. A **421**), p. 63c.
Arima, A., and F. Iachello, 1975, Phys. Rev. Lett. **35**, 1069.
Arima, A., and F. Iachello, 1976, Ann. Phys. (N.Y.) **99**, 253.
Arima, A., and F. Iachello, 1977, Phys. Rev. C **16**, 2085.
Arima, A., and F. Iachello, 1978a, Ann. Phys. (N.Y.) **111**, 201.
Arima, A., and F. Iachello, 1978b, Phys. Rev. Lett. **40**, 358.
Arima, A., and F. Iachello, 1979, Ann. Phys. (N.Y.) **123**, 468.
Arima, A., and F. Iachello, 1981, Annu. Rev. Nucl. Part. Sci. **31**, 75.
Arima, A., T. Ohtsuka, F. Iachello, and I. Talmi, 1977, Phys. Lett. B **66**, 205.
Bagnell, R. D., Y. Tanake, R. K. Sheline, G. Burke, and J. D. Sherman, 1977, Phys. Lett. B **66**, 129.
Bagnell, R. D., Y. Tanake, R. K. Sheline, G. Burke, and J. D. Sherman, 1979, Phys. Rev. C **20**, 42.
Baker, F. T., 1985, Phys. Rev. C **32**, 1430.
Balantekin, A. B., B. R. Barrett, and S. Levit, 1983, Phys. Lett. B **129**, 153.
Barfield, A., 1986, Ph.D. thesis (University of Arizona).
Barfield, A. F., J. L. Wood, and B. R. Barrett, 1986, Phys. Rev. C **34**, 2001.
Barrett, B. R., 1984, in *Proceedings of the International Summer School on the Nucleon Nucleon Interaction and Nuclear Many Body Problems,* edited by S. S. Wu and T. T. S. Kuo (World Scientific, Singapore), p. 415.
Berg, U. E. P., *et al.*, 1984, Phys. Lett. B **149**, 59.
Bes, D. R., 1963, Nucl. Phys. **49**, 544.
Bes, D. R., P. Federman, E. Maqueda, and A. Zuker, 1965, Nucl. Phys. **65**, 1.
Bijker, R., and A. E. L. Dieperink, 1982, Phys. Rev. C **26**, 2688.
Bohle, D., G. Kuchler, A. Richter, and W. Steffen, 1984, Phys. Lett. B **148**, 260.
Bohle, D., A. Richter, W. Steffen, A. E. L. Dieperink, N. LoIudice, F. Palumbo, and O. Scholten, 1984, Phys. Lett. B **137**, 27.
Bohr, A., and B. R. Mottelson, 1953, K. Dan. Vidensk. Selsk. Mat. Fys. Medd. **27**, No. 16.
Bohr, A., and B. R. Mottelson, 1975, *Nuclear Structure,* Vol. II (Benjamin, Reading, MA).
Bohr, A., and B. R. Mottelson, 1982, Phys. Scr. **25**, 28.
Bolotin, H. H., A. E. Stuchbery, I. Morrison, D. L. Kennedy, C. G. Ryan, and S. H. Sie, 1981, Nucl. Phys. A **370**, 146.

Borghols, W. T. A., N. Blasi, R. Bijker, M. N. Harakeh, C. W. De Jager, J. B. van der Laan, H. De Vries, and S. Y. Van Der Werf, 1985, Phys. Lett. B **152**, 330.
Brink, D. M., A. F. R. de Toledo Piza, and A. K. Kerman, 1965, Phys. Lett. **19**, 413.
Bucurescu, D., G. Cata, D. Cutoiu, G. Constantinescu, M. Ivascu, and N. V. Zamfir, 1986, Z. Phys. A **324**, 387.
Bucurescu, D., G. Cata, D. Cutoiu, G. Constantinescu, M. Ivascu, and N. V. Zamfir, 1987, Z. Phys. A **327**, 241.
Burke, D. G., W. F. Davidson, J. A. Cizewski, R. E. Brown, E. R. Flynn, and J. W. Sunier, 1985, Can. J. Phys. **63**, 1309.
Burke, D. G., B. L. W. Maddock, and W. F. Davidson, 1985, Nucl. Phys. A **442**, 424.
Castanos, Q., P. Federman, and A. Frank, 1981, in *Interacting Boson-Fermi Systems in Nuclei,* edited by F. Iachello (Plenum, New York), p. 21.
Castanos, O., P. Federman, A. Frank, and S. Pittel, 1982, Nucl. Phys. A **379**, 61.
Castanos, O., A. Frank, and P. Federman, 1979, Phys. Lett. B **88**, 203.
Castanos, O., A. Frank, P. Hess, and M. Moshinsky, 1981, Phys. Rev. C **24**, 1367.
Castanos, O., A. Frank, and P. Van Isacker, 1984, Phys. Rev. Lett. **52**, 263.
Casten, R. F., 1985a, Phys. Lett. B **152**, 145.
Casten, R. F., 1985b, Phys. Rev. Lett. **54**, 1991.
Casten, R. F., A. Aprahamian, and D. D. Warner, 1984, Phys. Rev. C **29**, 356.
Casten, R. F., D. S. Brenner, and P. E. Haustein, 1987, Phys. Rev. Lett. **58**, 658.
Casten, R. F., and P. von Brentano, 1985, Phys. Lett. B **152**, 22.
Casten, R. F., P. von Brentano, and A. M. I. Haque, 1985, Phys. Rev. C **31**, 1991.
Casten, R. F., P. von Brentano, K. Heyde, P. Van Isacker, and J. Jolie, 1985, Nucl. Phys. A **439**, 289.
Casten, R. F., and J. A. Cizewski, 1978, Nucl. Phys. A **309**, 477.
Casten, R. F., and J. A. Cizewski, 1984, Nucl. Phys. A **425**, 653.
Casten, R. F., and J. A. Cizewski, 1987, Phys. Lett. B **185**, 293.
Casten, R. F., D. H. Feng, J. N. Ginocchio, and C. L. Wu, 1986, Mod. Phys. Lett. **1**, 161.
Casten, R. F., W. Frank, and P. von Brentano, 1985, Nucl. Phys. A **444**, 133.
Casten, R. F., and D. D. Warner, 1982, Phys. Rev. Lett. **48**, 666.
Casten, R. F., and D. D. Warner, 1983, in *Progress in Particle and Nuclear Physics, Vol. 9, Collective Bands in Nuclei,* edited by D. Wilkinson (Pergamon, Oxford), p. 311.
Casten, R. F., D. D. Warner, and A. Aprahamian, 1983, Phys. Rev. C **28**, 894.
Casten, R. F., D. D. Warner, D. S. Brenner, and R. L. Gill, 1981, Phys. Rev. Lett. **47**, 1433.
Casten, R. F., and A. Wolf, 1987, Phys. Rev. C **35**, 1156.
Catara, F., M. Sambataro, A. Insolia, and A. Vitturi, 1986, Phys. Lett. B **180**, 1.
Chakraborty, Manab, V. K. Brahmam Kota, and Jitendra C. Parikh, 1981, Phys. Lett. B **100**, 201.
Chen, Hsi-Tseng, and A. Arima, 1983, Phys. Rev. Lett. **51**, 447.
Chuu, D. S., C. S. Han, S. T. Hsieh, and M. M. King Yen, 1984, Phys. Rev. C **30**, 1300.
Cizewski, J. A., R. F. Casten, G. J. Smith, M. L. Stelts, W. R. Kane, H. G. Börner, and W. F. Davidson, 1978, Phys. Rev. Lett. **40**, 167.
Cizewski, J. A., E. R. Flynn, Ronald E. Brown, D. L. Hanson, S. D. Orbesen, and J. W. Sunier, 1981, Phys. Rev. C **23**, 1453.
Cizewski, J. A., E. R. Flynn, Ronald E. Brown, and J. W. Sunier, 1979, Phys. Lett. B **88**, 207.
Cline, D., 1971, *Les Noyaux de Transition, Colloquium on Intermediate Nuclei* (Institut National de Physique, Orsay), p. 4.
Davidson, W. F., *et al.*, 1981a, J. Phys. G **7**, 455.
Davidson, W. F., *et al.*, 1981b, J. Phys. G **7**, 843.
Davydov, A. S., and G. F. Filippov, 1958, Nucl. Phys. **8**, 237.
de Leo, R., M. Pignanelli, W. T. A. Borghols, S. Brandenburg, M. N. Harakeh, H. J. Lu, S. Y. Van Der Werf, C. W. De Jager, J. B. van der Laan, and H. De Vries, 1985, Phys. Lett. B **162**, 1.
deShalit, A., and H. Feshbach, 1974, *Theoretical Nuclear Physics* (Wiley, New York).
Dieperink, A. E. L., 1979, in *Interacting Bosons in Nuclear Physics,* edited by F. Iachello (Plenum, New York), p. 129.
Dieperink, A. E. L., 1981, Nucl. Phys. A **358**, 189c.
Dieperink, A. E. L., 1983, in *Progress in Particle and Nuclear Physics, Vol. 9, Collective Bands in Nuclei,* edited by D. Wilkinson (Pergamon, Oxford), p. 121.
Dieperink, A. E. L., 1984, in *Proceedings of the International Workshop on Collective States in Nuclei,* Suzhou, PRC ..., edited by Li-Ming Yang, Xiao-Qian Zhou, Gong-Ou Xu, Shi-Shu Wu, and Da Hsuan Feng (Nucl. Phys. A **421**, 189c).
Dieperink, A. E. L., F. Iachello, A. Rinat, and C. Cresswell, 1978, Phys. Lett. B **76**, 135.
Dieperink, A. E. L., and O. Scholten, 1980, Nucl. Phys. A **346**, 125.
Dieperink, A. E. L., O. Scholten, and F. Iachello, 1980, Phys. Rev. Lett. **44**, 1747.
Dieperink, A. E. L., and G. Wenes, 1985, Annu. Rev. Nucl. Part. Sci. **35**, 77.
Dobeš, J., 1985, Phys. Lett. B **158**, 97.
Dobeš, J., 1987, Nucl. Phys. A **369**, 424.
Doran, C. E., H. H. Bolotin, A. E. Stuchbery, and A. P. Byrne, 1986, Z. Phys. A **325**, 285.
Dukelsky, J., G. G. Dussel, and H. M. Sofia, 1981, Phys. Lett. B **100**, 367.
Dukelsky, J., J. Fernandez Niello, H. M. Sofia, and R. P. Perazzo, 1983, Phys. Rev. C **28**, 2183.
Dumitrescu, T. S., and I. Hamamoto, 1982, Nucl. Phys. A **383**, 205.
Duval, P. D., and B. R. Barrett, 1981a, Phys. Lett. B **100**, 223.
Duval, P. D., and B. R. Barrett, 1981b, Phys. Rev. C **23**, 492.
Duval, P. D., and B. R. Barrett, 1982, Nucl. Phys. A **376**, 213.
Duval, P. D., D. Goutte, and M. Vergnes, 1983, Phys. Lett. B **124**, 297.
Eastham, D. D., P. M. Walker, J. R. H. Smith, D. D. Warner, J. A. R. Griffith, D. E. Evans, S. A. Wells, M. J. Fawcett, and I. S. Grant, 1987, Phys. Rev. C **36**, 1583.
Elliott, J. P., 1958a, Proc. R. Soc. London, Ser. A **245**, 128.
Elliott, J. P., 1958b, Proc. R. Soc. London, Ser. A **245**, 562.
Elliott, J. P., 1985, Rep. Prog. Phys. **48**, 171.
Elliott, J. P., J. A. Evans, and P. Van Isacker, 1986, Phys. Rev. Lett. **57**, 1124.
Elliott, J. P., and M. Harvey, 1963, Proc. R. Soc. London, Ser. **272**, 557.
Emling, H., 1984, in *Electromagnetic Properties of High-Spin Nuclear Levels* (Annals of the Israel Physical Society, Vol. 7), edited by Gvirol Goldring and Michael Haas (Hilger, Bristol), p. 161.
Engel, J., 1986, Phys. Lett. B **171**, 148.
Engel, J., and F. Iachello, 1985, Phys. Rev. Lett. **54**, 1126.
Erokhina, K. I., A. D. Efimov, I. Kh. Lemberg, and V. M. Mikhailov, 1985, Yad. Fiz. **41**, 596 [Sov. J. Nucl. Phys. **41**, 3860

(1985)].
Faessler, Amand, S. Kuyucak, A. Petrovici, and L. Petersen, 1985, Nucl. Phys. A **438**, 78.
Federman, P., and S. Pittel, 1977, Phys. Lett. B **69**, 385.
Federman, P., and S. Pittel, 1978, Phys. Lett. B **77**, 29.
Federman, P., and S. Pittel, 1979, Phys. Rev. C **20**, 820.
Federman, P., S. Pittel, and R. Campos, 1979, Phys. Lett. B **82**, 9.
Feng, D. H., 1986, in *Few Body Methods: Principles and Applications,* edited by T. K. Lim, C. G. Bao, D. P. Hou, and S. Huber (World Scientific, Singapore), p. 603.
Fewell, M. P., 1986, Phys. Lett. B **167**, 6.
Fewell, M. P., G. J. Gyapong, R. H. Spear, M. T. Esat, A. M. Baxter, and S. M. Burnett, 1985, Phys. Lett. B **157**, 353.
Frank, A., 1986, private communication.
Frank, W., H. Harter, and P. von Brentano, 1987, private communication.
Gallagher, C. J., Jr., and V. G. Soloviev, 1962, K. Dan. Vidensk. Selsk. Mat. Fys. Skr. **2**, No. 2.
Gast, W., *et al.*, 1984, Z. Phys. A **318**, 123.
Gelberg, A., and P. von Brentano, 1987, private communication.
Gelberg, A., and A. Zemel, 1980, Phys. Rev. C **22**, 937.
Gelletly, W., J. R. Larysz, H. G. Börner, R. F. Casten, W. F. Davidson, W. Mampe, K. Schreckenbach, and D. D. Warner, 1985, J. Phys. G **11**. 1055.
Gelletly, W., J. R. Larysz, H. G. Börner, R. F. Casten, W. F. Davidson, W. Mampe, K. Schreckenbach, and D. D. Warner, 1987, J. Phys. G **13**, 69.
Gelletly, W., P. Van Isacker, D. D. Warner, G. Colvin, and K. Schreckenbach, 1987, Phys. Lett. B **191**, 240.
Gill, R. L., R. F. Casten, D. D. Warner, D. S. Brenner, and W. B. Walters, 1982, Phys. Lett. B **118**, 251.
Gill, R. L., D. D. Warner, H. Mach, A. Piotrowski, A. Wolf, J. C. Hill, F. K. Wohn, J. A. Winger, and B. Fogelberg, 1986, Phys. Rev. C **33**, 1030.
Gilmore, R., 1979, J. Math. Phys. **20**, 891.
Gilmore, R., C. M. Bowden, and L. M. Narducci, 1975, Phys. Rev. A **12**, 1019.
Gilmore, R., and D. H. Feng, 1978a, Phys. Lett. B **76**, 26.
Gilmore, R., and D. H. Feng, 1978b, Nucl. Phys. A **301**, 189.
Ginocchio, J. N., 1980, Ann. Phys. (N.Y.) **126**, 234.
Ginocchio, J. N., and M. W. Kirson, 1980a, Phys. Rev. Lett. **44**, 1744.
Ginocchio, J. N., and M. W. Kirson, 1980b, Nucl. Phys. A **350**, 31.
Ginocchio, J. N., T. Otsuka, R. D. Amado, and D. A. Sparrow, 1986, Phys. Rev. C **33**, 247.
Goettig, L., Ch. Droste, A. Dygo, T. Morek, J. Srebrny, R. Broda, J. Styczen, J. Hattuk, H. Helppi, and M. Jaaskelainen, 1981, Nucl. Phys. A **357**, 109.
Goutte, D., 1984, in *Interacting Boson-Boson and Boson-Fermion Systems,* edited by O. Scholten (World Scientific, Singapore), p. 241.
Grechukhin, D. P., 1963, Nucl. Phys. **40**, 422.
Greenwood, R. C., *et al.*, 1978, Nucl. Phys. A **304**, 327.
Greiner, W., 1966, Nucl. Phys. **80**, 417.
Grosse, E., *et al.*, 1981, Phys. Scr. **24**, 337.
Han, C. S., D. S. Chuu, S. T. Hsieh, and H. C. Chiang, 1985, Phys. Lett. B **163**, 295.
Hanewinkel, H., *et al.*, 1983, Phys. Lett. B **133**, 9.
Haque, A. M. I., *et al.*, 1986, Nucl. Phys. A **455**, 231.
Harter, H., A. Gelberg, and P. von Brentano, 1985, Phys. Lett. B **157**, 1.
Harter, H., P. von Brentano, and A. Gelberg, 1986, Phys. Rev. C **34**, 1472.
Harter, H., P. von Brentano, A. Gelberg, and T. Otsuka, 1987, Phys. Lett. B **188**, 295.
Hatch, R. L., and S. Levit, 1982, Phys. Rev. C **25**, 614.
Helmer, R. G., C. W. Reich, R. J. Gherke, R. C. Greenwood, and R. A. Anderl, 1977, Phys. Rev. C **15**, 1453.
Hersman, F. W., *et al.*, 1983, Phys. Lett. B **132**, 47.
Heyde, K., J. Jolie, P. Van Isacker, J. Moreau, and M. Waroquier, 1984, Phys. Rev. C **29**, 1428.
Heyde, K., P. Van Isacker, R. F. Casten, and J. L. Wood, 1985, Phys. Lett. B **155**, 303.
Heyde, K., P. Van Isacker, J. Jolie, J. Moreau, and M. Waroquier, 1983, Phys. Lett. B **132**, 15.
Heyde, K., P. Van Isacker, M. Waroquier, and J. Moreau, 1984, Phys. Rev. C **29**, 1420.
Heyde, K., P. Van Isacker, M. Waroquier, G. Wenes, Y. Gigase, and J. Stachel, 1983, Nucl. Phys. A **398**, 235.
Heyde, K., P. Van Isacker, M. Waroquier, G. Wenes, and M. Sambataro, 1982, Phys. Rev. C **25**, 3160.
Hsieh, S. T., H. C. Chang, M. M. King Yen, and D. S. Chuu, 1986, J. Phys. G **12**, L167.
Iachello, F., 1979, in *Interacting Bosons in Nuclear Physics,* edited by F. Iachello (Plenum, New York), p. 1.
Iachello, F., 1981a, in *Nuclear Structure,* edited by K. Abrahams, K. Allaart, and A. E. L. Dieperink (Plenum, New York), p. 53.
Iachello, F., 1981b, Nucl. Phys. A **358**, 89c.
Iachello, F., 1983a, Hyperfine Interact. **15/16**, 11.
Iachello, F., 1983b, in *Progress in Particle and Nuclear Physics, Vol. 9, Collective Bands in Nuclei,* edited by D. Wilkinson (Pergamon, Oxford), p. 5.
Iachello, F., 1984, in *Nuclear Shell Models,* edited by M. Vallières and B. H. Wildenthal (World Scientific, Singapore), p. 279.
Iachello, F., and A. Arima, 1974, Phys. Lett. B **53**, 309.
Iachello, F., and A. Arima, 1987, *The Interacting Boson Model* (Cambridge University Press, Cambridge, England).
Iachello, F., and A. D. Jackson, 1982, Phys. Lett. B **108**, 151.
Iachello, F., and O. Scholten, 1979, Phys. Rev. Lett. **43**, 679.
Iachello, F., and I. Talmi, 1987, Rev. Mod. Phys. **59**, 339.
Janssen, D., R. V. Jolos, and F. Donau, 1974, Nucl. Phys. A **224**, 93.
Kaup, U., and A. Gelberg, 1979, Z. Phys. A **293**, 311.
Kirson, M. W., and A. Leviatan, 1985, Phys. Rev. Lett. **55**, 2846.
Krane, K. S., 1973, Phys. Rev. C **8**, 1494.
Kumar, K., 1970, Phys. Rev. C **1**, 369.
Kumar, K., 1972, Phys. Scr. **6**, 270.
Kumar, K., 1975, in *The Electromagnetic Interaction in Nuclear Spectroscopy,* edited by W. D. Hamilton (North-Holland, Amsterdam), p. 55.
Kuyucak, S., and I. Morrison, 1987, Phys. Rev. Lett. **58**, 315.
Lange, J., K. Kumar, and J. Hamilton, 1982, Rev. Mod. Phys. **54**, 119.
Leviatan, A., 1984, Phys. Lett. B **143**, 25.
Leviatan, A., 1986, Ph.D. thesis (Weizmann Institute of Science).
Leviatan, A., A. Novoselsky, and I. Talmi, 1986, Phys. Lett. B **172**, 144.
Lipas, P. O., 1962, Nucl. Phys. **39**, 468.
Lipas, P. O., 1983, in *Progress in Particle and Nuclear Physics, Vol. 9, Collective Bands in Nuclei,* edited by D. Wilkinson (Pergamon, Oxford), p. 511.

Lipas, P. O., 1984, in *International Review of Nuclear Physics,* Vol. 2, edited by T. Engeland, J. Rekstad, and J. S. Vaagen (World Scientific, Singapore), p. 33.
Lipas, P. O., 1986a, in *International Summer School on Hyperfine Interactions and Physics with Oriented Nuclei,* edited by E. Rotter (Charles University, Prague), p. 175.
Lipas, P., 1986b, in *Nuclear Structure, Reactions and Symmetries,* edited by R. A. Meyer and V. Paar (World Scientific, Singapore), p. 921.
Lipas, P. O., E. Hammarén, and P. Toivonen, 1984, Phys. Lett. B **139**, 10.
Lipas, P. O., J. Kumpulainen, E. Hammarén, T. Honkaranta, M. Finger, T. I. Kracikova, I. Prochazka, and J. Ferencci, 1983, Phys. Scr. **27**, 8.
Lipas, P. O., P. Toivonen, and E. Hammarén, 1987, Nucl. Phys. A **469**, 348.
Lipas, P. O., P. Toivonen, and D. D. Warner, 1985, Phys. Lett. B **155**, 295.
Loewenich, K., K. O. Zell, A. Dewald, W. Gast, A. Gelberg, W. Lieberz, P. von Brentano, and P. Van Isacker, 1986, Nucl. Phys. A **460**, 361.
Loludice, N., and F. Palumbo, 1978, Phys. Rev. Lett. **41**, 1532.
Maglione, E., A. Vitturi, C. H. Dasso, and R. A. Broglia, 1983, Nucl. Phys. A **404**, 333.
Maino, G., T. Martinelli, E. Menapace, and A. Ventura, 1981, Lett. Nuovo Cimento **32**, 235.
Maino, G., and A. Ventura, 1982a, Lett. Nuovo Cimento **34**, 79.
Maino, G., and A. Ventura, 1982b, Lett. Nuovo Cimento **34**, 533.
Maino, G., A. Ventura, P. Van Isacker, and L. Zuffi, 1986, Phys. Rev. C **33**, 1089.
Maino, G., A. Ventura, L. Zuffi, and F. Iachello, 1984, Phys. Rev. C **30**, 2101.
Maino, G., A. Ventura, L. Zuffi, and F. Iachello, 1985, Phys. Lett. B **152**, 17.
McGowan, F. K., 1981, Phys. Rev. C **24**, 1803.
McGowan, F. K., and W. T. Milner, 1981, Phys. Rev. C **23**, 1926.
McGrory, J. B., 1978, Phys. Rev. Lett. **41**, 533.
McGrory, J. B., 1979, in *Interacting Bosons in Nuclear Physics,* edited by F. Iachello (Plenum, New York), p. 121.
Menzen, G., A. Wolf, H. Lawin, G. Lhersonneau, and K. Sistemich, 1985, Z. Phys. A **321**, 593.
Mheemeed, A., *et al.*, 1984, Nucl. Phys. A **412**, 113.
Mikhailov, V. M., 1966, Izv. Akad. Nauk. SSSR Ser. Fiz. **30**, 1339.
Moinester, M. A., J. Alster, G. Azuelos, and A. E. L. Dieperink, 1982, Nucl. Phys. A **383**, 264.
Morrison, I., 1986, J. Phys. G **12**, L201.
Morrison, I., A. Faessler, and C. Lima, 1981, Nucl. Phys. A **372**, 13.
Morrison, I., and J. Weise, 1982, J. Phys. G **8**, 687.
Novoselsky, A., and I. Talmi, 1986, Phys. Lett. B **172**, 139.
Otsuka, T., 1981, Phys. Rev. Lett. **46**, 710.
Otsuka, T., A. Arima, F. Iachello, and I. Talmi, 1978, Phys. Lett. B **76**, 139.
Otsuka, T., A. Arima, and N. Yoshinaga, 1982, Phys. Rev. Lett. **48**, 387.
Otsuka, T., and M. Sugita, 1987, in *Proceedings of the International Conference on Nuclear Structure through Static and Dynamic Moments,* Australia (Organizing Committee, Melbourne), Vol. I, p. 98.
Ower, H., *et al.*, 1982, Nucl. Phys. A **388**, 421.
Paar, V., 1979, in *Interacting Bosons in Nuclear Physics,* edited by F. Iachello (Plenum, New York), p. 163.
Passoja, A., J. Kantele, M. Luontama, R. Julin, E. Hammarén, P. O. Lipas, and P. Toivonen, 1986, J. Phys. G **12**, 1047.
Piepenbring, R., 1986, Proceedings of the XVIII Summer School on Nuclear Structure, Mikolajk, Poland, unpublished.
Piepenbring, R., 1987, in Proceedings of the Sixth International Symposium on Capture Gamma-Ray Spectroscopy, Leuven, Belgium, edited by P. van Assche, unpublished.
Pittel, S., and J. Dukelsky, 1985, Phys. Rev. C **32**, 335.
Pittel, S., J. Dukelsky, R. P. J. Perazzo, and H. M. Sofia, 1984, Phys. Lett. B **144**, 145.
Ratna Raju, R. D., 1981, Phys. Rev. C **23**, 518.
Ratna Raju, R. D., 1982, J. Phys. G **8**, 1663.
Raman, S., C. H. Malarkey, W. T. Milner, C. W. Nestor, and P. H. Stelson, 1987, At. Data Nucl. Data Tables **36**, 1.
Richter, A., 1985, in *Nuclear Structure 1985,* edited by R. Broglia, G. B. Hagemann, and B. Herskind (Elsevier, The Netherlands), p. 469.
Riedinger, L. L., N. R. Johnson, and J. H. Hamilton, 1969, Phys. Rev. **179**, 1214.
Robinson, S. J., W. D. Hamilton, and D. M. Snelling, 1983, J. Phys. G **9**, 961.
Rowe, D. J., and F. Iachello, 1983, Phys. Lett. B **130**, 231.
Sage, K. A., and B. R. Barrett, 1980, Phys. Rev. C **22**, 1765.
Sage, K. A., P. R. Goode, and B. R. Barrett, 1982, Phys. Rev. C **26**, 668.
Sakai, M., 1984, At. Data Nucl. Data Tables **31**, 399.
Sala, P., A. Gelberg, and P. von Brentano, 1986, Z. Phys. A **323**, 281.
Sambataro, M., and G. Molnar, 1982, Nucl. Phys. A **376**, 201.
Scharff-Goldhaber, G., and J. Weneser, 1955, Phys. Rev. **98**, 212.
Schiffer, K., A. Dewald, A. Gelberg, R. Reinhardt, K. O. Zell, Sun Xianfu, and P. von Brentano, 1986, Z. Phys. A **323**, 487.
Scholten, O., 1979a, Kernfisisch Versneller Instituut Internal Report No. 63.
Scholten, O., 1979b, in *Interacting Bosons in Nuclear Physics,* edited by F. Iachello (Plenum, New York), p. 17.
Scholten, O., 1980, Ph.D. thesis (Kernfisisch Versneller Instituut, Groningen).
Scholten, O., 1983, Phys. Lett. B **127**, 144.
Scholten, O., F. Iachello, and A. Arima, 1978, Ann. Phys. (N.Y.) **115**, 325.
Scholtz, F. G, and F. J. Hahne, 1983, Phys. Lett. B **123**, 147.
Schreckenbach, K., *et al.*, 1982, Phys. Lett. B **110**, 364.
Scott, S. M., W. D. Hamilton, P. Hungerford, D. D. Warner, G. Jung, K. D. Wunsch, and B. Pfeiffer, 1980, J. Phys. G **6**, 1291.
Scott, S. M., D. D. Warner, W. D. Hamilton, P. Hungerford, G. Jung, K. D. Wunsche, and B. Pfeiffer, 1979, J. Phys. G **5**, L187.
Shi, Z.-R., R. F. Casten, J. Stachel, and A. M. Bruce, 1985, in *Capture Gamma-Ray Spectroscopy and Related Topics—1984,* AIP Conference Proceedings No. 125, edited by S. Raman (AIP, New York), p. 435.
Soloviev, V. G., 1965, Nucl. Phys. **69**, 1.
Soloviev, V. G., 1986, Z. Phys. A **324**, 393.
Soloviev, V. G., and N. Yu Shirikova, 1981, Z. Phys. A **301**. 263.
Stachel, J., N. Kaffrell, N. Trautmann, K. Broden, G. Skarnemark, and D. Ericksen, 1984, Z. Phys. A **316**, 105.
Stachel, J., P. Van Isacker, and K. Heyde, 1982, Phys. Rev. C **25**, 650.
Sun, Hong-Zhou, M. Moshinski, A. Frank, and P. Van Isacker, 1983, KINAM **5**, 135.

Sun, Hong-Zhou, Mei Zhang, and Da Hsuan Feng, 1985, Phys. Lett. B **163**, 7.
Talmi, I., 1971, Nucl. Phys. A **172**, 1.
Talmi, I., 1983, in *Progress in Particle and Nuclear Physics, Vol. 9, Collective Bands in Nuclei,* edited by D. Wilkinson (Pergamon, Oxford), p. 27.
Theuerkauf, J., H. Harter, P. von Brentano, and R. F. Casten, 1987, Z. Phys. A **326**, 65.
van der Laan, J. B., A. J. C. Burghardt, C. W. De Jager, and H. De Vries, 1985, Phys. Lett. B **153**, 130.
Van Isacker, P., 1983, Phys. Rev. C **27**, 2447.
Van Isacker, P., 1987, Nucl. Phys. A **465**, 497.
Van Isacker, P., and Jin-Quan Chen, 1981, Phys. Rev. C **24**, 684.
Van Isacker, P., K. Heyde, J. Jolie, and A. Sevrin, 1986, Ann. Phys. (N.Y.) **171**, 253.
Van Isacker, P., K. Heyde, M. Waroquier, and G. Wenes, 1981, Phys. Lett. B **104**, 5.
Van Isacker, P., K. Heyde, M. Waroquier, and G. Wenes, 1982, Nucl. Phys. A **380**, 383.
Van Isacker, P., J. Jolie, K. Heyde, and A. Frank, 1985, Phys. Rev. Lett. **54**, 653.
Varley, B. J., R. Moscrop, S. Babkair, C. J. Lister, W. Gelletly, and H. G. Price, 1985, in *Capture Gamma-Ray Spectroscopy and Related Topics—1984,* AIP Conference Proceedings No. 125, edited by S. Raman (AIP, New York), p. 709.
Vergados, J. D., 1968, Nucl. Phys. A **111**, 681.
Warner, D. D., 1981, Phys. Rev. Lett. **47**, 1819.
Warner, D. D., 1984, in *Proceedings of the Workshop on Bosons in Nuclei,* edited by D. H. Feng, S. Pittel, and M. Vallières (World Scientific, Singapore), p. 133.
Warner, D. D., 1986, Phys. Rev. C **34**, 1131.
Warner, D. D., and R. F. Casten, 1982a, Phys. Rev. Lett. **48**, 1385.
Warner, D. D., and R. F. Casten, 1982b, Phys. Rev. C **25**, 2019.
Warner, D. D., and R. F. Casten, 1982c, Phys. Rev. C **26**, 2690.
Warner, D. D., and R. F. Casten, 1983, Phys. Rev. C **28**, 1798.
Warner, D. D., R. F. Casten, and W. F. Davidson, 1980, Phys. Rev. Lett. **45**, 1761.
Warner, D. D., R. F. Casten, and W. F. Davidson, 1981, Phys. Rev. C **24**, 1713.
Warner, D. D., Z. R. Shi, W. Gelletly, H. G. Börner, F. Hoyler, K. Schreckenbach, and P. Van Isacker, 1987, in Proceedings of the Sixth International Symposium on Capture Gamma-Ray Spectroscopy, Leuven, Belgium, edited by P. van Assche, unpublished.
Wenes, G., P. Van Isacker, M. Waroquier, K. Heyde, and J. Van Maldeghem, 1981, Phys. Lett. B **98**, 398.
Wilets, L., and M. Jean, 1956, Phys. Rev. C **102**, 788.
Wolf, A., Z. Berant, D. D. Warner, R. L. Gill, M. Shmid, R. E. Chrien, G. Peaslee, H. Yamamoto, J. C. Hill, F. K. Wohn, C. Chung, and W. B. Walters, 1983, Phys. Lett. B **123**, 165.
Wolf, A., and R. F. Casten, 1987, Phys. Rev. C **36**, 851.
Wolf, A., R. F. Casten, and D. D. Warner, 1987, Phys. Lett. **190**, 19.
Wolf, A., D. D. Warner, and N. Benczer-Koller, 1985, Phys. Lett. B **158**, 7.
Wood, John L., 1984, in *Proceedings of the International Workshop of Collective States in Nuclei,* Suzhou, PRC . . . , edited by Li-Ming Yang, Xiao-Qian Zhou, Gong-Ou Xu, Shi-Shu Wu, and Da Hsuan Feng (Nucl. Phys. A **421**), p. 43c.
Wood, L., and I. Morrison, 1985, J. Phys. G **11**, L201.
Wu, C.-L., D. H. Feng, X.-G. Chen, J.-Q. Chen, and M. W. Guidry, 1986, Phys. Lett. B **168**, 313.
Wu, Hua-Chuan, 1982, Phys. Lett. B **110**, 1.
Xu, Gong-Ou, 1984, in *Proceedings of the International Workshop on Collective States in Nuclei,* Suzhou, PRC . . . , edited by Li-Ming Yang, Xiao-Qian Zhou, Gong-Ou Xu, Shi-Shu Wu, and Da Hsuan Feng (Nucl. Phys. A **421**), p. 275c.
Yen, M., M. King, S. T. Hsieh, H. C. Chiang, and D. S. Chuu, 1984, Phys. Rev. C **29**, 688.
Yoshida, N., A. Arima, and T. Otsuka, 1982, Phys. Lett. B **114**, 86.
Yoshinaga, N., Y. Akiyama, and A. Arima, 1986, Phys. Rev. Lett. **56**, 1116.
Zhang, Mei, M. Vallières, R. Gilmore, Da Hsuan Feng, Richard W. Hoff, and Hong-Zhou Sun, 1985, Phys. Rev. C **32**, 1076.
Zuffi, L., P. Van Isacker, G. Maino, and A. Ventura, 1987, Nucl. Instrum. Methods A **255**, 46.